1995

Climate Forcing: Observations From Chinese Loess Plateau And A Perspective Of The Influence Of Ocean-ridge Processes

Jingtai Han

献给我的母亲

Dedicated to my mother who passed away during this study

ISBN 0-612-03456-9

Name JINGTAI HAN

Dissertation Abstracts International is arranged by broad, general subject categories. Please select the one subject which most nearly describes the content of your dissertation. Enter the corresponding four-digit code in the spaces provided.

Geology | 0372 | U·M·I

SUBJECT TERM | SUBJECT CODE

Subject Categories

THE HUMANITIES AND SOCIAL SCIENCES

COMMUNICATIONS AND THE ARTS
Architecture 0729
Art History 0377
Cinema 0900
Dance 0378
Fine Arts 0357
Information Science 0723
Journalism 0391
Library Science 0399
Mass Communications 0708
Music 0413
Speech Communication 0459
Theater 0465

EDUCATION
General 0515
Administration 0514
Adult and Continuing 0516
Agricultural 0517
Art 0273
Bilingual and Multicultural 0282
Business 0688
Community College 0275
Curriculum and Instruction 0727
Early Childhood 0518
Elementary 0524
Finance 0277
Guidance and Counseling 0519
Health 0680
Higher 0745
History of 0520
Home Economics 0278
Industrial 0521
Language and Literature 0279
Mathematics 0280
Music 0522
Philosophy of 0998
Physical 0523
Psychology 0525
Reading 0535
Religious 0527
Sciences 0714
Secondary 0533
Social Sciences 0534
Sociology of 0340
Special 0529
Teacher Training 0530
Technology 0710
Tests and Measurements 0288
Vocational 0747

LANGUAGE, LITERATURE AND LINGUISTICS
Language
- General 0679
- Ancient 0289
- Linguistics 0290
- Modern 0291

Literature
- General 0401
- Classical 0294
- Comparative 0295
- Medieval 0297
- Modern 0298
- African 0316
- American 0591
- Asian 0305
- Canadian (English) 0352
- Canadian (French) 0355
- English 0593
- Germanic 0311
- Latin American 0312
- Middle Eastern 0315
- Romance 0313
- Slavic and East European 0314

PHILOSOPHY, RELIGION AND THEOLOGY
Philosophy 0422
Religion
- General 0318
- Biblical Studies 0321
- Clergy 0319
- History of 0320
- Philosophy of 0322

Theology 0469

SOCIAL SCIENCES
American Studies 0323
Anthropology
- Archaeology 0324
- Cultural 0326
- Physical 0327

Business Administration
- General 0310
- Accounting 0272
- Banking 0770
- Management 0454
- Marketing 0338

Canadian Studies 0385
Economics
- General 0501
- Agricultural 0503
- Commerce-Business 0505
- Finance 0508
- History 0509
- Labor 0510
- Theory 0511

Folklore 0358
Geography 0366
Gerontology 0351
History
- General 0578
- Ancient 0579
- Medieval 0581
- Modern 0582
- Black 0328
- African 0331
- Asia, Australia and Oceania 0332
- Canadian 0334
- European 0335
- Latin American 0336
- Middle Eastern 0333
- United States 0337

History of Science 0585
Law 0398
Political Science
- General 0615
- International Law and Relations 0616
- Public Administration 0617

Recreation 0814
Social Work 0452
Sociology
- General 0626
- Criminology and Penology 0627
- Demography 0938
- Ethnic and Racial Studies 0631
- Individual and Family Studies 0628
- Industrial and Labor Relations 0629
- Public and Social Welfare 0630
- Social Structure and Development 0700
- Theory and Methods 0344

Transportation 0709
Urban and Regional Planning 0999
Women's Studies 0453

THE SCIENCES AND ENGINEERING

BIOLOGICAL SCIENCES
Agriculture
- General 0473
- Agronomy 0285
- Animal Culture and Nutrition 0475
- Animal Pathology 0476
- Food Science and Technology 0359
- Forestry and Wildlife 0478
- Plant Culture 0479
- Plant Pathology 0480
- Plant Physiology 0817
- Range Management 0777
- Wood Technology 0746

Biology
- General 0306
- Anatomy 0287
- Biostatistics 0308
- Botany 0309
- Cell 0379
- Ecology 0329
- Entomology 0353
- Genetics 0369
- Limnology 0793
- Microbiology 0410
- Molecular 0307
- Neuroscience 0317
- Oceanography 0416
- Physiology 0433
- Radiation 0821
- Veterinary Science 0778
- Zoology 0472

Biophysics
- General 0786
- Medical 0760

EARTH SCIENCES
Biogeochemistry 0425
Geochemistry 0996
Geodesy 0370
Geology 0372
Geophysics 0373
Hydrology 0388
Mineralogy 0411
Paleobotany 0345
Paleoecology 0426
Paleontology 0418
Paleozoology 0985
Palynology 0427
Physical Geography 0368
Physical Oceanography 0415

HEALTH AND ENVIRONMENTAL SCIENCES
Environmental Sciences 0768
Health Sciences
- General 0566
- Audiology 0300
- Chemotherapy 0992
- Dentistry 0567
- Education 0350
- Hospital Management 0769
- Human Development 0758
- Immunology 0982
- Medicine and Surgery 0564
- Mental Health 0347
- Nursing 0569
- Nutrition 0570
- Obstetrics and Gynecology 0380
- Occupational Health and Therapy 0354
- Ophthalmology 0381
- Pathology 0571
- Pharmacology 0419
- Pharmacy 0572
- Physical Therapy 0382
- Public Health 0573
- Radiology 0574
- Recreation 0575
- Speech Pathology 0460
- Toxicology 0383

Home Economics 0386

PHYSICAL SCIENCES
Pure Sciences

Chemistry
- General 0485
- Agricultural 0749
- Analytical 0486
- Biochemistry 0487
- Inorganic 0488
- Nuclear 0738
- Organic 0490
- Pharmaceutical 0491
- Physical 0494
- Polymer 0495
- Radiation 0754

Mathematics 0405
Physics
- General 0605
- Acoustics 0986
- Astronomy and Astrophysics 0606
- Atmospheric Science 0608
- Atomic 0748
- Electronics and Electricity 0607
- Elementary Particles and High Energy 0798
- Fluid and Plasma 0759
- Molecular 0609
- Nuclear 0610
- Optics 0752
- Radiation 0756
- Solid State 0611

Statistics 0463

Applied Sciences

Applied Mechanics 0346
Computer Science 0984

Engineering
- General 0537
- Aerospace 0538
- Agricultural 0539
- Automotive 0540
- Biomedical 0541
- Chemical 0542
- Civil 0543
- Electronics and Electrical 0544
- Heat and Thermodynamics 0348
- Hydraulic 0545
- Industrial 0546
- Marine 0547
- Materials Science 0794
- Mechanical 0548
- Metallurgy 0743
- Mining 0551
- Nuclear 0552
- Packaging 0549
- Petroleum 0765
- Sanitary and Municipal 0554
- System Science 0790

Geotechnology 0428
Operations Research 0796
Plastics Technology 0795
Textile Technology 0994

PSYCHOLOGY
General 0621
Behavioral 0384
Clinical 0622
Developmental 0620
Experimental 0623
Industrial 0624
Personality 0625
Physiological 0989
Psychobiology 0349
Psychometrics 0632
Social 0451

ABSTRACT

This study involves improving knowledge of the climatic and environmental changes during the past 3 million years in the region of the Chinese Loess Plateau and the forcing mechanisms of global glacial-interglacial climate oscillations during the Quaternary. Loess sections consisting of loess-paleosol sequence, fluviolacustrine sequence, and the red clay formation were selected for detailed study. Laboratory methods used included analyses of paleomagnetism, ^{14}C dating, bulk sample mineralogy, grain-size distribution, clay mineralogy, major and trace element geochemistry, iron geochemistry, stable carbon-isotopes, carbonate content, organic matter content, pollen and pedo-micromorphology by photomicroscopy and SEM.

The fluviolacustrine sequence in the Shijiawan section was deposited between 3.05 and 1.9 Ma B.P. with a dominant alluvial facies. The red clay formation was developed under a constant warm-dry climate 2.7 Ma ago. The paleovegetation in the southern Guanzhong basin was of typical sage steppe type during the period of 3.0-2.7 Ma B.P. Evidence suggests that the red clay was derived from the northwest deserts by aeolian transport, indicating dust deposition started long before the major loess accumulation. The dustfall rate in the late Pliocene is much lower than in the Quaternary, implying that the Siberian cold high was abruptly intensified 2.6 Ma B.P. Pollen evidence, pedological studies and dustfall rate indicate that a profound climatic change and regional climate regime replacement were coincident with the advent of the first Quaternary glaciation. As demonstrated, the Quaternary climate in the loess plateau responded strongly to the

world glacial-interglacial signals which are related to the sea level-coastal position-precipitation linkage.

As has been suggested by many workers, the last and rapid deglaciation must be linked to major changes in ocean circulation. It is difficult to explain this change by changes in solar insolation alone. In fact, the albedo changes might have worked to maintain the ice age. A first attempt has been made to examine if ice loading could have contributed to asthenosphere flow and intensified ocean ridge volcanism which in turn could perturb ocean circulation patterns and increase atmospheric CO_2. The first modeling results suggest that the process could be of quantitative significance.

ACKNOWLEDGEMENTS

First, I am grateful to my supervisor, Dr. Williams S. Fyfe for his instructions, encouragement and financial support throughout my study. It is his generosity and humanity that fostered my long journey of thinking on the frustrating questions faced in my study. Under extremely difficult financial situations, he still took full responsibility to support me. He shared my feelings and gave me a thorough understanding whenever I met any kinds of difficulty and provided inspiration for further endeavour. His broad knowledge enlightened me when I was in darkness. His constructive comments and patient proof reading led to completion of the thesis. Behind each line of the thesis lie his untiring work and precious time. What he did for me is far beyond my words of appreciation. For this, I am deeply indebted to him for the rest of life.

I would like to thank Dr. H.C. Palmer for help with paleomagnetic measurements, Dr. Fred Longstaffe for carbon isotope analysis, and Dr. Stephen Hicock for help in experiments of grain-size and carbonate concentration and for the free access to his lab.

Special thanks are conveyed to Dr. Weiming Liu for his great help in computer modelling. He spent numerous hours on the model establishment and generously allowed the use of his computer program. Without this help, the modelling could not have been realized for the thesis.

I would like to thank Dr. Chales Wu for XRF and iron geochemistry analyses, Y. Cheng for XRD analysis, P. Middlestead for carbon isotope analysis, Prof. Terasmae and Fuhua Yan for pollen analysis, W. Logan for organic matter analysis, John Forth and

G. Wood for preparation of thin sections of paleosols.

I would also like to thank Dr. Mike Powell and Ms. M. McMahon who provided much help whenever needed.

I especially thank Kim Law who made great efforts on proof reading of the entire manuscript, and Fagan Roxane who read through some chapters.

My Chinese colleagues, Dr. Jiaqi Liu, Jiakuan Huang, Zhonglin Qi and Zhongli Ding are gratefully acknowledged for facilitating my study and field work. Dr. D.W. Mo provided the literature I needed for checking plant nomenclature and some plant samples.

I wish to express my deep appreciation to my former supervisor, Dr. Liu Tungsheng for his encouragement.

I am grateful to Dr. Michael Anketell of Manchester who helped me find a great supervisor, Prof. Williams S. Fyfe.

This study was supported by NSERC grants to W.S. Fyfe and a China NSF grant to the author.

Lastly, I would appreciate my family for creating a good environment for the thesis writting.

献给我的母亲

Dedicated to my mother who passed away during this study

TABLE OF CONTENTS

LIST OF PLATES

LIST OF TABLES

LIST OF FIGURES

CHAPTER 1

INTRODUCTION

1.1. Purpose of this Study

This study is designed to document the paleoclimatic changes over the past 3 million years of the Chinese Loess Plateau and in particular, to address the following issues:

1. Genesis of the Red Clay formation and the related environment;
2. The amplitudes of climatic variations in the central Loess Plateau during the Quaternary period;
3. The temporal trend of the climate in the region since late Pliocene;
4. The linkage of climate change between North China and global systems;
5. The forcing mechanism of the global glacial climate oscillations during the Pleistocene.

1.2. Methods

A wide-scale field investigation was conducted throughout the loess plateau, and several sections were selected for detailed study (see Figures 1-1 and 1-3). The Shijiawan section, composed of a loess-paleosol sequence and an underlying fluviolacustrine sedimentary sequence, was targeted to document the transitional processes of climatic shift from the late Pliocene to the early Pleistocene, to reconstruct the climatic conditions in the late Pliocene, and to estimate the climate conditions implied by the best developed paleosol layer "S5" in the Chinese loess sequences. The Chang'an section was chosen for the paleosol S5 study. The Yanyu primary section and Luochuan section (Fig. 1-1), consisting of a red clay formation and a loess-paleosol sequence, were studied to extract climatic information contained in the red clay formations. The Ziwu and another Yanyu site were chosen for stable carbon-isotopic studies of modern vegetation and related soils to establish the criterion for interpretation of isotopic signatures in paleosols.

Field observations and systematic sampling were followed by a variety of laboratory analyses, and paleomagnetism and radio-carbon dating were used for chronostratigraphy. To obtain environmental and climatic information, analyses including stable carbon-isotopes of organic matter, grain-size distribution, clastic mineralogy and clay mineralogy by XRD, XRF, and REEs, titrations for carbonates, iron-valence ratios and organic matter content, micromorphology of soil by photomicroscopy and scanning electron microscopy, and pollen analysis were conducted. To test the idea that the mid-ocean ridge processes could have played a leading role in pacing the Quaternary glacial cycles, a computer-based finite-element elastic model of the Earth was established to investigate the climatic influence of pulsative magmatism at mid-ocean ridges induced by the Earth's surface loading with ice sheets during glacial periods. Descriptions of the techniques employed will be given in related chapters where necessary.

1.3. Organization

Chapter 1 describes the physical character of the study area and summarizes previous work done on both the regional topics and general issues, climate forcing of the Quaternary glacial-interglacial oscillations. Chapter 2 includes descriptions of the selected working sections and determinations of their ages. The stable carbon-isotope signatures of modern vegetation and organic matter in related soils are discussed in Chapter 3, providing the basis for paleoclimatic interpretation. In Chapter 4, the climate conditions of the best developed paleosol in the Chinese loess sequences is evaluated. Chapter 5 focuses on the climate reconstructions of the late Pliocene from the fluvio-lacustrine sequence and the red clay formations. The origin of the red clay is also discussed. Temporal variations of climate in the Chinese Loess Plateau through the past 3 million years and a linkage between the regional and global climate change on a glacial cycle scale is proposed in Chapter 6. In Chapter 7, the possible influence of mid-ocean ridge processes on glacial cyclicity is investigated with a finite-element elastic spheric model of the Earth. Chapter 8 is comprised of conclusions and future work.

1.4. General Physiography and Geologic Setting

The Chinese Loess Plateau is located in central to western China, with an area of about 440,000 km^2 (Liu et al., 1985). The Qilian Mountains and the Qinling Mountains form the southern boundaries of the loess plateau, while the Taihang Mountains (a natural obstacle for northwesterly winds), form the east border of the plateau. In the northwestern regions the loess plateau links up with the deserts of northwestern China. The main body of the plateau is distributed within the area between 35-40°N and 100-115°E, comprising a loess belt extending NWW-SEE (Figure 1-1). Presently, the climate in this region varies from semi-humid in the southeast to semi-arid in the northwest, a climatic transition regime between humid and arid zones. The mean annual precipitation in the southernmost region is 600 to 700 mm and decreases to about 250 mm in the

Figure 1-1. Distribution of the Chinese Loess Plateau. Locations of the important sections mentioned in the thesis are indicated. The outlined square denotes the major study area and is shown in Figure 1-3. (from Liu et al., 1989).

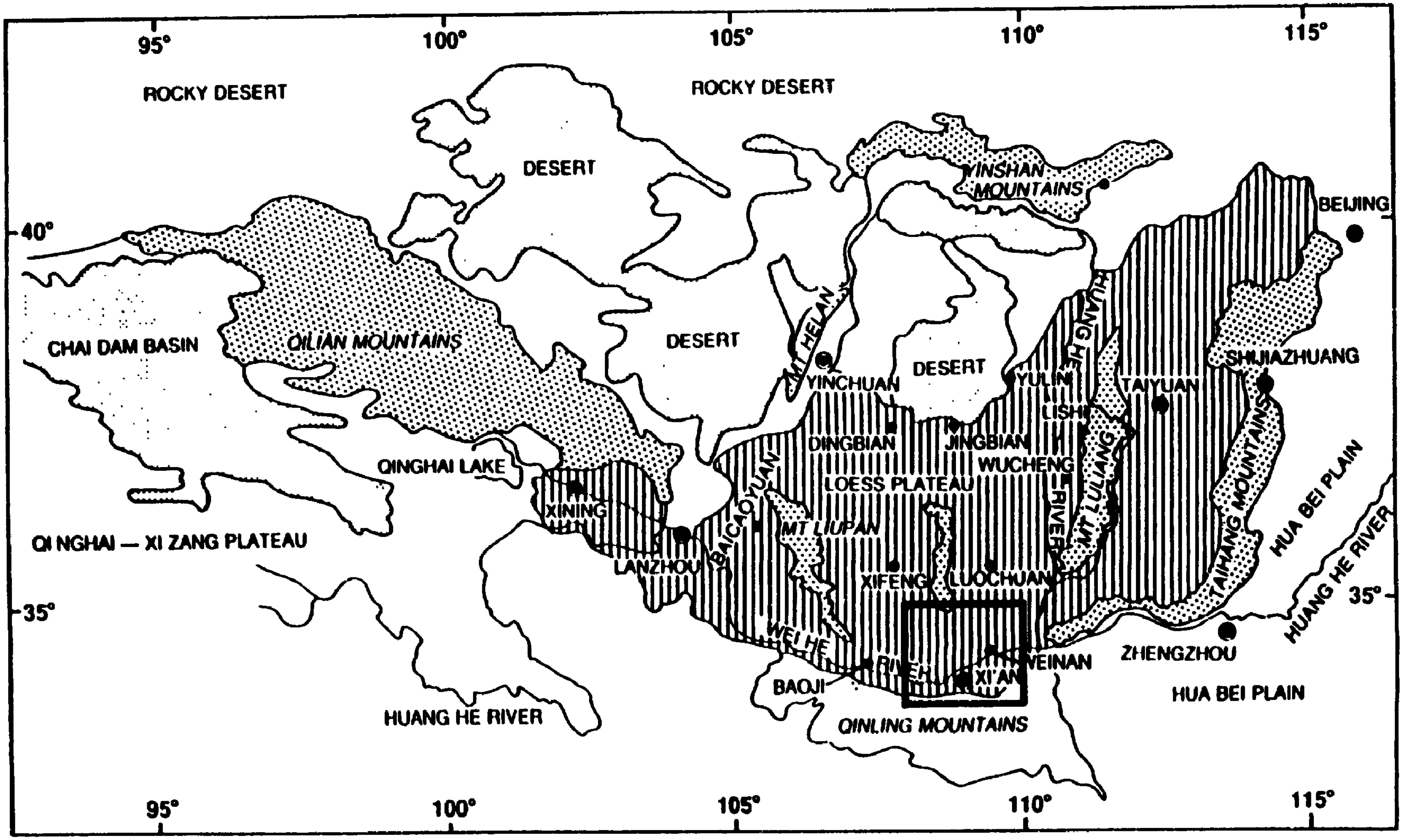
95°
100°
105°
110°
115°
40°
35°
ROCKY DESERT
ROCKY DESERT
DESERT
DESERT
DESERT
YINSHAN MOUNTAINS
BEIJING
CHAI DAM BASIN
QILIAN MOUNTAINS
MT HELAN
YINCHUAN
YULIN
HUANG HE
TAIYUAN
SHIJIAZHUANG
LISHI
DINGBIAN
JINGBIAN
WUCHENG
MT LULIANG
TAIHANG MOUNTAINS
HUA BEI PLAIN
QINGHAI LAKE
LOESS PLATEAU
RIVER
XINING
BAICAOYUAN
MT LIUPAN
QI NGHAI — XI ZANG PLATEAU
LANZHOU
XIFENG
LUOCHUAN
HUANG HE RIVER
WEI HE
RIVER
WEINAN
ZHENGZHOU
BAOJI
XI'AN
QINLING MOUNTAINS
HUA BEI PLAIN
HUANG HE RIVER

Figure 1-2. Distribution of the mean annual rainfall (mm) in the Loess Plateau. (from Liu et al., 1989).

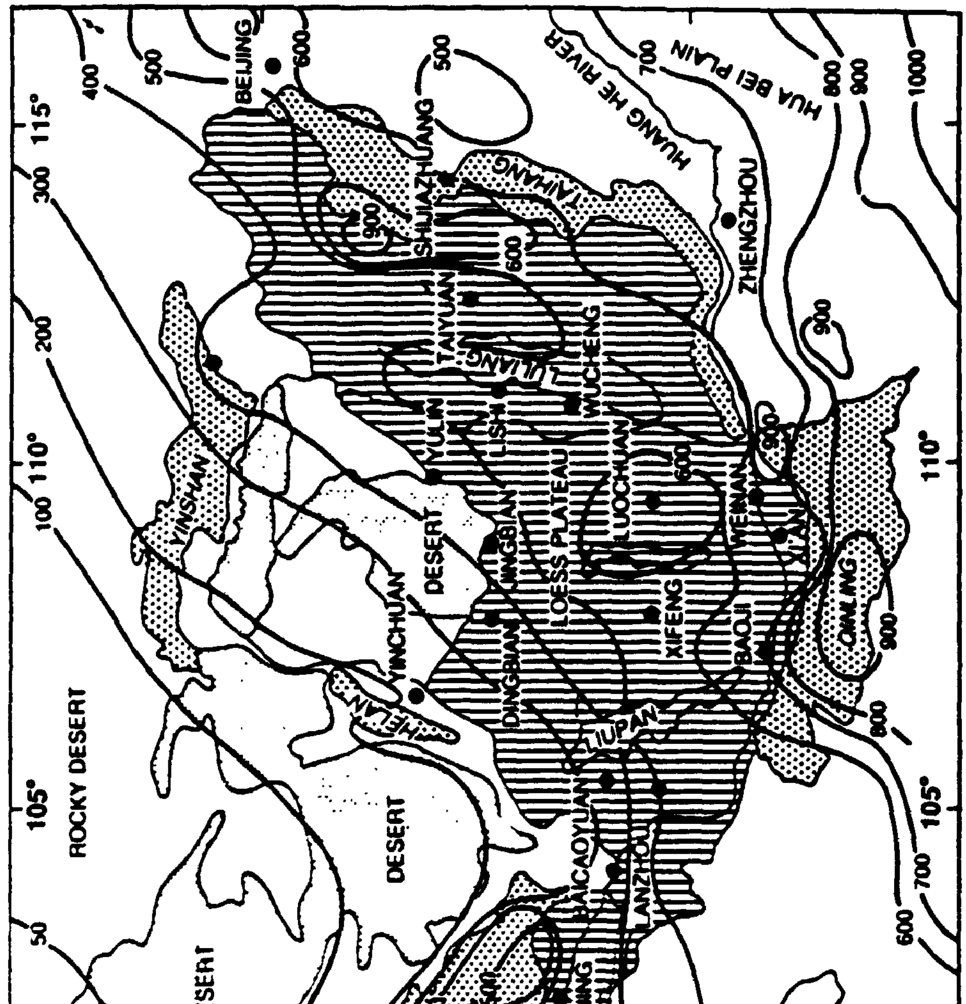
ROCKY DESERT
ROCKY DESERT
CHAI DAM BASIN
DESERT
DESERT
DESERT
YINCHUAN
HELAN
YINSHAN
YULIN
TAIYUAN
SHIJIAZHUANG
BEIJING
TAIHANG
LULIANG
LISHI
WUCHENG
LUOCHUAN
LOESS PLATEAU
DINGBIAN
JINGBIAN
XIFENG
BAOJI
WEINAN
QINLING
LIUPAN
LANZHOU
XINING
QILIAN
QINGHAI — XI ZANG PLATEAU
HUANG HE RIVER
HUA BEI PLAIN
ZHENGZHOU
40°
35°
95°
100°
105°
110°
115°

Figure 1-3. Map of the major study area showing locations of the Qinling Mountains and the Guanzhong Basin. The ticked lines show the normal faults defining the margins of the Weihe Graben (Guanzhong Basin). Symbol I, distribution areas of the red clay formation; symbol II, distribution areas of late Pliocene fluviolacustrine sequences. (produced from satellite images of 1975 and China Map Press, 1984).

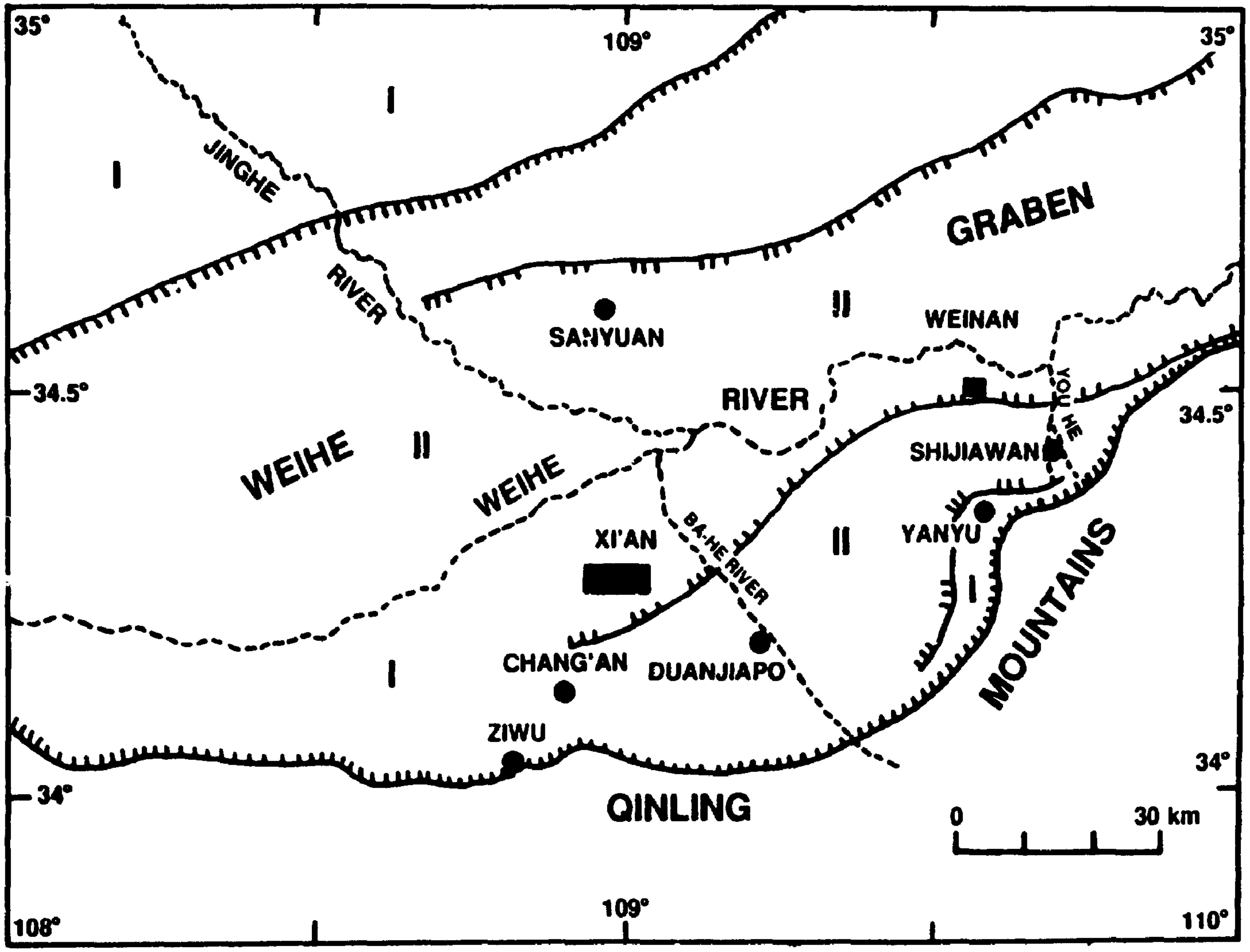
35°
109°
35°
I
I
JINGHE
GRABEN
RIVER
II
WEINAN
SANYUAN
34.5°
RIVER
YOU HE
34.5°
WEIHE
II
SHIJIAWAN
WEIHE
YANYU
XI'AN
BA-HE RIVER
II
I
MOUNTAINS
I
CHANG'AN
DUANJIAPO
ZIWU
34°
34°
QINLING
0
30 km
109°
108°
110°

northwestern regions near the deserts (see Figure 1-2). The change in annual temperature is similar to the change in precipitation, decreasing northwestwards across the loess plateau.

The major study area is in the southern part of the central loess plateau, the Weihe basin (Guanzhong Basin). The Weihe river lies in a median line of the basin from west to east (Figure 1-3) and links to the Huanghe (Yellow) river as a first grade major tributary (see Figure 1-1). The basin is characterized by wide and smooth terraces mainly composed of reworked loess. On the north side of the river, mega-terraces constitute the major body of the Guanzhong Plain, and each terrace is about 10 km in width. On the south side, the basin is segmented by tributaries of the Weihe river and divided into platform belts (see Plate 1-1).

The Weihe graben was formed in the early Cenozoic (Chinese Academy of Geology, 1974), but a faulting event along the Ba-he river can be speculated to have occurred about 5 million years ago (cf. Zheng et al., 1991). This is manifested by the difference in lithostratigraphy between both sides of the river. On the western side, the bedrock is overlain by the red clay formation and subsequently covered with a loess sequence. On the eastern side, the red clay is absent. Instead, a fluviolacustrine sequence was developed until early Pleistocene as indicated by the Shijiawan section. The graben lake disappeared for the most part during the period of 1.5-1.8 million years B.P., and then loess was deposited on the fluviolacustrine sequence. Presently, the entire basin is covered with thick loess and interbedded paleosols. The Qinling mountains, the southern margin of the basin, also delineates the southernmost limit for loess deposition (Figure 1-3). The spatial distribution of the Cenozoic strata is illustrated in Figures 1-3, 1-4 and

Figure 1-4. Sketch of a cross section from Yanyu to Shijiawan. See locations in Figure 1-3.

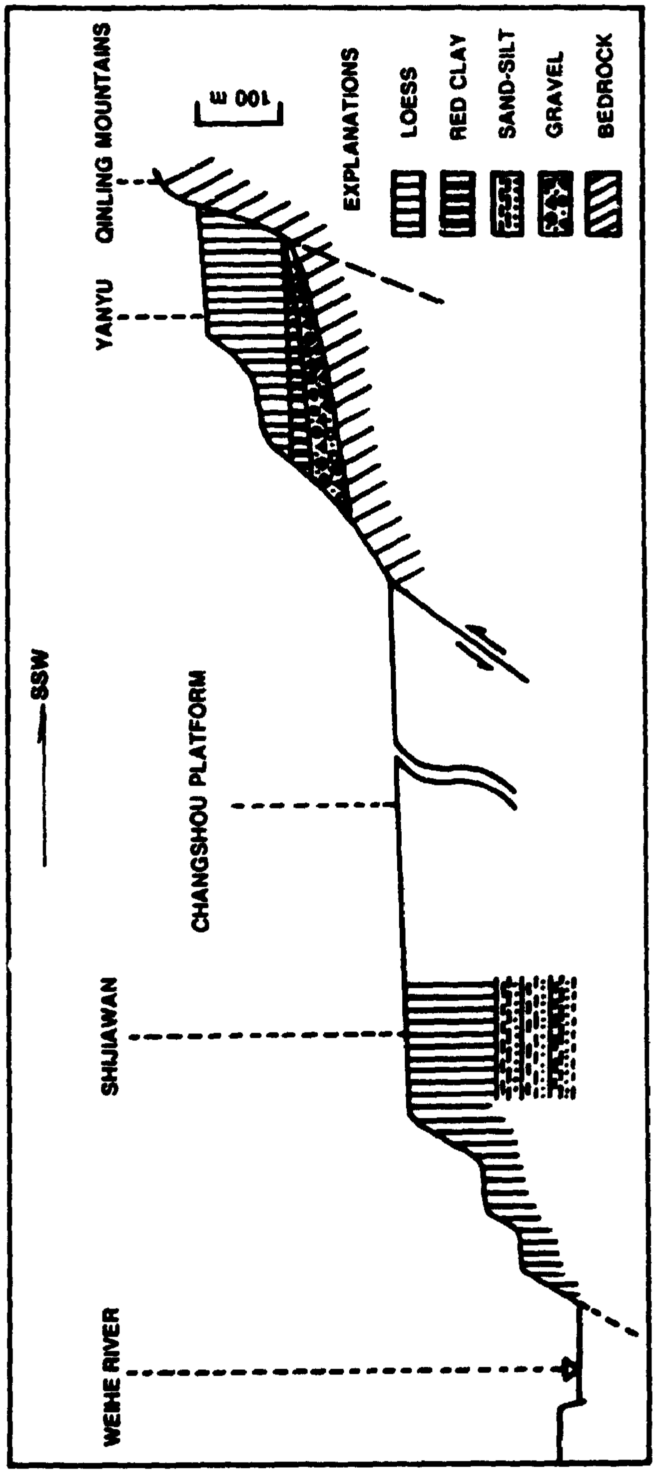
WEIHE RIVER
SHIJIAWAN
CHANGSHOU PLATFORM
YANYU
QINLING MOUNTAINS
SSW
100 m
EXPLANATIONS
LOESS
RED CLAY
SAND-SILT
GRAVEL
BEDROCK

1-5. Due to differential uplift within the graben basin, loess platforms developed on the south side of the Weihe river. These provided abundant natural outcrops for detailed geological studies.

1.5. Previous Studies of the Cenozoic Paleoclimate in the Chinese Loess Plateau

1.5.1. Loess Deposits

Through the work of many generations, the investigation of the Chinese loess has achieved significant progress. Over one hundred years ago, the German scholar F.V. Richthofen (1877, 1882) first proposed an aeolian origin of the Chinese loess (subaerial deposit). In the 1930's, Obruchev (cf. Liu, 1965) developed the idea of wind-blown deposition of the Chinese loess after his observations in Europe, central Asia and China. From the 1930's to 1950's, the Cenozoic strata in the Chinese Loess Plateau re studied and subdivided based on field observations and vertebrate fossils (eg., Teilhard de Chardin and Young, 1930, 1931; Young, 1934; Masukenkichi and Todatatsu, 1944). Systematic studies were initiated in the late 1950's by T.S. Liu and his research team . The major accomplishments of their first decade of study were compiled in three monographs, *The Loess along the Middle Reaches of the Huanghe River* (Liu, 1964), *The Loess Deposits of China* (Liu, 1965), and *The Composition and Texture of Loess* (Liu, 1966). Wide-scale field observations and laboratory analyses indicated that loess of all ages is very similar in mineralogical composition and grain-size. Over a wide spatial range, systematic variations in thickness and grain-size composition have been found, both decreasing from northwest to southeast. These characteristics lead to a convincing

Figure 1-5. Sketch of a cross section from Duanjiapo to Shijiawan. For explanations of the symbols see Figure 1-4 and for locations see Figure 1-3.

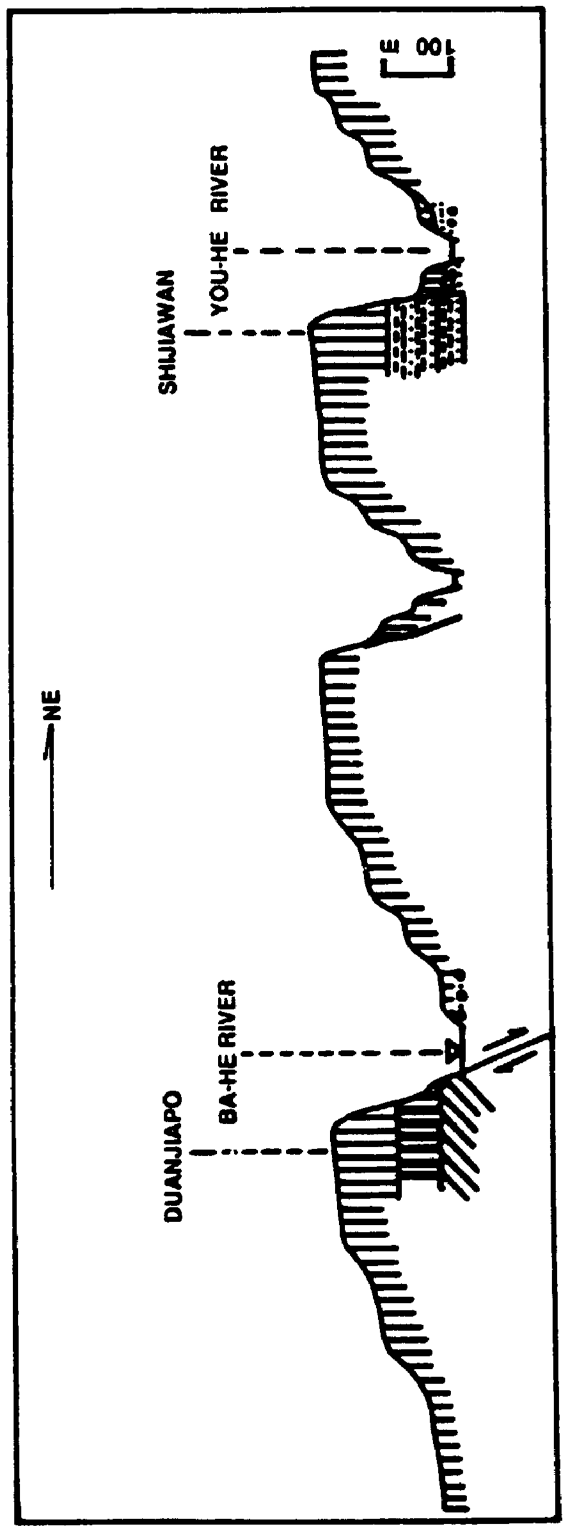
SHIJIAWAN
YOU-HE RIVER
100 m
NE
DUANJIAPO
BA-HE RIVER

Plate 1-1. Photographs showing the south side of the Weihe (Guanzhong) Basin. The upper-plate was taken at Yanyu village near the northern margin of the Qinling Mountains (on the upper-right corner). The Yanyu section is shown at lower-right corner. Multiple loess platforms of the southern Guanzhong Basin constitute the southernmost area of the Chinese Loess Plateau. The lower plate is a distant view of the Changshou Yuan (platform). The Shijiawan section is located in a short valley cutting the platform.

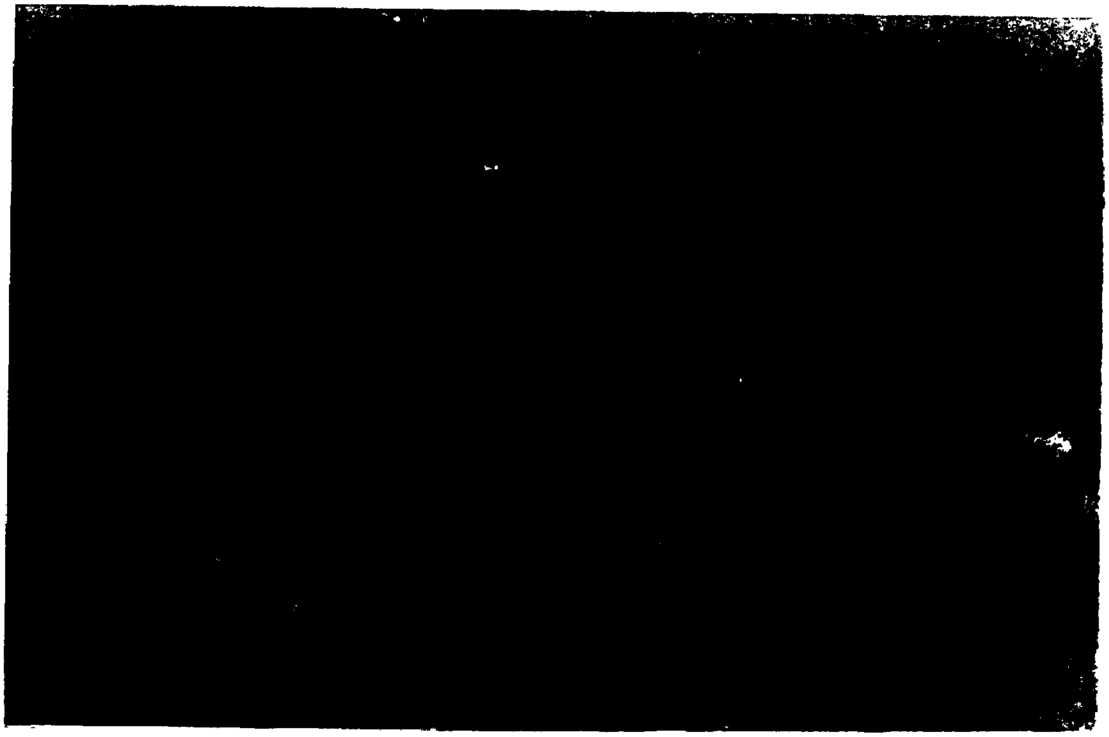

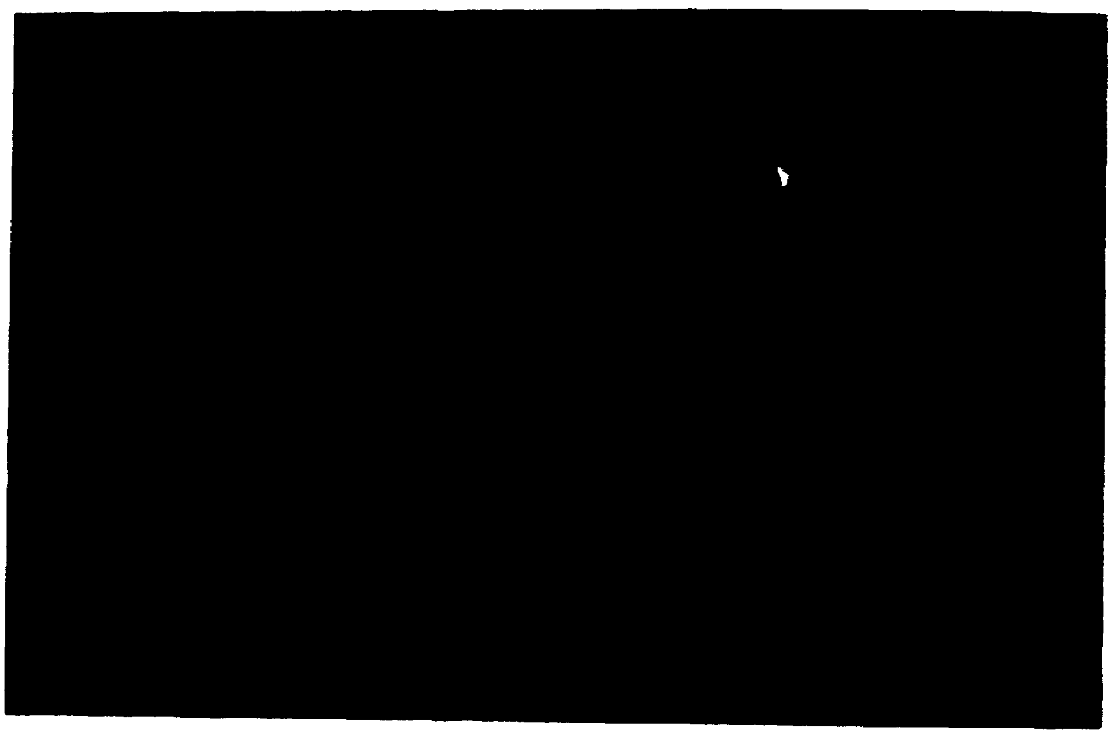

conclusion that loess in the Chinese Loess Plateau is an aeolian deposit originating from the deserts.

Since the 1970's, Chinese loess research has concentrated on individual sections, and great interest has been given to temporal changes in various profiles. During this period, three major topics have been stressed: 1) chronostratigraphy of the loess-paleosol sequences; 2) environmental and climatic implications of the loess-paleosol sequences; and 3) comparison of the climatic record in the loess-paleosol sequences with global climate change documented from deep sea sediments. The books *Loess and the Environment* (Liu, 1985) and *The Recent Research of Loess in China* (Sasajima and Wang, 1984) represent the major achievements obtained in 1970s. After an international workshop on loess research in Xi'an in 1985, research on the Chinese loess-paleosol sequences was rejuvenated and characterized by global cooperation (Liu, 1987, 1991). The key sections with detailed studies are at Luochuan (Heimugou), Xifeng, Xi'an (Liujiapo) and Baoji (locations shown in Figure 1.1). The main conclusions were:

1. The accumulation of the Chinese loess sequence started at about 2.4 Ma B.P. in the Luochuan section (Heller and Liu, 1982) and at approximately 2.5 Ma B.P. in other sections (Sun et al., 1985, Ding et al., 1990);

2. The climatic fluctuations recorded in the loess-paleosol sequences are indicated by mineralogy, grain-size and chemical compositions (Liu and Yuan, 1987) and also by pedogenic studies. The loess layers and paleosols represent cold-dry and warm-wet climate episodes respectively (Liu, 1985; Ding, 1988; Guo, et al., 1991). The amplitude of the climatic fluctuations are manifested by variations of magnetic susceptibility along loess profiles (Heller and Liu, 1986; Liu et al., 1988, 1991; Wang et al., 1990; Maher

and Thompson, 1991, 1992).

3. The climatic oscillations recorded in the loess-paleosol sequences are well correlated with the variations of $\delta^{18}O$ values in deep sea sediments (Liu and Yuan, 1987; Liu, 1988, 1991; Heller et al., 1987; Kukla, 1987; Ding et al., 1991; An et al., 1991; Maher and Thompson, 1992), suggesting that the Chinese loess-paleosol sequences completely reflect the climate changes throughout the past 2.5 million years and indicate a global significance of the regional climate oscillations.

1.5.2. Red Clay Formations and Fluviolacustrine Sequences

In the early part of the century, the red clay formations in North China were subdivided according to field observations and vertebrate fossils (Anderson, 1923; Teilhard de Chardin and Young, 1930, 1931; Young, 1934a). The pink-red clay was named the Jingle Formation and ascribed as late Pliocene in age. Meanwhile, another red clay formation was identified as the Baode formation, which differed from the Jingle Formation by its dark-red colour, and was considered to be early Pliocene in age.

These red clay formations were interpreted to have been formed in a rather warm and humid climate and were thought to be fluviolacustrine in origin or formed by oxidation of lacustrine sediments. Similar conclusions were obtained by later studies (eg., Pei et al., 1963; Li et al., 1984; Mo and Derbyshire, 1991; Chen, 1994), though the origin remains controversial (Liu et al., 1988; Mo and Derbyshire, 1991). Recent magnetostratigraphic studies indicate that the red clay deposition ended with the advent of the loess deposition (Zheng et al., 1991; Tedford et al., 1991; Chen, 1994).

The widely exposed fluviolacustrine sequences in the Guanzhong Basin were of great interest, especially paleontologically, in the middle of the century (eg., Young, 1934b; Pei and Huang, 1959; Cao et al., 1966). The Sanmen Series (sequence) in the literature is, in actuality, the sedimentary sequence in the lower part of the Shijiawan section. Abundant vertebrate fossils have been exhumed from the silt layers throughout the sequences and a standard fauna named the You-he Fauna was established for the Cenozoic biostratigraphic correlations in North China (Xue, 1981). Chronostratigraphic work on this sequence started only after the paleomagnetic dating method became available. At this time, there was no constraint on the lower boundary of the sequence. The oldest stratum reached is about 3.2 million years at Sanmen Gorge (He et al., 1984). The age of the upper boundaries was reported to vary with locations, indicating a diachronous disappearance of the lake. The retreat of the graben lake began from west to east and from the south margin to the center (Sun, 1987).

In summary, although these have been some detailed insights into the regional climate and environmental changes through the past 3 million years, there are still some major questions unanswered, namely:

1. The origin of the red clay formations and their climatic implications.

2. The transitional change of the climate from late Pliocene to early Pleistocene.

3. The amplitude of the climatic oscillations in the Chinese Loess Plateau-- a more convincing estimation of the climate extremes, the worst and the best states.

4. The relationship of secular climate oscillations between the regional loess deposits and deep sea sediment reco...

1.6. An Overview on the Forcing Mechanisms of the Quaternary Glacial Cycles

1.6.1. The Dominant Theories of the Ice Ages

The driving mechanisms of Quaternary glaciation have attracted great interest in a broad scientific community. Over 120 years ago, astronomical forcing of glaciation was first postulated by French astronomical scientists (cf. Imbrie and Imbrie, 1979). Following this idea, Croll (1875) calculated variations of insolation caused by orbital parameters, eccentricity, obliquity and precession, and speculated that the glaciations should have occurred repeatedly. But modern astronomical theory of the ice ages has been attributed to Milankovitch because of the accurate physical description for the related parameters he employed and the precise mathematical approach (Milankovitch, 1941). A real renaissance of the astronomical theory of glaciation, however, began only after the first stable oxygen-isotope data from deep sea sediments were published (Emiliani, 1955) and the relationship between the variations in marine $\delta^{18}O$ and the continental ice volume were confirmed by Shackleton (1967) and Shackleton and Opdyke (1973). The modern Milankovitch theory was essentially established by the work of Hays et al. (1976), Berger (1976), Imbrie and Imbrie (1979, 1980), CLIMAP Project Members (1981), and Berger et al. (1984). Later research concentrated on the linkage between the orbital theory and glacial cycles by tuning the periodic signals of insolation dominated by 41 and 23/19 kyr at high north latitudes to fit the geological observations of the 100 kyr cycle, and on the transmission of the regional signal of the northern hemisphere into global significance in the models (Weertman, 1976; Oerlemans, 1980; Birchfield et al., 1981; Birchfield, 1985; Denton et al., 1986; Peltier, 1987). More recently, an ocean-circulation mode switch mechanism was proposed targeting the rapidity and global synchroneity of the last deglaciation (Broecker and Denton, 1989) with a rapid increase in geological findings (e.g., Bond et al., 1992; Lehman and Keigwin, 1992; Broecker, 1994). These theories are reviewed below and shown, with geologic evidence, that they have failed to explain many fundamental problems.

Milankovitch (1941) emphasized the ice-climate link by postulating that summer insolation anomalies near 65°N controlled ice-sheet oscillations. However, a severe difficulty with a simple linear relation emerged from the power spectra of orbital variations and the marine oxygen-isotope record (Hays et al., 1976). The orbital variations show the strongest power at the 41,000-year tilt and 23,000/19,000-year precession periods, and comparatively little power at the eccentricity periods near 94,000 and 125,000 years at 65°N latitude (Hays et al., 1976; Imbrie et al., 1984; Peltier, 1987). On the other hand, the marine oxygen-isotope records consistently show dominant power at 100,000 years and less power at the 41,000-year and 23,000/19,000-year periods (Imbrie, 1985). The 100,000-year dominant cycle in late Quaternary glaciations is characterized by a long period of ice-sheet growth with some fluctuations and sudden deglaciations spaced at about 100,000 years apart marking glaciation terminations (Broecker and van Donk, 1970). Hence, a puzzle facing the theory is that the dominant and asymmetric 100,000-year rhythm revealed by fluctuations of the late Quaternary ice sheets is not predicted by the Milankovitch hypothesis.

Time-dependent ice-sheet models can test whether this enigma is resolved by nonlinear ice-sheet response to summer insolation forcing at about 65°N latitude (Weertman, 1976; Pollard et al., 1980; Oerlemans, 1980; Birchfield et al., 1981; Pollard, 1982, 1983; Peltier and Hyde, 1984; Hyde and Peltier, 1985; Peltier, 1987). These ice-sheet models have many similarities. They consider a north-south profile along a typical flowline through a Northern Hemisphere ice sheet and neglect east-west flow. The northern ice-sheet margin is fixed at the edge of a polar sea. The southern margin and ice thickness are allowed to vary. Changes in accumulation and ablation that determine mass balance on the ice-sheet surface are strongly elevation dependent. The ice-sheet model is coupled with a geophysical model of glacial isostatic adjustments that strongly influence surface ice elevations and, in turn, ice-sheet extent, because accumulation and ablation rates are elevation dependent. Model input is summer insolation anomalies that are superimposed on the ice sheet by north-south migration of the climate point, hence changing mass balance. Model output is expressed in terms of ice-volume changes that lag insolation forcing. Experiment (model) success is measured by the degree to which ice-volume output simulates marine oxygen-isotope curves, taken to represent the actual ice-sheet fluctuations during glacial cycles.

In early experiments, the model ice sheet responded linearly to insolation forcing caused almost entirely by precession (23,000/19,000 year) and obliquity (41,000 year); response at the 100,000-year frequency was negligible (Weertman, 1976; Pollard et al., 1980). The results of subsequent experiments more closely simulated the marine oxygen-isotope record, largely because a time lag for isostatic deformation caused amplification of some ice-sheet retreat phases (Oerlemans, 1980; Birchfield et al., 1981). But even these modeling experiments showed differing results that depend on the time scale of isostatic adjustment (Peltier, 1982). Some of the existing weaknesses (not enough 100,000-year spectral power and incomplete ice-sheet recession during interglaciations) were rectified by adding a calving term that accentuated rapid retreat each 100,000 years (Pollard, 1982, 1983, 1984; Birchfield, 1985).

The most recent version of the ice-sheet model emphasizes the role of glacial isostasy in producing glacial terminations (Peltier and Hyde, 1984; Hyde and Peltier, 1985; Peltier, 1987). With a new description of glacial isostatic adjustment that is particularly sensitive to the choice of mantle viscosity, this version gives an adequate replication of the marine oxygen-isotope record (Peltier and Hyde, 1984; Peltier, 1987). The actual mechanism that produces terminations depends critically on accentuated isostatic sinking beneath maximum ice-sheet loads. Once this situation is achieved, a positive summer insolation anomaly forces the southern margin of the ice sheet to retreat into the low-elevation depression that is maintained by delayed isostatic response. This causes a sharply negative mass balance because of the strong dependence of ablation on elevation. The resulting steeper ice slope caused by enhanced ablation induces southward ice flow greatly. Hence, northern ice is transferred into a low southern depression, where it melts rapidly. By this mechanism, the ice-sheet model produces a sawtoothed 100,000-year cycle of glaciation from higher-frequency Milankovitch summer forcing at 65°N latitude.

The ice-sheet model addresses only terrestrial ice sheets, despite the probable existence of marine ice-sheet components at the last glacial maximum. To overcome this shortcoming, Denton and Hughes (1983) and Denton et al. (1986) suggested a conceptual model of global ice sheets that incorporates marine mechanisms along with terrestrial dynamics. Sea-level changes initiated by the variations of terrestrial ice sheets were a critical interlocking mechanism among marine ice-sheet components in both polar hemispheres. Hence, these marine components fluctuated in phase with Northern Hemisphere terrestrial components. An important result of this addition to the terrestrial model is that the Antarctic Ice Sheet fluctuates in accord with Northern Hemisphere ice sheets through a sea-level linkage.

While the last glaciation in the southern hemisphere was as severe as in the northern hemisphere, even for mountain glaciers in the tropical regions, and the deglaciations are globally synchronous (Porter, 1981a,b, 1988; Suggate, 1978; Skinner and Porter, 1987; Mercer, 1984; Nelson et al., 1985), which have been confirmed by studies of Antarctic and Greenland ice cores (Royer et al., 1983; Jouzel et al., 1987, 1989; Hammer et al., 1985; Lorius et al., 1990). Therefore, changes in the southern hemisphere paleo-atmosphere have to be incorporated into any explanation of the 100 kyr cycle. In the case of the ice-sheet-climate link, this requires that the Northern Hemisphere ice sheets drive global climate through a thermal impact on the atmosphere. In other words, for the model to correctly explain ice-age climate, Northern Hemisphere ice sheets must have transmitted regional Milankovitch summer half-year insolation variations near 65°N latitude into a global climate signal. Herein lie the difficulties of the ice-climate link. A general circulation model of the atmosphere coupled with a static mixed-layer ocean (Manabe and Broccoli, 1985) demonstrated that the climatic influence of large North American and Eurasian ice sheets was restricted to the Northern Hemisphere, and that expansion of the Antarctic Ice Sheet was not large enough to significantly influence the Southern Hemisphere's climate. The observation that the beginning of the last glacial termination is registered nearly simultaneously in both hemispheres including polar ice cores, argues against the ice-climate link, for it does not allow the time lag necessary for

Northern Hemisphere ice-sheet shrinkage to cause the rapid Southern Hemisphere warming recorded by the collapse of alpine glaciers. As well, the climate record denies that Milankovitch summer insolation anomalies directly caused ice recession of the last deglaciation because of nearly identical timing and severity of the onset of the last termination in both hemispheres where summer insolation anomalies are opposite. Furthermore, unlike North American ice sheets, Southern Hemisphere alpine glaciers collapsed under opposite insolation forcing with little or no role played by delayed isostatic sinking, but both collapses were simultaneous.

To overcome these difficulties, an ocean-circulation mode switch mechanism was postulated (Broecker and Denton, 1989). This concept is based on the studies of paleo-ocean nutrient distribution patterns traced from foraminiferal tests which had inhabited the ocean at various depths. It is revealed that the vertical distribution patterns during the last glacial period are quite different from today (Boyle and Keigwin, 1987; Duplessy et al., 1988). Therefore, this study reached the conclusion that deepwater circulation of the North Atlantic Ocean was probably shut down or greatly reduced during glacial periods. This is confirmed by the most recent studies (Bond et al., 1992, 1993; Lehman et al., 1994; Blanchon and Shaw, 1995), though a controversy on the intensity of the circulation has arisen (Venum et al., 1992; Lehman and Keigwin, 1992; Fichefet et al., 1994; Rahmstorf, 1994). The ocean-circulation-climate linkage emphasizes the importance of North Atlantic deep water circulation in maintaining the climate of the region and adjacent areas, and its critical role in the fluctuations of North American and European ice sheets. It is suggested that massive meltwater from North American ice sheets discharged into the ocean, diluted the salinity of the surface water and interrupted

Atlantic deep water production thus causing the Atlantic conveyor belt to shut down, which is exemplified by the Younger Dryas cold event. In this situation, the Atlantic deep water circulation led the regional climate to global significance through energy balance in the sea and influence on the atmosphere (Blanchon and Shaw, 1995).

1.6.2. Critical Problems

Although orbital parameters have largely been accepted as the primary forcing in the Quaternary glacial-interglacial climate oscillations, this theory is challenged by many critical problems. The ocean circulation mode switch model adequately explains global synchroneity and rapidity of deglaciation, which greatly enhanced our understanding of climate change. Some problems, however, still remain.

The secular variations of insolation induced by orbital parameters have no significant difference in amplitude and manner throughout the last 5 million years (Berger and Loutre, 1991), but world-wide glaciation occurred at about 2.5 Ma B.P. The dominant glacial cycle shifted from 40 ka before, to 100 ka after the Brunhes/Matuyama boundary (Ruddiman and Raymo, 1988; Kukla and An, 1989).

The glacial cycles did not follow the most powerful periodicity of the orbital forcing (Imbrie et al., 1984; Ruddiman, 1987) and were out of phase with the insolation variations (Broecker and Denton, 1989; Winograd et al., 1992; Crowley and Kim, 1994).

According to the ocean circulation mode switch model, the "Atlantic conveyor belt" probably closed down (or was greatly weakened) during glaciation periods. This would increase the temperature gradient polarwards and keep tropical regions warmer because the main pathway of surface heat transport in the ocean was locked. However, this is probably not the case as documented by observations of similar cooling from tropical to polar regions during glaciations (e.g., Porter, 1981, 1988).

Studies of polar ice cores have revealed that the concentration of atmospheric CO_2 always changed in phase with temperature (Jouzel et al., 1989; Chappellaz et al., 1990; Lorius et al., 1990) and no time lag has been distinguished at present (Ruddiman, 1987). The positive contribution of enhancement of atmospheric CO_2 is undoubtedly accepted, but how could it rise so rapidly during a postglacial period? The biological pump mechanism does not adequately explain this phenomenon (Boyle and Keigwin, 1985, 1986; Boyle, 1988a).

I am of the opinion that one aspect has been ignored in previous searching for the forcing mechanisms of Quaternary glacial cyclicity. The heat flux at mid-ocean ridges from the earth's interior might play an important role in secular climate change. During the last glacial maximum, the global sea level dropped about 130 to 170 m (Hughes et al., 1981; Chappell and Shackleton, 1986; Shackleton, 1988), and most of this water was loaded on the northern hemisphere. Estimated thickness of the Laurentide and Fennoscandian ice sheets are on the order of 3500-4000 m (CLIMAP, 1981: Denton and Hughes, 1981). The effect of the massive ice sheet load depressing the crust can still be detected by gravity anomalies (Peltier, 1987). The rebounding uplift in central ice sheets (e.g., the Hudson Bay) reaches about 300 m (cf. Peltier, 1985; Begin et al., 1993). This implies that the massive load shift of the ice sheets between ocean and continents has profound effects on the global stress field and deformations of the earth's crust, and in turn on the magma output at mid-ocean ridges. Unfortunately, this has not received any serious considerations (see Chapter 7).

1.7. Summary

Previous work both on regional climate change of the Chinese Loess Plateau and on forcing mechanisms of global glaciations during the late Cenozoic provides the basis for this study, but also leaves many unsolved problems for further research. My thesis is dedicated to this task.

CHAPTER 2

STRATIGRAPHY AND THE CHRONOLOGY

2.1. General Features of the Cenozoic strata

The Cenozoic strata in the Chinese Loess Plateau include the loess-paleosol sequence, the red clay formation, the fluviolacustrine sequence and a cemented sandstone. The cemented sandstone is an early Tertiary sediment and is not included in this study. The nature of the contact between these sequences can be classified as two major types. The first contact type is that of the red clay formation, which is deposited on the cemented sandstone, and is overlain by the loess-paleosol sequence. It is exposed in Yanyu, Duanjiapo and Baoji areas in the Guanzhong Basin (see Figure 1-1, 1-3, Area I, the distribution area of the Red Clay formation) as well as in the central part of the Loess Plateau with various bedrocks (eg., Luochuan, Xifeng, etc.). This type of sequence covers most of the loess plateau. The second type is characterized by the loess-paleosol sequence which is underlain by a fluviolacustrine sequence without exposure of cemented bedrocks. It can be found in the central Guanzhong Basin as observed in the Shijiawan section, and is also common in many graben basins in the Shanxi province.

On a large scale, the thickness of the loess-paleosol sequence and the number of interbedded paleosols differ from one place to another. In the central part of the loess plateau, the thickness is about 170 m in Xifeng (Liu et al., 1987), 140 m in Luochuan (Liu, 1985), and 160 m in Baoji (Ding, 1988).

Large scale field observations indicate that there are some loess and paleosol units characteristic of all sections. Thus they have been used as markers for stratigraphic correlation. The ninth and fifteenth loess-units (counted from top to bottom) are remarkably coarser and thicker, and are referred to as the first sandy loess and second sandy loess, respectively (Liu, 1985). The S5 (the fifth paleosol unit) is the best developed paleosol complex in the Chinese loess sequence and is a very useful marker layer. It contains three pedons with two thin interbedded loess layers. In most sections, the two lower pedons are truncated and slightly less-developed than in the upper one. Using these marker layers and magnetostratigraphic constraints, Ding et al. (1991) made a correlation of the loess-paleosol sequences distributed in the major Loess Plateau. Field observations for the present study indicated that pedogenic intensities and preservations of the loess and paleosol layers vary with location. Detailed stratigraphic correlations of the loess-paleosol sequences on a large scale must involve individual dating of each section and at least some independent age-controls are needed.

The loess/red clay boundary has been dated at about 2.4 to 2.5 Ma B.P. by paleomagnetic studies (Heller and Liu, 1982; Liu et al., 1987; Ding et al., 1991; Zheng et al., 1991). This age marks the end of the red clay accumulation and the beginning of the loess deposition. The boundary of the Matuyama and Gauss magneto-stratigraphic chrons occurs at the top of the red clay formations in Luochuan and Xifeng, whereas it is detected in the bottom loess layer in the Guanzhong Basin (eg., Baoji, Xi'an, Duanjiapo, and Yanyu). This discrepancy in timing of the loess/red clay boundary could be attributed to erosion or disturbance which may have occurred during the transitional period, as indicated by a sharp contact of the loess and the red clay or a thin sand/gravel layer existing between them.

Like that of the loess-paleosol sequence, the thickness of the red clay formation changes from site to site. It is about 60 m thick in the Lantian section (Zheng et al., 1991), 30 m in the Baoji section (Ding, 1988) and 10 m in the Yanyu section. In the central part of the major loess plateau, the lower boundary of the red clay is either not exposed (eg., in the Xifeng section) or poorly exposed as in the Luochuan section.

The fluviolacustrine sequence in the Guanzhong graben is characterized by alternations of silty clay and sand layers. The thickness varies from area to area, depending on natural outcrops. The age of the upper boundary is paleomagnetically determined as 1.8 Ma in the western margin and 1.2 Ma in the centre, as is summarized in Chapter 1. Therefore, the boundary-age in my study section, the Shijiawan section, still needs to be determined.

In this chapter, the study sections are briefly described, the dating methods and results are presented and discussed, and a regional stratigraphic comparison and correlation are attempted.

2.2. Study Sections for Paleomagnetic Dating

2.2.1. Shijiawan Section

Shijiawan village is situated approximately 20 km southeast of the Weinan city, 70 km east of Xi'an (see Figure 1-3). The Shijiawan section is 300 m northwest of the village in a deep valley at the margin of the Changshou Platform.

The section consists of a loess-paleosol sequence (in the upper part) and a fluviolacustrine sequence (in the lower part). The thickness of the whole section is about 250 m (see Figure 2-1). The loess-paleosol sequence contains 36 paleosol layers with a

Figure 2-1. The Shijiawan section, consisting of loess-paleosol sequence and fluviolacustrine sequence.

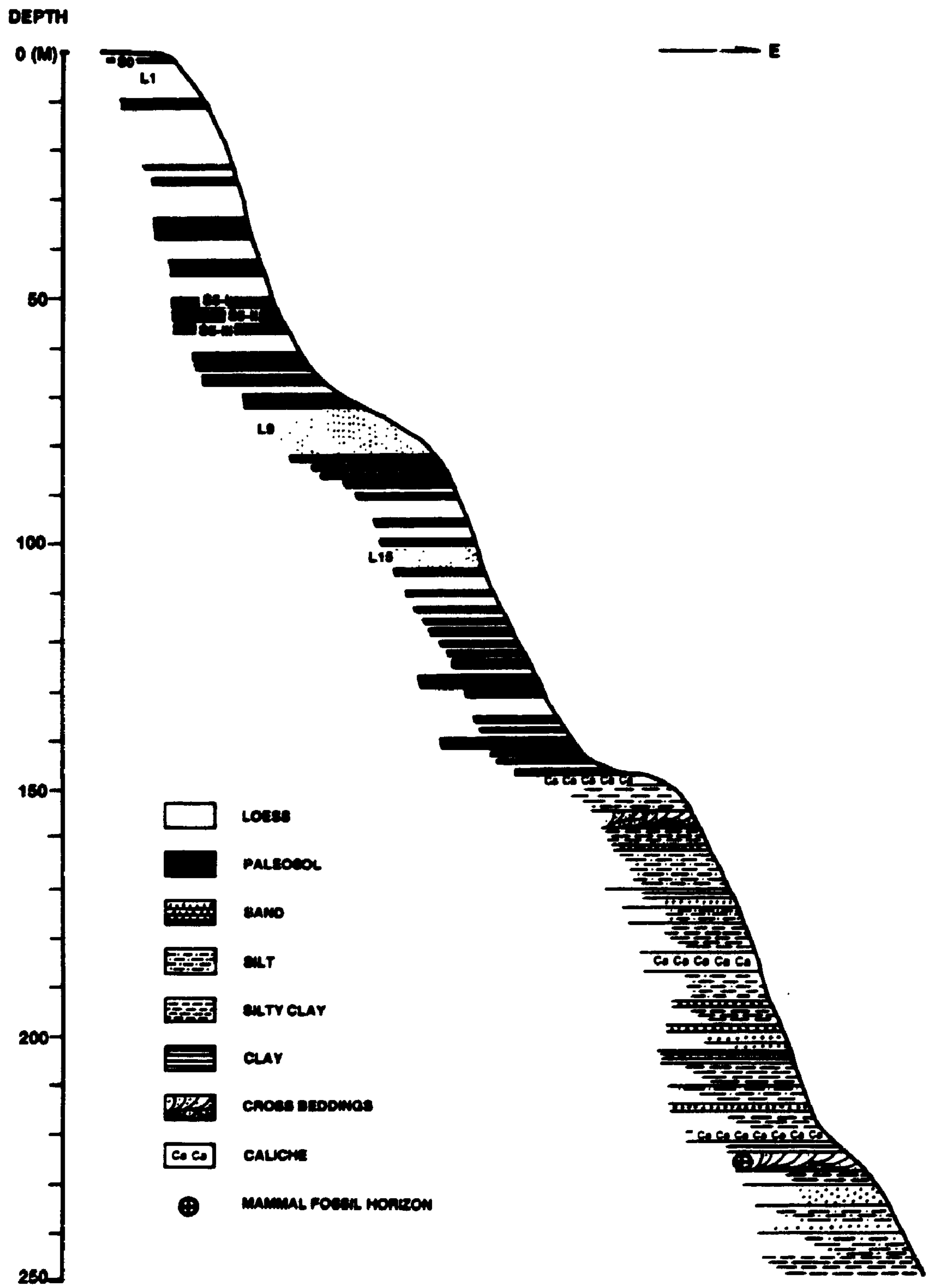
DEPTH
0 (M)
50
100
150
200
250
E
L1
L9
L15
LOESS
PALEOSOL
SAND
SILT
SILTY CLAY
CLAY
CROSS BEDDINGS
CALICHE
MAMMAL FOSSIL HORIZON

total thickness of 148 m. The "S5" in this section includes three paleosol layers separated by two interbedded loess layers. L9 (the first sandy layer) and L15 are characterized by loose texture, coarse grain-size and great thickness, and are easily identified. A rough comparison with other sections using the marker layers indicates that the loess and paleosol layers are notably thicker, but the lower part of the loess-paleosol sequence is not complete. The bottom layer would conventionally be classified as L27. The fluviolacustrine sequence is composed of silty clay and sand beds with a total thickness of about 100 m.

Samples were generally taken in 50 cm intervals for paleomagnetic analysis and in 20 cm intervals in horizons suspected of containing magnetic polarity reversals. A total of 486 vertically oriented specimens were collected from the whole section.

2.2.2. Yanyu Section

Yanyu village is 30 km south of Weinan city. The Yanyu section is located in the southeastern valley, 200 m from the village, and about 5 km from the northern slope of the Qinling Mountains. The local relief is featured as a mountain front hill. This section is comprised of a loess-paleosol sequence, a red clay formation, a sand-gravel complex and a cemented sandstone and mudstone.

The loess-paleosol sequence in this section is 94 m in thickness. Compared with other sections, the top layers above S5 are missing. The lower boundary smoothly contacts the red clay formation (see Figure 2-2, Plate 2-1). The red clay formation thickness ranges from 7 to 12 m (thickens from upstream in the south to downstream northwards). The underlying gravel layer, consisting of poorly-rounded and poorly-sorted

Figure 2-2. The Yanyu section, consisting of loess-paleosol sequence and the red clay formation.

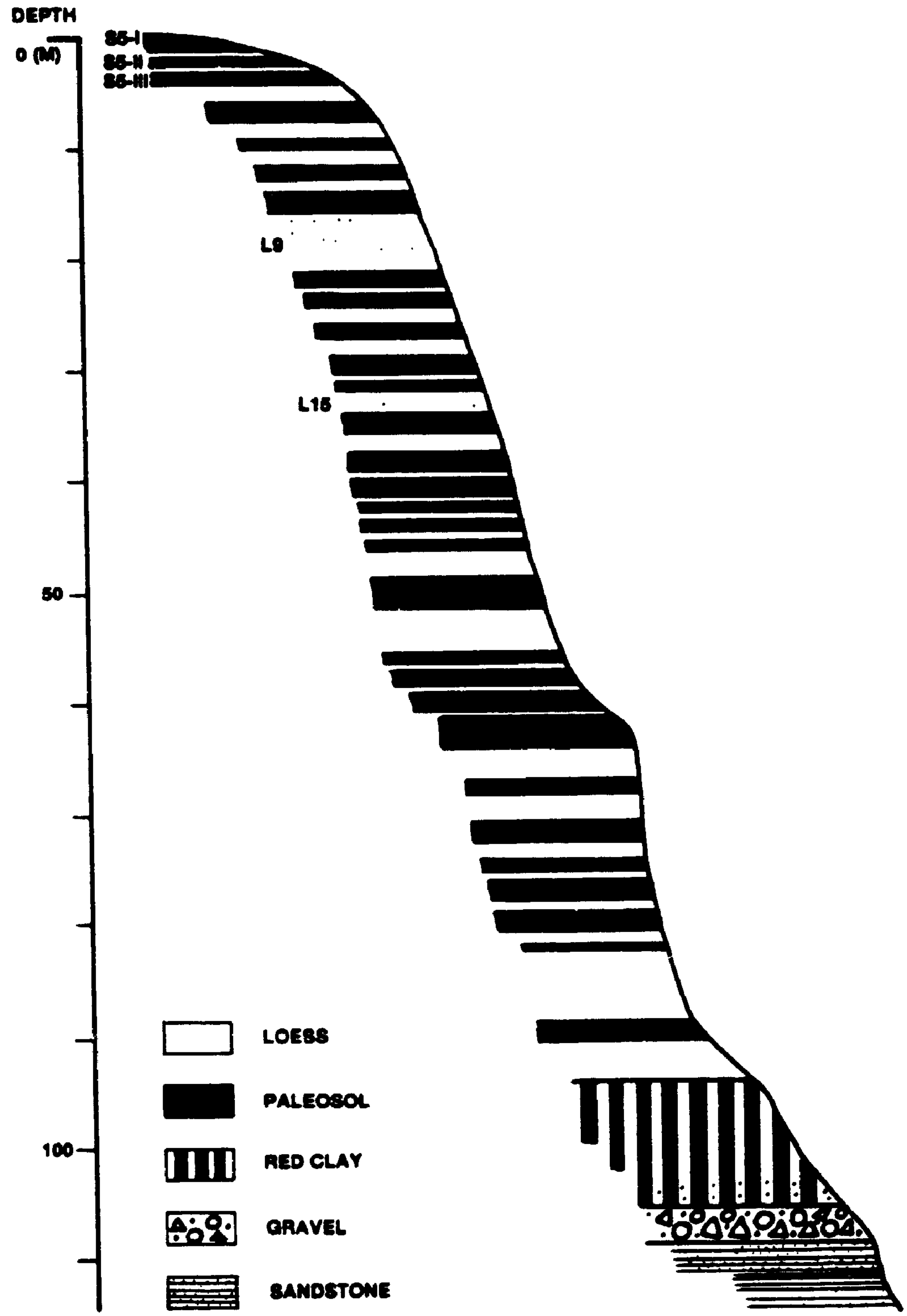
DEPTH
0 (M)
50
100
S5-I
S5-II
S5-III
L9
L15
LOESS
PALEOSOL
RED CLAY
GRAVEL
SANDSTONE

gravels, is about 5 m thick, but transforms into a sand-gravel sequence downstream. At the mouth of the valley, it reaches approximately 40 m in thickness.

Beneath the gravel layer lie the cemented sandstone and mudstone which are believed to be early Tertiary deposits (Chinese Academy of Geology, 1973).

The visible difference between the loess-paleosol sequence and the red clay formation is in their different background colours. In contrast to the yellowish loess, the red clay formation is always pink-red or dark red through profiles (Plate 2-1).

This section has been studied magnetostratigraphically (e.g., Ding, 1988). The purpose of the paleomagnetic measurements was to confirm the position of the Matuyama/Gauss Boundary and to obtain the lower boundary age of the red clay formation in this profile. Some 32 vertically oriented samples were collected from the lower horizon of L32 down to the red clay in 30 cm intervals for the loess and top of the red clay formation, and 50 cm interval for the rest of the exposure.

2.3. Paleomagnetic Measurement and Results

The vertically oriented samples are shaped as cylinders which are 2 cm in diameter and length. Measurements were conducted in the former Geophysics Department by Dr. Palmer with a spinner magnetometer. The natural remanent magnetization of all specimens were triply measured by placing them up-side down for one week after each series of measurements. All specimens were progressively thermo-demagnetized in intervals of 50 °C from 200 °C to 665 °C or up to their measurable limit for the instrument in order to obtain a stable characteristic remanent magnetization (ChRM) as shown in Figure 2-3.

Figure 2-3. Orthogonal projections of natural remanent Magnetization vector paths of paleosol and fluviolacustrine sediment specimens with progressive thermal demagnetization.

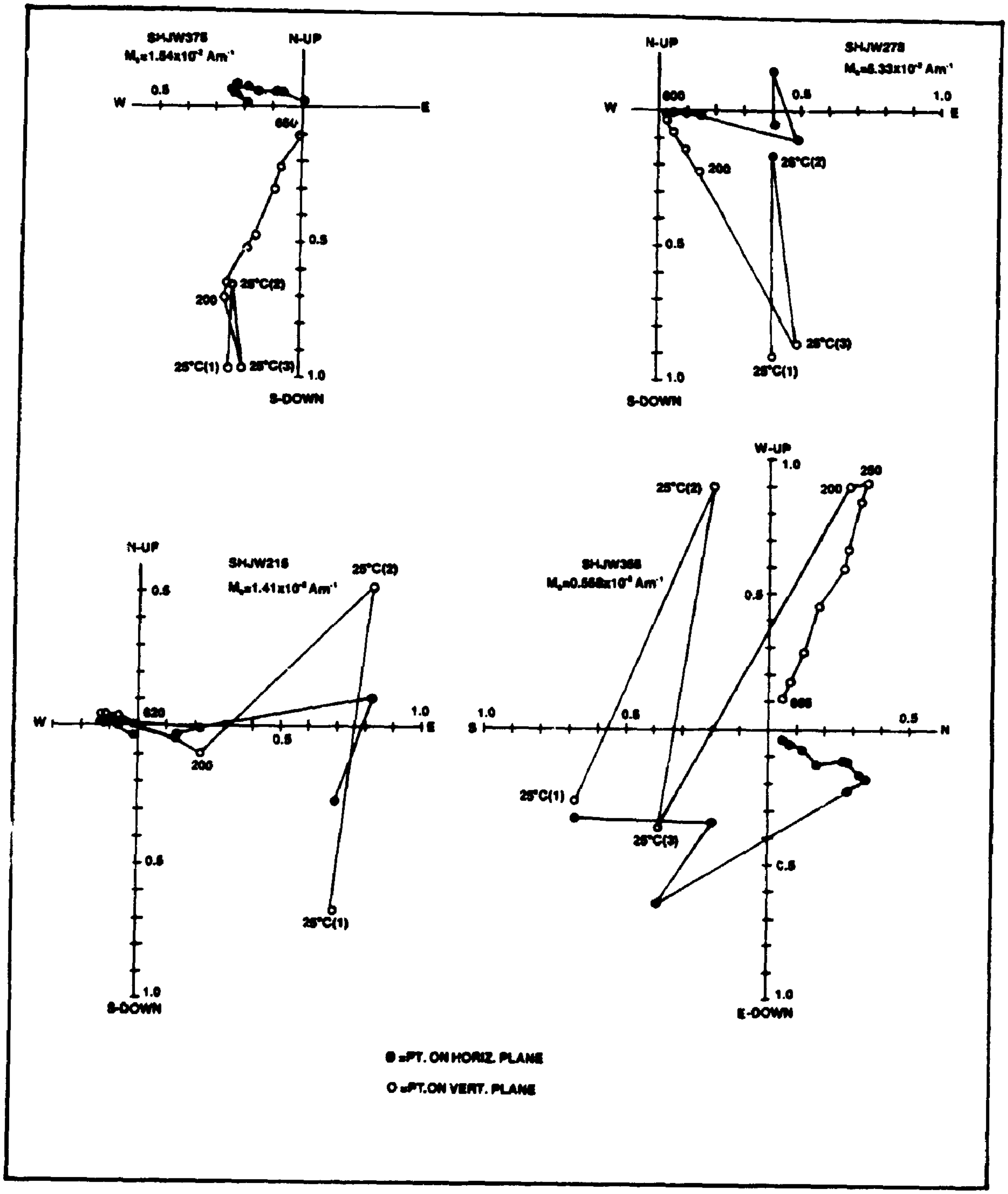
SHJW375
N-UP
W
E
S-DOWN
25°C(1)
25°C(2)
25°C(3)
200
SHJW278
N-UP
S-DOWN
25°C(1)
25°C(2)
25°C(3)
200
SHJW215
N-UP
S-DOWN
25°C(1)
25°C(2)
200
SHJW388
W-UP
E-DOWN
S
N
25°C(1)
25°C(2)
25°C(3)
200
● =PT. ON HORIZ. PLANE
○ =PT. ON VERT. PLANE

Plate 2-1. Photos showing a smooth contact of loess with the underlying red clay formation. Left, taken from Longhua, Shanxi province, east part of the Chinese Loess Plateau. Right, The lower part of the Yanyu section. The loess/red clay boundaries in both sites are pointed by black arrows. Above the boundaries are the loess-paleosol sequences and below the boundaries is the Red Clay Formation.

The ChRM polarity (inclination) is defined by progressive thermal demagnetization and plotted against depth (Figures 2-4, 2-5).

2.4. Discussion

2.4.1. The Brunhes/Matuyama Boundary

As shown in Figure 2-4, the first magnetic polarity reversal occurred in the upper horizon of the paleosol unit S8 in the Shijiawan section. This is consistent with the results from the Luochuan sections (Heller and Liu, 1982, 1984; Heller et al., 1987). Some studies on other sections show the boundary in the loess unit L8, just above S8 (Liu et al., 1987; Ding, 1988; Zheng et al., 1991). Heller et al. (1987) attributed the discrepancy to deviations of variable stratigraphic recording techniques applied by the individuals. This could not be the case because the loess bed L8 and the paleosol S8 are very distinct in colour and texture in most profiles. Field observations show that a short period of erosion is very common during the transition from paleosol to loess deposition as indicated by truncated paleosol layers. Therefore, very short events like the magnetic polarity reversals, could not be expected to have been recorded in exactly the same horizon in the whole loess plateau, and small differences are to be expected.

2.4.2. The Jaramillo Subchron

From S11 to L15 (between 90 and 106 m in depth), variations in the ChRM inclinations show a complicated pattern (see Figure 2-4). A similar phenomenon has been reported in the Xifeng section (cf. Liu et al., 1987). To avoid erroneous measurement, more samples were added and investigated. It was found that these unexpected polarity

Figure 2-4. The lithology and magnetostratigraphy of the Shijiawan section.

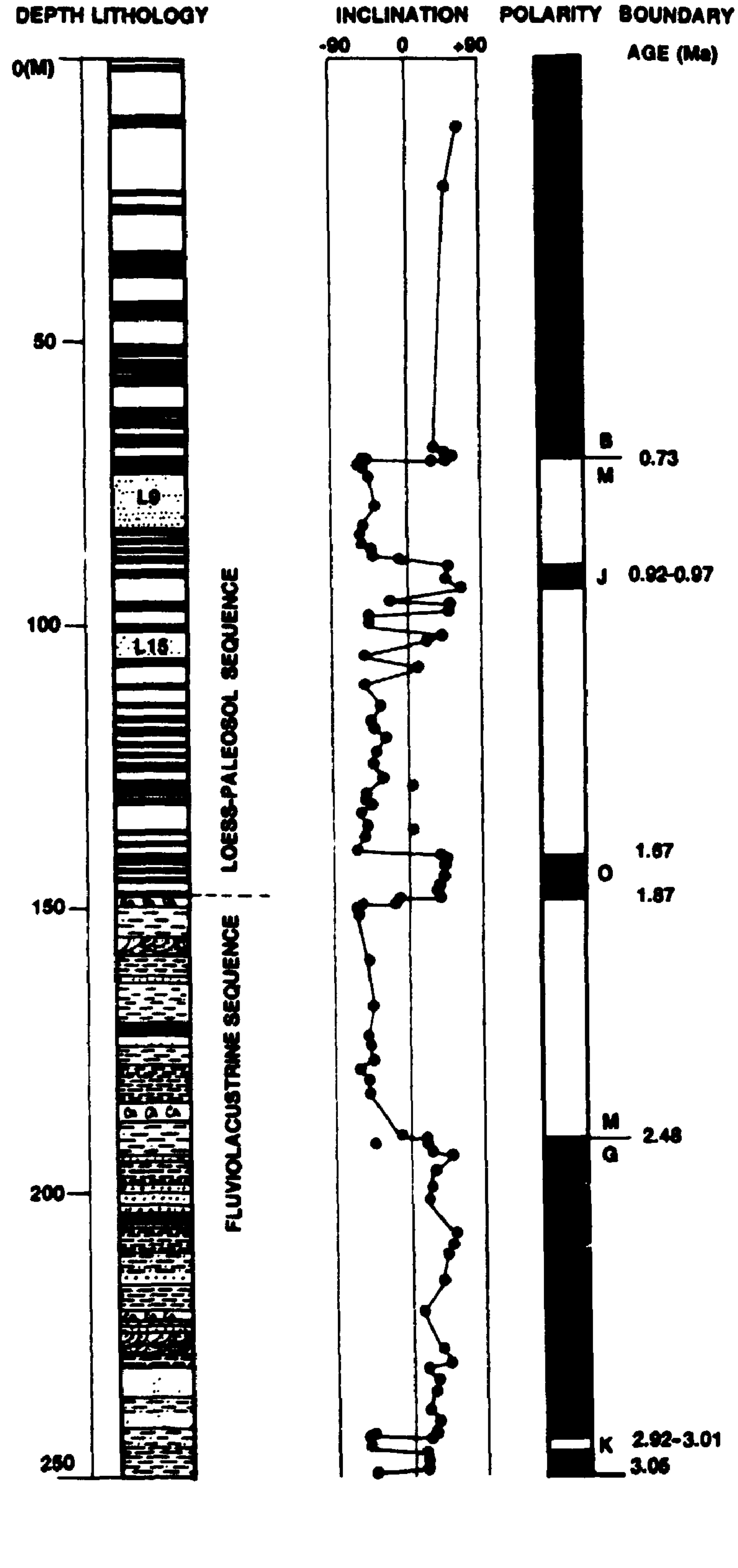
DEPTH LITHOLOGY
INCLINATION
POLARITY BOUNDARY
AGE (Ma)
-90 0 +90
0(M)
50
100
150
200
250
L9
L15
LOESS-PALEOSOL SEQUENCE
FLUVIOLACUSTRINE SEQUENCE
B
M
0.73
J 0.92-0.97
1.67
O
1.87
M
G
2.48
K 2.92-3.01
3.05

Figure 2-5. Lithology and magnetostratigraphy of the lower part of the Yanyu section for defining the horizon of the M/G boundary.

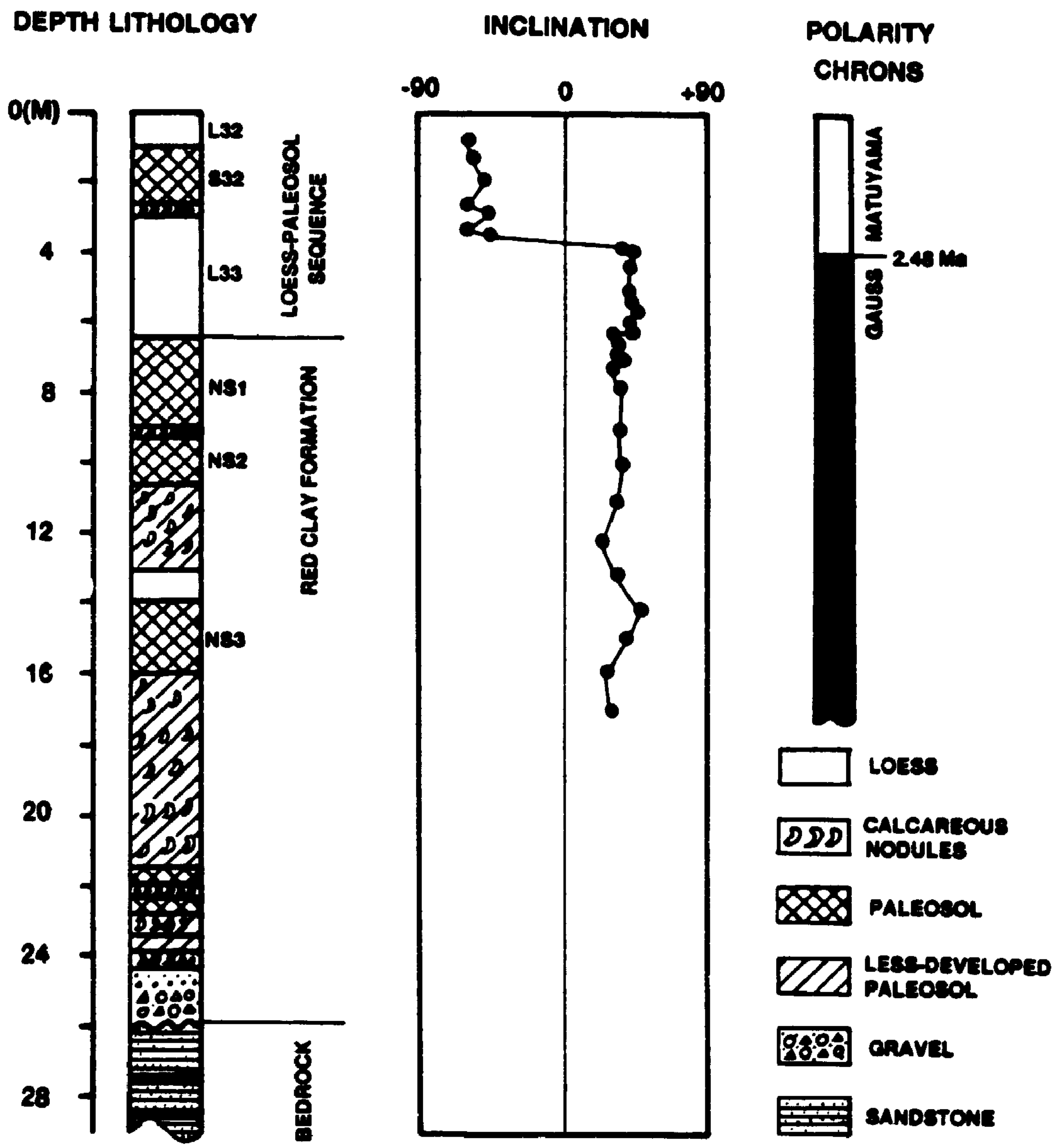
DEPTH LITHOLOGY
INCLINATION
POLARITY CHRONS
0(M)
4
8
12
16
20
24
28
L32
S32
L33
NS1
NS2
NS3
LOESS-PALEOSOL SEQUENCE
RED CLAY FORMATION
BEDROCK
-90
0
+90
MATUYAMA
2.48 Ma
GAUSS
LOESS
CALCAREOUS NODULES
PALEOSOL
LESS-DEVELOPED PALEOSOL
GRAVEL
SANDSTONE

changes are not the result of mis-orientation of the specimens. The fact is that the remanent magnetization intensities decrease very sharply when heated at 300 °C and soon down to the noise level when further heated during progressive thermal demagnetization. The reason behind this is not clear. As the Jaramillo subchron has a time-interval of 70,000 years, it should not span more than two loess-paleosol cycles. Therefore, it is reasonable to match this event to the normal polarity stage between the top of the L12 and the bottom of the L13 (Figure 2-4).

2.4.3. The Olduvai Subchron

The results clearly show that the ChRM normal polarity occurs again at 142 m in depth. It continues to 148.2 m in the paleosol layer, just above the lithologic boundary between the loess-paleosol sequence and the fluviolacustrine sequence. This normal polarity interval covers four loess-paleosol alternations. Thus, in this section, the Olduvai event defines the end of the fluviolacustrine deposition and the beginning of loess accumulation at about 1.9 Ma B.P.

2.4.4. The Matuyama/Gauss Boundary

In the Shijiawan section, the M/G (Matuyama/Gauss) boundary occurs in a sandy silt bed of the fluviolacustrine sequence (Figure 2-4). In the Yanyu section, the M/G boundary is detected in the bottom loess layer (correlated to the L33 in the Baoji section, Ding et al., 1991) above the red clay formation (Figure 2-5). This is consistent with the results from Baoji (Ding, 1988) and Duanjiapo (Zheng et al., 1991) in the Guanzhong Basin, but slightly different from the central part of the major Loess Plateau where the

M/G boundary is in the upper horizon of the red clay formation (Heller and Liu, 1982, 1984; Liu et al., 1987). A possible explanation would be that the central part of the loess plateau was subjected to a redeposition by water flowing during the period between loess and red clay, which is indicated by the erosion surface or a mixing layer of red clay with loess on the top of the red clay formation. Therefore, the present results lead to the conclusion that the loess deposit was initiated about 2.5 million years ago, a little earlier than the M/G boundary.

The question remaining is the timing of the end of red clay accumulation. Although the answer cannot directly be found from paleomagnetic results, field observations provide assistance in approaching this problem. As shown in Plate 2-1, the overlying loess is smoothly deposited on red clay as it successively followed the paleosols in the loess-paleosol sequence. There is no evidence indicating a large hiatus between them. Paleomagnetic results from the Lantian section show a 9 m thickness of red clay accumulated during the interval of 2.92-2.5 Ma B.P. (Zheng et al., 1991), similar to the Xifeng section (Liu et al., 1987). Therefore, 2.5 Ma B.P. has been chosen as the commencement of the Chinese loess accumulation and the end timing of the red clay formation.

2.4.5. The Kaena Subchron

Approximately 48 m below the M/G boundary in the Shijiawan section, an abnormal polarity zone is clearly demonstrated close to the bottom, which can be correlated with the Kaena subzone. It indicates that the oldest age of the fluviolacustrine sequence in the Shijiawan section is about 3.05 Ma according to the polarity time scale of Mankinen and Dalrymple (1979).

In the Yanyu section, the Kaena subchron cannot be detected. Though it cannot be concluded that the entire red clay of this section was deposited within the interval from 2.92 to 2.5 Ma B.P., for our sampling did not reach the bottom due to loose texture, the upper 6 m seems to have formed in this time-interval.

2.5. Stratigraphic correlations

A framework of stratigraphic correlation for the Cenozoic in the Chinese Loess Plateau is shown in Figure 2-6. The following points are stressed.

1. The Shijiawan section, representing the last 3 million years, accumulated continuously in terms of secular climate change. The lithologic boundary between the fluviolacustrine sediments and the overlying loess is dated at about 1.9 Ma B.P. Thus the fluviolacustrine sequence has the potential to provide the information for the climate transition from late Pliocene to early Pleistocene.

2. The Chinese loess-paleosol sequence follows the end of the red clay accumulation at about 2.5 Ma B.P. without any significant interruption. Erosion of the red clay formation before loess deposition is only a local phenomenon.

3. The loess-paleosol sequence in the Brunhes chron can clearly be correlated for all the established sections. The best developed paleosol unit, S5, consists of either one complex of multiple layers or a combination of three separate pedons, and can be identified without confusion.

4. As in Figure 2-6, the discrepancies in the magnetic polarity boundaries suggest different accumulation-erosion histories between individual localities.

Figure 2-6. Correlation of litho-, magneto- and chrono-stratigraphy of the Cenozoic strata in various locations of the Chinese Loess Plateau. Lithologic symbols seen in other figures of this chapter. Data from Heller and Liu (1982) for the Luochan section, X.M. Liu et al. (1987) for the Xifeng section, Ding (1988) for the Baoji section, and Zheng et al. (1991) for the Duanjiapo section.

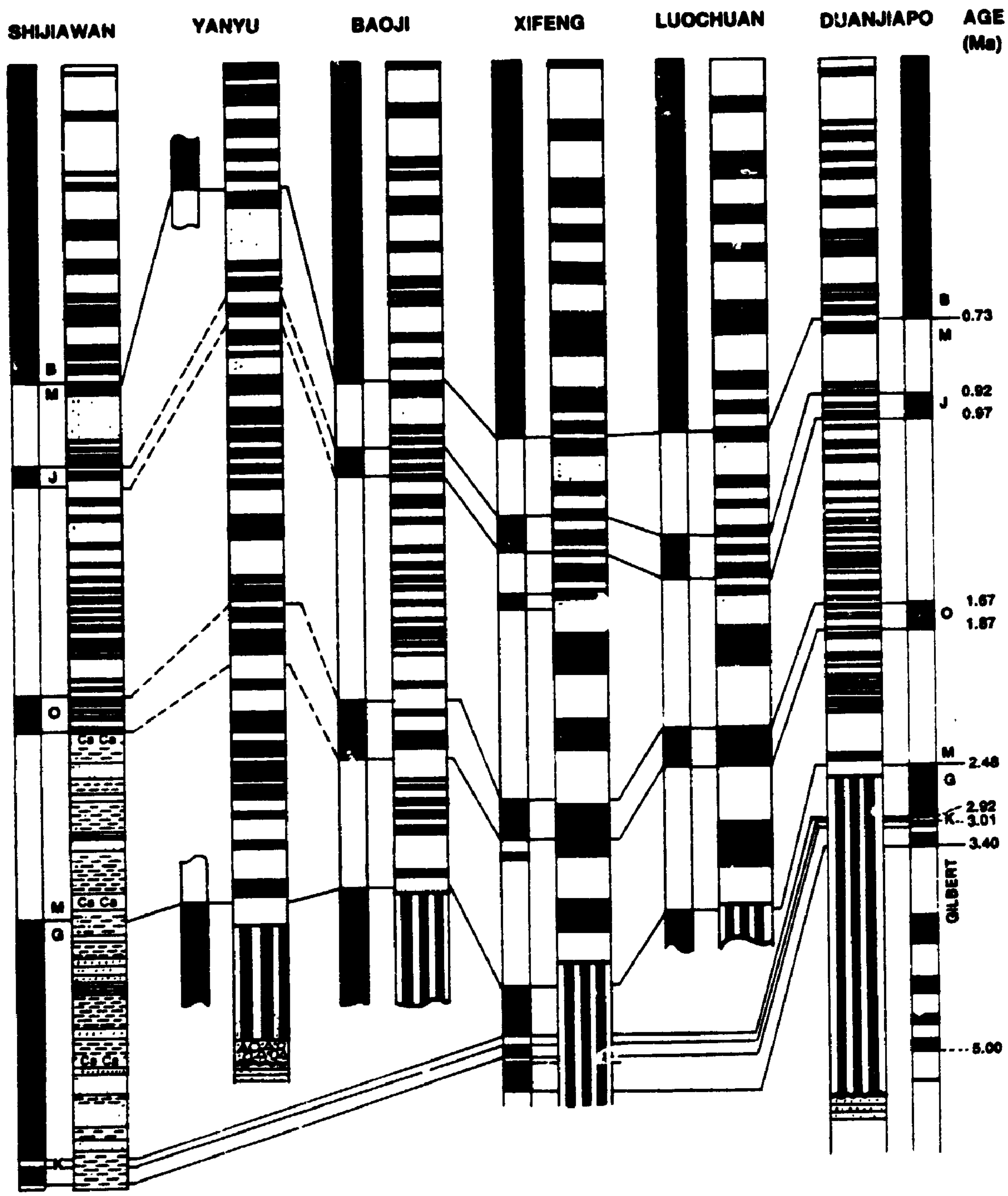
SHIJIAWAN
YANYU
BAOJI
XIFENG
LUOCHUAN
DUANJIAPO
AGE (Ma)
B
M
J
O
G
K
0.73
0.92
0.97
1.67
1.87
2.48
2.92
3.01
3.40
GILBERT
5.00
Ca Ca

CHAPTER 3

$\delta^{13}C$ SIGNATURES OF REGIONAL VEGETATION AND RELATED SOILS

3.1 Introduction

Plants can be classified into three groups based on their photosynthetic pathways: C3, C4 and CAM. C3 plants, including virtually all trees, most shrubs, herbs and cool-season grasses, have $\delta^{13}C$ values ranging from -23 to -35 permil and average about -27 permil (Deines, 1980). C4 plants, mainly composed of warm-season grasses and sedges (Bender, 1971), are characterized by a narrow $\delta^{13}C$ range from -10 to -14 permil, averaging about -13 permil (Deines, 1980; O'Leary, 1988). CAM plants, of which the most abundant are succulent plants which grow mainly in conditions under water and CO_2 stress (Bender et al., 1973), have a wide range in $\delta^{13}C$ values that covers C3 and C4 plants. When plant tissues fall into soil or are deposited in sediments, they experience decomposition and the organic composition will change. But the $\delta^{13}C$ values of organic matter generally remain close to that of the vegetation from which it is derived (Deines, 1980; DeLaune, 1986; Balesdent et al., 1987; Martin et al., 1990; Ambrose and Sikes, 1991). If vegetation is a mixture of C3 and C4 plants, the carbon isotope signature of the soil organic matter reflects the proportion of C3 and C4 plants in the total biomass influx. Therefore, the stable carbon isotope composition of organic matter from sediments has been extensively used for tracing paleovegetation and related climate (Krishnamarthy et al., 1982; Schwartz et al., 1986; Dorn et al., 1987; Guillet et al., 1988; Goodfriend, 1990; Ambrose and Sikes, 1991; Cerling et al., 1993; Sukumar et al., 1993). These results, however, have shown that the ecological and climatic significance of the organic carbon isotope signature can vary from region to region.

Previous studies on the upper part of the loess-paleosol sequence in the Chinese Loess Plateau have been reported by Lin et al. (1991) and An et al. (1993). But the relationship of the $\delta^{13}C$ between vegetation and its related soil organic matter in the region has not received detailed investigation. Therefore, it is necessary to elucidate this relation if $\delta^{13}C$ signatures of organic matter are intended to be used for paleoecological and paleoclimatic reconstructions of the region.

This chapter focuses on the organic carbon isotope compositions of modern plants and related soils in the Guanzhong basin, the southernmost part of the central Chinese Loess Plateau. In particular, the relationship between vegetation and related soils in organic carbon- isotope composition will be described, and the climatic significance of C4 plant-abundance in this region will be discussed.

3.2 Regional Vegetation and Related Soils

The modern natural vegetation in the Guanzhong basin is represented mainly by two types, the semi-arid steppe and the semi-humid grass-forest. Today they have been destroyed in most areas due to long-period cultivation. Two floras minimally influenced by human activities were selected for this study.

3.2.1 Steppe vegetation and its soil

This type of vegetation is found close to Yanyu village in the Weinan District of

Shaanxi Province (109°33', 34°20', see Figure 1-3). The local relief is characterized by rugged loess hills. Annual rainfall and annual mean temperature are about 580 mm and 13.3 °C, respectively (Sun, 1989). The main floral components are herbs and grasses, mainly *Artemisia sacrorum, Artemisia giraldi* and *Stipa bungeana*, and shrubs, *Zizyphus spinosa*, *Vitex chinensis*, and *Lespedeza bicolor*. These are also the common species in the loess plateau as well as in north China (Institute of Botany, Academia Sinica, 1960; China Map Press, 1984; Liu et al., 1985).

Underneath the steppe cover, the modern soil is developed from silty loess. Pedogenic features are not strongly developed, with only A and C horizons present. Carbonates are only weakly leached and can be detected at about 10 cm below the surface. Scattered small calcareous nodules are formed at depths of approximately 20 to 40 cm (see Figure 3-2).

3.2.2 Grass-Shrub Mixed Forest and the Soil

The grass-shrub mixed forest flora is found on the piedmont of the Qinling Mountains, south of Ziwu village, 20 km south of Xi'an (108°53'E, 34°0'N, see Figure 1-3). Because of its altitude and topography, the annual mean precipitation in this area is about 200 mm more than the adjacent plain. Trees are the dominant plants, forming about 70% of the total cover. The major species are *Populus davidiana, Platycladus orientalis, Juniperus chinensis* and *Pyrus ussuriensis*. *Robinia pseudocacia* is a human-planted species. Shrubs (mainly including *Vitex chinensis, Zizyphus spinosus* and *Lespedeza bicolor*), herbs (*Artemisia sacrorum, Artemisia giraldi*) and grasses (*Bothriochloa isochaemum, Bromus japonicus*) grow in open patches and only make up a minor portion of the vegetation.

The soil profile in this site contains horizons A, Bw and C (the definitions of the soil horizons from Catt, 1990). The parent materials are slope-wash from weathered granites. Carbonates have not been detected in this profile. Clay particles have accumulated in the Bw horizon to some extent. In the C horizon, the parent materials contain a large amount of coarse sand and angular gravels. The total pedogenic thickness is about 50 cm.

3.3 Sampling and Laboratory Methods

Plant samples were air dried, and different organs (leaves, stems, roots etc.) were separated. Each sample was then treated with 5% HCl for 2 hours to remove carbonate, rinsed with tapwater, then dried at 80°C. After drying, the plant samples were ground into powder. Soil samples were treated somewhat differently. After removal of plant debris, the sample was ground and passed through a 100-mesh sieve. The sample was then treated with 20% HCl to remove carbonate and then washed with distilled water (the solution was centrifuged before being decanted). This process was repeated until the sample solution became neutral. The sample was then dried and re-ground. Tests using carbonate-free soil samples showed that treatment with 20% HCl did not affect the organic matter content or its carbon isotopic composition.

Acidified samples were mixed with pure CuO (plus Pt wire) and transferred into quartz sample tubes for combustion. CO_2 produced by the combustion was purified with cold-traps and then further purified by exposure to a sulphur scrubber. Its isotopic composition was measured using a Fisons OPTIMA dual inlet, gas-source mass spectrometer. Results are reported using the standard δ-notation as permil (‰) relative to the PDB standard (Craig, 1957). Standards (NBS#21, Carbon Rod) were reproducible to better than ±0.05‰, and the average value obtained for NBS#21 (-28.09‰) compares well with the accepted value (-28.1‰). The reproducibility for duplicate samples of plant tissues and soils was normally better than ± 0.04‰ and ± 0.20‰, respectively. The larger error, obtained for soil materials mainly reflects the heterogeneity of samples with low organic matter content.

3.4 Results and Discussion

3.4.1 $\delta^{13}C$ Values of the Floras and Related Top Soils

The results listed in Table 3-1 show that all tree species have $\delta^{13}C$ values between -28.9 and -24.6‰. The *Robinia pseudoacacia L.* leaf has the lowest $\delta^{13}C$ value whereas the *Juniperus chinensis* twig has the highest. Different tissues from the same plant have similar $\delta^{13}C$ values. Leaves are usually enriched in ^{12}C by about 1 permil relative to woody tissue such as twigs and roots, a result that is consistent with previous studies (Deines, 1980; O'Leary, 1981; Leavit and Long, 1982). All shrub plants in the two sites have relatively low $\delta^{13}C$ values, ranging from -27.0 to -27.9‰. The difference in $\delta^{13}C$ values between plant organs is very small. Most herb plants in both sites are of the C3 variety. Their $\delta^{13}C$ values range from -25.7 to -28.6‰. Only one species of the major plants appears to be a C4 plant with a $\delta^{13}C$ value -16.0 (see Table 3-1).

The $\delta^{13}C$ values of top soil samples reflect the carbon isotopic composition of the modern vegetation (see Table 3-2). In order to understand how the $\delta^{13}C$ values of soil organic matter are close to the source flora, it was assumed that each major plant species

Table 3-1. $\delta^{13}C$ values of major plants in Yanyu and Ziwu areas.

Plant Species	Tissues	$\delta^{13}C$ (‰) PDB	Type/Abund. (%)
	Plants in Yanyu		
Zizyphus spinosus	Twig + Root	-27.92	shrub/20
Lespedeza bicolor	Root	-27.03	shrub/20
	Twig	-27.14	
Artemisia giraldi	Stem	-27.09	herb/ 30
	Root	-27.30	
Stipa bungeana	Whole Plant	-25.66	herb/ 25
	Plants in Ziwu		
Plalycladus orientalis	Leaf	-27.51	tree/ 10
	Twig	-26.49	
Robinia pseudoacacia L.	Leaf	-28.82	tree/ 5
	Twig	-28.03	
Juniperus chinensis	Leaf	-25.83	tree/ 20
	Twig	-24.58	
	Root	-24.73	
Populus davidiana	Root	-26.75	tree/ 20
Pyrus ussuriensis	Leaf	-27.86	tree/ 5
	Twig	-27.66	
Vitex chinensis	Root	-27.30	shrub/10
	Stem + Leaf	-27.33	
Artemisia sacrorum	Root	-28.10	herb/ 10
	Stem	-28.40	
Themeda triadra var. japonica	Whole	-15.99	herb/ 10
Bothriochloa ischaemum	Whole	-28.64	herb/ 10
	Major tree species in North China		
Quercus liaotungensis	Leaf + Twig	-26.49	tree
Pinus tabulaeformis	Leaf + Twig	-27.16	tree

contributed its organic matter coverage-proportionally to the surface horizon, and the $\delta^{13}C$ values of the surface horizon for the Ziwu and Yanyu sites was calculated using the following equation

$$\delta^{13}C_{s.h} = \Sigma P^{i}_{coverage} \times \tfrac{1}{2}(\delta^{13}C^{i}_{leaf} + \delta^{13}C^{i}_{root\ or\ twig})$$

Here $\delta^{13}C_{s.h}$ represents the $\delta^{13}C$ value of organic matter in the surface horizon and $P^{i}_{coverage}$ means the coverage (see Table 3-1) for the ith plant species in the sampling site; the term $\tfrac{1}{2}(\delta^{13}C^{i}_{leaf} + \delta^{13}C^{i}_{root\ or\ twig})$ means that the $\delta^{13}C$ value of the ith plant species is a mean value contributed equally by its leaves and other organs (roots and/or twigs).

As a result, the difference in $\delta^{13}C$ values of the organic matter between the measured and the calculated for surface horizon is less than 1 permil. Therefore, it indicates that the $\delta^{13}C$ signatures of soil organic matter precisely reflect the source vegetation.

3.4.2 $\delta^{13}C$ Signatures in the Grass-Mixed Forest Soil Profile

The $\delta^{13}C$ values of the modern soil profile in Ziwu are plotted in Figures 3-1 (also see Table 3-2). The $\delta^{13}C$ values along the Ziwu profile change from -26.7 at the top to -24.0‰ in the upper 10 cm, and then decrease slightly with depth. This variation could be explained by the fact that herb plant roots, especially of the C4 grasses, penetrate to shallower depths and that their residuals are mainly distributed in the upper horizons of the soil profile. Tree and shrub plants (all of C3 type) can reach much deeper horizons, and thus contribute a major portion to the organic carbon in lower soil horizons.

Table 3-2. $\delta^{13}C$ values of soil organic matter in the Ziwu and Yanyu profiles.

Sample Number	Depth (cm)	$\delta^{13}C$ (‰) PDB
Ziwu Soil		
ZW0	0-5	-26.71
ZW1	10-15	-24.03
ZW2	25-30	-24.37
ZW3	40-45	-25.38
Yanyu Soil		
YY0	0-5	-27.09
YY1	10-15	-25.86
YY2	30-35	-24.51
YY3	45-50	-18.81

Figure 3-1. $\delta^{13}C$ values of organic matter in the Ziwu soil profile. Modern vegetation in this site is a grass-shrub mixed forest. The lower horizontal scale indicates the equivalent percentage of C4 flora, assuming a +1 per mil enrichment in soil relative to plant $\delta^{13}C$ values. The end point $\delta^{13}C$ values are set at -26 per mil for 100% C3 (typical forest) and -15 per mil (according to the local C4 plant $\delta^{13}C$ value) for 100% C4 (typical grassland).

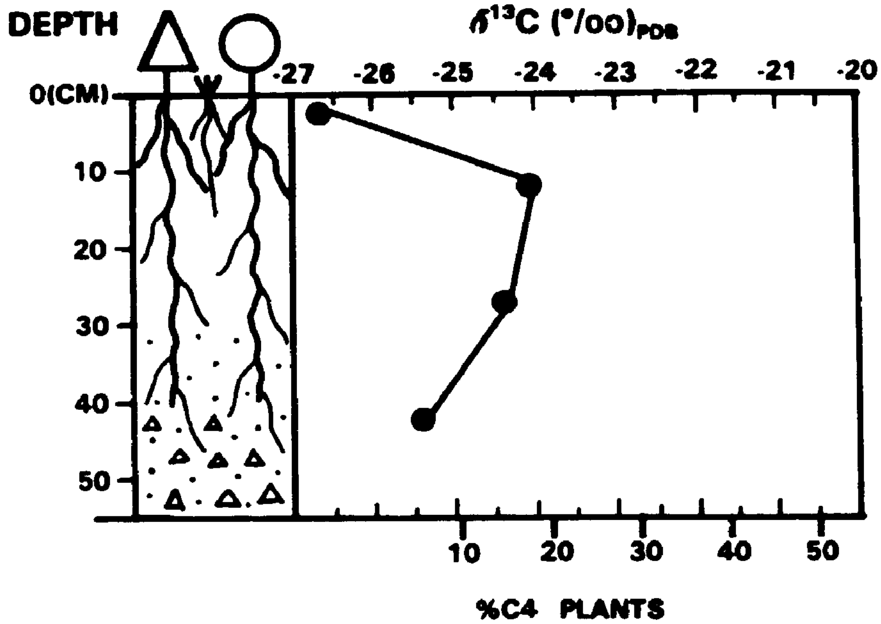
DEPTH
$\delta^{13}C$ (°/oo)$_{PDB}$
-27 -26 -25 -24 -23 -22 -21 -20
0(CM)
10
20
30
40
50
10 20 30 40 50
%C4 PLANTS

Figure 3-2. $\delta^{13}C$ values of organic matter in the Yanyu soil profile. Modern vegetation in this site is shrub mixed steppe. The radiocarbon dating was conducted by University of Waterloo Isotope Lab. Explanation for the lower horizontal scale is the same as that in Figure 3-1.

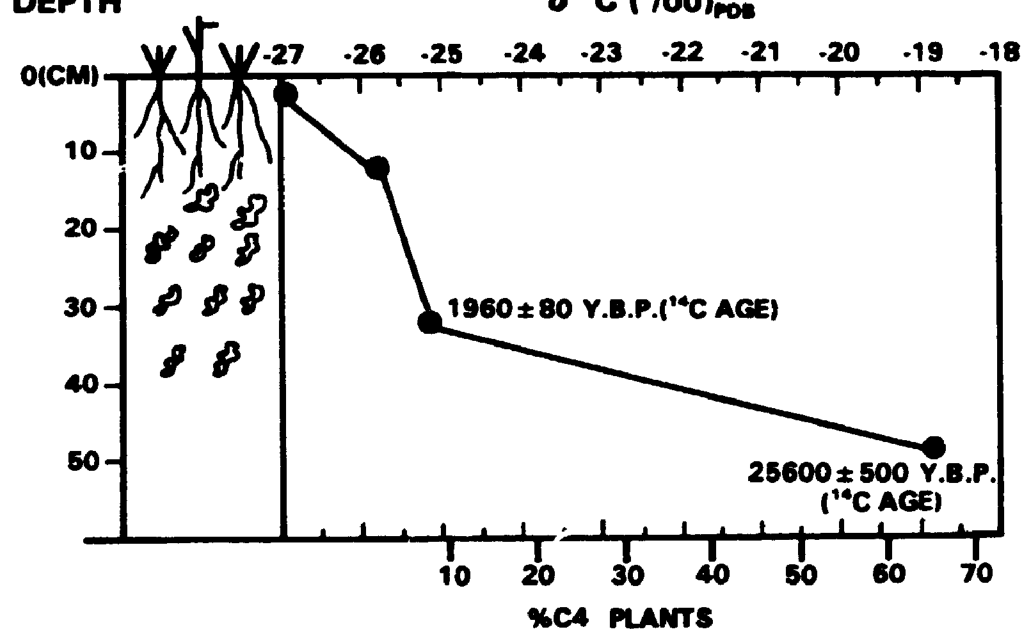
DEPTH
δ13C (°/oo)PDB
-27 -26 -25 -24 -23 -22 -21 -20 -19 -18
0(CM)
10
20
30
40
50
1960 ± 80 Y.B.P.(14C AGE)
25600 ± 500 Y.B.P.
(14C AGE)
10 20 30 40 50 60 70
%C4 PLANTS

Therefore, such patterns could be typical for $\delta^{13}C$ variations of organic matter along a soil profile on which a grass-mixed forest vegetation (containing some C4 plant species) exists.

3.4.3 $\delta^{13}C$ variation through the steppe soil profile

The Yanyu soil is vegetated by shrub-mixed steppe type. The $\delta^{13}C$ values increase with depth, from -27.1 at the top to -19.8‰ at the bottom of the profile (see Fig. 3-2). As shown by Table 3-1, all major plants of this site today have $\delta^{13}C$ values less than -25‰.

The change in the $\delta^{13}C$ value of organic matter in the deeper soil horizons cannot be derived from the modern native vegetation, as the soil organic matter may only be expected to have +1 to +3 per mil of enrichment in $\delta^{13}C$ values relative to those plants according to the discussion in last section and other studies (cf. Ladyman and Harkness, 1980; Becker-Heidmann and Scharpenseel, 1986). To explain these high values, C4 plants must have contributed a considerable proportion to the total organic matter at depth. For the Yanyu site, the C4 plant materials at depth could only come either from transport with loess materials or from native vegetation replacement.

The loess parent materials of the soil in Yanyu may have included some organic matter. The amount of organic matter transported is very low, normally bellow 0.02% as measured in loess samples. As the soils have a minimum of 0.5% organic matter, the high $\delta^{13}C$ value cannot be explained by such inclusion.

Radiocarbon dating indicates that the organic matter in different horizons of the profile does not have the same age (see Figure 3-2), which would suggest that variations of $\delta^{13}C$ values in the Yanyu soil profile may have originated from vegetational change. As shown in Figure 3-2, C4 plants contribute over 60% of the organic matter at the 45 to 50 cm levels (about 25,000 years B.P.), about 10% at the 30 to 35 cm levels (about 2000 years B.P.), and very little at surface horizon (0 to 5 cm). This shift pattern of the $\delta^{13}C$ values has been found in the Holocene soils elsewhere in the Chinese Loess Plateau (cf. Lin et al., 1991, Fig.2,3). This suggest that it is a regional rather than a local phenomenon.

3.4.4 Abundance of C4 plants and climate

Studies indicate that the abundance of C4 plants is closely related to either the minimum temperature or water supply during the growing seasons (e.g., Teeri and Stowe, 1976; Tieszen et al., 1979; Livingstone and Clayton, 1980; Young and Young, 1983; Cerling and Hay, 1986; Hattersley, 1983). In most cases, warmer and drier climates favour colonization of tropic or subtropic species, which generally includes more C4 plants. The climate over the Chinese Loess Plateau is strongly controlled by the east Asian monsoon, which simultaneously provides major rainfall and additional heat to the affected regions (Lin, 1981). Therefore, in contrast to areas controlled by the Indian monsoon, a warmer climate in the Chinese Loess Plateau means wetter rather than drier conditions. Thus, the definite climatic meaning of the abundance of C4 plants in this region should be investigated with care.

As C4 plants occur usually as minor components in the modern floras of steppe and forest in the region, it is difficult to directly constrain the climatic meaning of a C4 plant-dominated flora. C4 species in this region mainly are Gramineae, Chenopodeaceae and Compositae etc. They are more commonly observed on unstable ground surfaces as pioneer species, which suggests that these C4 plants are more resistant to harsh weather. The C4 dominant flora colonized about 25,000 years ago which is close to the time of the last glacial maximum, should imply a cold-dry climate. Recent detailed chronological study indicates that that period is marked by typical loess-accumulation (Liu et al., 1994). Pedogenic studies have indicated a north temperate dry-grassland soil developed during that time (Guo et al., 1994), under a climate much colder and drier than today. The C4-dominant flora may also correlate to a low level of atmospheric CO_2 of the last glacial (Barnola et al., 1987) which could have promoted C4 expansion (cf. Moor, 1994; Robinson, 1994). Therefore, abundant C4 plants in the Chinese loess Plateau suggest drier and colder climatic conditions, not drier and warmer.

3.4.5 Concluding Notes

A stable carbon-isotope study on the modern vegetation and related soils in the southern Chinese Loess Plateau leads to the following conclusions.

1) Most modern plants in southern Chinese Loess Plateau are C3 varieties. The $\delta^{13}C$ values in the top soil horizon of the two sites investigated (Ziwu and Yanyu) are around -26 per mil, corresponding to the combined biomass flux of all plants in the local floras.

2) Apparent differences in the major contribution depth of plant roots between trees and grasses have been observed in the field and revealed in the stable carbon isotope data. The ^{14}C dating suggests the major contribution depth of modern grasses and herbs is restricted to within about 10 to 15 cm in the Yanyu profile, and this depth is similar

in the Ziwu soil profile.

3) The maximum value (about -24‰) of the $\delta^{13}C$ in the Ziwu profile is found at about 10 cm in depth. This reflects the greatest contribution of C4 plants to the soil organic matter. The upper and lower horizons of the profile basically reflect C3 plant features with $\delta^{13}C$ values around -26‰. This $\delta^{13}C$ curve (Figure 3-1) should be typical for a grass-mixed forest soil profile.

4) The presence of abundant C4 vegetation in the Chinese Loess Plateau implies that the climatic conditions were drier and colder, rather than drier and warmer in the past.

CHAPTER 4

CLIMATIC FACTORS AND THE BEST DEVELOPED PALEOSOL IN THE LOESS SEQUENCE

4.1. Introduction

Chinese studies on modern large-scale dust storm events suggest that loess materials are dust, sorted and transported from the western inland deserts by northwesterly winds which are principally controlled by the Siberian cold-high pressure regime (Liu, 1985, Liu et al., 1981, 1989). The loess deposition rate was much higher during cold periods when the Cold-High was stronger, and formed the loess beds in the loess-paleosol sequence. Evidence shows that deposition was greatly reduced or nil when the climate was dominated by the summer monsoon (the winter cold-high is relatively weak) during interglacial episodes (Liu et al., 1981, 1985, 1989; An et al., 1993), and the surface loess was subjected to weathering and pedogenesis. Therefore, the loess and paleosol alternations of the past 2.5 million years show cold and warm climate fluctuations of great interest to Quaternary paleoclimatic studies.

Based on field observations, early studies of the Chinese loess confirmed that the "red bands" interbedded in loess successions in the loess plateau are buried soils (Zhu, 1958; Shi, 1958; Liu et al., 1959). Later, Liu et al. (1964) and Zhu (1965) showed that the loess has been deposited under dry-cold climatic periods whereas the buried soils formed during warm and slightly more humid climatic episodes than today. They showed that the paleosols could be classified into modern soil types which are typical of the south. An early study of the paleosols and their microfabrics was conducted by H.Z. Zhu (1963), who found illuvial features (oriented clay) in the B horizons. Aiming at documenting paleoclimatic implications of the loess and paleosols, Lu and An (1979) first classified the middle Pleistocene paleosols (from S1 to S14) in the Luochuan section into five types based on carbonate content, SiO_2/Al_2O_3 ratios and micromorphology. An and Wei (1980) and Tang (1981) were among the first who applied and emphasized soil micromorphological features. They focused on the paleosol S5 and interpreted it as brown cinnamon soil (in Luochuan) or as a brown forest soil (in Wugong of the Guanzhong Basin). More systematic studies of the paleosols were made by Liu et al. (1985). They estimated the climatic conditions according to comparison of their pedogenetic features in micromorphology and multiple geochemical and mineralogical indices with modern soils. Stressing pedogenic diagnostic horizons, Ding (1988) modified the criteria for the paleosol classification and climatic factors for each paleosol layer in the Baoji section. Guo et al. (1991) investigated the climatic implications of the paleosols in the Xifeng section and reached the conclusion that a short period of forest development had occurred in Xifeng which is located in a warm temperate semi-arid to semi-humid grassland zone today. Overall, the previous studies of the paleosols employed similar methodologies (comparison of the paleosols with modern soil orders), and obtained similar conclusions, which is that the S5 was developed under a typical forest in the Guanzhong Basin. Though the later studies pointed out some fundamental problems in the earlier studies, they are still questionable. The following problems exist in the studies to date.

1) Climatic interpretations of the paleosols are based on analogy, but it is not known whether the Holocene/modern soils have reached a state which adequately reflects

the modern climate.

2) For soils formed in short periods, many pedogenic features are largely a reflection of parent materials, which means it is not appropriate to compare paleosols to modern soils which developed from different parent materials.

3) Even for the paleosols developed from loess, it is difficult to compare them until the pedogenic duration is determined; chemical weathering processes depend on both climate and time, even if other factors are similar.

4) Palynological studies failed to provide evidence supporting the conclusion obtained from the Luochuan section (cf. Liu et al., 1985). Thus re-evaluation of paleoclimate of the loess-paleosol sequence is still necessary.

Considering the climatic change in the Chinese Loess Plateau, our interest is in the oscillation amplitudes during the Quaternary period, emphasizing the best climatic conditions which had ever existed in this region during the Quaternary. For this purpose, the best developed paleosol S5 of the loess sequence was chosen in our study. This chapter presents evidence for its pedogenic features from field observation and detailed laboratory analyses of grain size, mineralogy, clay mineralogy, chemistry and carbon isotopes of organic matter for two S5 profiles, the Shijiawan section and the Chang'an section, and then considers the climatic implications.

4.2. Field-Observation Features of S5

Both profiles of the paleosol S5 from Shijiawan and Chang'an (see Figures 1-1 and 1-3) contain three pedons which are separated by two interbedded loess layers. Only the upper pedon has an A horizon, while the others were truncated, leaving the Bt and

Table 4-1. Field observations of the S5 in the Shijiawan section.

Subdivision of S5	Pedogenic Horizon	Thickness (cm)	Description
S5-I	A	50	Dark brown clayey loam, friable, medium granular structure; abundant pseudomycelia in the upper part that decreased downward; diffuse smooth boundary.
	Bt1	50	Reddish brown silty clay; friable, very strong fine-subangular blocky structure; bright red, continuous thick clay coating and black Fe-Mn film; smooth boundary.
	Bt2	80	Reddish brown clay loam, dense, firm, weak medium-coarse subangular blocky structure; medium-thick clay coatings without Fe-Mn film; wavy boundary.
	CCa	40	Grey to dark yellow loam; dense, firm. Large calcareous nodules cemented together. The individual size can exceed 40 cm with irregular shapes.
	C1w	40	Light tan loam; firm with light-coloured calcic pseudomycelia.
S5-II	2Bt1	55	Reddish brown clayey loam, strong, medium-sized angular blocky structure; medium clay coating with some Fe-Mn films; well-developed large cracks with white carbonate precipitates; diffuse boundary.
	2Bt2	130	Dark-brown clayey loam, strong-fine subangular blocky structure; bright-red thick clay coating with Fe-Mn film; progressively changes into coarse blocky structure.
	C2w	60	Reddish brown loam; dense, firm, weak subangular-blocky structure; intermittent thin clay coatings; diffuse boundary.
S5-III	3Bt1	95	Reddish brown clayey loam, strong medium-fine subangular blocky structure; bright-red thick clay coatings with abundant black Fe-Mn films; smooth boundary.
	3Bt2	70	Reddish brown clayey loam; dense, firm, weak, coarse-subangular blocky structure; discontinuous thin clay coatings. In the bottom, colour shifts to light-brown; wavy boundary.
	C3Ca	95	Grey-yellow loam matrix with large carbonate nodules cemented together; diffuse boundary.
L6	C3	310	Grey-yellow silt loam; dense, firm with scattered large carbonate nodules.

C horizons. Compared with the S5 in Luochuan, these profiles are notably thicker (cf. Liu et al., 1985). The pedogenic horizons of each pedon have been subdivided according to pedogenic features and are described in Table 4-1. The best developed paleosol layer of the S5 unit is the upper pedon (S5-I, see Plate 4-1) whose Bt horizons have the thickest clay coatings and the most abundant Fe-Mn film in the two profiles.

4.3. Methods

Bulk samples were taken from all pedogenic horizons of the S5 in the Shijiawan and Chang'an sections. Grain-size determinations were made by the hydrometer method (cf. Catt, 1990). Mineralogy of the bulk samples were determined by X-ray diffraction spectrometry (XRD) and thin section microscopy. The samples were gently ground and reacted with 10% HCl to remove carbonate cement before attempting a clay mineralogical study. Clay fractions (<2 μm) were separated in a dispersing solution (5% sodium hexametaphosphate) according to Stokes' Law (assuming mean particle density of 2.65 g/cm^3). The separated clay fractions were saturated with Mg^{2+} by shaking for 2 hours with 100 ml of 1 N $MgCl_2$ solution, a procedure described by Catt (1990). The clay minerals were identified by X-ray diffraction on oriented slides. The chemical composition of bulk samples was analyzed by an X-ray fluorescence spectrometer. Trace elements were analyzed by Bondar-Clegg Geochemical Lab in Toronto. The ferrous iron content was determined by a titration method. Samples were dissolved in cold HF in the presence of a known amount of ammonium metavanadate (AMV), an oxidising agent. The ferrous iron present in the sample was oxidised quantitatively by the pentavalent vanadium, and the excess V^{5+} was titrated against standardized ferrous ammonium

Plate 4-1. Photos showing the paleosol S5-I. Left, the Chang'an section. Right, the Shijiawan section.

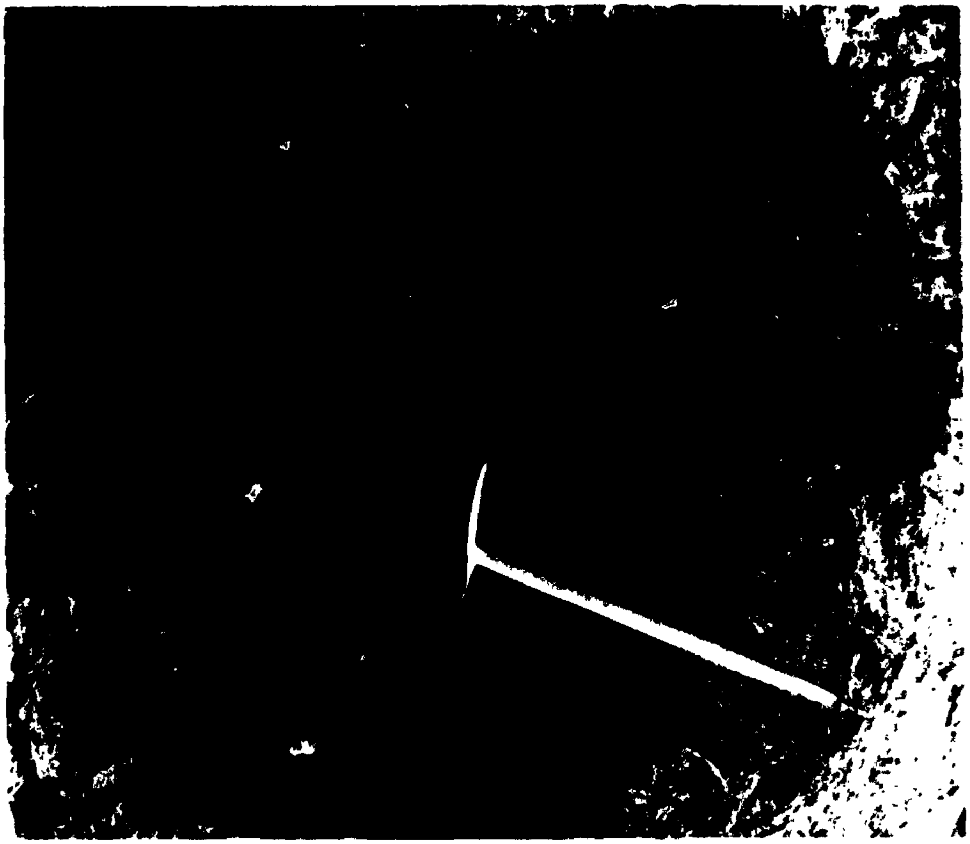

sulphate (FAS). The method is described in detail by Wu (1984). The organic matter was determined by a modified Walkley-Black method. The stable carbon-isotope composition of organic matter was measured using the procedures described in Chapter 3. The carbonate content was determined with the Chittick apparatus (Dreimanis, 1962).

4.4. Results and Discussion

In this section, the analytical data for both the Shijiawan and Chang'an profiles are presented. In order to avoid confusion, discussions are focused on the Shijiawan profile.

4.4.1. Grain-size Distribution

Granulometric analyses of S5 in the Shijiawan and Chang'an sections are listed in Table 4-2. Silt (4-9ϕ, equivalent to 0.063-0.002 mm) is the major component and clay ($>9\phi$, i.e. <0.002 mm) the second major component in all the samples throughout the profiles. Sand (0-4ϕ, 1-0.063 mm) makes a negligible contribution. The obvious variations of the grain-size composition along the profiles are found in the clay-sized fraction. In the Shijiawan section (samples W27 to 31), clay-sized particles increase with depth and reach maximum proportion in the Bt horizon (W29), then decrease downwards and reach the minimum at the C horizon (W31). In contrast, the coarser grains ($<4\phi$, >0.063 mm) are enriched in upper horizons. In the Chang'an section, the minimum clay content occurs in the A horizon. This implies that a profound clay fraction was intensively eluviated from the A horizon during pedogenesis and the post-pedogenic deposition of loess was mixed with the top soil layer.

Table 4-2. Grain-size distribution of S5 in the Shijiawan and Chang'an sections.

Sample#	horizon	<3ϕ	3-4ϕ	4-5ϕ	5-6ϕ	6-7ϕ	7-8ϕ	8-9ϕ	9-10ϕ	>10ϕ
W27	A	--	0.4	6.0	17.6	17.0	16.0	8.0	6.0	29.0
W28	A-Bt1	--	0.4	4.6	20.0	22.5	7.5	7.0	6.5	31.5
W29	Bt1	--	0.1	10.9	10.0	15.0	14.0	5.5	5.5	39.0
W30	Bt2	--	0.1	8.4	11.5	17.	15.7	6.8	6.0	34.0
W31	Cw	--	<0.1	9.9	20.0	22.5	9.5	8.5	9.5	20.0
CHA1	A	--	0.2	18.3	16.5	18.0	11.0	8.0	4.0	23.0
CHA2	A	--	0.4	9.6	17.0	23.0	12.0	10.0	6.0	27.0
CHA3	Bt1	--	0.4	5.1	22.5	14.0	13.0	8.0	7.0	30.0
CHA4	Bt1	--	0.4	3.6	14.0	21.0	14.0	7.0	6.0	34.0
CHA5	Bt1	--	0.4	5.6	14.0	16.0	13.0	6.0	6.0	39.0
CHA6	Bt2	--	0.3	4.2	14.5	18.0	14.0	7.0	7.0	35.0
CHA7	Cw	--	0.2	4.8	18.0	17.0	14.0	7.0	6.0	31.0

4.4.2. Whole-rock Mineralogy

In general, whole-rock mineralogy of the S5 paleosol in both profiles is quite uniform with major minerals such as quartz, feldspar and mica present (Figures 4-1 and 4-2). Calcite is the most mobile constituent among all the minerals throughout the profiles, but it was not detected in the Bt horizons. Total amounts of chlorite and kaolinite (indicated by the height of the 7 Å peak) reached the lowest values in the Bt1 horizons (samples W29 and CHA5 in the Shijiawan and Chang'an sections, respectively).

4.4.3. Clay Mineralogy

Separated clay fractions were analyzed by X-ray diffraction and data are presented in Figures 4-3 and 4-4. The major clay mineral present in the profiles is illite, as indicated by peaks at 3.34, 4.98 and 10.05 Å. The minor minerals are chlorite, kaolinite, smectite and irregularly interstratified minerals.

Chlorite (the peaks 3.56, 4.72 and 14.25 Å in un-treated samples) decreased from the A horizon (W27) to the Bt1 horizon (W29), and then increased with depth. The presence of kaolinite throughout the profile, and also in the loess sample (Y01), was indicated by a decrease in the 14.1 Å peak in the heated samples (equivalent to the peak of about 14.2 Å in the unheated samples). It is evident that in the sample W29, a 7.1 Å peak still exists but the peaks around 14 Å are hardly seen.

In the Bt horizon (W29), a notable amount of vermiculite exists as evidenced by the 4.46 Å peak in the untreated sample and the 4.51 Å peak in the glycol-saturated sample. The existence of smectite is revealed by the peaks around 17 Å in glycol-treated samples and a rather stable peak at 14.2 Å in the untreated samples in which chlorite

Figure 4-1. XRD spectra of bulk samples of the S5-1 from the Shijiawan section.

2

PM-1 3½"x4" PHOTOGRAPHIC MICROCOPY TARGET
NBS 1010a ANSI/ISO #2 EQUIVALENT

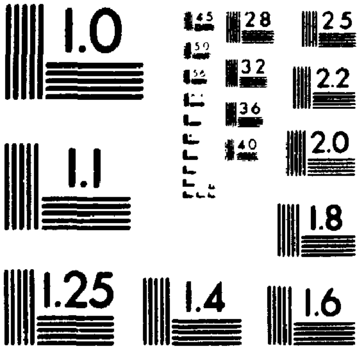

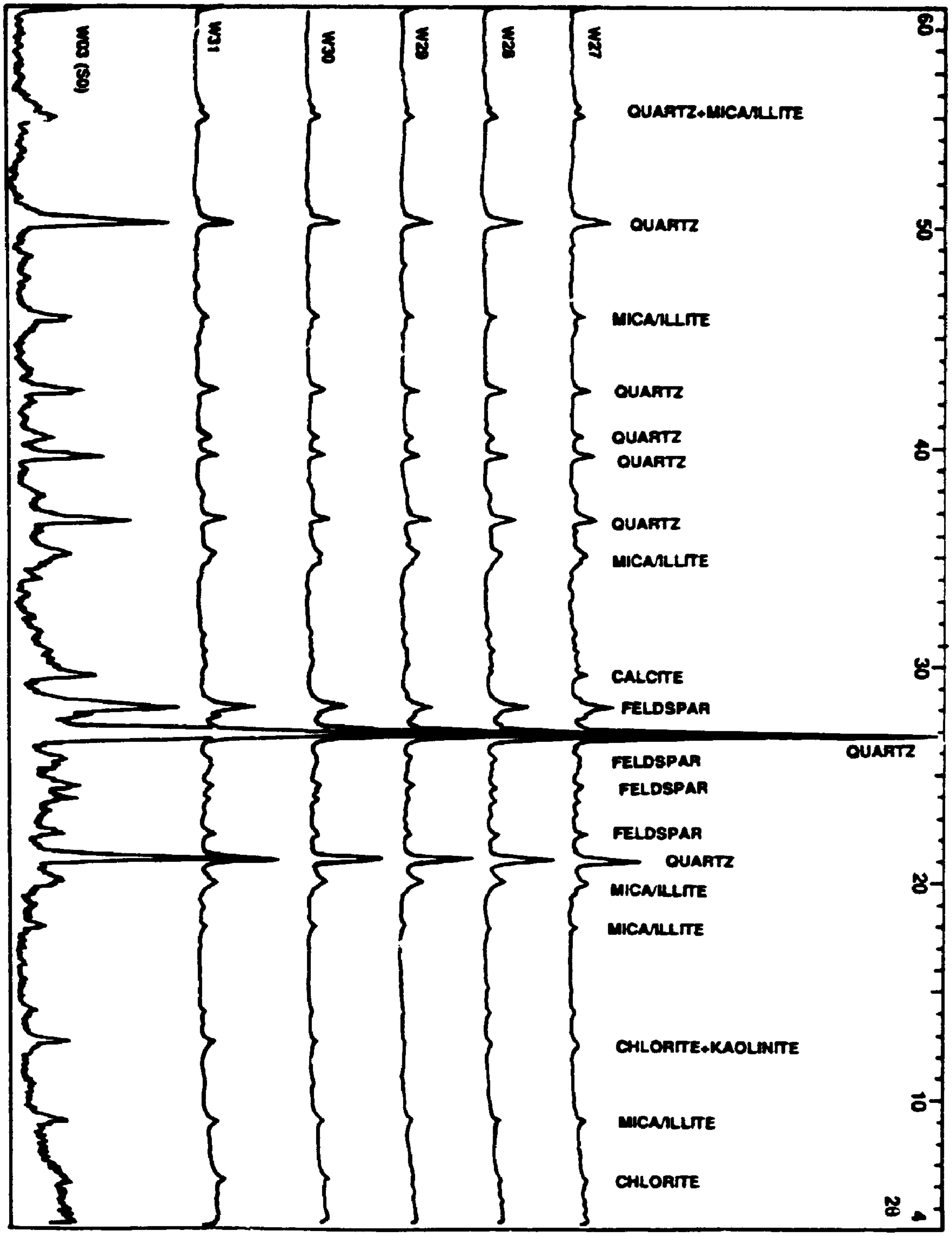

QUARTZ+MICA/ILLITE
QUARTZ
MICA/ILLITE
QUARTZ
QUARTZ
QUARTZ
QUARTZ
MICA/ILLITE
CALCITE
FELDSPAR
QUARTZ
FELDSPAR
FELDSPAR
FELDSPAR
QUARTZ
MICA/ILLITE
MICA/ILLITE
CHLORITE+KAOLINITE
MICA/ILLITE
CHLORITE
W03 (S0)
W31
W30
W29
W28
W27
60
50
40
30
20
10
4
2θ

Figure 4-2. XRD spectra of bulk samples of the S5-I from the Chang'an section.

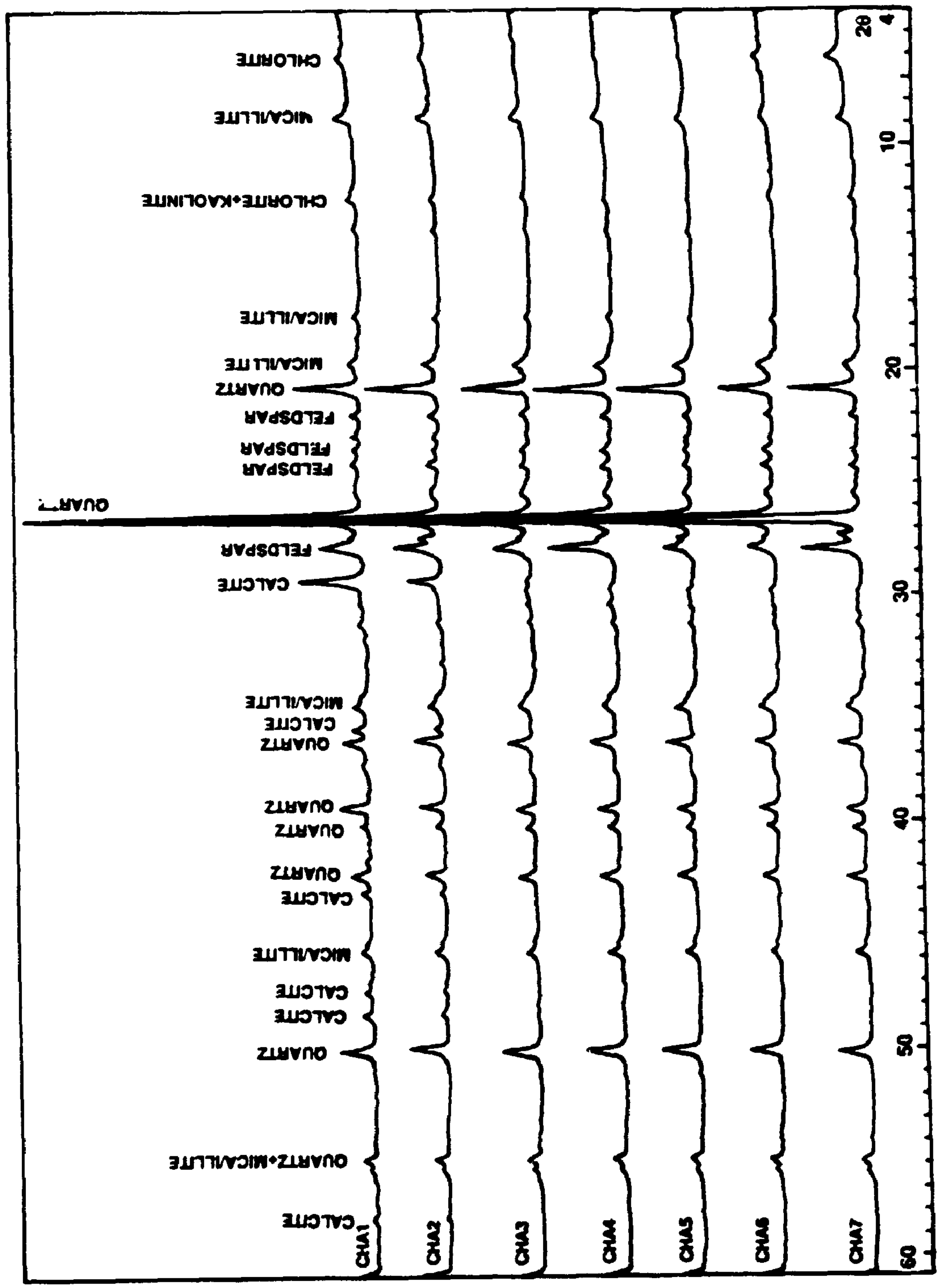

CHLORITE
MICA/ILLITE
CHLORITE+KAOLINITE
MICA/ILLITE
MICA/ILLITE
QUARTZ
FELDSPAR
FELDSPAR
FELDSPAR
QUARTZ
FELDSPAR
CALCITE
MICA/ILLITE
CALCITE
QUARTZ
QUARTZ
QUARTZ
QUARTZ
CALCITE
MICA/ILLITE
CALCITE
CALCITE
QUARTZ
QUARTZ+MICA/ILLITE
CALCITE
CHA1
CHA2
CHA3
CHA4
CHA5
CHA6
CHA7
2θ
4
10
20
30
40
50
60

Figure 4-3. XRD spectra of clay minerals in paleosol S5-I from the Shijiawan section. A, untreated oriented samples. B, glycol-treated samples. C, samples heated at 560°C for 4 hours. Sample Y01 taken from a loess layer.

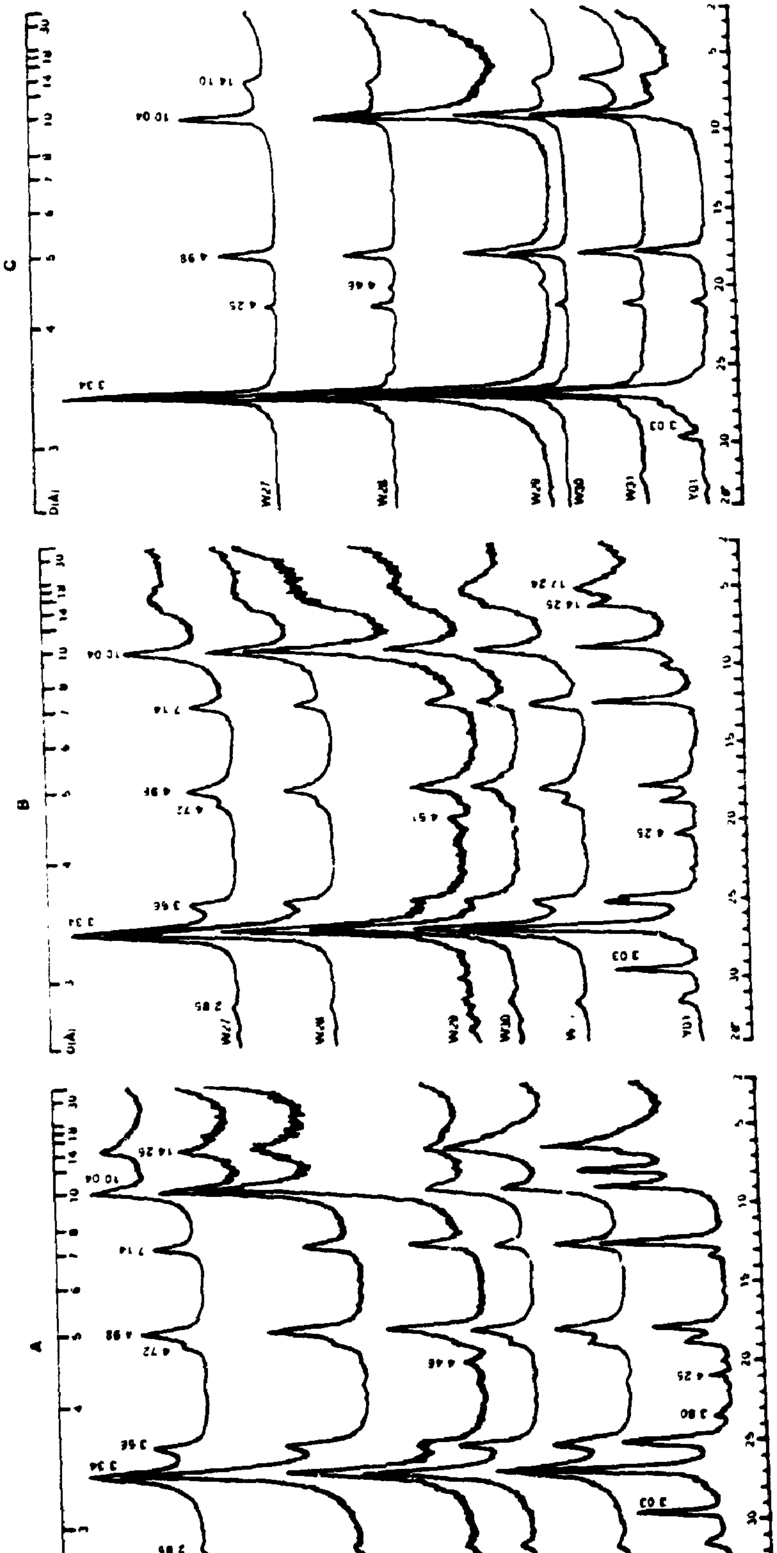

Figure 4-4. XRD spectra of clay minerals in paleosol S5-I from the Chang'an section. A, untreated oriented samples. B, glycol-treated samples. C, heated samples at 560°C for 4 hours.

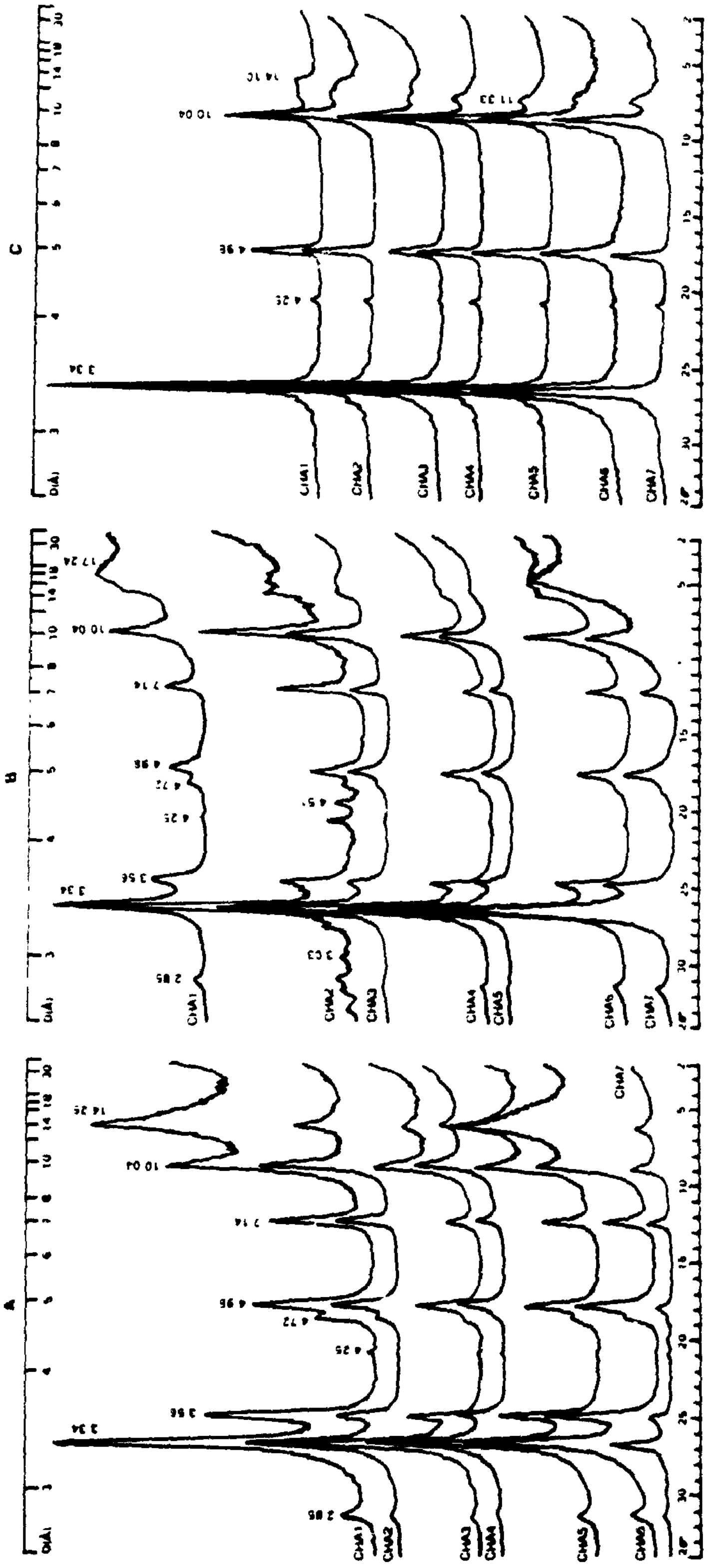
A
B
C
CHA1
CHA2
CHA3
CHA4
CHA5
CHA6
CHA7
3.34
10.04
4.96
7.14
3.56
4.25
4.72
14.25
2.85

barely exists. Irregularly interstratified minerals which were shown by a wide range of peaks between 14 and 30 Å in glycol-saturated samples increased with depth from the A to Bt1 horizon (W27 to W29 in the Shijiawan section and CHA1 to CHA5 in the Chang'an section). Very small amounts of quartz and calcite present in some samples were detected with peaks at 3.03, 4.25 and 2.85 Å.

4.4.4. Bulk Chemical Composition

Chemical analyses of the S5 paleosol for the two sections are presented in Table 4-3. In concordance with the mineralogical assemblage, the chemical composition throughout the profiles is dominated by SiO_2 and Al_2O_3, while CaO is the most variable. The highest concentrations of CaO occur in the A and C horizons, while the lowest concentrations occur in the Bt horizon. The total iron slightly increased from the A horizon to the Bt horizon and then decreased with depth. The variation of Al_2O_3 through the profiles has a similar pattern to that of total iron, and attains the highest value in the Bt horizon. The total loss of weight during ignition (LOI) depends mainly on the amount of organic matter, carbonate and swelling clay minerals present. For discussion of chemical weathering of the major elements through profile, carbonate concentration in each sample was determined, and the major chemical constituents were subsequently recalculated and listed in Table 4-4. The maximum concentration of organic matter in both sections is less than 0.2% (see Figure 4-5) and was neglected in the calculation. In the Shijiawan section, the variation of LOI percentage does not follow the pattern of the carbonate, implying that the clay minerals containing interlayer water are more abundant in the Bt horizon.

Table 4-3. Major chemical constituents of S5 in the Shijiawan and Chang'an sections.

Sample#	Horizon	SiO_2	TiO_2	Al_2O_3	Fe_2O_3	MnO	MgO	CaO	K_2O	P_2O_5	Na_2O	LOI
W27	A	63.4	0.8	14.6	5.7	0.1	2.2	2.1	2.9	0.08	0.9	6.8
W28	A-Bt1	64.0	0.8	14.7	5.8	0.1	2.0	1.6	2.9	0.29	1.1	6.5
W29	Bt1	62.0	0.7	15.7	6.4	0.1	2.1	1.0	3.0	0.07	0.7	7.7
W30	Bt2	62.9	0.8	15.3	6.2	0.1	2.2	0.8	2.9	0.06	0.9	6.8
W31	C1w	63.9	0.8	14.6	5.8	0.1	2.3	1.2	2.9	0.14	1.0	6.2
W32	2Bt1	63.2	0.8	15.0	5.8	0.1	2.2	1.5	3.0	0.07	1.1	6.5
W33	2Bt2	63.9	0.8	15.2	6.0	0.1	2.1	0.9	2.9	0.09	0.9	6.5
W34	C2w	65.4	0.8	14.4	5.5	0.1	2.2	1.4	2.8	0.12	1.2	6.0
W35	3Bt1	64.2	0.8	14.6	5.9	0.1	2.0	1.2	2.9	0.08	1.0	6.2
W36	3Bt2	64.6	0.7	14.7	5.6	0.1	2.3	1.3	2.9	0.14	1.3	6.0
W37	C3	58.5	0.7	13.0	5.0	0.1	2.2	7.2	2.5	0.13	1.4	9.6
L32	Loess	56.6	0.7	13.1	5.1	0.1	2.2	7.7	2.5	0.12	0.9	10.6
CHA1	A	58.4	0.7	13.1	5.1	0.1	2.1	7.0	2.5	0.13	1.2	9.0
CHA2	A	63.0	0.8	13.7	5.3	0.1	1.9	3.7	2.7	0.10	1.1	6.5
CHA3	Bt1	65.2	0.8	15.1	5.9	0.1	2.0	1.1	2.9	0.10	1.1	5.0
CHA4	Bt1	65.9	0.9	14.9	5.8	0.1	1.8	0.9	2.9	0.08	1.1	5.4
CHA5	Bt1	66.2	0.9	15.6	6.2	0.1	1.7	0.8	2.9	0.10	1.1	4.8
CHA6	Bt2	63.4	0.8	16.0	6.4	0.1	2.1	0.9	2.9	0.11	0.9	5.4
CHA7	CB	64.0	0.8	15.6	6.2	0.1	2.3	1.0	2.7	0.11	1.1	5.3
CHA8	CB	64.3	0.8	15.3	6.0	0.1	2.1	0.8	2.9	0.10	1.0	6.0
YGS0	A	62.7	0.7	15.1	5.9	0.1	1.8	1.4	2.7	0.09	1.0	7.4

Table 4-4. Major chemical constituents of the S5 in the Shijiawan and Chang'an sections after removal of carbonates.

Sample# /Horizon	SiO_2	TiO_2	Al_2O_3	Fe_2O_3	MnO	MgO	CaO	K_2O	P_2O_5	Na_2O	LOI	$CaCO_3$
W27/A	64.46	0.77	14.86	5.76	0.11	2.21	1.45	2.92	0.08	0.93	6.41	1.15
W28/A-B	64.71	0.79	14.87	5.84	0.11	2.01	0.85	2.89	0.29	1.06	5.79	0.77
W29/Bt1	62.22	0.74	15.79	6.46	0.11	2.10	0.74	2.98	0.07	0.65	7.54	0.41
W30/Bt2	62.98	0.76	15.31	6.16	0.10	2.19	0.72	2.87	0.06	0.94	6.75	0.16
W31/Cw	64.26	0.75	14.70	5.85	0.09	2.34	0.93	2.77	0.14	1.01	5.99	0.50
$CA1/A_{up}$	66.04	0.80	14.85	5.81	0.10	2.33	0.61	2.78	0.15	1.31	4.45	11.52
$CA2/A_{lo}$	66.82	0.88	14.58	5.57	0.12	1.98	0.50	2.86	0.11	1.12	4.24	5.73
CA3/Bt1	65.67	0.82	15.22	5.89	0.11	1.97	0.69	2.94	0.10	1.11	4.72	0.74
CA4/Bt1	66.10	0.87	14.98	5.77	0.12	1.82	0.71	2.91	0.08	1.13	5.23	0.33
CA5/Bt1	66.24	0.87	15.60	6.11	0.12	1.74	0.69	2.93	0.10	1.06	4.76	0.12
CA6/Bt2	63.48	0.76	16.03	6.36	0.11	2.06	0.84	2.87	0.11	0.88	5.38	0.12
CA7/Cw	64.22	0.77	15.66	6.18	0.10	2.26	0.85	2.74	0.11	1.12	5.20	0.14
CA8/Cw	64.50	0.77	15.33	5.99	0.14	2.05	0.67	2.94	0.10	1.02	5.92	0.12
LCS5/Bt	64.35	0.76	15.24	5.97	0.10	2.19	0.63	2.89	0.08	0.80	6.37	0.16

4.4.5. Trace Elements

Some 32 trace elements were analyzed for S5 from the Shijiawan section by the neutron activation method and data are listed in Table 4-5. Major changes through the profile occur with Mo, Ni, Co, Zn, As, Sb, Ba, Cr, Cs, La, Ce, Sm, Sc, Lu, The, U, Br, and Rb Based on their behaviours through the profile, the elements can be classified into three groups.

Like ferrous iron, Zn, Ni, Co, La, Ce, Sc, and Rb have the highest concentrations in the A horizon and the lowest concentrations in the CCa (Ca accumulation) horizon, reflecting that they reside mainly in the primary clastic minerals. The second group, including As, Sb, Cr, W, Cs, Th, U, and Br, reach the maximum concentrations in the best developed Bt horizon and the minimum concentrations in the CCa horizon, exhibiting a clear relationship with clay content. For the third group, involving noble metals like Au, Ir, Ag, etc., no obvious trend has been found through the profile. Barium behaves very similarly to calcium, indicating a close relation to carbonate.

4.5. Pedogenic Processes

4.5.1. Clay Translocation and Transformation

Grain-size analyses show that clay content increases with depth and reaches the highest value in the Bt horizon, which is consistent with the presence of the thickest clay coatings and suggests that the major process associated with the clay concentration is illuviation rather than argillation (Birkeland, 1974). The migration of clay minerals reflects the pedogenic conditions with a pH of no more than 7. This process can only

Table 4-5. Trace elements in S5 in the Shijiawan section

Sample#/ Horizon	Au ppb	Ir ppb	Ag ppm	Zn ppm	Mo ppm	Ni ppm	Co ppm	Cd ppm	As ppm	Sb ppm	Se ppm	Te ppm
W27/A	<2	<50	<2	190	2	59	25	<5	17.0	1.8	<5	<10
W28/AB	6	<50	<2	200	1	39	17	<5	18.0	1.8	<5	<10
W29/Bt	<2	<50	<2	140	<1	25	21	<5	20.0	2.0	<5	<10
W30/CCa	<2	<50	<2	110	2	<10	<5	<5	4.1	0.5	<5	<10
W31/Cw	<2	<50	<2	140	<1	50	19	<5	15.0	1.7	<5	23
W32/2Bt1	3	<50	<2	160	<1	47	20	<5	19.0	1.9	<5	<10
W33/2Bt2	<2	<50	<2	200	1	64	18	<5	19.0	2.0	<5	<10
W34/2BC	<2	<50	<2	190	<1	29	17	<5	16.0	1.9	<5	<10
W35/3Bt1	<2	<50	<2	160	<1	25	19	<5	17.0	1.8	<5	<10
W37/3C	<2	<50	<2	200	<1	38	15	<5	16.0	1.7	<5	<10

Sample#/ Horizon	Ba ppm	Cr ppm	Sn ppm	W ppm	Cs ppm	La ppm	Ce ppm	Sm ppm	Eu ppm	Tb ppm	Yb ppm	Lu ppm
W27/A	630	120	<100	2	9.1	50	110	6.5	3	0.9	5	0.6
W28/AB	660	130	<100	3	9.5	43	100	6.1	<1	1.1	4	0.3
W29/Bt	580	100	<100	4	11.0	43	90	6.6	2	0.9	4	0.4
W30/CCa	5000	34	<100	<1	2.3	11	21	1.9	<1	<0.5	<2	<0.2
W31/Cw	550	87	<100	3	9.2	40	83	6.4	2	1.2	4	0.4
W32/2Bt1	590	92	<100	3	10.0	40	89	6.4	<1	0.9	3	0.3
W33/2Bt2	610	110	<100	2	11.0	47	100	7.5	1	1.2	5	0.5
W34/2BC	600	100	<100	3	10.0	43	85	6.9	<1	1.1	4	0.4
W35/3Bt1	570	90	<100	2	9.2	41	87	6.9	1	1.2	4	0.5
W37/3C	550	95	<100	1	7.7	37	81	6.3	<1	0.9	4	<0.2

Sample#/ Horizon	Sc ppm	Hf ppm	Ta ppm	Th ppm	U ppm	Br ppm	Rb ppm	Zr ppm
W27/A	18.0	8	1.7	15.0	3.1	<0.5	200	<200
W28/AB	16.0	8	1.5	16.0	3.5	0.6	190	<200
W29/Bt	17.0	6	1.5	16.0	3.2	3.4	190	<200
W30/CCa	4.2	3	<0.5	3.9	1.3	<0.5	38	<200
W31/Cw	14.0	7	1.5	15.0	2.9	<0.5	180	<200
W32/2Bt1	16.0	7	1.3	16.0	3.3	<0.5	190	<200
W33/2Bt2	16.0	7	1.2	17.0	3.3	<0.5	210	<200
W34/2BC	14.0	6	1.3	16.0	3.3	<0.5	180	490
W35/3Bt1	14.0	7	1.4	15.0	3.2	<0.5	170	<200
W37/3C	13.0	6	1.2	14.0	3.1	<0.5	170	<200

occur when carbonate is completely leached out.

The downward decrease of chlorite, and occurrence of vermiculite in the Bt horizon (W29) implies that the clay minerals have been subjected to transformation. Vermiculite is most likely of pedogenic origin (Tan, 1994). According to previous studies, vermiculite may be derived from chlorite and micas (cf. Yatsu, 1988; Evans, 1992), and micas are readily altered to vermiculite by the extraction of potassium, and chlorite by oxidation of Fe^{2+} (Ross, 1975; Ross and Kodama, 1976). Our chemical data, however, show that potassium increased and magnesium decreased in the Bt horizon, which seems to favour a chlorite-alteration, as is suggested by the clay mineralogical study. A pH value less than 7 is necessary for the transformation of chlorite into vermiculite (Birkeland, 1974).

The XRD spectra of ethylene glycol-treated samples demonstrate that smectite exists in all horizons but is less abundant in the Bt horizon, and irregular interstratified minerals make up a notable portion in the Bt horizon. The possibility of a decreased smectite signal resulting from alteration of smectite into kaolinite needs to be further confirmed. Regardless of the pathways, the pH values required by the process must be in the range of 5-7 (Birkeland, 1974; Yatsu, 1988), similar to that of the chlorite-vermiculite transformation.

Overall, the following alterations may have occurred.

Chlorite - Mg^{2+}, Fe^{2+} $\rightarrow$ Vermiculite + interstratified material;

Illite - K^+ $\rightarrow$ Vermiculite + interstratified material;

Smectite - H_4SiO_4 $\rightarrow$ Kaolinite.

4.5.2. Variations of the Major Chemical Constituents

Carbonate analyses indicate that the Bt horizon has experienced complete decalcification, and secondary carbonate accumulation has occurred in the CCa horizon at 1.9-2.6 m depths below the S5 surface as observed in the field. The carbonate depletion in the Bt horizon is consistent with the clay mineralogical data. The presence of carbonate in the upper horizons as indicated by chemical data is due to post-pedogenic carbonate leaching from overlying loess, which is suggested by the fact that the carbonate in the A horizon exists as white coatings or pseudomycelia on the cracks.

Besides $CaCO_3$, SiO_2 and Al_2O_3 are the second most pronounced labile constituents. SiO_2 decreases with illuviation whereas Al_2O_3 varies inversely to SiO_2. Microscopic study of the clastic minerals revealed that quartz and feldspars did not suffer serious alteration. The chemical data also indicate that potassium, magnesium and sodium are incorporated in the silicates (see Table 4-4) with only a slight change. Therefore, a higher SiO_2/Al_2O_3 ratio in the Bt horizon is mainly the result of clay translocation. To evaluate the degree of chemical weathering, the chemical index of alteration (CIA) was calculated as proposed by Nesbit and Young (1982). It is presented by using molecular proportions:

$$CIA = \langle Al2O3/(Al2O3 + CaO + Na2O + K2O) \rangle \times 100$$

where CaO is the amount of CaO incorporated in the silicate minerals. Here the CaO content used is from the data after removal of carbonates as shown in Table 4-4. Variations can be seen from Table 4-6 and Figure 4-5.

Table 4-6. CIA values of S5-I in the Shijiawan and Chang'an sections.

Shijiawan Section		Chang'an Section	
Horizon	CIA	Horizon	CIA
A	66.96	A	70.30
AB	69.86	A	71.45
Bt1	73.68	Bt1	70.85
Bt2	71.96	Bt1	70.39
Cw	69.82	Bt1	71.64
		Bt2	72.48
		Bt2	71.18
		Cw	71.59

Figure 4-5. Graphic illustrations of variations in clay-sized fraction and some chemical factors through paleosol S5-I. Solid circles represent samples from the Shijiawan section, open circles represent samples from the Chang'an section.

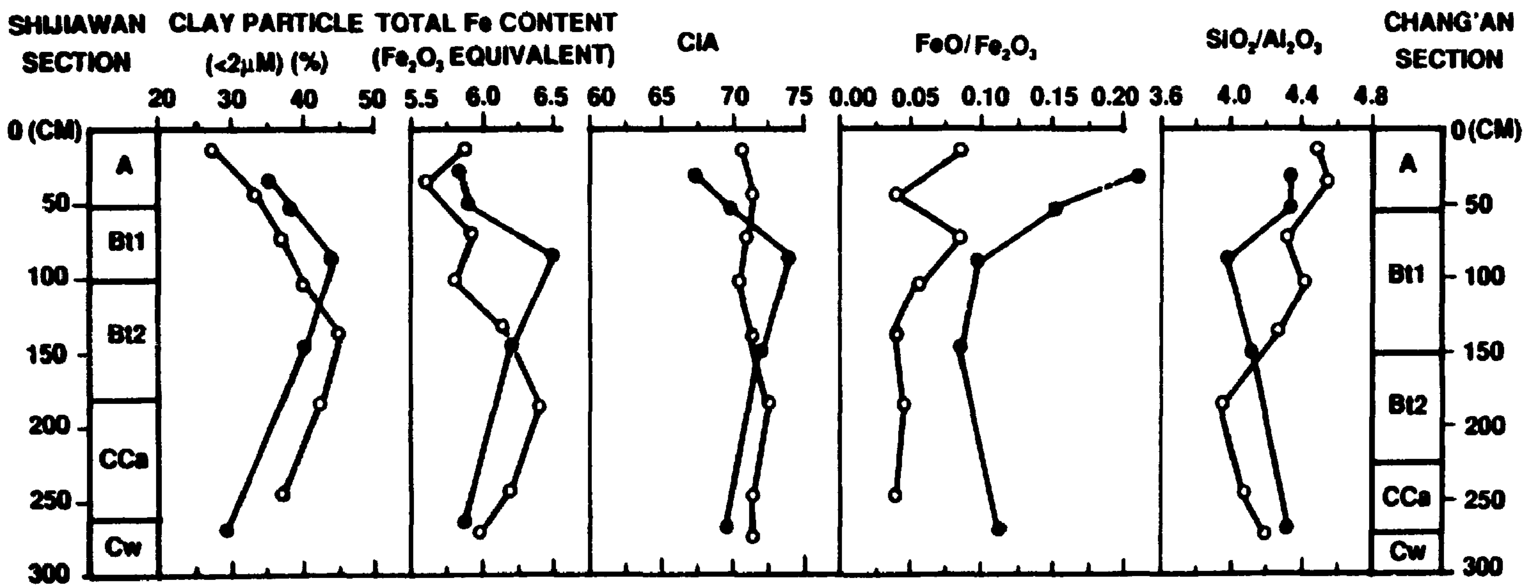

SHIJIAWAN SECTION
CLAY PARTICLE (<2μM) (%)
TOTAL Fe CONTENT (Fe_2O_3 EQUIVALENT)
CIA
FeO/Fe_2O_3
SiO_2/Al_2O_3
CHANG'AN SECTION
20 30 40 50
5.5 6.0 6.5
60 65 70 75
0.00 0.05 0.10 0.15 0.20
3.6 4.0 4.4 4.8
0 (CM) 50 100 150 200 250 300
A
Bt1
Bt2
CCa
Cw

It is demonstrated that the CIAs for all horizons are slightly different. The highest value found in the Bt horizons and the lowest in the A horizon of the Shijiawan section suggest that the chemical variations have resulted mainly from mechanical translocation of clay-size particles, and that chemical weathering in the S5 is slight. In fact, similar results of chemical composition between loess and paleosols have been shown by previous studies with large number of samples (e.g., Liu et al., 1985). Unfortunately, these were not taken into consideration in their paleoclimatic interpretation, probably because these data do not favour their impression in terms of the presumed contrast between loess and paleosols as is visualized in colour (for dada refer to Liu et al., 1985, p240-243).

The variable trend of the CIA through the Chang'an profile does not follow the pattern observed in the Shijiawan section, and may be attributed to other factors (eg., drainage conditions, aggradation etc.) associated with the relatively low altitude of the river-terrace when the S5 was developing.

The total iron content varies in a trend similar to that of Al_2O_3 and the clay content (see Table 4-4 and Figure 4-5). Compared with parent loess, the total iron is slightly concentrated with highest value in the most-developed illuvial horizon, while the highest concentration of FeO is found in the A horizon. Magnetic susceptibility measurements indicate the highest values in the A horizon. This coincidence implies that FeO is principally concentrated in magnetite, suggesting a weak chemical alteration and leaching process experienced by the S5 in Shijiawan, although it may largely have been comminuted during pedogenesis. Higher concentrations of Fe_2O_3 resulted from fine hematite translocated with clay migration and in situ oxidation of magnetite.

Fe-Mn films in the Bt horizon were observed in the field and confirmed by SEM analysis. It will be argued that it is an indicator of leaching conditions rather than gleying or pseudogleying conditions (seasonally over-saturated with water). Further discussion will be given in Chapter 5.

4.6. $\delta^{13}C$ signatures of Organic Matter and Paleovegetation

The stable carbon-isotope composition of organic matter in S5-I was determined and presented graphically in Figure 4-6. Obviously, C4 plants constituted a pronounced portion of the paleovegetation. The isotopic signatures changed notably along the profiles, and these variations follow a similar pattern in both sections. The highest $\delta^{13}C$ values occur in the Bt horizon and lowest values occur in the top and bottom horizons. Measurements of the organic matter content in the two sections (see Figure 4-6) indicate that the highest concentration occurred at depths around 1.0 m in Shijiawan, which is consistent with clay illuviation. This may be partly attributed to migration of organic matter, but the pronounced difference in $\delta^{13}C$ values between the A and Bt horizons can only be explained by a pedogenic history with both vegetational change and loess deposition. Therefore the leaching processes seem to have a minor vertical mixing influence on organic matter distribution. Gradual decrease of organic matter content in the Shijiawan section from 1.0 m to the bottom suggests that below the depth of about 1 m, there is no other pedogenic A horizon buried. The $\delta^{13}C$ variation in this depth range could be explained by the difference in organic matter contribution depths between C3 and C4 plants. Above 1.0 m depth, it most likely reflects a progressive floral change. For the Chang'an section, two separate vegetation histories are suggested according to changes in organic matter concentration.

Figure 4-6. $\delta^{13}C$ signatures of organic matter in paleosol S5-I from the Shijiawan and Chang'an sections. Solid circles represent the samples from Shijiawan, and open circles represent the samples from Chang'an. The equivalent percentage of C4 plants is explained in Figure 3-1.

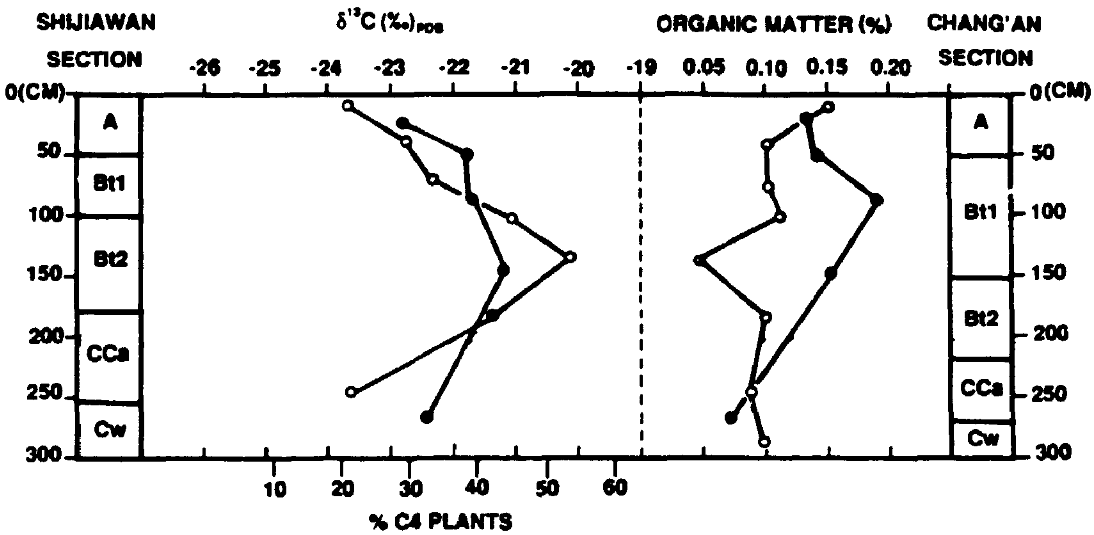
SHIJIAWAN
SECTION
δ13C (‰)PDB
-26 -25 -24 -23 -22 -21 -20 -19
ORGANIC MATTER (%)
0.05 0.10 0.15 0.20
CHANG'AN
SECTION
0(CM)
50
100
150
200
250
300
A
Bt1
Bt2
CCa
Cw
10 20 30 40 50 60
% C4 PLANTS

Overall, the stable carbon-isotope evidence reveals that during the S5-I development, the regional vegetation experienced a profound change, from a flora with about 50% C4 plants to floras with about 20% C4 plants, at least indicating that a typical forest never stood for an identifiable period. A very short depth range for C3-dominated $\delta^{13}C$ signatures in the upper horizon is demonstrated in both sections. If these low $\delta^{13}C$ values were derived from a forest, such low values should have been maintained for a much longer depth range, because tree roots are commonly distributed over 1 m in depth in this region as observed today, and their contributions to $\delta^{13}C$ value could not be masked by C4 grasses of the minor floral constituents especially at greater depth. Therefore, the occurrence of C3-dominated $\delta^{13}C$ signatures in the upper horizon in the both sections does not seem to reflect a forest flora, because many herbs and grasses in this region are C3 as discussed in Chapter 3 (referred to Figure 3-1). In the Shijiawan section, relatively stable $\delta^{13}C$ values (reflecting about 40% C4 plants) would suggest that the paleovegetation of the S5-I was dominated by grassland with a minor portion of trees. In Chang'an, a grassland with more than 50% C4 plants is clearly indicated by the $\delta^{13}C$ record (see Figure 4-6).

4.7. Climatic Evaluation

Most previous paleoclimatic studies on the loess-paleosol sequences have estimated paleoclimate by the correlation of pedogenic features of paleosols with modern soils and by analogy with the climatic conditions (mean annual temperature and rainfall). As previously mentioned, the methodology employed is quite questionable, because it is very difficult to constrain the effects of parent material and pedogenic duration which cannot be neglected in climatic interpretation. For example, consider two soils (A and B) with the same parent material, relief and complete decalcification, if A is just half of B in pedogenic duration, it must be double B in leaching-effective rainfall. But an equal precipitation might be estimated without consideration of time-effect.

The magnetic susceptibility (MS) record in the Chinese loess-paleosol sequence provides another approach to the paleoprecipitation. Heller et al. (1993), Maher et al. (1994), and Liu et al. (1995) statistically demonstrated a good relationship between MS of modern soils and annual precipitation in the regions of the Chinese Loess Plateau. Using such relations, the MS signals in the loess-paleosol sequences were interpreted in terms of paleorainfalls. In fact, the mechanism behind this relation is still poorly understood, although the MS of the loess and paleosols is convincingly demonstrated to be greatly enhanced by pedogenesis (Heller and Liu, 1984; Zhou et al., 1990; Maher and Thompson, 1991; Zheng et al., 1991; Verosub et al., 1993). Our measurement of the MS indicated that the most intensively pedogenic paleosol (S5-I) in the Shijiawan section does not possess the highest MS, in agreement with the Baoji section which is also located in the Guanzhong basin (cf. Wang et al., 1990). When a soil achieves complete decalcification, high precipitation will lead to oxidation of superparamagnetic grains of magnetite, the major MS contributor for the loess and paleosols (Maher and Taylor, 1988; Verosub et al., 1993), and hence to a decrease of the MS. Therefore, a steady state of MS for pedogenic origin suggested by Maher et al. (1994) is very limited in terms of consideration of climatic conditions and time-length of pedogenesis. A large discrepancy of MS-interpreted paleoprecipitation for the S1 in Xifeng between Heller et al. (1993) and Maher et al. (1994) (Maher- about 150-200 mm more than today without consideration of pedogenic duration; Heller- equal or slightly less than today with consideration of the pedogenic duration) indicates that the pedogenic enhancement of MS is time-dependent. Furthermore, it has been found by this study that the MS enhancement is also affected by the organic matter content and leaching state. Therefore, a proper interpretation of paleoclimatological significance of the MS signatures and its climofunction validity needs additional work.

As approximated by Kukla et al. (1988), Kukla and An (1989) and Ding et al. (1991), the pedogenic duration of the S5-I is about 40-50 ka. Assuming 10% of calcite in the parent loess and $1.7 g/cm^3$ of the specific weight (Liu et al., 1966) at 25°C and $3.5x10^{-3}$ atm. of pCO_2 in the subsoil zone with a saturate solubility about 0.2g/litre (cf. Richardson and Mcsween, 1989), $2.55x10^5$ cm of the leaching-effective rainfall was calculated to be necessary for a 3 m column of loess to be completely decalcified. A calibration of the effectiveness of regional rainfall for carbonate leaching based on a Holocene soil indicates the effectiveness of the annual precipitation is about 15%, i.e., the total amount of natural rainfall is about 6.7 times as much as the calculated effective rainfall required for complete decalcification. For S5-I in the Shijiawan section, if about 600 mm of today's local rainfall is used in the calculation, the complete decalcification would be acquired after 27 ka, a time-length far less than the actual duration. Our chemical analyses show other labile constituents (e.g., MgO, Na_2O, K_2O, etc.) with little significant change, indicating no obvious advance of chemical leaching other than decalcification. As is observed today, the annual rainfall in this region is concentrated in July, August, September and October, and a seasonal water-saturated state can be expected. Once a complete decalcification in the upper horizon is achieved, clay mineral migration takes place readily. Therefore, the climatic conditions reflected by S5-I in Shijiawan and Chang'an, as well as the whole Guanzhong basin are at best similar to, or even drier than today. The vegetation during that period was dense grassland-dominant, which is necessary for the formation of the well-developed clay coatings and later Fe-Mn films.

A further discussion on the amplitudes of the Pleistocene climate oscillations in the Chinese Loess Plateau will be given in Chapter 6.

CHAPTER 5

CLIMATIC CHANGE IN THE PERIOD OF LATE PLIOCENE-EARLY PLEISTOCENE

5.1. Introduction

From the data of Chapter 2, it has been shown that the fluviolacustrine sequence in the lower part of the Shijiawan section was formed during a period from 3.05 to 1.9 Ma B.P., and the upper red clay formation in the Yanyu section was formed in the interval 2.9-2.5 Ma. In this chapter, the intention is to discuss the climatic reconstruction of the period from late Pliocene to early Pleistocene (3.0 to 1.9 Ma) based on sedimentary and palynological analyses, and stable carbon-isotopes of organic matter. Through laboratory analyses of grain-size distribution, major chemical composition, clay mineralogy and other pedogenic studies, the provenance of the red clay and its paleoclimatic implications are discussed.

5.2. Sedimentary Analysis of the Fluviolacustrine Sequence

5.2.1. Major Sedimentary Features

The lithologic features of the fluviolacustrine sequence in the Shijiawan section (Figure 5-1) are summarized as follows.

1. The grain size data of the sequence indicates deposition with strong rhythms and sedimentary cycles. Each cycle starts with a coarse sand bed and then switches to a poorly sorted loam or silty clay bed. The top layer of most of the sedimentary cycles is

Figure 5-1. A lithologic column with descriptions of the fluviolacustrine sequence shown in the lower part of the Shijiawan section.

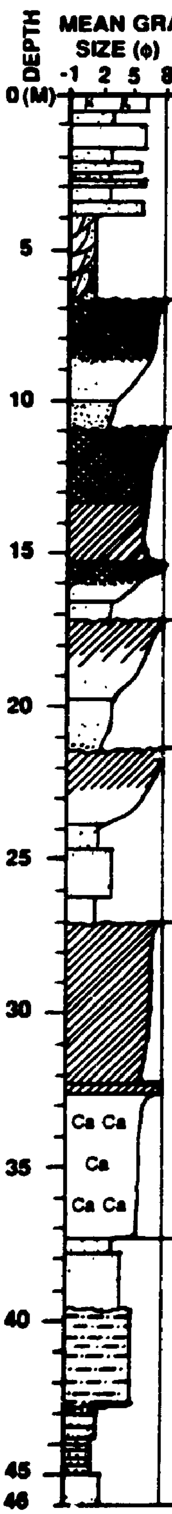

DESCRIPTION

Sand and sandy loam alternations.
Sand beds: Feldspathic litharenite, light grey to yellow grey, loose, poorly sorted and sub-rounded.
Sandy loam beds: Dark grey, poorly sorted, massive structure, firm, rich in biotite. The uppermost sand bed is well-cemented with $CaCO_3$.
Bottom: a coarse sand bed with some gravels (~2 mm), moderately sorted, large cross beddings; sharp boundary.

Upper: Reddish brown silty clay, dense, firm, large angular blocky structure, bright red clay coating; paling downwards; abundant gleying halos and black mottles, massive structure in subzones; coarse sand increases with depth; smooth boundary.
Lower: Grey-yellow to grey green sandy loam, poorly sorted, dense, firm; containing silty clay crumbs; abundant yellowish rust halos; sharp boundary.

Upper: Reddish brown silty clay with coarse sand, dense, firm, strong large-medium blocky structure at top, weakening downwards, abundant clay coatings and Fe-Mn films; massive structure with rusty mottles in subzones; fairly strong blocky structure with thick clay coatings in the lower horizon; smooth boundary.
Lower: Pale brown sandy silt and fine sand, poorly sorted, rusty yellow and grey green mottles, abundant dark minerals; semi-cemented; sharp boundary.

Upper: Brown red silty clay, dense, firm, large angular blocky structures coated with Fe-Mn film, abundant grey-blue mottles; paling downwards; coarse sand increases with depth; smooth boundary.
Lower: Yellowish brown fine sand with coarse sand, dense, firm, poorly sorted, massive structure, abundant biotite; sharp boundary.

Upper: Pale brown silty clay, dense, firm, weak angular blocky structure, abundant black films and rusty yellow mottles; lower horizon contains ~20% coarse sand; smooth boundary.
Lower: Sandy silt bed alternations, yellowish green to grey green in colour, fairly sorted, rich in rust halos; the bottom layer is a grey-white fine sand bed with abundant biotite, loose; sharp boundary.

Upper: Yellowish brown loam, dense, firm, large angular blocky structure and pellety crumb structure; more abundant clay fraction, small Fe-Mn nodules and rusty halos in the subzone; smooth boundary.
Lower: A pale pink Ca precipitation bed with small Ca-nodules; well cemented; silty clay matrix; sharp boundary.

Sand and silt bed alternations. From top to bottom:
1. Dark green fine sand with grey-white and rusty yellow halos; containing some small Ca-nodules; loose, sharp boundary.
2. Grey-blue silt, dense, firm, developed rusty yellow halos, containing some small Ca-nodules.
3. Grey clayey silt with developed horizontal beddings; abundant biotite in the lower part.
4. Dark grey sand bed with interbedded thin silt lenticles; sharp boundary.

CONTINUED

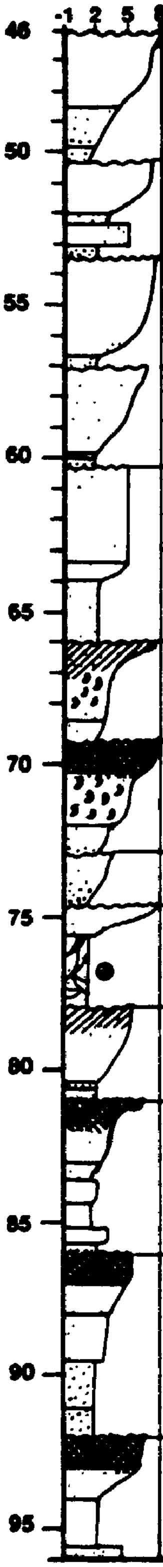

DESCRIPTION

Upper: Dull reddish brown silty clay, weak angular blocky structure; abundant black spots; coarse sand increases downwards; smooth boundary.
Lower: Grey-green coarse sand, poorly sorted, poorly rounded; abundant Ca-nodules; the bottom is well-cemented; sharp boundary.

Upper: Grey-yellow silty clay, dense, firm, poorly sorted, massive structure with rusty halos; coarse sand and fine gravels increase downwards; smooth boundary.
Lower: grey-white fine sand bed and loam bed alternation, poorly sorted, dense, massive structure; sharp boundary.

Upper: Pink-grey silty clay, large angular blocky structure with rusty halos; coarse sand increases downwards; smooth boundary.
Lower: Coarse-sandy loam, poorly sorted, grey blue to rusty yellow in colour, semi-cemented, sharp boundary.

Upper: Reddish coarse-sandy loam, dense, hard, massive structure; coarse sand increases downwards; smooth boundary.
Lower: Sandy beds, grey-white to yellowish white in colour, medium to fine in size, loose or firm; sharp boundary.

Upper: Pale brown sandy loam with poorly sorted and poorly rounded fine gravels, dense, firm, abundant grey-blue and rusty mottles, Ca-nodules in the lower horizon.
Lower: Sandy bed with fine gravels, poorly sorted and poorly rounded, yellowish green to black in colour, firm in the upper horizon but loose in the lower; abundant amorphous manganese precipitated in the lower part; sharp boundary.

Upper: Dull pink-grey loam, dense, firm, massive structure with rusty and pale blue halos; coarse sand increases downwards.
Lower: Fine sand with fine gravels, poorly sorted, containing small Ca-nodules in the lower part; sharp boundary.

Upper: Bright reddish brown silty clay, strong blocky structure, thick clay coatings with weakly developed Fe-Mn films; coarse sand increases downwards.
Middle: Small-sized Ca-nodules accumulation zone, red loam matrix with coarse sand.
Lower: Yellowish brown fine sand, containing coarse sand and red clay crumbs, semi-cemented.

Brick-red sandy clay, massive structure; abundant coarse sand and red clay crumbs in the lower horizon, rich in dark minerals; sharp boundary.

Upper: Pink brown clay with coarse sand, massive structure with rusty yellow halos, rich in black carbon film; coarse sand increases downwards.
Lower: Thick coarse sandy layer, grey-yellow to grey-white in colour, loose, well-developed large cross beddings, contains elephant fossils; sharp boundary.

Upper: Dark pink-grey silty clay with coarse sand, medium-angular blocky structure with rusty yellow and grey-blue mottles, rich in carbon films; coarse sand increases downwards; smooth boundary.
Lower: Sandy beds, light grey, rusty yellow and light pink in colour, coarse to fine in grain-size, poorly sorted; top part is well-cemented with $CaCO_3$; Sharp boundary.

Upper: Sandy clay with varicolored mottles, poorly sorted, fine blocky structure; containing fairly sorted fine sandy l[illegible]nticles; smooth boundary
Lower: Medium-sized sand, loose; sharp boundary.

Upper: Dull brown-red sandy clay, poorly sorted, fairly strong blocky structure, thick clay coatings; blocky structure weakens downwards, smooth boundary.
Middle: Pale reddish brown sandy clay, poorly sorted massive structure with rusty yellow mottles; coarse sand increases downwards, smooth boundary.
Lower: Rusty yellow coarse sand, containing small-sized gravels; bottom is cemented with $CaCO_3$; sharp boundary.

Upper: Dark reddish brown sandy clay, dense, strong large blocky structure with blue-grey mottles, thick clay coatings; coarse sand increases downwards; smooth boundary.
Middle: Dark grey to pale brown coarse sand with gravels, loose.
Lower: Pale brown sandy silt, poorly sorted semi-cemented.

characterized by relatively pure fine sediments. Approximately 20 cycles exist in the Shijiawan section.

2. Except for the middle part of the section (the interval from 40 m to 66 m in depth), each cycle was succeeded by a pedogenic period, which is manifested by occurrences of a Bt horizon with clay coatings and black Fe-Mn films, strongly developed blocky structure of the B horizon, and a carbonate accumulation horizon CCa.

3. Most of the beds are poorly sorted and exhibit massive structure. Sedimentary bedding is rarely found. With the exception of the sand layers, most beds show a bimodal size distribution. High frequencies of the grain-size distribution show coarse sand (about 1 mm) and fine silt or clay (<0.01 mm) fractions.

4. Most sedimentary beds are not stable in spatial extension and change their facies on a scale of hundreds of meters.

5. In the upper part of the sequence (0-66 m in depth), the fine-grained layers have a yellowish colour, very similar to that of the loess, and there is no difference from the loess of the region in the grain-size distribution pattern. In the lower part of the sequence (66-102 m), the fine-grained beds have reddish colour with a bimodal size distribution pattern, and the fine-size fraction is similar to that of the red clay. Therefore, this suggests that the major portion fine-grained sediments in the upper part of the sequence are reworked loess, and in the lower part are reworked red clay. According to grain-size composition and colour, the first typical reworked loess occurs at 61 m in depth and the last typical reworked red clay occurs at about 70 m.

5.2.2. Depositional Process

From the major sedimentary features discussed above, the fluviolacustrine sequence in the Shijiawan section shows a typical alluvial origin. Each sedimentary cycle contains coarse sand and silty layers, reflecting a hydraulic rhythm which is mainly controlled by paleohydrology. Obviously, the poorly sorted beds reflect a different hydraulic condition and suggest that they were formed by flooding. The coarse sand beds, especially those with abundant large cross-bedding, represent river-channel deposition. During flooding events, large amounts of fine-grained material were eroded from loess- or red clay-covered ground surface by rainwater discharged into river and deposited, which forced the river channel to shift. Combined with channel sediments, the flood deposition forms the binary structure of the sequence. Once the floodplain was high enough and acquired a stable surface, pedogenesis could take place. With evolution of the graben, a new sedimentary episode terminated the previous cycle. In this scenario, the sedimentary beds fluctuated from coarse channel sand to poorly sorted flood material (sand-mixed loam or silty clay). The thick and pure fine-grained top horizon of each cycle suggests that the post-depositional pedogenesis was accompanied by red clay or loess accumulation under subareal conditions. The deeper continuous carbonate accumulation zones reflects the paleo- groundwater table.

Overall, the conventionally called fluviolacustrine sequence in the Shijiawan section was mainly of fluvial deposition, and little seems to be of lacustrine origin. Variations in grain-size composition reflect cyclic deposition. Approximately 20 depositional cycles in the Shijiawan section started with channel sand deposition and ended with poorly sorted fine flood materials which are mainly reworked loess or reworked red clay. Most cycles involve a post-depositional pedogenic period. The first bed of reworked loess occurs at 56 m in depth, about 16 m below the Matuyama/ Gauss boundary, marking the beginning of loess deposition in this region. The cyclicity of the deposition reflects the river-channel shift, which could be caused by episodic tectonics or climatic fluctuations or both. More work is needed to confirm such a relationship.

5.2.3. Deposition Rate

With paleomagnetic dating constraints and an assumption of constant tectonic depression, the deposition rate can be estimated. The whole fluviolacustrine sequence in the Shijiawan section was dated in the period of 3.0 to 1.9 Ma B.P (see Chapter 2). The upper part (above the M/G boundary, from 2.48 to 1.9 Ma) has a thickness of about 40 m. Thus the mean deposition rate is approximately 6.9 cm/10^3 yr. The lower part (between the M/G boundary and the Kaena event, a period from 2.92 to 2.48 Ma B.P.) is 54 m in thickness, with an average deposition rate of 12 cm/10^3 yr. Using these data, a chronological framework of the sequence was constructed and is shown in Figure 5-2.

5.3. Palynological Data and Stable Carbon-Isotope Analysis

Some 57 samples through the sequence (excluding coarse sand beds) were taken for pollen analysis, and processed with laboratory methods for clastic sediments which are described as follows.

Samples were treated with 10% HCl to remove carbonate, passed through a 150 μm sieve, and then treated with HF to digest silica. The samples were then washed with distilled water and sieved through a 7 μm screen to remove silica gel and fine particles, and dehydrated with glacial acetic acid. A mixed acid (acetolysis and sulphuric acid at a ratio of 8:1) was added to remove organic material. Samples were washed, centrifuged, and mounted in silicon oil. Pilot samples were examined in the Microfossil Lab of Brock University, and the major analysis of pollen was conducted in the Pollen Laboratory of the Geological Institute, State Seismological Bureau of China. The results are presented in Figure 5-2.

All of the samples contain low concentrations of pollen, which may reflect a high depositional rate as suggested by its sedimentary environment (floodplain). Based on pollen concentration and assemblage, the whole sequence in the Shijiawan section is divided into three pollen zones, which is coincident with lithological subdivisions. The upper zone (Zone I) is 0-40 m in depth, just covering the interval between the beginning of the Olduvai subchron and the Matuyama/Gauss boundary. In this zone, each sedimentary cycle involves a thick developed pedogenic layer in a reworked loess bed. The middle zone (Zone II) refers to the interval from 40 to 66 m in depth, i.e. from the M/G boundary to the depth of 26 m below the boundary, covering a period from 2.48 to 2.7 Ma B.P. In this stage, no obvious indications of pedogenesis have been found. The lower zone (Zone III) includes the interval from 66 m to the bottom of the sequence of this section, and indicates a duration from 2.7 to 3.05 Ma B.P. The lower zone coincides the range of reworked red clay.

The upper pollen zone (1.90-2.48 Ma B.P.) is dominated by non-arboreal species. Some arboreal pollen has been found in most samples, and constitutes a notable portion (the highest ratio is near 50%) in some horizons. *Pinus* (Pine) is the major arboreal species in all the samples which contain arboreal pollen. *Quercus, Juglans, Ulmus, Rhus* and *Betula* are found in some samples, but constitute only a minor fraction.

Figure 5-2. Diagrams showing pollen spectra and $\delta^{13}C$ variations along the fluviolacustrine profile in the Shijiawan section. Chronological data were obtained by interpolations using age-constraints of paleomagnetic boundaries (details seen in the text). The pollen zone II, represented by open unshaded area in the pollen spectra, indicates a low concentration (usually <20 grains/10 gram).

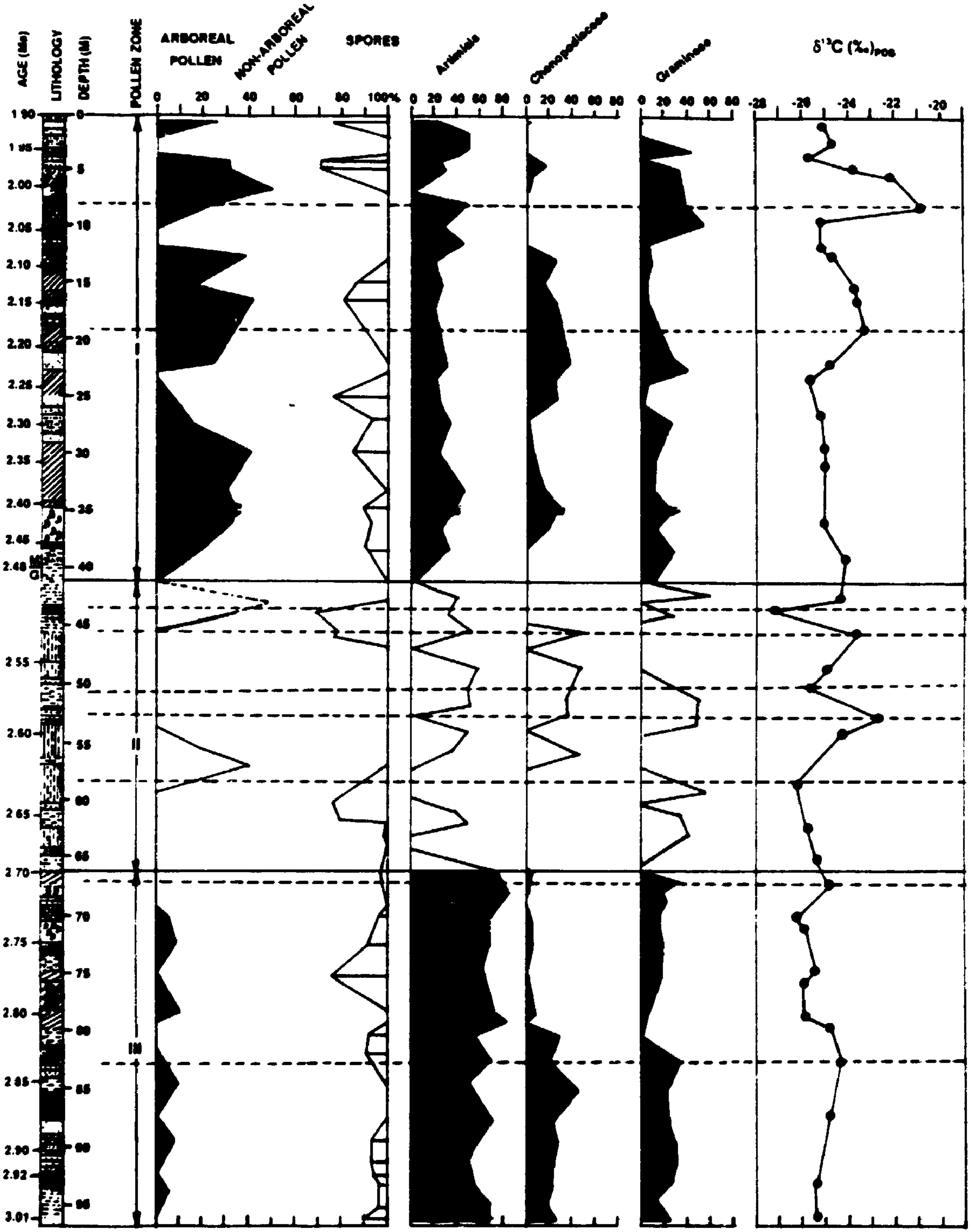
AGE (Ma)
LITHOLOGY
DEPTH (M)
POLLEN ZONE
ARBOREAL POLLEN
NON-ARBOREAL POLLEN
SPORES
Chenopodiaceae
Gramineae
I
II
III

Euphorbiaceae, *Abies*, *Castanea*, *Salix*, *Leguminosae*, *Engelhardtia*, Solanaceae and Cypressaceae are present in only a few samples. The major non-arboreal pollen types are *Artemisia*, Chenopodiaceae and Gramineae. *Humulus* and Compositae occur in some beds, and a few shrub taxa (*Corylus* and Ericaceae) were detected in some samples. In the lower part of this zone, some of spores commonly exist with taxa of *Selaginella*, Polypodiaceae, *Polypodium* and Filicales. Compared with the lower pollen zone, non-arboreal pollen in the upper zone has proportionataly more Gramineae and Chenopodiaceae but less *Artemisia*.

The middle zone (2.48-2.70 Ma B.P.) is characterized by very low pollen concentrations. There is very little diversity among the existing pollen taxa. Arboreal pollen and spores are rarely found. Except *for Artemisia* and Chenopodiaceae, the presence of the other species is negligible.

In the lower zone (2.7-3.0 Ma B.P.), non-arboreal species dominate all samples. The major taxa are *Artimisia*, Chenopodiaceae and Gramineae. Compositae commonly occur through the lower zone. As a minor constituent, *Selaginella* (spores) are also commonly present. These non-arboreal species constitute over 90% of the total pollen. Arboreal pollen present consists essentially of a single genus, *Pinus*, with very few *Salix* and *Betula* pollen grains in the lower bed and the uppermost bed of this zone. Generally, the lower zone shows a constant pollen concentration, exclusively dominated by non-arboreal species with narrow diversity.

5.4. Stable Carbon-Isotope Analysis

Some 40 samples were chosen for stable carbon-isotope analysis of organic matter (see methods described in Chapter 3). Due to low concentration of organic matter (0.022-0.067%) and thus higher heterogeneity, the reproducibility of $\delta^{13}C$ values is between 0.5 and 1.2 permil. The results obtained are presented in Figure 5-2. As discussed in Chapter 3, the $\delta^{13}C$ signature of organic matter depends on the source material and reflects a ratio of C3/C4 plants in the organic matter. As the sedimentary material was mainly derived from the pathways (floodplain sediments), the organic matter is a mixture of local vegetation, and should be identical to that of pollen in the sediments. Although more negative $\delta^{13}C$ values (around -26 permil) do not necessarily imply a forest flora (as is demonstrated by organic carbon-isotope study on modern vegetation and related soils in this region), it is useful for examining the validity of the conclusion from pollen analysis.

The variations in $\delta^{13}C$ signatures show good agreement with the pollen assemblage throughout the sequence (see Figure 5-2). In the lower zone, $\delta^{13}C$ values are close to -25 permil with a narrow range between -24 to -26, which is consistent with the pollen results that *Artemisia* (a C3 species) persistently exists as a dominant species throughout the interval. In contrast, Chenopodiaceae and Gramineae (C4 species) are only a minor component. A notably higher value of -24 permil coincides with a relative abundance of C4 plants. In the middle zone, the $\delta^{13}C$ signature fluctuated from a high value of -22 to a low of -27.5 permil and these data agree with the pollen data that the ratio of C3/C4 species (but all are non-arboreal plants) varies drastically. The lowest value corresponds to an abundance of *Artemisia* and the highest corresponds to abundant C4 species, Chenopodiaceae and/or Gramineae. In the upper zone, a pronounced $\delta^{13}C$ high was detected in an intensive pedogenic layer, corresponding to a large proportion of C4 plants as indicated by pollen spectra.

5.5. Paleovegetation and Paleoclimatic Interpretation

The fact that stable carbon-isotope signatures show agreement with pollen results indicates the pollen assemblage obtained from each bed is representative of the paleovegetation.

The pollen data (see Figure 5-2) indicate that the evolution of vegetation in this region experienced three major stages during the period from 3.05 to 1.9 Ma B.P. as suggested by the three pollen zones. From 3.0 to about 2.7 Ma., the vegetation was characterized by a typical steppe which was dominated by a dry-resistant species, *Artemisia*. Furthermore, the few arboreal pollen grains found are restricted to pine species, which seem to be from a remote source because of their high propagational capacity (cf. Færi and Iverson, 1989). Obviously, the vegetation represented by this period is of a relatively dry steppe type, substantially without trees. Consistency in the species assemblage and proportions of each species suggests that such a steppe flora lasted through the period of 3.0-2.7 Ma B.P. without any significant change, implying that the climate during that period was persistently dry. As indicated by the lithologic study, this stage coincides with reworked red-clay deposition. Therefore, the lower pollen zone substantially reflects the floral features and climate of the red clay formation.

The upper pollen zone (2.48-1.9 Ma B.P.) shows that a pronounced arboreal component existed, although its abundance varied largely. The arboreal pollen contains a large diversity including some thermophilous genera such as *Juglans*, *Ulmus* etc. The non-arboreal pollen also includes a variety of species. Pollen of Gramineae and some fern species are more abundant in the upper zone than in the lower zone. These observations indicate that the early Pleistocene flora was mainly forest-grassland, reflecting a climate that was significantly wetter than the late Pliocene (the lower zone, the reworked red clay stage). It should be noted that the abundance of the arboreal component fluctuated frequently and significantly with a dominant amplitude from zero to about 45%. At least three large cycles are demonstrated. Although they cannot be correlated to regional climatic episodes due to uncertainty in the climatic significance of the sedimentary cycles, the floral variations indicate that the climate has periodically changed in the early Pleistocene, which is characteristic of the ice ages.

Pollen analysis indicates that the middle zone (2.7-2.48 Ma B.P.) has the lowest concentration of both pollen and organic matter. The absence of arboreal pollen in this zone indicates the paleovegetation was probably related to a grassland. Interestingly, sedimentary facies analysis indicates the flood plains experienced little pedogenesis, which is the most distinct feature of the other zones. This could suggest that erosion-deposition processes were more active than in other periods, implying a poorly vegetated ground surface in the region. The $\delta^{13}C$ signatures show large fluctuations in the middle zone, suggesting that the species in a sparse steppe vegetation altered frequently, and that the climate was unstable. These features indicate that the climate was in a transition period from a relative stable state in the late Pliocene to glacial-interglacial fluctuations in the Pleistocene.

5.6. Late Pliocene Red Clay and Climatic Implication

5.6.1. Description of the Red Clay Profiles

The reddish colour is the most distinctive feature of the red clay formation throughout the profiles, although it varies between dark red and light red (Plate 2-1).

Detailed descriptions of the Yanyu section (Figure 2-5) are presented in Table 5-1. The lithologic units of N2S1 through N2S4 in Table 5-1 belong to red clay formation. The overlying strata L32 and S32 are the lowermost part of the loess-paleosol sequence.

Besides a reddish background colour, the red clay has the following features. Similar to the loess-paleosol sequence, the red clay formation comprises multiple soil layers which implies periodic pedogenesis, but the pedogenic intensity appears stronger in the red clay formation as suggested by thicker B horizons and abundantly thick clay coatings and Fe-Mn films. Carbonate nodules are usually scattered in very thick bands with small scorious shapes rather than in a precipitated bed (see Plate 5-1), and are commonly nucleated on small red clay chunks with black Fe-Mn films. This suggests that the red clay experienced multiple pedogenic periods with carbonate addition.

5.6.2. Grain-size Analysis

Grain-size analysis was conducted on the lowest loess-paleosol cycle and the upper part of the red clay formation in the Yanyu and the Luochuan sections. The results are presented in Table 5-2.

The sand (>0.063 mm) fraction constitutes a negligible proportion but shows a slightly higher concentration in the upper horizon of each pedogenic cycle in the Yanyu section. It can also be noted that this fraction increases downwards through the section. In the Luochuan section, no sand-sized grains were detected in any of the samples. This is attributed to the fact that the Yanyu section is situated in a basin margin close to the Qinling Mountains, while the Luochuan section is in a central basin.

The clay fraction (<0.002 mm) is more abundant in the red clay than in loess,

Table 5-1. Field description of the red clay formation in the lower part of the Yanyu section.

Lithologic Subdivision	Pedogenic Horizon	Thickness (cm)	Description
L32	C/Y1	320	Yellow-brown loam; dense and firm.
S32	A/Y2	40	Yellow-brown clayey loam; spongy structure.
	Bt/Y3,4,5	120	Bright brown-red silty clay; very strong blocky structure; thick and continuous clay coatings and Fe-Mn films but decreased downward.
	CCa	45	Yellowish grey calcareous nodules; Hard and dense; large size (diameter: 10-30 cm).
	C/Y6,7	320	Yellow-brown loam, dense, reddened at bottom; smooth boundary.
N2S1	A/Y8	35	Brown silty clay with little coarse sand; granular structure; small amount of pseudocellia; smooth boundary.
	Bt/Y9,10,11	180	Bright dark red clay; very strong fine blocky structure; thick clay coatings and black-brown Fe-Mn coatings (dark blue fresh fracturing surface); large blocky structure in the middle; colour becomes dull dark red; structure weakened downward; thick clay coatings through the horizon; blue clay spots occur in the lower horizon.
	CCa/Y12	20	Grey red-brown clay with small carbonate nodules containing large amount of grey clay chunks rich in Fe-Mn films; smooth boundary.
N2S2	Bt/Y13,14	120	Bright dark red clay with coarse sand; very strong blocky structure; abundant dark blue clay chunks; thick clay coatings with Fe-Mn films; dull dark reddishbrown colour in the lower horizon.
	CCa/Y15,16	250	Pale reddish brown carbonate nodules with clay matrix; small size with scorious shapes in the upper 2.05 m; clay chunks with Fe-Mn film as nuclei; large-sized nodules in the lower 45 cm.
	C/Y17	100	Reddish brown silty clay; dense; small to medium sized calcarious nodules scattered through the horizon; smooth boundary.
N2S3	A/Y18	50	Brown red silty clay; dense, medium-granular structure; possessing Fe-Mn film;smooth boundary.
	Bt/Y19,20	120	Bright reddish brown clay; strong blocky structure; thick Fe-Mn coating and clay coating; very abundant blue clay chunks and small calcareous nodules in the bottom level.
	CCa/Y21-26	550	Pale reddish brown silty clay with abundant scattered small calcareous nodules; high proportion of the matrix silty clay in the nodules; clay chunks with thick Fe-Mn film and Clay coating are common nuclei; most are voidal with large calcite crystals in the interior; matrix with loose structure.
N2S4	Bt/Y27	40	Dark reddish brown clay with large amount of sand and silt; strong blocky structure; firm and friable; abundant pseudocellia covering very developed black Fe-Mn coatings; smooth boundary.
	CCa/Y28-30	200	Alternations of brown red sandy loam and yellow brown nodules; nodules connected together forming carbonate beds; very abundant Fe-Mn films in the carbonate beds; largegravels commonly occur through the interval; diminishedupstream and thickened downstream.
Gravel layer	Basement	120	Poorly sorted and poorly rounded gravel layer with sandymatrix; various thicknesses; unconformity with the underlying bedrock.

Table 5-2. Grain-size distribution of red clay formation in the Yanyu and Luochuan sections.

Sample#	horizon	<3ϕ	3-4ϕ	4-5ϕ	5-6ϕ	6-7ϕ	7-8ϕ	8-9ϕ	9-10ϕ	>10ϕ
YANYU										
Y01	L32	--	0.3	6.2	28.5	13.5	11.5	11.0	10.5	18.5
Y02	S32-A	--	0.4	5.1	16.1	16.0	15.2	9.8	8.8	28.2
Y03	S32-B	--	0.5	14.5	9.0	11.0	11.0	6.0	6.0	42.0
Y04	S32-B	--	0.5	8.0	13.5	22.0	8.0	7.0	6.2	34.8
Y05	S32-B	--	0.4	7.6	23.0	14.5	11.5	9.0	7.2	26.8
Y07	L33	--	1.1	5.9	17.0	18.0	13.0	11.2	10.8	23.0
Y08	N2S1-A	1.5	0.7	15.8	13.0	11.0	11.0	9.0	7.0	31.0
Y09	N2S1-B	2.8	1.2	6.0	13.0	16.0	9.0	7.0	7.0	38.0
Y10	N2S1-B	1.0	0.3	4.7	9.5	10.5	12.0	5.0	4.0	53.0
Y11	N2S1-B	--	1.1	16.9	8.0	10.0	10.0	10.0	6.0	40.0
Y12	N2S1-C	--	1.2	7.8	12.0	8.0	9.0	9.0	9.0	43.0
Y13	N2S2-B	3.5	1.5	6.0	9.0	13.0	11.0	8.0	7.5	40.5
Y14	N2S2-B	3.5	1.5	7.0	8.0	12.0	8.0	7.0	6.0	47.0
Y15	N2S2-C	--	0.8	3.2	9.0	11.0	14.0	9.0	9.0	44.0
Y16	N2S2-C	--	1.5	4.0	8.5	11.0	10.0	10.0	9.0	46.0
LUOCHUAN SECTION										
LCH4	S32-B	--	0.1	2.4	19.5	12.0	14.0	10.0	8.0	34.0
LCH5	L33	--	0.2	8.8	28.0	17.0	12.0	6.0	5.0	23.0
LCH6	N2S1-B	--	0.2	5.3	16.5	13.0	12.0	6.0	7.0	40.0
LCH8	N2S1-B	--	0.2	3.8	19.2	9.8	10.0	8.0	8.0	41.0

and reaches the highest concentrations in the best-developed Bt horizons. Compared with the loess-paleosol sequence, the variation of the clay fraction in the profile is less, which can be explained by the fact that the red clay experienced multi-pedogenic processes as indicated by clay coatings and Fe-Mn films even in the CCa horizon.

5.6.3. Major Chemical Constituents

As shown in Tables 5-3 and 5-4, CaO appeared to be the most mobile constituent with a low value of 0.91% and a high value of 16.59 %. For insight into the chemical change which is masked by carbonate leaching, the carbonate concentration in each sample was determined. After removal of carbonate, the major element concentrations were recalculated and listed in Table 5-4.

From the adjusted results listed in Table 5-4, it is clear that the major element composition of the red clay formation is substantially uniform through each section and between the Yanyu and Luochuan sections, and very similar to the loess. As with the paleosols interbedded in loess, SiO_2 reaches the lowest value in the best clay-illuvial horizon, while Al_2O_3 changes inversely to SiO_2. Compared with paleosols in loess, these changes are notably small. All samples of the red clay have concentrations of SiO_2 and Al_2O_3 similar to that of the overlying paleosols. Total iron (Fe_2O_3 equivalent) shows a relatively higher concentration in the red clay formation than in the loess-paleosol sequence, and is slightly enriched in the Bt horizon but does not exceed the value obtained in the overlying paleosol (sample Y03-S32-Bt: 6.71% in loess sequence; sample Y10-NS1-Bt: 6.67% in red clay). Therefore, the chemical change caused by pedogenesis in the red clay seems no more intensive than in the overlying paleosols.

Table 5-3. Major chemical constituents of the red clay formation in the Yanyu and Luochuan sections.

Sample#	Horizon	SiO_2	TiO_2	Al_2O_3	Fe_2O_3	MnO	MgO	CaO	K_2O	P_2O_5	Na_2O	LOI
Y01	L32	56.6	0.7	13.1	5.1	0.1	2.2	7.7	2.5	0.12	0.9	10.6
Y02	S32-A	62.3	0.8	14.6	5.7	0.1	2.1	2.3	3.0	0.07	0.8	7.5
Y03	S32-B	61.6	0.7	16.1	6.7	0.1	2.1	0.9	3.1	0.07	0.3	7.8
Y04	S32-B	63.6	0.7	15.3	6.1	0.1	2.3	0.9	3.0	0.07	0.5	7.1
Y05	S32-B	64.2	0.7	14.9	5.8	0.1	2.4	1.4	2.8	0.11	0.5	6.9
Y06	L33	60.0	0.7	12.8	4.9	0.1	2.1	6.0	2.4	0.12	1.0	9.0
Y07	L33	61.7	0.8	14.6	5.9	0.1	2.2	2.2	2.9	0.12	0.7	7.8
Y08	N2S1-A	63.8	0.8	14.9	5.8	0.1	2.0	1.4	3.2	0.07	0.6	6.7
Y09	N2S1-B	63.2	0.8	15.1	6.0	0.1	1.9	1.1	3.0	0.06	0.5	7.1
Y10	N2S1-B	60.9	0.7	16.5	6.7	0.1	2.3	1.0	3.1	0.08	0.1	8.4
Y11	N2S1-B	62.5	0.8	15.7	6.2	0.1	2.2	1.0	2.9	0.08	0.3	7.6
Y12	N2S1-C	58.9	0.7	14.5	5.8	0.1	2.1	4.4	2.7	0.09	0.3	9.4
Y13	N2S2-B	61.3	0.8	15.4	6.0	0.1	2.5	1.4	3.0	0.10	0.2	8.4
Y14	N2S2-B	59.7	0.7	15.9	6.3	0.1	2.4	1.7	2.9	0.05	0.1	9.4
Y15	N2S2-C	44.1	0.6	11.1	4.5	0.1	1.8	16.6	2.0	0.16	0.0	17.6
Y16	N2S2-C	61.9	0.8	15.4	6.1	0.1	2.3	2.2	3.0	0.11	0.4	7.8
LCH4	S32-B	63.1	0.8	15.9	6.3	0.1	2.6	1.0	3.0	0.06	0.6	6.2
LCH5	L33	58.9	0.7	13.6	5.3	0.1	2.4	6.2	2.6	0.14	0.7	8.9
LCH6	N2S1-B	61.6	0.8	15.7	6.3	0.1	2.2	2.2	2.9	0.06	0.4	6.9
LCH7	N2S1-B	61.8	0.8	15.9	6.4	0.1	2.3	1.9	3.0	0.07	0.3	6.7
LCH8	N2S1-B	60.8	0.8	16.0	6.4	0.1	2.5	2.5	3.0	0.08	0.3	7.7

√

Table 5-4. Major chemical constituents of the red clay in the Yanyu and Luochuan sections after removal of carbonates.

Sample# /Horizon	SiO_2	TiO_2	Al_2O_3	Fe_2O_3	MnO	MgO	CaO	K_2O	P_2O_5	Na_2O	LOI	$CaCO_3$
Y01/L32	62.89	0.75	14.52	5.72	0.10	2.44	2.26	2.78	0.13	0.96	6.87	10.08
Y02/S32A	63.54	0.78	14.89	5.85	0.11	2.16	1.23	3.02	0.07	0.83	6.78	1.98
Y03/S32B	61.77	0.73	16.18	6.71	0.10	2.13	0.72	3.12	0.07	0.33	7.69	0.25
Y04/S32B	63.76	0.74	15.33	6.12	0.09	2.29	0.75	2.96	0.07	0.54	7.00	0.16
Y05/S32B	65.07	0.75	15.04	5.88	0.09	2.37	0.95	2.83	0.11	0.51	6.61	0.75
Y06/L33	65.73	0.75	13.99	5.38	0.08	2.32	1.15	2.64	0.13	1.05	5.58	8.80
Y07/L33	62.55	0.77	14.84	5.95	0.10	2.23	1.40	2.91	0.12	0.73	7.32	1.37
Y08/NS1A	64.40	0.82	15.00	5.89	0.11	1.99	0.85	3.20	0.07	0.60	6.32	1.00
Y09/NS1B	63.65	0.80	15.16	5.99	0.11	1.94	0.73	3.05	0.06	0.46	6.82	0.66
Y10/NS1B	60.93	0.71	16.53	6.67	0.10	2.25	0.87	3.07	0.08	0.14	8.38	0.10
Y11/NS1B	62.46	0.79	15.74	6.19	0.11	2.19	0.91	2.87	0.08	0.27	7.58	0.00
Y12/NS1C	62.02	0.77	15.29	6.10	0.10	2.19	1.63	2.86	0.09	0.35	7.55	5.06
Y13/NS2B	62.14	0.77	15.59	6.12	0.11	2.57	0.68	3.01	0.10	0.19	7.95	1.28
Y14/NS2B	60.56	0.72	16.16	6.42	0.09	2.40	0.89	2.94	0.05	0.14	8.87	1.37
Y15/NS2C	61.36	0.78	15.38	6.23	0.10	2.53	1.21	2.71	0.22	0.00	7.33	28.08
Y16/NS2C	63.69	0.79	15.81	6.30	0.10	2.40	0.62	3.09	0.11	0.45	6.77	2.81
LC4/S32B	63.40	0.75	15.09	6.33	0.11	2.56	0.71	3.06	0.06	0.63	6.49	0.50
LC5/L33	[illegible]	0.78	15.08	5.90	0.09	2.62	0.74	2.83	0.16	0.82	5.04	9.93
LC6/NS1B	62.96	0.79	16.06	6.43	0.10	2.26	0.92	3.01	0.06	0.40	6.10	2.23
LC7/NS1B	62.25	0.80	16.31	6.57	0.11	2.32	0.62	3.07	0.07	0.35	5.83	2.32
LC8/NS1B	62.53	0.77	16.50	6.62	0.11	2.55	0.88	3.06	0.08	0.30	6.58	2.98

TiO_2, MnO, K_2O and even MgO show little change in concentration throughout the profiles. Na_2O appears depleted in the red clay formation relative to the loess-paleosol sequence.

5.6.4. Clay Mineralogy

The XRD spectra of the clays present in the red clay formation from the Yanyu section and the Luochuan section are shown in Figure 5-3. Basically, the clay mineralogy of the red clay is very similar to that in the loess. The major constituents are illite (peaks 3.34, 4.98 and 10.05 Å), chlorite (peaks 3.56, 4.72 and 14.2 Å), smectite (peak 17.2 Å in glycol-treated samples) and irregularly interstratified material (wide peak band between 14 and 18 Å or more in glycol-treated samples). Incomplete collapse of smectite and interstratified clays (indicated by peaks between 10 and 14 Å in the heated samples) suggest that these minerals contain some interlayer hydroxyl aluminium or iron (cf. Catt, 1990). The presence of kaolinite is indicated by the relatively stable intensity (peak height) of the 7.1 Å peak when chlorite content decreases (see sample Y09). Small amounts of quartz (4.25 Å peak) and calcite (2.85 and 3.03 Å) exist in some samples. The presence of vermiculite cannot be confirmed, but at most it constitutes a negligible part, if any, because chlorite exists in fairly constant amounts in most samples.

In the best developed B horizon (sample Y10 in the Yanyu section), there is significant enrichment of irregularly interstratified clays and depletion of chlorite and smectite. The changes in the combination of clay minerals through pedogenic horizons in the red clay formation show a similar trend as in the overlying paleosols in the loess sequence, more abundant chlorite and smectite in the C horizons and depleted chlorite

Figure 5-3. XRD spectra of clay minerals. Samples Y01-Y16 are from the Yanyu section and LC4-LC8 from the Luochuan section. A, untreated oriented samples; B, glycol-treated samples; C, samples heated at 560°C for 4 hrs.

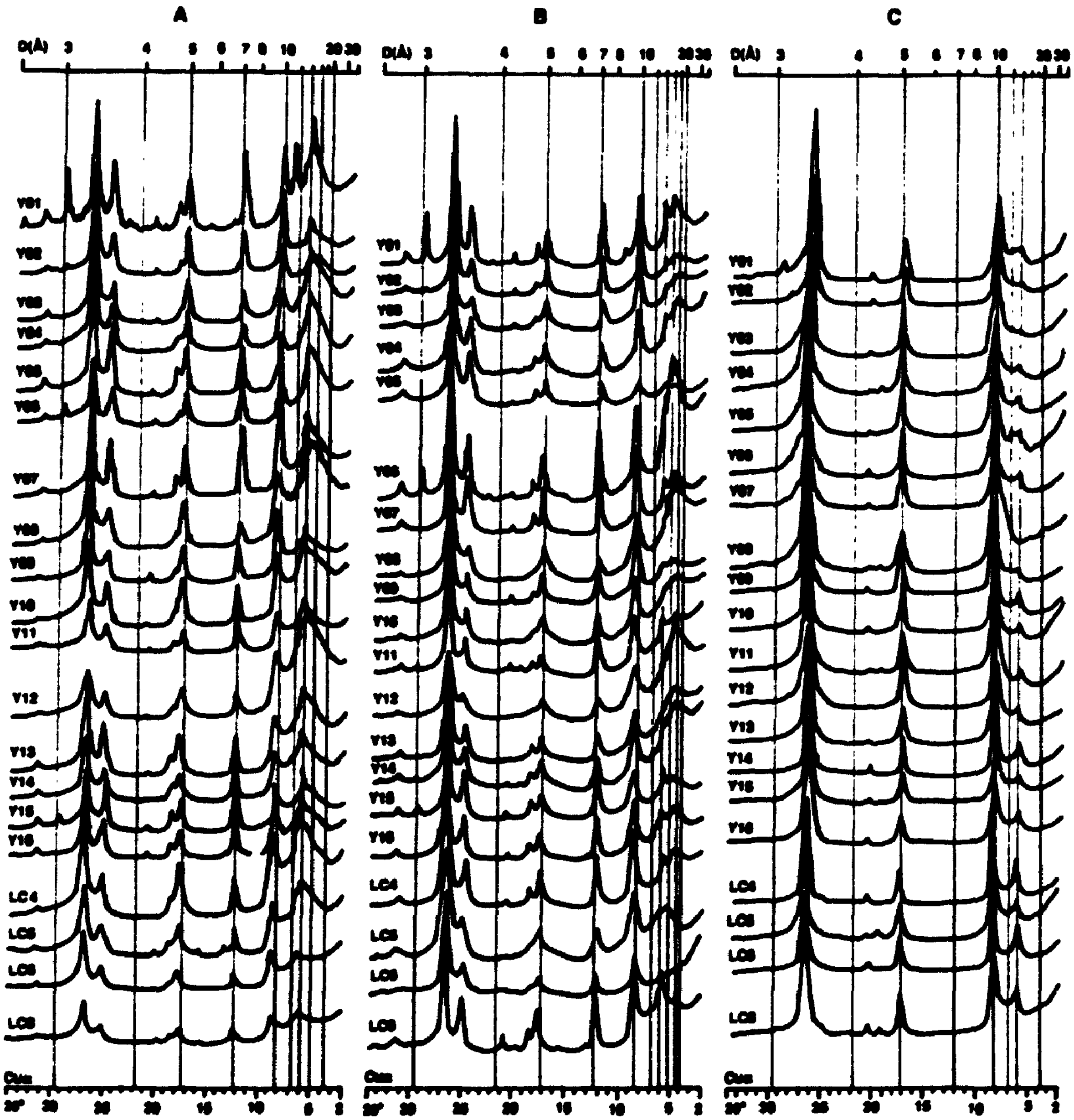
A
B
C
D(Å)

in the A horizon (compare the pedogenic cycle represented by samples Y08 to Y12 in the red clay with paleosol S32 represented by samples Y02 through Y07). The major clay mineralogical difference between the red clay formation and the overlying loess sequence is the presence of abundant interstratified clays in all the red clay horizons as indicated by the glycol-treated samples (which is correlated with the high percentages of the loss on ignition (L.O.I.) in the chemical analytic data, (see Table 5-4)). This may reflect the multiple pedogenic processes which occur in the red clay formation. Another distinct feature of clay mineralogy in the red clay is that chlorite is present in significant proportions, but disappears in the loess-derived paleosol S5 in the Shijiawan section as has been shown in Chapter 4.

5.6.5. Provenance of the Red Clay

As briefly mentioned in Chapter 1, the origin of the red clay formation remains controversial.

Field observations indicate that the red clay formations overlie a large variety of bedrocks with various topography in a large range of altitudes. It occurs as the basement of the loess-paleosol sequence in basins (e.g., Luochuan, Xifeng in Shaanxi Province, and many graben basins in Shanxi Province), or as rugged hills extensively exposed near deserts in the western provinces (such as north Shaanxi, south Ningxia, east Gansu etc.).

The occurrence of the red clay formation with a vast distribution range is consistent with the range of the loess, from the desert margin in west and northwest China to the North China Plain in the east. Great thicknesses were observed in the regions close to the deserts, and they exceed 100 m in South Ningxia. In the Guanzhong basin, a 61.5 m thick red clay section was reported (Zheng et al., 1991), but commonly it is between 10 and 50 m. That means a thickness gradient from the northwest desert to the southeast regions exists.

Grain-size distribution patterns of the red clay in the studied sections follow that of the loess, they are restricted to sizes less than 0.063 mm, and uniform between sections, even though there is a 300 km distance between the Yanyu section and the Luochuan section, supporting an aeolian origin.

The chemical composition of the red clay in the two distantly separated sections all show a large amount of calcite, indicating slight chemical weathering during pedogenesis. Furthermore, the two identical sections in terms of mineralogy and grain-size with different bedrocks, deny a local provenance of the red clay from bedrock weathering. The fact that these analyses demonstrate no significant difference in chemical composition between the red clay and the loess suggests a similar source, both derived from deserts in the northwest. Massive structure characterizes the red clay formation, as observed in loess, also suggesting the same transport agent.

It should be stressed that faunal and floral fossils are good environmental indicators for a period of pedogenesis or deposition, but they cannot provide the evidence of the material source as was suggested by previous studies (e.g., Anderson, 1923; Chen, 1994). In some regions the red clay has been reworked and shows some hydrogenic features. However, it is not representative of the general case, nor the indicator of primary origin.

5.6.6. Pedogenic Processes and Climatic Implications

Thick clay coatings are commonly observed throughout the red clay profiles and have been confirmed by photomicroscopy. As discussed in Chapter 4, their development requires a temporarily water-saturated pedoclimate and a fixed ground surface, thus suggesting a dense vegetation cover. Calcareous nodules in the red clay formation are commonly nucleated on clay chunks with Fe-Mn films, implying that the horizons in which these nodules accumulated had been thoroughly decalcified and then later received renewed carbonate leaching from pedogenic processes. Scorious shaped nodules randomly scattered in a rather thick band (see Plate 5-I) suggest that the post-pedogenic carbonate leaching occurred continuously throughout the red clay formation. This requires the dustfall rate to be relatively constant (no obvious episodes of fast and low deposition as implied by loess and paleosols), and slow enough (relative to the pedogenic rate) to allow the new material to achieve thorough decalcification and the previously formed nodules to be leached to some extent to obtain the scorious shapes observed. Therefore, a stable pedoclimate and constant low dustfall rate required by the red clay formation can be suggested.

Clay mineralogical studies show a pronounced depletion of smectite and enrichment of irregularly interstratified material in the B horizon. Unlike the paleosol S5 in the Shijiawan section and the overlying paleosol S32 in the Yanyu section, significant amounts of chlorite exist in all the horizons in the red clay formation, and a decrease was only observed in the best developed Bt horizons (see figure 5-4). Furthermore, the presence of vermiculite is clearly demonstrated in the Bt horizon of the S5 in the Shijiawan section which is situated about 30 km away from the Yanyu section in the same

Figure 5-4. Graphic illustrations of variations in the clay-sized fraction and some chemical factors through the lower part of the Yanyu section. The interval from L32 to L33 belongs to the loess-paleosol sequence, and the interval from NS1 to the bottom is for the red clay formation.

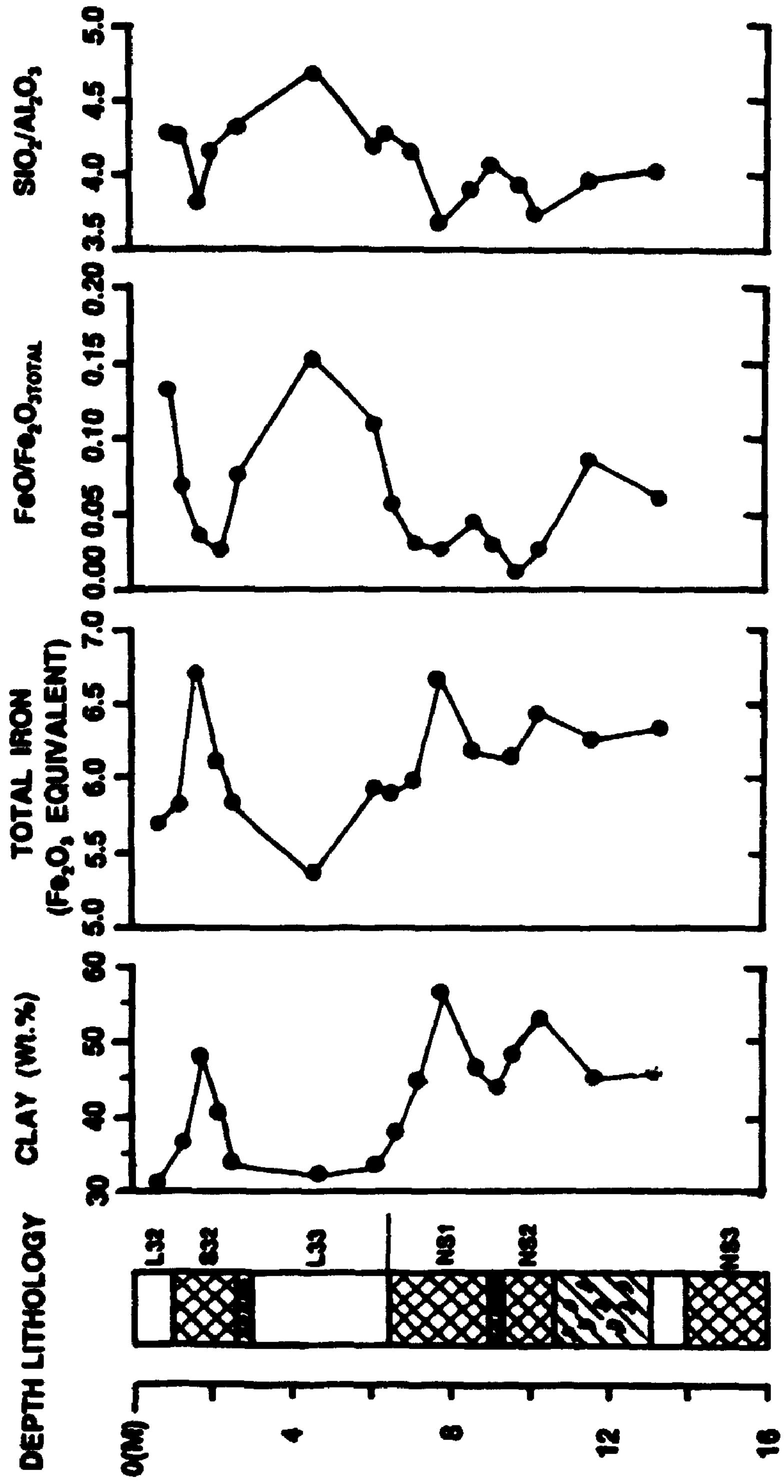
SiO$_2$/AL$_2$O$_3$
3.5
4.0
4.5
5.0
FeO/Fe$_2$O$_{3TOTAL}$
0.00
0.05
0.10
0.15
0.20
TOTAL IRON
(Fe$_2$O$_3$ EQUIVALENT)
5.0
5.5
6.0
6.5
7.0
CLAY (Wt.%)
30
40
50
60
DEPTH LITHOLOGY
0(M)
4
8
12
16
L32
S32
L33
NS1
NS2
NS3

basin. It is evident that clay mineral transformations and/or alterations in the red clay are less intensive than in the S5, implying a drier pedoclimate during the formation of the red clay. This provides an argument against the widely held opinion that the red clay formation reflects a humid subtropic climate.

Chemical analyses indicate little change in MnO, MgO and K_2O through the red clay profile. This is comparable with the overlying loess, indicating only slight chemical alteration during pedogenesis, which may suggest low precipitation.

The uppermost horizon of calcareous nodules with small size occurs at 180 cm in depth, similar to the leaching depth of the overlying paleosol S32. As has been mentioned previously, the nodules in the red clay were precipitated on a former clay illuvial horizon. This suggests carbonate saturation was caused entirely by water loss. On the other hand, the carbonate saturation as indicated by calcareous nodule formation in loess was favoured by both the original detrital calcite content and water loss. In this aspect, the formation depth in the red clay would be notably greater than in the loess-derived paleosols if the pedoclimate is the same. Therefore, it seems to reflect a drier climate during the red clay development than during the formation of the overlying paleosol in the Quaternary loess sequence.

As shown in Figure 5-4, the total iron content reaches its highest value in the B horizon, similar to the value in the overlying paleosol S32. Clay content shows a similar variation, suggesting that this process was mainly caused by mechanical translocation of fine particles. An inverse change in SiO_2 is attributable to clay mineral migration, because quartz is dominant in the silt fraction, while depleted in clay-sized fraction. Compared with the loess-paleosol cycles in the Quaternary, smaller variations in FeO/Fe_2O_3,

SiO_2/Al_2O_3, total iron and clay content throughout the red clay profile provide further evidence for a climatic interpretation that the red clay formation was developed under a rather stable and drier pedoclimate with a low dustfall rate.

Compared with the overlying paleosol, the red clay contains slightly but systematically less Na_2O and a larger clay sized fraction in both sections (see Table 5-4). This could be a function of in situ weathering or a difference in source materials. As Na_2O in the red clay mainly resides in silt-sized albite, clay particle-enriched material should be depleted in Na_2O. It is suggested that a low dustfall rate implies weak wind strength and a larger clay-sized fraction in the dust.

The dominant feature of the red clay is its colour, which can lead to a tropic or subtropic climatic interpretation. Previous studies on soil rubefication (reddening) show that it is related to an increase in hematite (Kemp, 1985; Barron and Torrent, 1986). Guillet and Souchier (1982) stress the importance of almost neutral pH and a strong seasonal climate with hot-dry summers. Schwertmann et al. (1982) show that the rubefication of the soils on silt or clayey moraines in southern Germany positively correlates with an increase in mean annual temperature and inversely correlates to an increase in mean annual precipitation. But it was also suggested that relatively high humidity is necessary for rubefication (Gardner and Pye, 1981). Birkeland (1974) considers that the rubefication is largely related to age.

For understanding the factors related to reddening, and to avoid the aging factor, the paleosol S5-I in the Shijiawan and Chang'an sections was selected. The S5 in the Chang'an section has a more reddish colour, a greater clay fraction, a lower FeO/Fe_2O_3 ratio and a lower concentration of organic matter than the Shijiawan S5. Therefore, rubefication in the loess seems to be related to fine hematite (in clay fractions), organic matter decomposition and ferrous iron oxidation. The required pedogenic conditions do not imply high precipitation as required by a forest environment.

It should be stressed that the abundant Fe-Mn films observed in the red clay and paleosols in loess (as confirmed by scanning electron microscopy) do not indicate a seasonal water-oversaturated pedo-condition, because the occurrence of the Fe-Mn films is restricted to the clay coated surface. If a water over-saturated condition was achieved and the water stagnated, the reducing condition should have been obtained for the horizons between the water table and the impervious layer, and the ferrous iron should have been observed in the soil matrix of the stagnating zone. Obviously, the well developed fine-blocky structure would collapse. Furthermore, there is no evidence of diffusion or migrating triotubules of ferrous iron in the matrix or in cracks as described by Pipujol and Buurman (1994). Therefore, the climatic implication of the Fe-Mn films in the red clay and in loess-derived paleosols is similar to clay coatings. It is also possible that microorganisms are an important factor.

5.7. Environmental Change During the Period of 3.0-1.9 Ma B.P.

5.7.1. Climate Change

Evidence obtained from fluviolacustrine sediments and red clay indicates a profound and drastic change in climate during the period from 3.0 to 1.9 Ma B.P. This change is marked by three distinct periods.

1) 3.05-2.7 Ma B.P. Climate in this period was characterized by being constant, warm and dry. Pollen data demonstrate a prolonged sage vegetation with a narrow

diversity, suggesting that the amount of precipitation was less than during the early Quaternary interglacials and conditions present today. Although a pollen flora of subtropic to warm temperate forest-grasslands was reported from a section located in the eastern central Guanzhong basin (Sun et al., 1987), this study shows no species typical of the subtropics, consistent with the study in the Jingle basin (Mo and Derbyshire, 1991) which is also located in a warm temperate zone. The occurrence of elephant fossils in the thick sand bed (about 2.8 Ma) in the Shijiawan section seem to indicate the later Pliocene climate could be warmer than today.

2). 2.7-2.48 Ma B.P. Palynological study, stable carbon isotope analysis and sedimentary facies analysis indicate that this period is characterized by scanty vegetation with frequent substitutions in plant taxa (all are non-arboreal C3 and C4 species) and intensive erosion, which implies a harsh and capricious climate. These characteristics probably reflect a climatic transition from a stable warm Pliocene condition to large warm-cold fluctuations in the Pleistocene. Sedimentary analyses indicate that this period includes the final stage (2.7-2.61 Ma B.P.) of the red clay formation and the early stage of loess deposition (2.61-2.48 Ma B.P.).

3). 2.48-1.9 Ma B.P. The climate fluctuated with large amplitudes, which is revealed by pollen combinations, especially by arboreal constituents, and variations in the sedimentary cycles. These features are more clearly visualized by the loess-paleosol alternations and have been discussed in numerous publications. Nevertheless, this study directly demonstrates the biological response. Floras fluctuated between forest grasslands with a wide diversity and sparse dry-steppe types with a few non-arboreal species, reflecting a climate which oscillated between warmer-wetter and cold-dry episodes. But it does not seem to be of the warm-dry fashion as occurred in the Pliocene.

5.7.2. Changes in the Aeolian Deposition Rate

As has been discussed above, the red clay and loess were all derived from deserts in the west and northwest. Using the data from the Lantian section which is well dated by Zheng et al. (1991), the 14 m red clay column formed in the Gauss Chron (from 3.4 to 2.48 Ma B.P.) implies a 1.56 cm/10^3 yr accumulation rate, a similar value to that obtained from the Baoji section (1.5 cm/10^3 yr) by Evans et al. (1990). During the Matuyama Chron (2.48-0.73 Ma B.p.), an 83.5 m column of loess-paleosols with a 4.64 cm/10^3 yr accumulation rate exists. In the same way, a 7.14 cm/ 10^3 yr rate is obtained for the Brunhes period. For comparison of dustfall rates in different periods, we express these data as a ratio of weight/$cm^2.10^3$ yr following the method used by Liu et al. (1985) with neglect of mass loss after deposition. The mean specific weight of each period is also adopted from Liu et al. (1985). Calculations show that the dustfall rates of the periods of 3.4-2.50 Ma, 2.50-0.73 Ma and 0.73-0 Ma B.P. are 3.10, 8.35 and 11.78 g/$cm^2.10^3$ yr, respectively. These rates are consistent with those obtained from the Luochuan section (see Table 5-5).

It is evident that the dustfall rate of the red clay formation is much lower than that of the loess-paleosol sequence. Such a remarkable change in dustfall rate implies an abrupt and great strengthening of the Siberian cold-high pressure center at about 2.5-2.7 Ma B.P., because the strength of the northwest winds in China is controlled by this cold-high (Liu et al., 1981, 1985; An at al., 1993). Furthermore, a warmer and drier climatic pattern in the later Pliocene period cannot be explained by the modern east Asian

Table 5-5 Dustfall rates through the past 3.4 Ma.

Periods (Ma B.P.)	Lantian Section ($g/cm^2.10^3$ yr)	Luochuan Section ($g/cm^2.10^3$ yr)	Mean Specific Weight (g/cm^3)
0-0.73	12.64	12.32	1.77
0.73-0.97	--	16.79	1.87
0.97-1.87	--	8.68	1.92
1.87-2.48	--	8.68	1.98
0.73-2.50	8.96	9.83	1.93
2.50-3.40	3.10	--	1.99

monsoon. Therefore, a profound change in the climate regime must have occurred.

Plate 5-I. Upper: A photo showing that the carbonate nodules in the red clay are scattered through a thick band. Scorious shapes suggest post-pedogenic leaching.

Lower: Loess deposits derived from marine sediments when seawater retreated from the region. Photo shows a loess section in Dalian, on the north margin of the Bohai Gulf (see text Chapter 6).

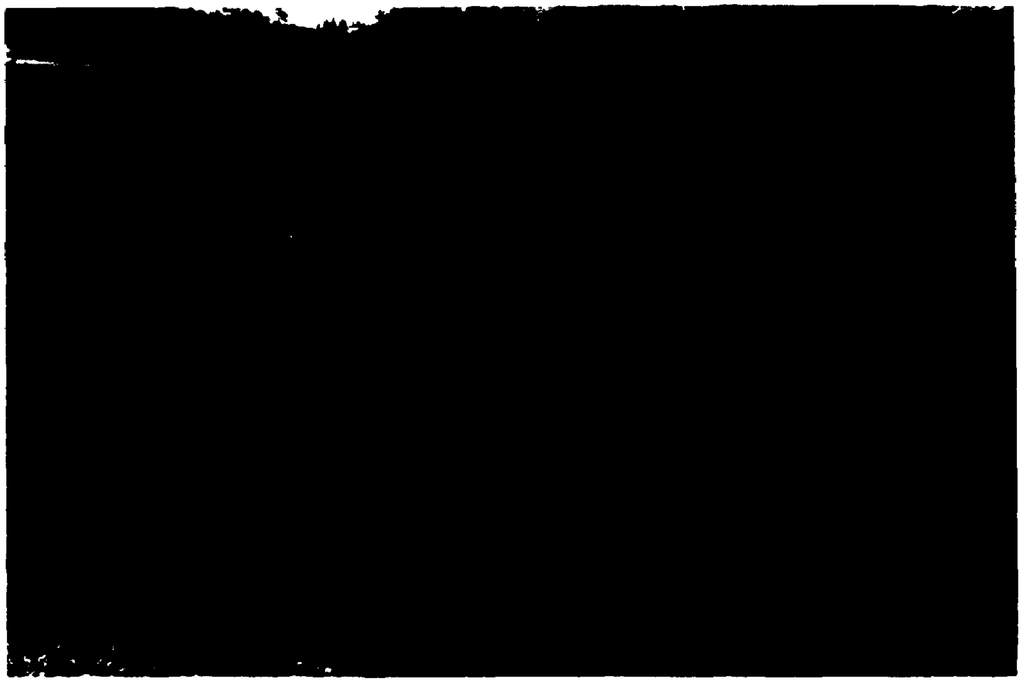

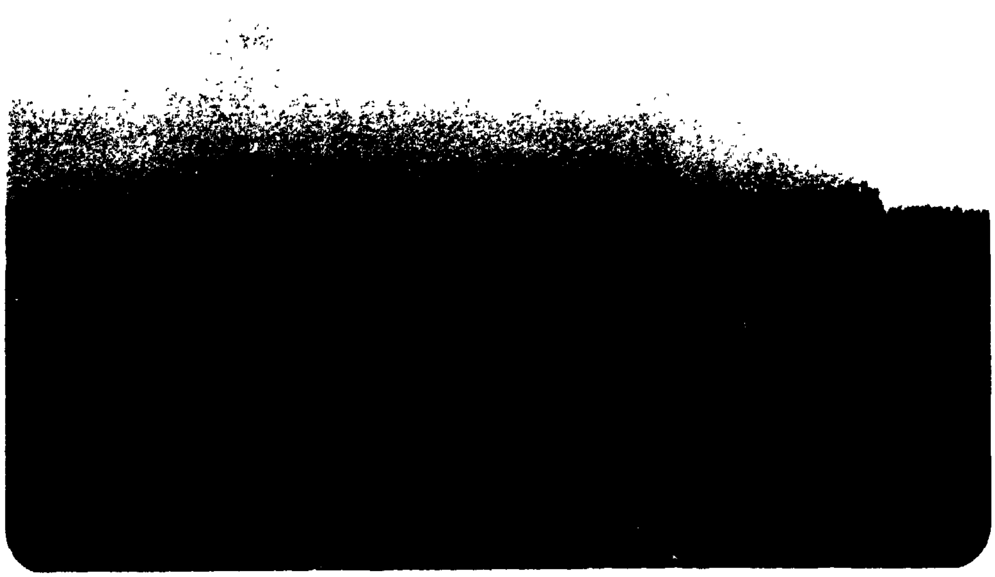

CHAPTER 6

CLIMATIC CHANGE IN THE LOESS PLATEAU DURING THE PAST THREE MILLION YEARS: THE GLOBAL SIGNIFICANCE

6.1. Introduction

Studies on the fluviolacustrine sequences, the red clay formation and the loess-paleosol sequences, demonstrate that the climate in the loess plateau has been subjected to profound changes during the past 3 million years, which include fluctuation in response to glacial-interglacial oscillations and an irreversible change marking a revolution in the climate regime. A relatively stationary warm and dry climate in the late Pliocene was replaced by oscillations between cold-dry and warm-wetter periods in the Quaternary. Many of the previous studies emphasize the influence of the Siberian cold-high air pressure cell on dust transport and loess accumulation and suggest that the Siberian High must have been greatly strengthened during glacial periods with an associated weakening of the southeast Asia monsoon (it is assumed that they compete against each other). Comparison of climatic records from the loess-paleosol sequences and deep sea sediments shows good agreement (Heller and Liu, 1984; Liu et al., 1985; X.M. Liu, 1987; Kukla, 1987; Ding et al., 1991; Heller and Evans, 1995), even for some rather short period cold events (An et al., 1991, 1993; Porter and An, 1995). However, the linkage between the regional record and global climatic signals is still under discussion. In this chapter, we will demonstrate a mechanism of sea level-precipitation interlock which transmitted global glacial-interglacial climate signals into central China.

As noted in field observations and confirmed by this study, a sharp change in sedimentary environment from "red clay" formation to loess accumulation suggests an abrupt shift of the regional climate pattern or a rapid reorganization of the environmental system at 2.5 Ma B.P. Early studies stressed the importance of the Tibetan Plateau uplift in the formation of the modern east Asia monsoon climate and the development of the desert-loess plateau coupled system (Zhang, 1981; Liu and Han, 1988; Ding et al., 1992). New evidence from the fluviolacustrine sequence and the red clay formation (see Chapter 5) indicates that the climatic transition from a Pliocene pattern to the modern east Asia monsoon was completed in a period of about 100 ka. This requires that any explanation must take the rapidity of the transition into serious consideration before it invokes an orogenic forcing for such a climate regime revolution. This time factor was ignored in previous studies (e.g., Ruddiman and Raymo, 1988; Ruddiman and Kutzbach, 1991; Liu and Han, 1988; Ding et al., 1992). Furthermore, the altitude of the Tibetan Plateau at 2.5 Ma is quite controversial (Harrison et al., 1992; Burbank et al., 1993; Coleman and Hodges, 1995). If the Tibetan plateau achieved its present height some 8 million years ago, its climatic significance in the worldwide glaciation (Ruddiman and Raymo, 1988; Ruddiman and Kutzbach, 1991) will be critically challenged and the timing of the reorganization of the east Asian physiological system and the forcing mechanism must be reconsidered. In this chapter, the role of the Tibetan Plateau uplift in the Quaternary global glaciation is considered with emphasis on the timing.

6.2. Linkage Between Climate of North China and Sea Level Change

Modern climate in most of China is dominated by two high pressure centres in different seasons, the south Pacific high pressure cell in summer and the Mongolian/Siberian high pressure cell in winter. The Indian oceanic monsoon only influences a small area in southwestern China. Therefore, the southeast monsoon is the major source of precipitation for most of the country and brings additional heat to those regions (cf., Lin, 1984). The winter monsoon, which is cold and dry, greatly influences the climate in winter and spring, especially in North China. Therefore, climatic conditions substantially reflect the intensities of the summer monsoon (east Pacific oceanic high) and the winter monsoon (Siberian cold-dry high).

The distribution patterns of mean annual temperature and precipitation in China show that the climatic conditions strongly relate to the distance from the east coast (the west Pacific margin). As shown by Figure 6-1, the precipitation decreases nearly linearly with distance away from the coastline. This relationship is evident for the past 18,000 years.

During the last glacial maximum, the sea level dropped 130-150 m in the East China Sea and 100-120 m in the South China Sea (Zhao, 1982; Wang, 1992). The east coast migrated seawards more than 600 km on average (and even over 1000 km for some regions) away from the present position (Winkler and Wang, 1993; Wang, 1995; cf., First Institute of Oceanography, State Oceanic Administration, 1984). The Bohai Gulf was exposed and subjected to deflation which resulted in thick loess deposition (Plate 5-1) in the coastal regions (Han, 1987). These types of sea shelf deserts occurred in a large area of the west Pacific margin, including the whole Bohai Gulf, the Yellow Sea, the East China Sea, the northern part of the South China Sea (Qin and Zhao, 1991), and even the

Figure 6-1. Modern mean annual precipitation (mm) in China (modified from Winkler and Wang, 1993). Areas which receive less than 300 mm are stippled and essentially coincide with areas where the aridity index is greater than 2. Arrows indicate the precipitation gradient and the summer monsoon directions. The broken line circle denotes the Siberian (Mongolian) cold high cell in winter. Data from Lin, 1984.

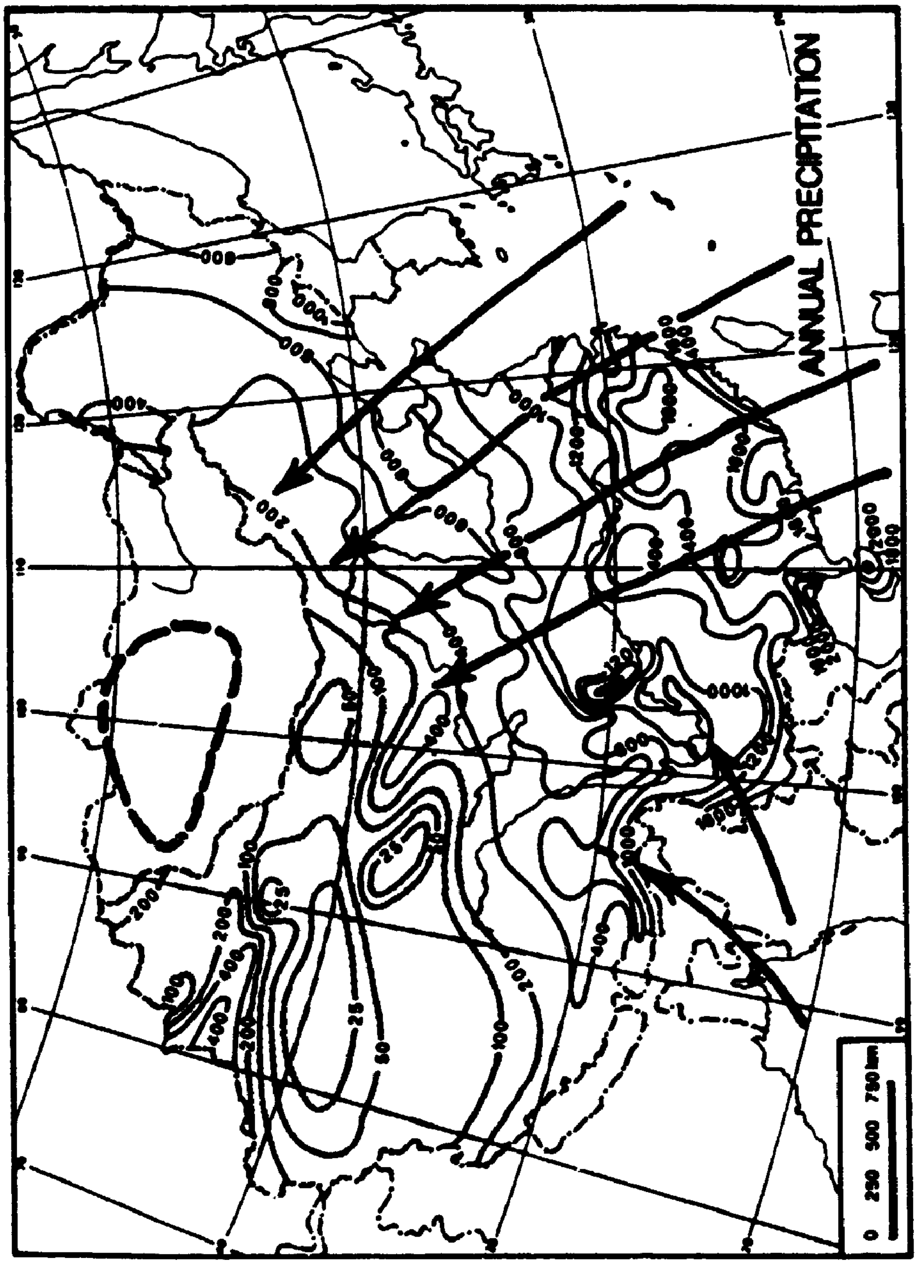
ANNUAL PRECIPITATION
0 250 500 750 km

Java Sea. Japan, Taiwan and the Hainan Island were connected to the continent (see Figure 6-3). *Bulcella frigida*, a cold-water foraminifer, shifted 5° southward in latitude and grew in the East China Sea, and spruce and fir forests covered most of Japan and expanded in China (Winkler and Wang, 1993). These forests grew at least 1200 m lower than at present in both the eastern and western mountain ranges of China, while frozen steppe covered large regions in the northern half of the country (Hou, 1979; Teachers College of northwest China, 1984; Ren et al., 1985).

In North China, a high stand of sea level was registered by a widespread transgression 6000 years B.P. It reached a position in the Beijing lowlands of the North China Plain as far as 100 km from the present margin (Zhao et al., 1980, 1982; Zhao and Zhang, 1985; Zhao and Qin, 1982), a view which is supported by Japanese studies (Matsushima, 1976). This is coincident with a major wetter episode during that time. Evidence indicates that most of China was warmer and wetter than at present and lake levels were higher throughout most of the country (see Figure 6-2). Therefore, it strongly suggests that the intensity of the summer monsoon in China is strictly interlocked to the west Pacific margin which is controlled by eustatic sea level change. By this linkage, the world glacial climate signals were transmitted into the regional climatic regime.

Taking today's precipitation gradient versus the distance from the west Pacific margin and the 200 mm mean annual isopluvial line as the southeast margin of the deserts as observed at present, the desert margin at 18 000 year B.P. should be roughly overlapping the modern 700 mm isopluvial line. That means, the whole loess plateau lay in a desert climate zone (see Figure 6-2), and the Guanzhong basin, the warmest and wettest region in the loess plateau could only have received 100 mm of annual rainfall.

Figure 6-2. Time series of paleoenvironmental parameters and paleoclimate in east Asia since the last glacial maximum (from Winkler and Wang, 1993). The locations indicated in the diagram include "north of 35 N" (the Coastal regions with latitudes higher than 35 °N), "south of 35 N (the coastal regions with latitudes lower than 35 °N), "loess plateau" (the Chinese Loess Plateau), "northeast" (Northeast China), "west" (west China), "south" (South China), "Q-X" (Qinghai-Xizang Plateau, The Tibetan Plateau), "Q-X & X" (Tiben Plateau and Xinjiang), and Japan.

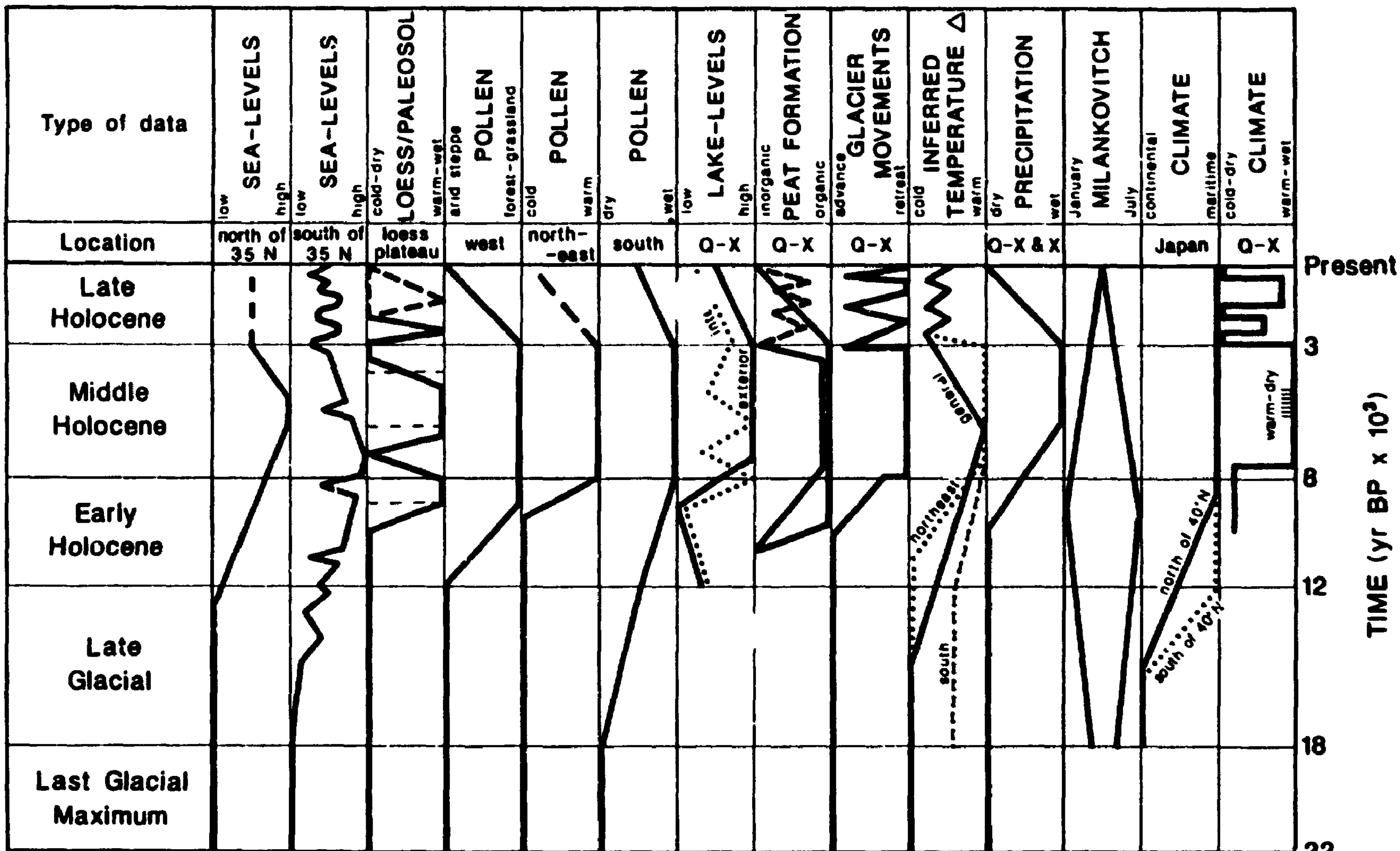
Type of data
Location
SEA-LEVELS
low
high
north of 35 N
SEA-LEVELS
low
high
south of 35 N
LOESS/PALEOSOL
cold-dry
warm-wet
loess plateau
POLLEN
arid steppe
forest-grassland
west
POLLEN
cold
warm
north-east
POLLEN
dry
wet
south
LAKE-LEVELS
low
high
Q-X
intl.
exterior
PEAT FORMATION
inorganic
organic
Q-X
GLACIER MOVEMENTS
advance
retreat
Q-X
INFERRED TEMPERATURE Δ
cold
warm
general
northeast
south
PRECIPITATION
dry
wet
Q-X & X
MILANKOVITCH
January
July
CLIMATE
continental
maritime
Japan
north of 40°N
south of 40°N
CLIMATE
cold-dry
warm-wet
Q-X
warm-dry
Late Holocene
Middle Holocene
Early Holocene
Late Glacial
Last Glacial Maximum
Present
3
8
12
18
22
TIME (yr BP x 10³)

Figure 6-3. A, relative paleoprecipitation map (modified from Winkler and Wang, 1993) at 18,000 year B.P. (showing areas wetter than, drier than, or the same as at present) constructed from biogeologic evidence (Ren et al., 1985). Black areas are the exposed shallow sea or continental shelves caused by sea level lowering at the last glacial maximum. The broken line is a 200 mm isopluvial line postulated by the distance from west pacific margin as suggested by a sea level-interlocked precipitation hypothesis (see text for explanation). B, Paleovegetation map at 18,000 year B.P. (from Winkler and Wang, 1993) constructed from the pollen and macrofossil evidence. Note the western China was totally vegetated by arid steppe. The heavy lines in the ocean denote the regions which became continental deserts matching the black areas shown in map A.

A

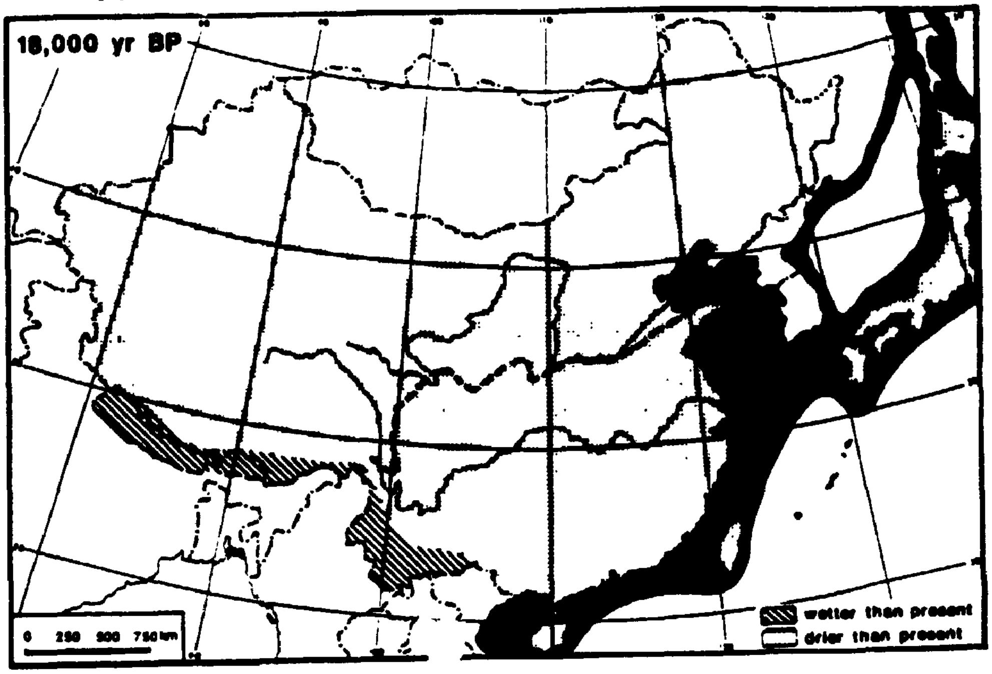
18,000 yr BP
0 250 500 750 km
wetter than present
drier than present

B

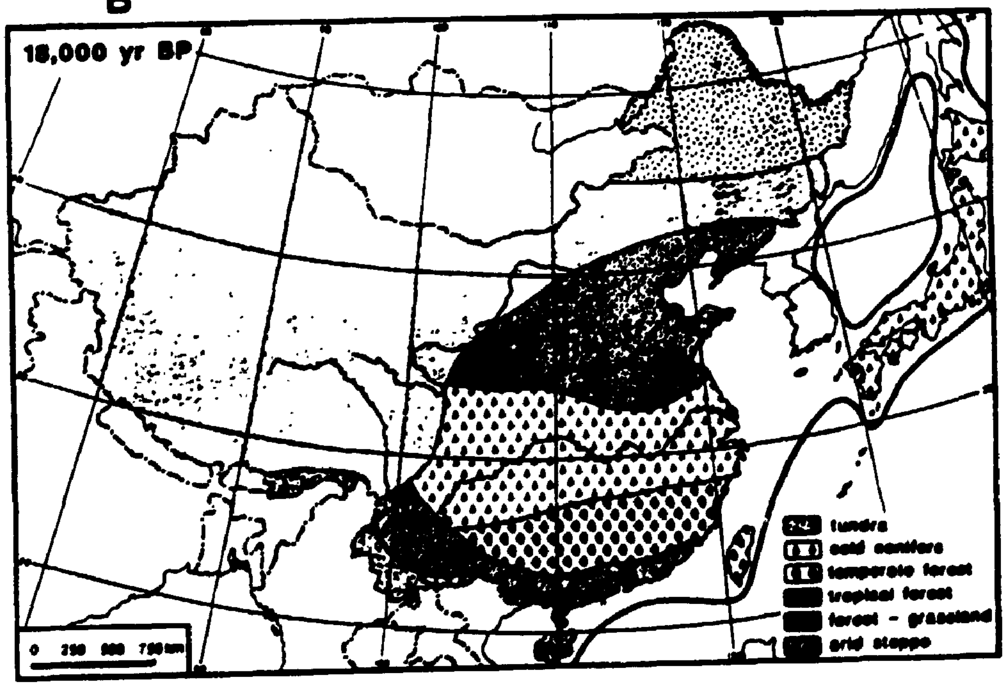
18,000 yr BP
0 250 500 750 km
tundra
cold conifers
temperate forest
tropical forest
forest - grassland
arid steppe

This is why the detrital calcite in the loess layers are preserved with little eluviation.

The inferred change in summer monsoon intensity actually results from the regional influence of the southeast Pacific high pressure cell. In other words, it is a combined result caused by changes in the distance from the coast and the absolute intensity of the southeast Pacific high. In fact, the Pacific High is affected by the sea surface temperature (SST). Higher SST causes greater evaporation and thus favours intensification of the southeast Asia monsoon. At the last glacial maximum, the SST in the south China Sea dropped 2-5 °C in mean annual values and 0.9-3.0 °C in summer (Wang, 1995). A 10-20% decrease in evaporation could be expected (cf. Lamb, 1972). This could have reduced the strength of the summer monsoon and further reduced the estimated paleoprecipitation during glacial periods. For individual locations and short periods, however, it is difficult to confirm such a relation. As observed in west Africa, the air humidity in drought years can be even higher than normal years (Blumenthal, 1990). The relations between SST and the summer monsoon intensity are more complicated than a simple linear relationship over a small time-scale, as observed by Barnett et al. (1991) and Ni and Qian (1991). This implies that errors on small scale localities may exist in the reconstructions.

As well, the proposed sea level-precipitation linkage cannot be used to estimate the climatic harshness which is governed by the northwest winter monsoon. The climatic harshness controller is the Siberian cold high. The winter monsoon intensity is expressed by the loess deposition rate and the grain-size distribution, whereas the summer monsoon influence is in the pedogenic intensity after deposition which modifies the depositional appearance. Caution must be taken in the interpretation of various parameters, for example, grain-size distribution, clay content, and mobile chemical constituents etc.

6.3. Relationship between the Summer Monsoon and the Winter Monsoon

^{10}Be flux studies indicate that the dust deposition rate in loess layers is much higher than in the paleosols (Shen et al., 1992, 1994; Beer et al., 1993), suggesting the different influences of the summer and winter monsoons. The simulated results of the winter global air temperature and pressure fields by Kutzbach et al. (1993) show 16-32 °C lower temperature and 8-16 mb higher air pressure in the high north of Asia during the last glacial maximum than at present, supporting a great intensification of the winter monsoon. The interbedded paleosol study of the loess sequence indicates a relatively stable ground surface necessary for clay coating development, which is consistent with a low dustfall rate. Therefore, such a competing relation between the summer and the winter monsoons is tenable on the glacial cycle time scale.

Study of the Younger Dryas cold event in the loess record suggests that both the summer monsoon and the winter monsoon were intensified during that period (An et al., 1991, 1993). Although the Younger Dryas event occurred at least as a hemispheric phenomenon (cf. Ruddiman and McIntyre, 1981; Dansgaard et al., 1989; Lindley and Thunell, 1990; Kudrass et al., 1991), global sea level had greatly risen since the last glacial maximum. Most areas of the west pacific margin were submerged, which must have greatly enhanced the influence of the southeast monsoon on inland China. On the other hand, this event is registered as a profound cooling. As observed by Huang et al. (1992), lower temperatures favour development of a blocking high over eastern Siberia and north China, lending support for the idea that the Siberian cold high could be strengthened by this event. Therefore, the binary intensification of the summer monsoon and winter monsoon inferred from the Younger Dryas study of the loess provides additional evidence for the sea level linked climate model in the loess plateau.

6.4. Correlations of Climatic Records Between the Loess Plateau and Deep Sea Cores

In the early 1980's, Liu and Yuan (1982) systematically correlated the climatic record in the loess-paleosol sequence of the Luochuan section with the marine oxygen isotope record. Great success was obtained by Heller and Liu (1984) using the magnetic susceptibility signature with more reliable paleomagnetic dating constraints. Subsequent correlations were made in more detail with different loess sections and different deep sea cores (e.g., X.M. Liu et al., 1987; Kukla, 1987; Kukla and An, 1989; Ding et al., 1991; Heller and Evans, 1995). Great similarity of these two types of climatic records suggests a strong response of the loess plateau to global climatic forcing, and has led to a wide acceptance of the loess magnetic susceptibility signature as a proxy terrestrial climate record in the paleoclimatological community (e.g., Morley and Dworetsky, 1991; Crowley and North, 1991). The following is an overview of the previous studies, with a correlation presented in Figure 6-4.

1. The Quaternary climate change recorded in the loess sequences is consistent with global glacial-interglacial oscillations implied by marine oxygen isotope signatures, suggesting a faithful and sensitive response of the east Asian monsoon regime in the loess plateau. As discussed in the previous section, this response is driven by west Pacific marginal shifts which are closely correlated with sea level change. Therefore, the loess-paleosol sequence has registered global climate change in amplitudes and timing at least

Figure 6-4. A, Comparison of the magnetic susceptibility in the Xifeng section (see Figure 2-6) and marine oxygen isotope record of DSDP 552A in central North Atlantic (modified from Kukla, 1987). The composite marine oxygen-isotope record is from Williams et al., 1988. Note the first abrupt decrease in magnetic susceptibility in the loess-paleosol sequence and oxygen-isotope index in marine sediments (the middle column) occurred between 2600 and 2400 ka. B, detailed comparison of the first 1.1 Ma of record (from Kukla, 1987).

A

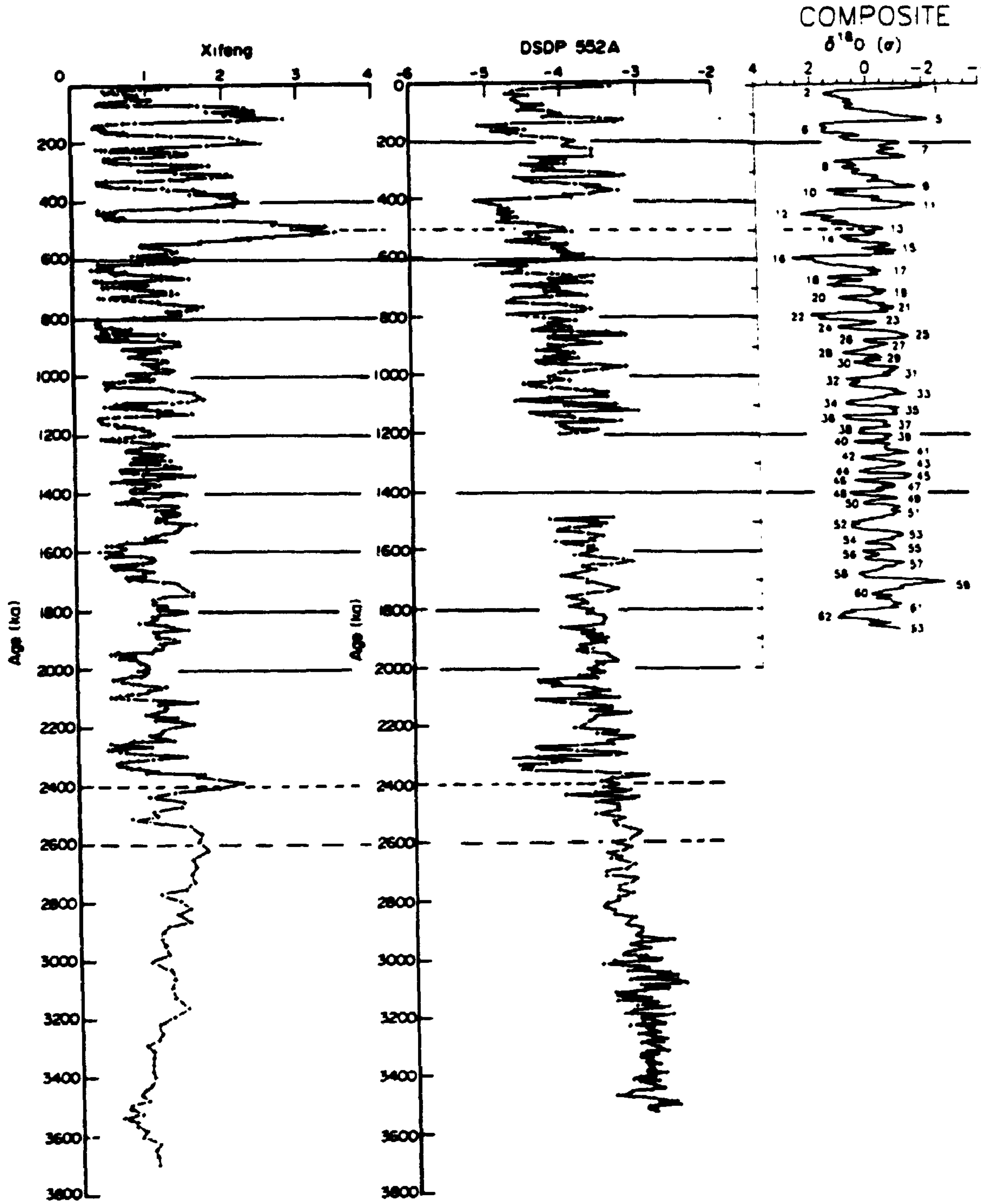

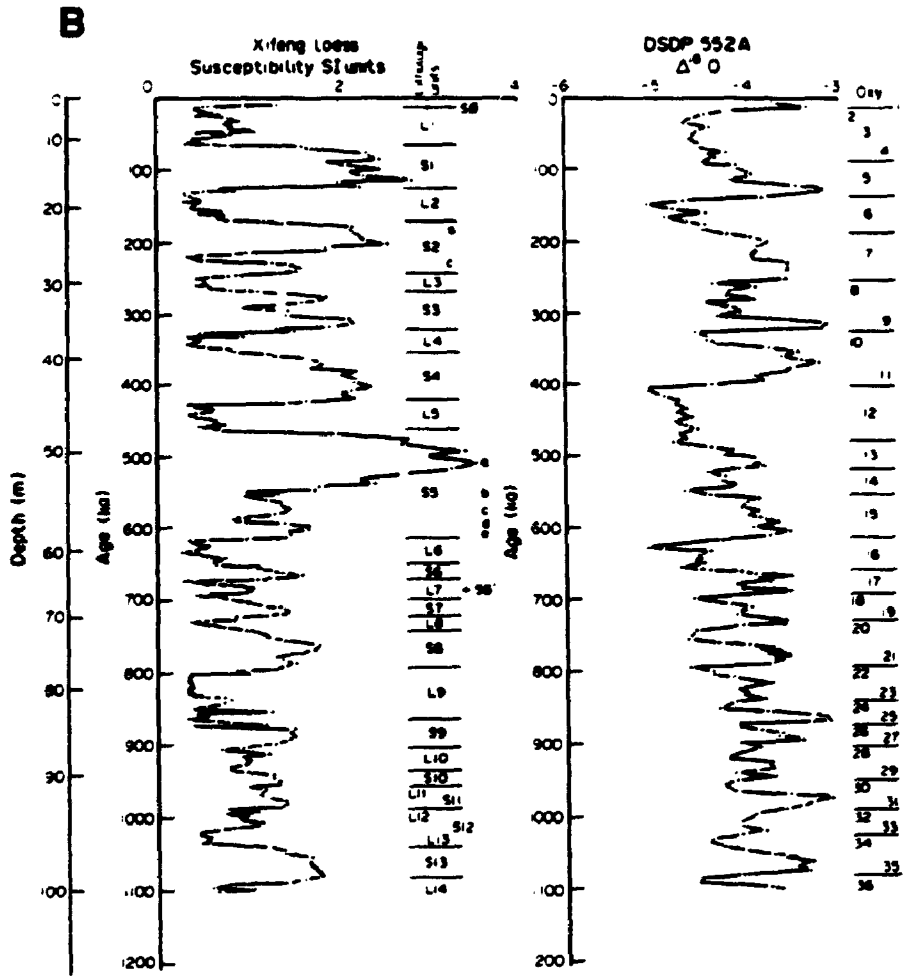
B
Xifeng Loess
Susceptibility SI units
DSDP 552A
Depth (m)
Age (ka)
Oxy

at glacial cycle time scale.

2. Both records show that a dramatic change in climatic pattern occurred 2.5 Ma ago (see Figure 6-4), from a stationary warm state to a style with frequent fluctuations, as is demonstrated by analyses of the fluviolacustrine sequence and the red clay formation discussed in Chapter 5.

3. Another profound change occurred at 600 kyr ago in that the glacial-interglacial oscillations shifted to a new manner with greater amplitude and for a longer period than before. This is clearly demonstrated by thicker loess layers and intensified pedogenesis (e.g., deeper B horizons, thicker clay coatings etc.).

4. Discrepancy between the two kinds of records lies in the relative amplitude. As suggested by the magnetic susceptibility in the Xifeng section, the S5 seems to reflect an interglacial climax throughout the Quaternary, but the corresponding oxygen isotope stage indicates a relatively weak interglacial period. The present study of S5 demonstrates that the S5 in the Guanzhong basin was vegetated by grassland-dominated flora, suggesting the climate was even drier than in the Holocene, and this is supported by the sea level-interlocked climate model. As pointed out earlier, the magnetic susceptibility enhancement and pedogenic features are greatly affected by factors such precipitation, pedogenic duration and dust deposition rate etc. Therefore, a final confirmation can be expected only when reliable and accurate dating results are available.

5. The magnetic susceptibility of the red clay formation in the Xifeng section shows relatively constant values, similar to the moderately developed paleosols in the loess sequence. Field observations of this section indicate that only the Bt horizon in the red clay formation possesses intermittent clay coatings. Therefore, the magnetic

susceptibility signals do suggest that the climatic conditions of the red clay are drier than that of S5. As revealed by this study, a typical grassland existed through the red clay development until 2.7 Ma ago.

6.5. A Rapid Transition of Climate Regime Between 2.7 and 2.6 Ma

6.5.1. Considerations from Modern Climate

The modern east Asian monsoon climate in China indicates that major rainfalls are closely related to the activities of both the southeast monsoon and the cool polar front which is maintained by the Siberian high pressure cell. The favourable condition for precipitation is in the intersection belt of the polar front and the southeast monsoon front. After winter, a long-term rain belt appears in South China in late April and May, showing that the southeast monsoon is restrained by the cold high. In late July and August, although dominated by the southeast monsoon, South China is characterised by hot-humid weather but with less precipitation, because the cold front retreats far from the region. In North China, most of annual precipitation is concentrated in July and August, which is attributed to active intrusions of both air fronts. Therefore, two conclusions can be reached. Firstly, that the southeast monsoon is necessary for large scale precipitation in this climate regime and secondly, that the cold high pressure centre is critical for setting the modern east Asian monsoon climate. The Pliocene long-period climate characteristic of warmer and drier than at present implies that either the cold high pressure centre was rather weak, or that the oceanic airmass could not reach the region, or both.

6.5.2. An Overview on the Uplift of the Tibetan Plateau

Many studies emphasize the importance of the Tibetan Plateau uplift in the Cenozoic (particularly since late Pliocene) for explaining the Quaternary glacial initiation (e.g., Ruddiman and Raymo, 1988; Ruddiman and Kutzbach, 1991) and the occurrence of the modern east Asian monsoon (e.g., Liu and Han; Ding et al., 1992). However, it can be pointed out that no consideration of the timing can be seen in the previous studies other than a postulated elevation threshold.

The evidence for the Tibetan Plateau uplift in the late Cenozoic will be summarized, and the critical challenge of timing to the orogenic forcing hypothesis of the Quaternary first glaciation will be shown in this section.

Bio-geologic evidence indicates that in late Pliocene, the Himalayan region was dominated by subtropical and warm deciduous flora (Hsu et al., 1973, Hsu, 1978; Li et al., 1979; Li, 1983, 1985; Han, 1988a). Well-developed karst and red lateritic weathering (with major clay mineral being kaolinite) also suggest a sustained wet subtropical climate in the Pliocene (Cui and Zheng, 1975; Han, 1988b). By comparison of the distribution elevation between the *Quercus semicarpifolia* fossil ed and modern flora nearby, 3000 m uplift of the Tibetan Plateau was suggested for the period since the late Pliocene (Hsu et al., 1973; Li et al., 1979). Mammalian fossils (*Hipparion* fauna) indicate that the Himalayas and Tibet were not an effective barrier to north-south faunal exchange until the late Pliocene (Li et al., 1979; Ji et al., 1981), supporting the conclusion obtained from fossil plants and pollen evidence. Accelerated uplift of the Tibetan Plateau since late Pliocene is suggested by earlier studies based on the following evidence. The lacustrine deposits containing *Hipparion* fauna in the Gyrong Basin are covered by the Gongbe

Conglomerate which belongs to the Matuyama chron (Wang and Li, 1985), suggesting an abrupt uplift-acceleration. Comprehensive studies in the Kashmir Valley conclude that the climatic pattern of Kashmir follows a global trend: the warming during the Pliocene, and the glacial-interglacial fluctuations during the Pleistocene (Agrawal, 1985; Agrawal et al., 1989). Conclusions of the accelerated uplift and climate shift in the late Pliocene are supported by the Siwalik Group studies (cf. Chaudhri, 1982; Bhatia and Kapoor, 1982).

Overall, evidence from inside the Tibetan Plateau and adjacent regions indicates a profound climate change and accelerated uplift of the Tibetan Plateau in the late Pliocene. The most important feature for this work is the timing of this change. Recently, the issue regarding the elevation of the Tibetan Plateau in the past 3 million years is strongly debated by Harrison et al. (1992) and Coleman and Hodges (1995). They argue that much of the present elevation of the Plateau was attained at least 8 million years ago. Obviously, this negates the hypothesis of tectonic forcing for the Quaternary glaciation initiation. The controversy about the dating will not be discussed in this thesis, however it must be stressed that the tectonic forcing hypothesis is still questionable even if the evidence employed is confirmed.

6.5.3 Challenge to the Hypothesis of Plateau-Uplift Forcing for Global Plio-Pleistocene Climate Change

Evidence from the fluviolacustrine sequence and the red clay formation indicates that the warm-dry climate lasted until 2.7 Ma, and was characterized by dry sage-grasslands and a low dust deposition rate. Some 100 ka later, it was replaced by a cold-dry climate with a remarkably enhanced dust deposition rate as indicated by the first loess deposition 2.6 million years ago. This marked a great and abrupt intensification of the Siberian cold high pressure center, and the establishment of modern east Asian monsoon.

Taking 1 mm/year of the maximum mean uplift of the Tibetan Plateau in the past 3 million years, a 100 m increase in elevation could be suggested for a period of 100 ka. The tectonic forcing hypothesis stresses that a threshold height greatly influences the planetary waves thus promoting ice sheet growth in North America. It seems unlikely that a 100 m increase in altitude of the plateau could lead to a striking change in planetary atmospheric circulation, stimulate a remote ice sheet initiation and cause rapid global glaciation within a period of some 100 ka.

6.5.4. Main Points on the Forcing Mechanism of the Quaternary Climate Regime Emergence

A large amount of evidence indicates that the loess deposition and climatic deterioration in North China occurred in timing with the occurrence of global glaciation as recorded by marine oxygen isotopes. This strongly suggests that the great intensification of the Siberian cold high pressure centre was produced by a glacial climate. This relationship is unanimously supported by atmospheric general circulation modelling experiments (e.g., Manaba and Broccoli, 1985; Kutzbach and Guetter, 1986; Kutzbach et al., 1993).

As reviewed, the Tibetan Plateau and its adjacent areas experienced climate change with the global trend and timing. Adopting the conclusion that the mean elevation of the Tibetan Plateau was about 1500 m at 2.5 Ma. B.P., the principal high Himalayas would have been 4000-4500 m above sea level. As observed, the modern snowline on the southern slope of southeast Tibetan Plateau is at 4500 m (Zhang, 1981). Therefore, it is reasonable to expect that ice caps and mountain glaciers existed on the high Himalayan ranges during the glacial period of the early Pleistocene, which would have greatly enhanced its blocking effect on the Indian oceanic airflow to the plateau and northward. With uplift of the plateau and global cooling, the ice caps on the high Himalayas became permanent and irreversibly restrained the Indian monsoon across the mountain chains. Furthermore, a low pressure cell was formed in the Tibetan Plateau in summer due to its high elevation (thin air) and low thermo-capacity (dry), which induces the southeast Pacific monsoon to move deeper into inland China. By blocking the Indian monsoon and producing a summer low pressure cell, the Tibetan Plateau intensified the influence of the southeast monsoon and northwest monsoon on the inland China climate, which is consistent with modelling experiments (Manaba and Terpstra, 1974).

Questions, however, still remain. What caused the Quaternary worldwide glaciation? What controlled the timing of the glacial cycles? Possible solutions to these questions will be addressed in the following chapter.

CHAPTER 7

POSSIBLE INFLUENCE OF OCEAN RIDGE PROCESSES ON SECULAR CLIMATE CHANGE

7.1. Introduction

As has been discussed, available theories of the Quaternary glacial climate have failed to explain many fundamental problems as listed below (for details refer to Chapter 1):

1. The occurrence of the Quaternary glaciation (cf. Imbrie et al., 1984; Berger, 1991);

2. Deglaciations out of phase with the maximum insolation anomalies in either the northern or the southern hemisphere (cf. Broecker and Denton, 1990; Crowley and Kim, 1994);

3. The periodicity shift at the B/M paleomagnetic polarity boundary, from fast to slow oscillations (say from dominant 41 ka cycle to 100 ka cycle (cf. Ruddiman and Raymo, 1988));

4. Glacial cycles did not follow the most powerful periodicity of the orbital forcing (cf. CLIMAP members, 1981; Imbrie et al., 1984);

5. The ocean circulation mode switch theory could not explain the similar severity of glaciation through tropics to polar regions and does not provide the mechanism of the mode flip-over (cf. Broecker and Denton, 1990, 1991);

6. The synchroneity of the enhancement of the atmospheric CO_2 and global

warming at the transition from glaciation termination to interglacial period (cf. Barnola et al., 1987; Jouzel et al., 1989; Ruddiman, 1987)).

This study also stresses a vital problem which has never been explained: the budget for rapid global warming. During the glacial maximum, North America (with latitudes higher than 40°) was totally covered with ice or snow, and most areas of high latitude in the both hemispheres were under similar conditions even for those without ice sheets. Snow albedo can be as high as 80-90% for fresh snow or over 50% for old snow (cf. Dickinson, 1992; Lydolph, 1985). This means about 70% loss of the solar radiation in those areas. It is known that the maximum change of the total insolation of the earth is about 0.2% (cf. Crowley and North, 1991) which is induced by eccentricity. Given that the ice sheet collapse model is correct (cf. Hughes, 1987), the ice cover on the earth was not reduced but enlarged, because high ice sheets were transported to lowlands or discharged into oceans, which would make a pronounced negative effect on the solar radiation absorption (the average continental albedo is 30% or less and ocean near zero, but sea ice albedo is near 50% on average). Taking the ice cover in both polar spheres from 40 or 50 degree in latitude during the last glacial maximum and 30% of increase in albedo on average, the albedo changes could have caused 4-7% loss in solar energy receipt on the earth. Therefore, the 0.2% increase in solar insolation, if it coincided with deglaciation, must have been completely destroyed by the effect of the expansion of ice and snow cover. However, an abrupt temperature increase at the time of the last glaciation termination has been observed from all records (polar ice cores, marine sediments, etc.).

Instead of the orbital forcing of the Quaternary glacial oscillation, other mechanisms must be explored. Mid-ocean ridge processes induced by ice sheet waning and waxing might be important in the forcing of the Glacial-interglacial cycles. During the last glacial maximum, great ice sheets on the surface of the earth would have had a great influence on the world's stress fields and have caused large deformation at the most vulnerable region of the earth in terms of mechanical strength, the world mid-ocean system, and have induced massive magma release from the deep earth. Once this process occurs, it could generate a rapid deglaciation and global warming by the following processes: (1) the evacuation of the space for the isostatic depression of the ice sheet loaded areas and thus complete collapse of the ice sheets, (2) direct heat release into the ocean, (3) stimulation of deep ocean circulation, and (4) driving CO_2 from ocean into the atmosphere. However, this subject has received little recognition in the past.

The first question to be raised is, could such a force be transmitted to the mid-ocean ridges? This will be examined below. The earthquake data show very uniform stress directions within individual plates (Tarling, 1981; Zoback, 1992). New evidence from the KTB project indicates that the lithosphere is strong enough to transmit tectonic force from plate boundaries (Zoback et al., 1993). The observed rebound in the glaciated areas is obvious, for example, the Hudson Bay region has rebounded approximately 300 m in the last 8000 years (Peltier, 1987) and the Finoscandia over 100 m (Stacey, 1977), clearly demonstrating the elastic properties of the lithosphere. Therefore, it should be feasible to examine the influence of the great ice sheet loading on the deformation of the ocean ridges by modelling the elastic response.

This chapter will present an elastic finite element spheric model, and then discuss the ocean ridge processes and the climate significance combined with the modelling results.

7.2. Earth Model Construction and Assumptions

To simulate the global deformation distribution of the crust caused by ice sheet loads, parameterization of the mechanical properties and structure of the solid earth must be assessed. Geophysical and seismological studies indicate that the solid earth is composed of multiple spheric layers with distinct mechanical properties. There are two major mechanical layers outside the core, the outermost lithosphere and the underlying asthenosphere. The mechanical properties of these two layers essentially control crustal deformation from surface loading. Many studies have shown that the lithosphere can be regarded as elastic material (e.g., Richardson et al., 1979; Erickson, 1993; Coblentz and Sardiford, 1994). Crustal isostasy depends on the viscous asthenosphere as suggested by earlier studies (Barell, 1919a,b; Haskell, 1935, 1936; McConnell, 1965; Peltier, 1982) and later seismological investigations.

In this computation, the solid earth is simplified as an elastic lithosphere over a viscous fluid, the asthenosphere. The structure in this model assumes that under steady-state conditions, the lithosphere is a closed spheric shell constituted by various types of plates with different thicknesses, and the asthenosphere is treated as a non-compressible fluid. Under such conditions, the gravitational isostasy with any load will not occur until the elastic lithospheric shell achieves its failure point. Before crustal failure, the crustal depression under ice sheet loading is elastic. In this case, all elastic deformation of the crust depends on the weight of the ice sheets and the strength of the elastic spheric shell. If the stress produced by ice sheet loads exceeds the elastic deformation range, the closed continuum lithospheric-shell will break up and deep magma may tend to erupt. The contribution of the viscous asthenosphere to surface loading-forced deformation is principally expressed by its drag force on the lithosphere. This function is represented by the springs attached to the lithosphere from the outer core of the earth as illustrated in Figure 7-1. Before lithospheric failure, the viscosity of the asthenosphere protects the elastic shell against deformation. Once the stress exceeds a critical value for lithospheric failure, magma is forced to erupt (or to be exposed at a depth lower than seafloor if the magma reservoir does not have enough pressure) from the asthenosphere onto the solid-earth's surface, which may cause collapse of the ice sheets. After the ice sheets are discharged, the viscosity of the asthenosphere helps the depressed crust to rebound. Therefore, by this mechanism, two major events might occur in the solid earth under ice sheet loads; (1) magma eruption (or exposure) and, (2) partial rebound of the crust because of the incomplete failure deformation protected by the drag force. This is supported by the fact that the 300 m of post-glacial rebound observed in the Hudson Bay area (Peltier, 1985; Begin et al., 1993) is much less than the expected value of 700 to 800 m (Flint, 1971).

Another important property of these viscous fluids is the duration of these processes. As observed, the isostatic process produced by the last deglaciation is still going on (cf. Peltier, 1982, 1988). In this study, interest is toward investigation of the deformations of the world mid-ocean ridges at the time of the last glacial maximum when the ice sheets achieved maximum loading on the earth's crust. Therefore, no time effect is involved in the model.

Figure 7-1. A spheric shell model of the planet Earth. The Earth's lithosphere is simplified into four typical plates with different thicknesses, continents, continental shelves, oceans and mid-ocean ridges. The centre of mass of the Earth is presumed to be fixed in its spatial position and thus is the Earth's core. Springs are attached on the lithosphere and the Earth's outer core along radius directions to simulate the viscous behaviour of the asthenosphere. (EPR = East Pacific Rise, and MAR = Mid-Atlantic Ridge)

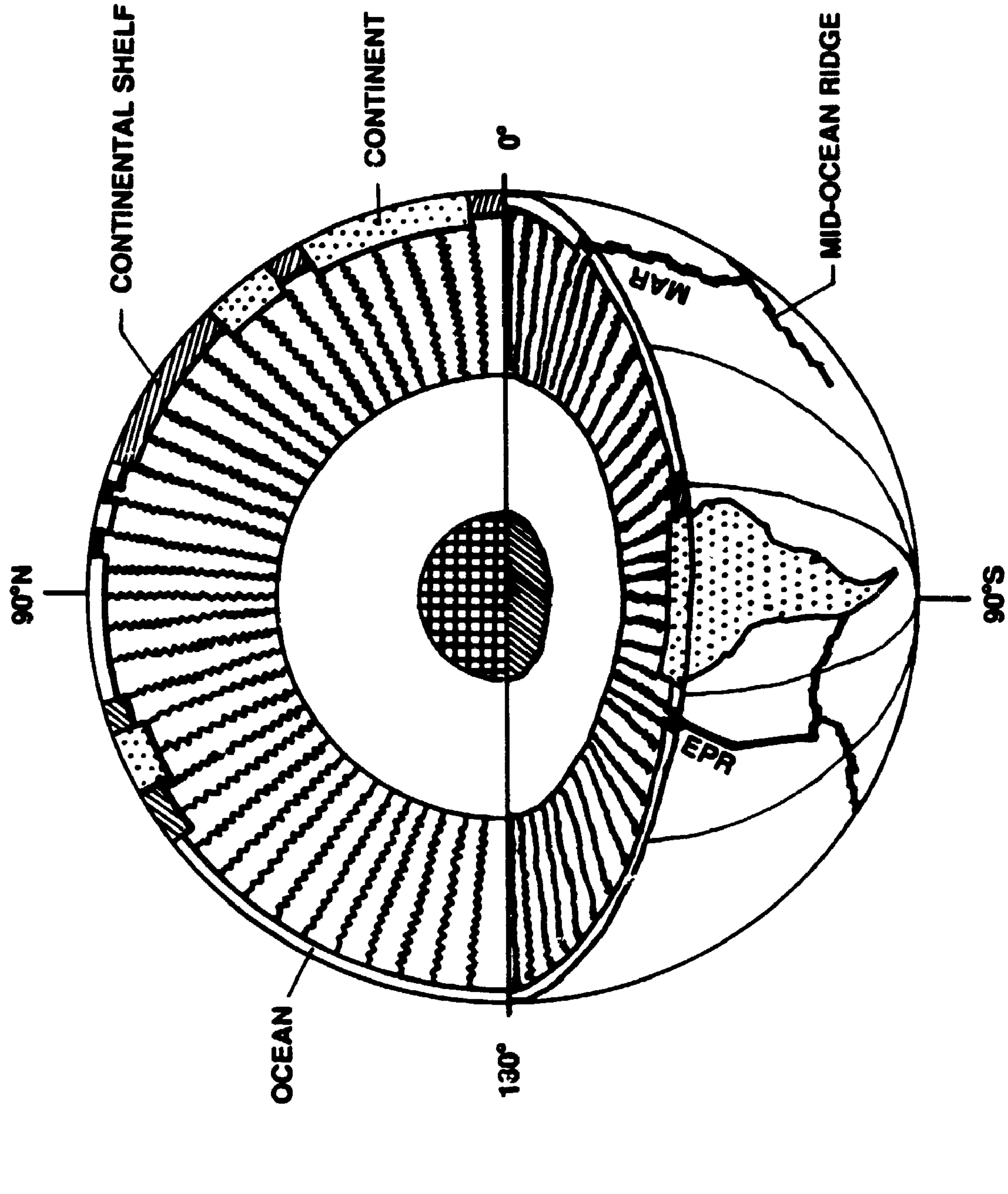
CONTINENTAL SHELF
CONTINENT
MID-OCEAN RIDGE
0°
90°N
90°S
130°
OCEAN
MAR
EPR

7.3. Methods

The computer program SSIAP written by W.M. Liu (1990) is used to establish the finite element model and calculate elastic deformation. Computation was conducted by the Cyber system of the computing centre at the University of Western Ontario. Parameters used in the calculation are listed in Table 7-1. Coordinates of the discretized elements and nodes for the spheric shell earth are listed in Appendices II and III.

The entire earth's lithosphere is treated as a spherical shell with different elastic thickness corresponding to continents (105 km), continental shelves (75 km), oceans (70 km), and mid-ocean ridges (20 km). The plate boundaries and continental shelf configurations are based on the map of *Earth's Dynamic Crust* (Garrett, 1985) and the *World Continental Shelves* (Heezen and Tharp, 1970). The width of ocean ridges is assumed as 0.1 degree of latitude/longitude (equivalent to ~11 km at the equator and 5.5 km at 60° latitude) in order to facilitate the element discretization. The finite-element grid is generally about 5° both in latitude and longitude except for mid-ocean ridges and plate boundaries. The total discretized system of the earth's lithosphere is represented by an elastic spherical shell which consists of 2122 nodes and 2355 elements (see Figures 7-2, 7-3, 7-4, and 7-5).

The thin shell elements which was originally developed by Clough and Felippa (1968) is used to discretize the earth's lithosphere. It is a quadrilateral element composed from four LCCT-9 (Linear Curvature Compatible Triangle with 9 bending degrees of freedom) thin plate elements. A triangular element can also be specified by defining only the first three nodes. Within each triangle, linear curvature can be represented by the interpolation functions. The membrane part of the element is a constant strain triangle.

Table 7-1. Parameters used in the models

Symbols	Parameters' description	Values
R_e	the Earth's radius	6371 km
R_{core}	the Earth's core radius	3471 km
Thickness of the lithosphere		
h_{cont}	thickness of continents	105 km
h_{shlf}	thickness of continental shelves	75 km
h_{ocean}	thickness of ocean lithosphere	70 km
h_{ridg}	thickness of mid-ocean ridges	20 km
E	Young's modulus	10^{12} dyn/cm^2
ρ_{ice}	density of the ice sheets	0.9 g/cm^3
ρ_{asth}	mean density of the asthenosphere	3.5 g/cm^3
V_{ice}	volume of the ice sheets at LGM	58x10^6 km^3
Δh_{sea}	sea level lowering at LGM	146 m
C_{rock}	specific heat of rocks	0.3 cal./g.°C
C_{water}	specific heat of water	1.0 cal./g.°C
T_{water}	temperature of deep ocean water	2 °C
T_{magma}	temperature of magma beneath ocean ridges	1200 °c
g	the Earth's gravitational acceleration	9.81 m/s^2

Figure 7-2. A finite-element mesh of the northern hemisphere of the Earth as viewed from the North Pole. The heavy lines are the combination of successive elements of mid-ocean ridges.

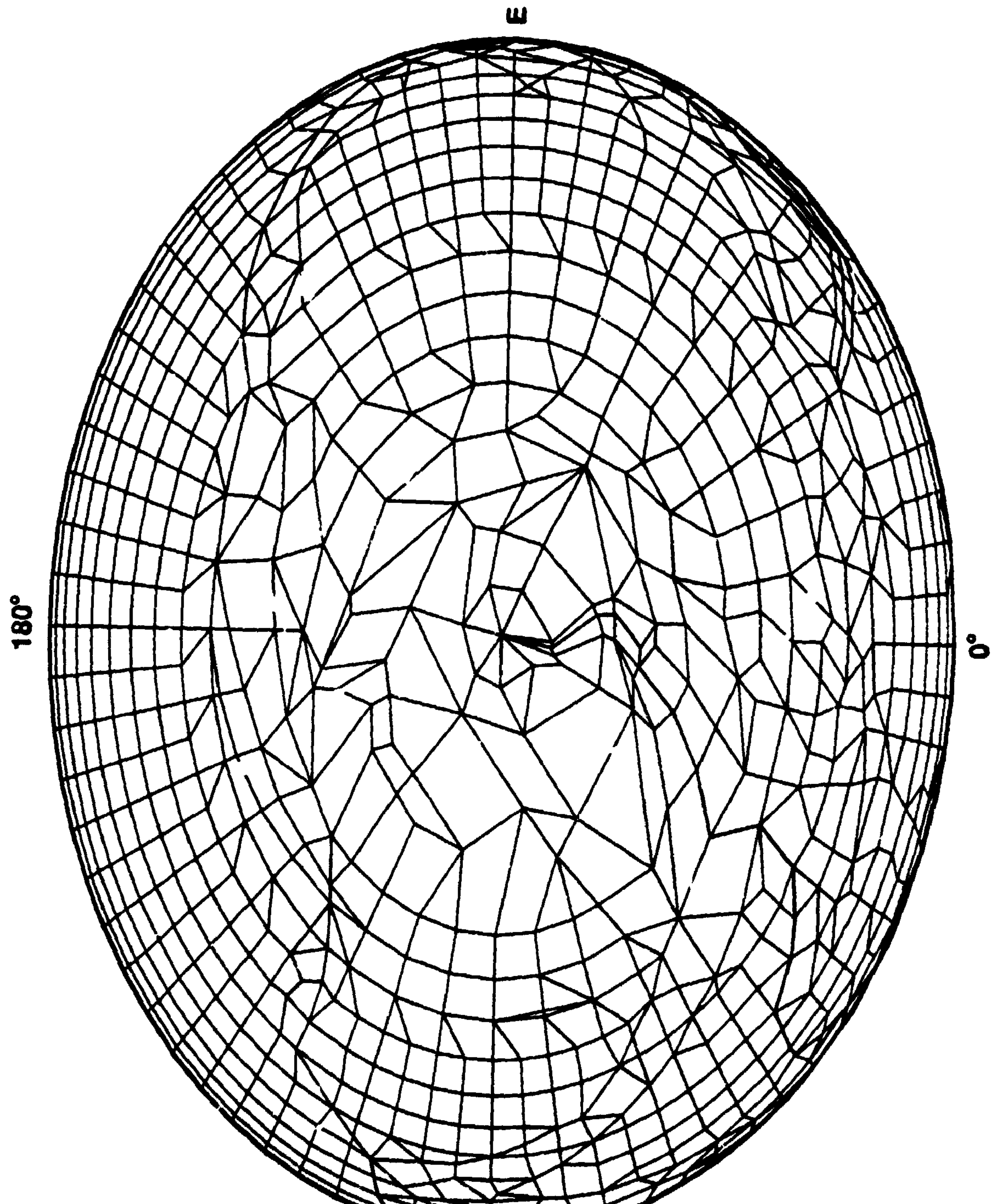
E
180°
0°
W

Figure 7-3. A finite-element mesh of the southern hemisphere of the Earth as viewed from the South Pole. The heavy lines are combinations of successive elements of mid-ocean ridges.

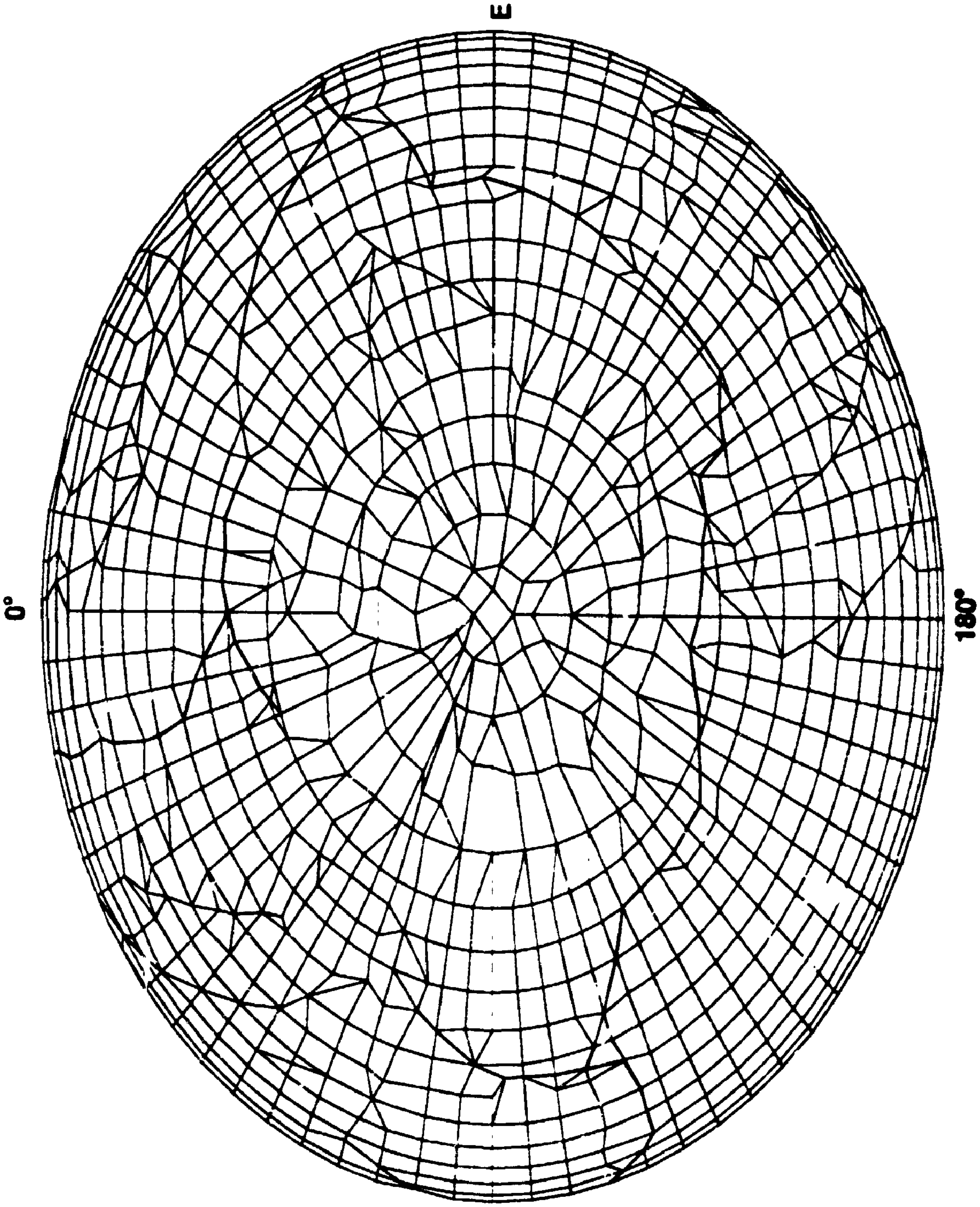
E
0°
180°
W

3

PM-1 3½"x4" PHOTOGRAPHIC MICROCOPY TARGET
NBS 1010a ANSI/ISO #2 EQUIVALENT

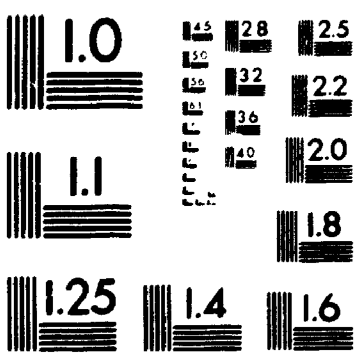

Figure 7-4. The finite-element mesh sector from 50°N to 50°S as viewed from 0° longitude, 0° latitude. The heavy lines are combinations of successive elements of mid-ocean ridges.

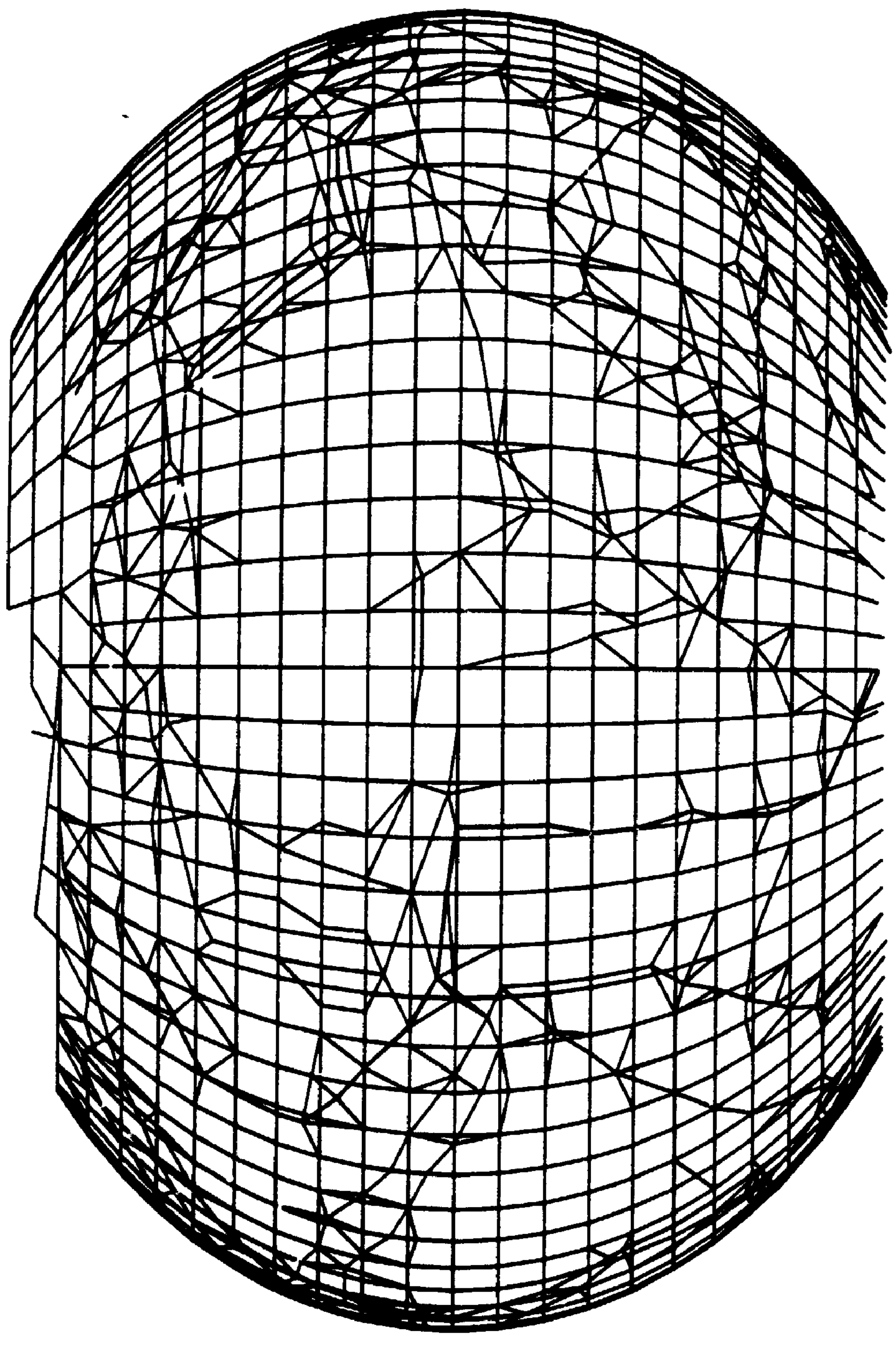

CRUST MESH FROM 50N TO 50S

Figure 7-5. The finite-element mesh sector from 35°N to 30°S as viewed from 0° longitude, 45°N. The heavy lines are combinations of successive elements of mid-ocean ridges.

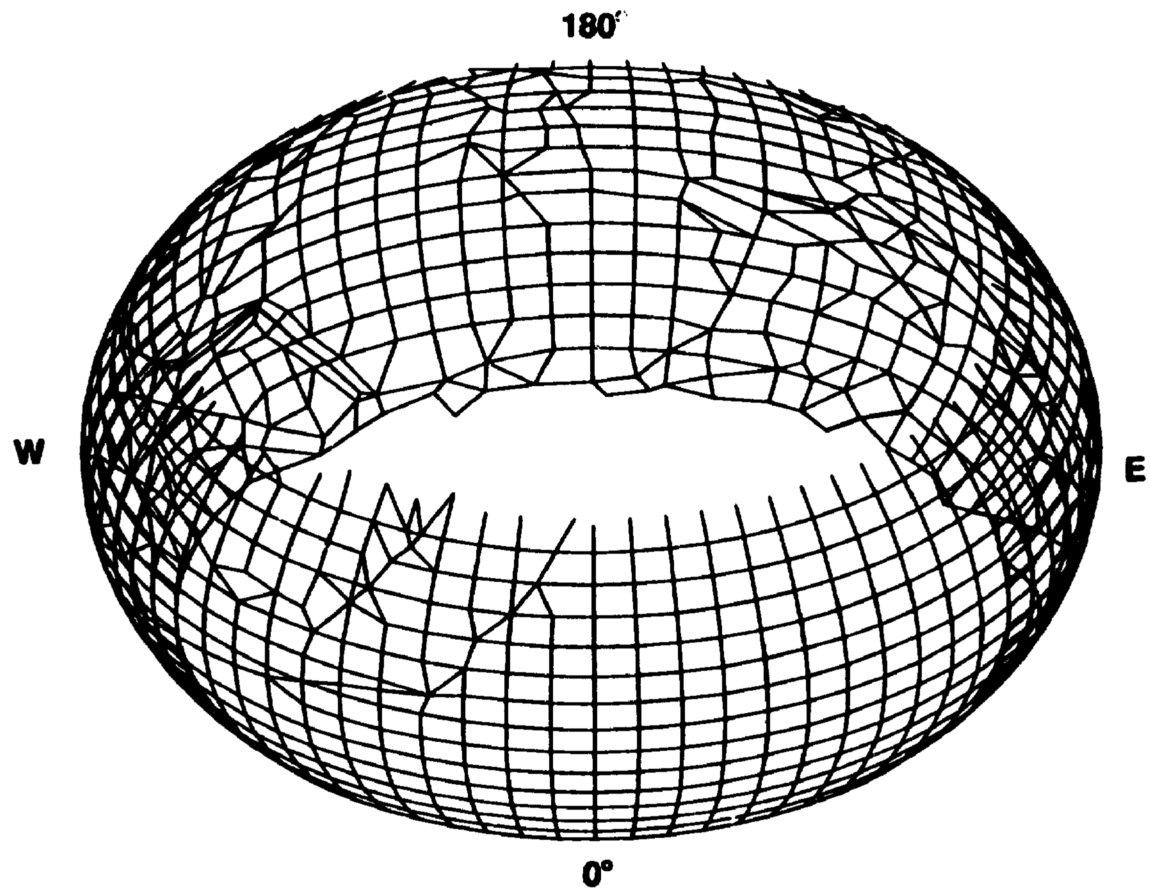
180°
W
E
0°

This element is a displace-based fully compatible element. Therefore, convergence is guaranteed when refining the mesh.

For modeling the displacements of the discretized lithosphere forced by the ice sheet loads in our elastic spherical model, a steady state is assumed, which means a condition of static equilibrium without ice sheet load. Therefore, the sum of all the forces (including gravity of the lithosphere, convection drag of the asthenosphere, Coriolis force etc.) acting on the lithosphere is zero. The distribution and size of the northern Hemisphere's ice sheets, as reconstructed by Denton and Hughes (1981, Fig.6-15) for the last glacial maximum has been applied to the model, and the effect of mountain glaciers and the Antarctic ice sheet has been neglected. Normal pressure loads representing the ice sheets are applied to each node of an element by averaging the total weight of ice on the element and distributing the weight equally to all the nodes of the element according to the equation

$$P_{node} = (1/n) \times \rho_{ice} \hat{H} \Delta S_i$$

where ρ_{ice} is the specific weight of the ice, $\hat{H}$ the mean thickness of the ice on the element, ΔS_i the area of element i in m^2 and n the number of nodes in the element. Here the ρ_{ice} adopted is 0.9 g/cm^3 (cf. Schilling and Hollin, 1981).

The Young's modulus E of the lithosphere is assumed to be 10^{12} $dyne/cm^2$, which is very close to the calculated value using the seismological data given by Anderson (1989) and others (eg., Erickson, 1993). We also assume that the mass geometric centre of the earth (the earth's core) is fixed in spatial position. Therefore, normal pressures along the earth's radius all act on the earth's central point. To simulate the reaction force of the viscous asthenosphere, springs are attached to all the finite element nodes. The stiffness coefficients of these springs are in the range of 10-20% of the membrane stiffness of the earth's lithosphere. It may need to be pointed out that, the length of springs is a changeable parameter in the model runs. The outcore of the earth in the model is substantially a definition of the mechanical spheric shell (layer) which is assumed to be not deformed by the ice sheet loading. In addition, the effect of the length of the springs on mechanical response can be compensated by the change of the stiffness coefficient. Therefore, in the model, the radius value and meaning of the earth's outcore are somewhat different from the conventional meanings, and the top of the outcore in the model refers to a stable solid boundary of the asthenosphere.

7.4. Modeling Results

In order to simulate the displacement of the world mid-ocean ridge system with finite-element elastic spherical shell models, a number of cases were tested for comparison. In the cases with the condition that the elastic thicknesses of continental, continental shelf, oceanic and mid-ocean ridge lithospheres are 35, 20, 10, and 5 km respectively (their actual crustal thicknesses), the output values seem too large (the maximum absolute displacement at mid-ocean ridges is 340 m) even though the stiffness coefficient of the underneath springs was as high as 40%. When the thicknesses of the lithosphere are changed to values similar to those widely adopted (105 km for continents, 75 km for continental shelves, 70 km for ocean, and 20 km for mid-ocean ridges; cf. Richardson et al., 1979) and the stiffness coefficients of the springs are put in the 10-20%

range of the membrane stiffness of the lithosphere, the computed results of displacement are less than the expected value of isostatic rebound for the Hudson Bay region (the computed depression is close to 600 m; the expected complete rebound is 700-800 m, cf. Flint, 1971). From a conservative perspective, discussions in the following section are directed to the results obtained from the latter case with a high stiffness coefficient (20%) as presented in Figures 7-6, 7-7 and 7-8. The related data are given in Appendix I.

7.5. Displacement at Global Mid-Ocean Ridge Systems Induced by the Ice Sheet Loads

Results demonstrate that the most significant deformation effect of the ice-sheets load appears in the Northern Hemisphere (see Figures 7-6,7, and 8, Appendix I). Most regions of the mid-ocean ridges are forced to spread, especially at the high latitudes of the north Atlantic Ocean. The spreading magnitudes (displacements) decrease from the latitude of the central Laurentide ice sheet southwards, and are much less in the Southern Hemisphere than in the Northern Hemisphere. Furthermore, changes in the orientation of the displacement show a complicated pattern at some sections of ocean ridges. For a detailed investigation into the deformation effect of the ice sheet loads on the ocean ridge system, the ridge system has been divided into sectors and discussed separately.

In the north Atlantic region, the mid-ocean ridges are subjected to the largest deformation in the global ocean ridge system. The maximum absolute value of the relative displacement of node pairs occurs at the point around 9°W, 72°N, the end point of tne transform fault east to the southeastern corner of Greenland and north to Iceland (see Figure 7-6). This displacement reaches approximately 100 m. In general, the displacement at ridges is tensile (toward spreading) with directions roughly perpendicular

Figure 7-6. Displacement of the world's mid-ocean ridges calculated by Model 3-1, northern hemisphere sector. Detailed data are shown in Appendix I. See text for explanation.

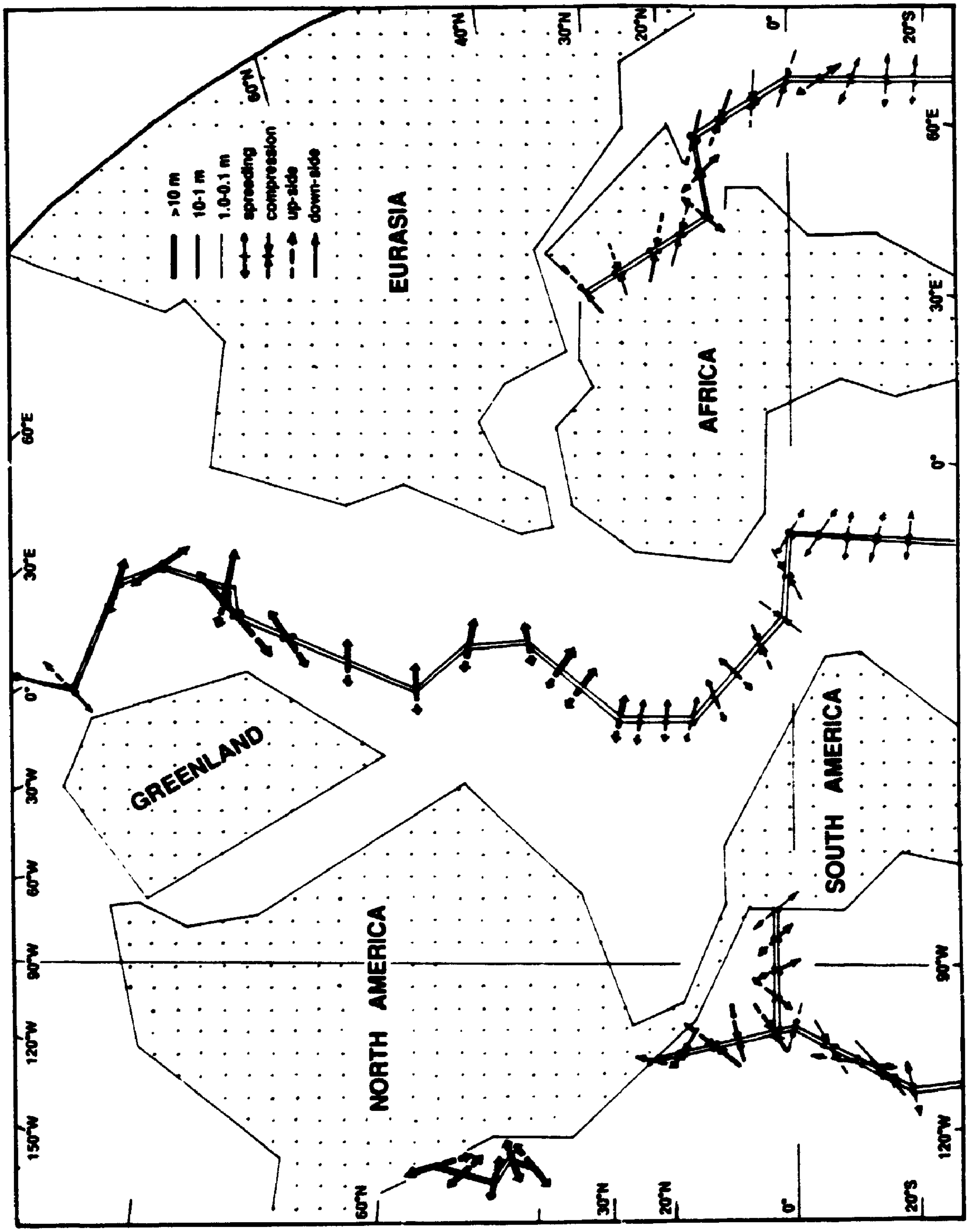
>10 m
10-1 m
1.0-0.1 m
spreading
compression
up-side
down-side
EURASIA
AFRICA
GREENLAND
NORTH AMERICA
SOUTH AMERICA
60°N
40°N
30°N
20°N
0°
20°S
150°W
120°W
90°W
60°W
30°W
0°
30°E
60°E

Figure 7-7. Displacement of the world's mid-ocean ridges calculated by Model 3-1, southern Indian-Pacific Ocean sector. All the relative displacements are in the range of 10-1 cm.

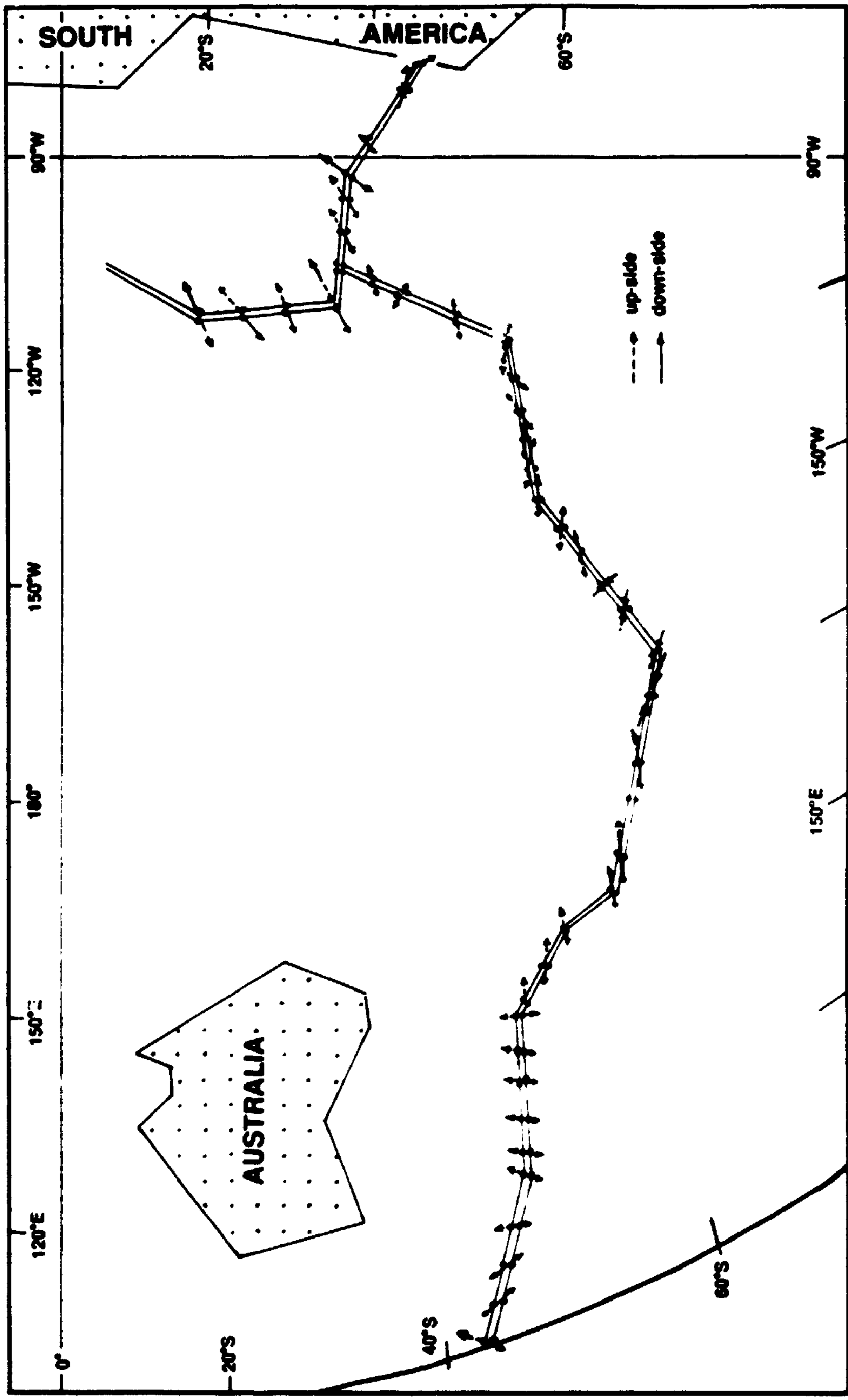
SOUTH
AMERICA
AUSTRALIA
up-side
down-side
20°S
60°S
90°W
120°W
150°W
180°
150°E
120°E
0°
40°S

Figure 7-8. Displacement of the world's mid-ocean ridges calculated by Model 3-1, Mid Atlantic-southern Indian ocean sector.

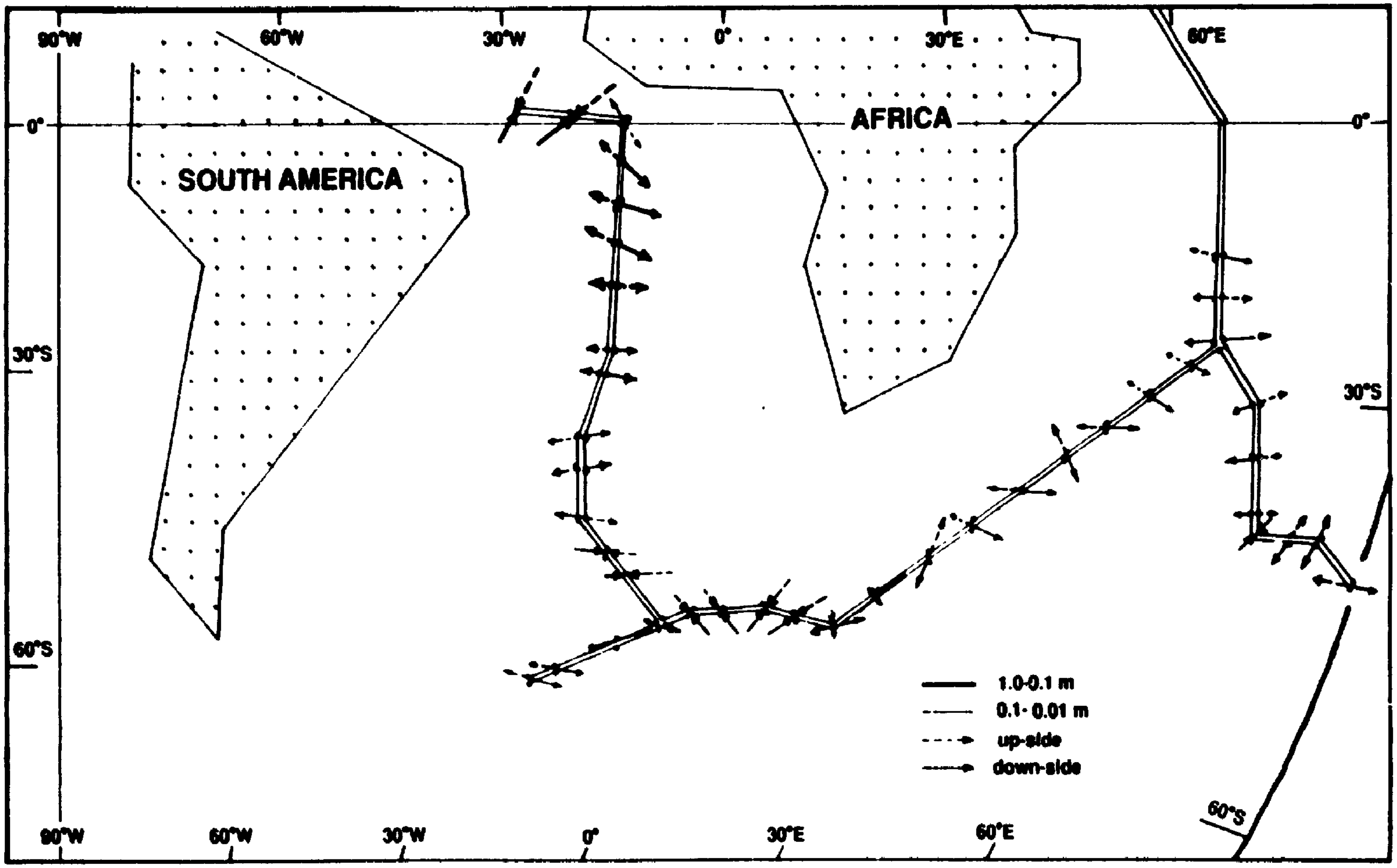
SOUTH AMERICA
AFRICA
90°W
60°W
30°W
0°
30°E
60°E
30°S
60°S
1.0-0.1 m
0.1- 0.01 m
up-side
down-side

to the ridge axes. The spreading amplitudes smoothly decrease from near 70°N down to the tropical region. For some ridge sections, however, the displacement orientation appears unstable. At the transform fault sections (see Figure 7-9), the displacements are orientated nearly parallel to the fault. This is common for all transform faults in the Northern Hemisphere Atlantic Ocean (compare Figure 7-6 with Figure 7-9). But in our model the whole ridge system, including transform faults, are treated as of the same width and same thickness, and without any discrimination. This implies that the ice sheet loads in the Northern Hemisphere did not favour these faults to develop into a normal ocean ridge, but exerted a compressive force against their widening.

In the Juan de Fuca Ridge, the forced displacements appear mainly to spread away from the ridge axes, except for the middle section in our model (See Figure 7-6). The magnitude of the displacement on average is about 10 m for the north segment, and 7 m for the south part.

The East Pacific Rise shows a very complicated pattern of deformation. The longitudinal section (north of 20°S) is compressed, but the latitudinal sections are forced to spread and the directions vary from one part to another (Fig.7.6).

Ocean ridges located in the Red Sea and in the central Indian Ocean show a minor deformation response to the ice sheet loading. The maximum horizontal translation is less than 1 m. The southeast Indian Ocean Ridge and the Pacific Antarctic Ridge received minimum influence of deformation. The magnitude of the displacements in these regions are all less than 10 cm. But their orientations might have certain implications and will be discussed further below.

Figure 7-9. The global mid-ocean ridge system (from RIDGE, 1994).

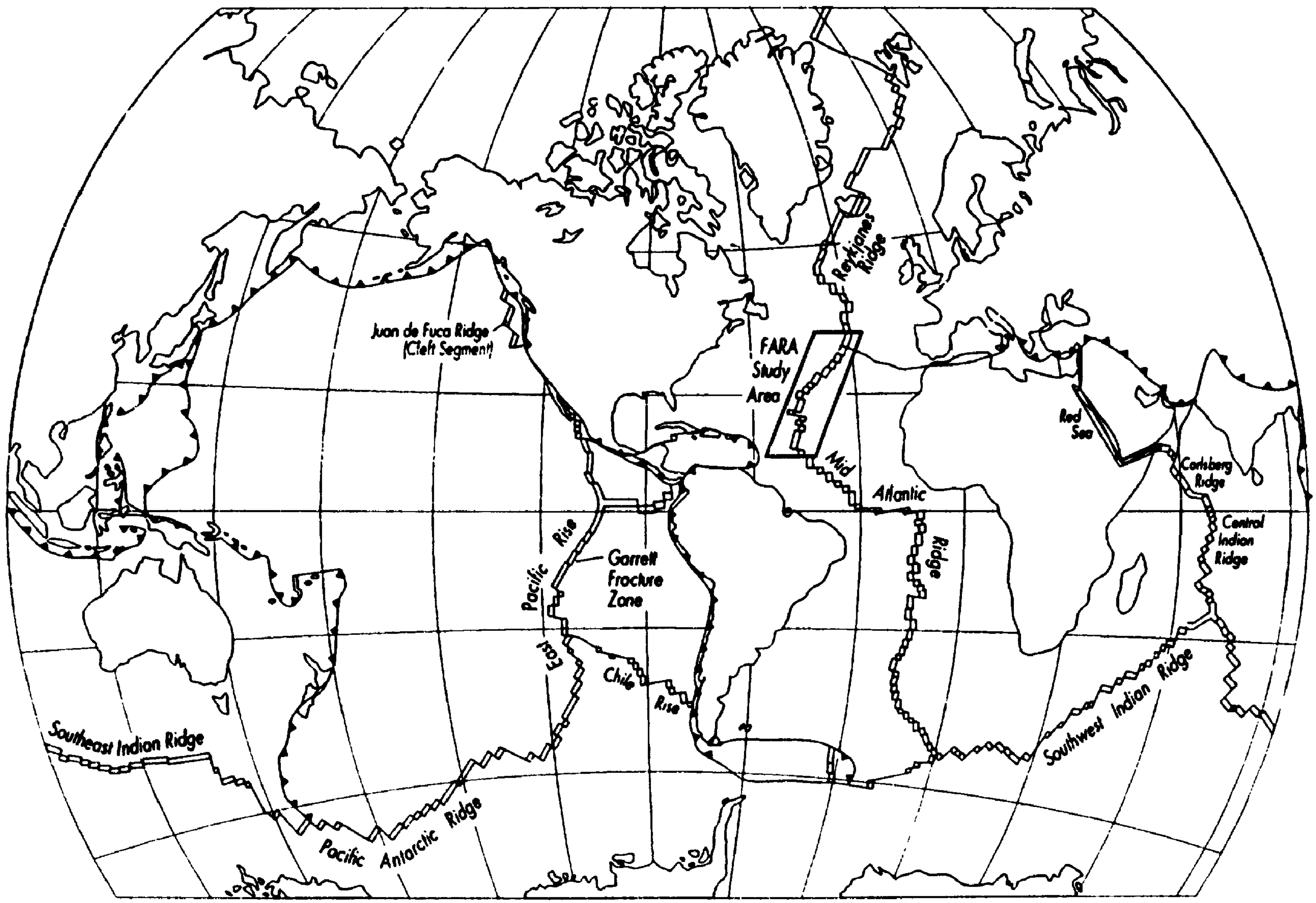

Juan de Fuca Ridge
(Cleft Segment)
FARA
Study
Area
Reykjanes
Ridge
Mid
Atlantic
Ridge
Red
Sea
Carlsberg
Ridge
Central
Indian
Ridge
Southwest Indian Ridge
Garrett
Fracture
Zone
East
Pacific
Rise
Chile
Rise
Southeast Indian Ridge
Pacific Antarctic Ridge

7.6. Topography of the World Mid-Ocean Ridges and the Ice Sheets Load Waning and Waxing

It is interesting to note that the modeling results (the calculated deformations) are coincident with the ridge styles. At the north Atlantic ridges, the ice sheet loads give the transform fault zones a compressive deformation which prohibits faults to spread in a perpendicular direction. Furthermore, in well-developed transform fault zones such as the section of Mid-Atlantic Ridge near the equator, the sections in the Pacific Antarctic Ridge and Southwest Indian Ridge, the deformation orientations are strongly altered (see Figures 7.6, 7.7, 7.8, 7.9). Similar features are also found at the Juan de Fuca Ridge and the East Pacific Rise. But as pointed out before in the model input, all the world's mid-ocean ridges are presented as continuous structures with uniform width and thickness. The coincidence of the ridge fashions with the ice sheet load forcing gives rise to an interesting question. Are the modern patterns of the world's mid-ocean ridge system markedly modified by repeated alternations of massive water loading on continents and ocean basins during the past ice ages?

In the modeling experiments, the East Pacific Rise suffered a compression with ice sheet loading in the northern hemisphere. This favours formation of positive topography of this ridge. Furthermore, because of the viscosity of the asthenosphere, the duration of isostatic rebound and relaxation are very much prolonged. As with the rebound resulting from the last ice sheet collapse, the relaxation will very likely still be acting at present, which should make a positive contribution to the faster spreading rate at the East Pacific Rise (see Figure 7-10).

In contrast, the negative topography of the north Atlantic ridges is consistent with

Figure 7-10. A conceptual model showing the influence of ice sheet loads in the northern hemisphere's continents on mid-ocean process of the East Pacific Rise. a, A presumed original state in the Earth's surface conditions without the ice sheet. Spreading at a normal speed equilibrating with magma production and all forces in the ridge system. b, As the ice sheets load, a lateral compressive force acts on the ridge axis, which forces the ridge edges to uplift and decreases the spreading rate. High ridge peaks build up during this stage. c, A phase showing the ice sheets discharged into oceans. The lateral compression ceases, and the prolonged relaxation due to the viscous asthenosphere response enhances the spreading rate, as observed today. Because the pressure in the magma source decreases with time, the altitude of the central ridge is lowered until lateral compressions are re-established. d, A renewed compression phase features a new episode of high ridge-peaks build up.

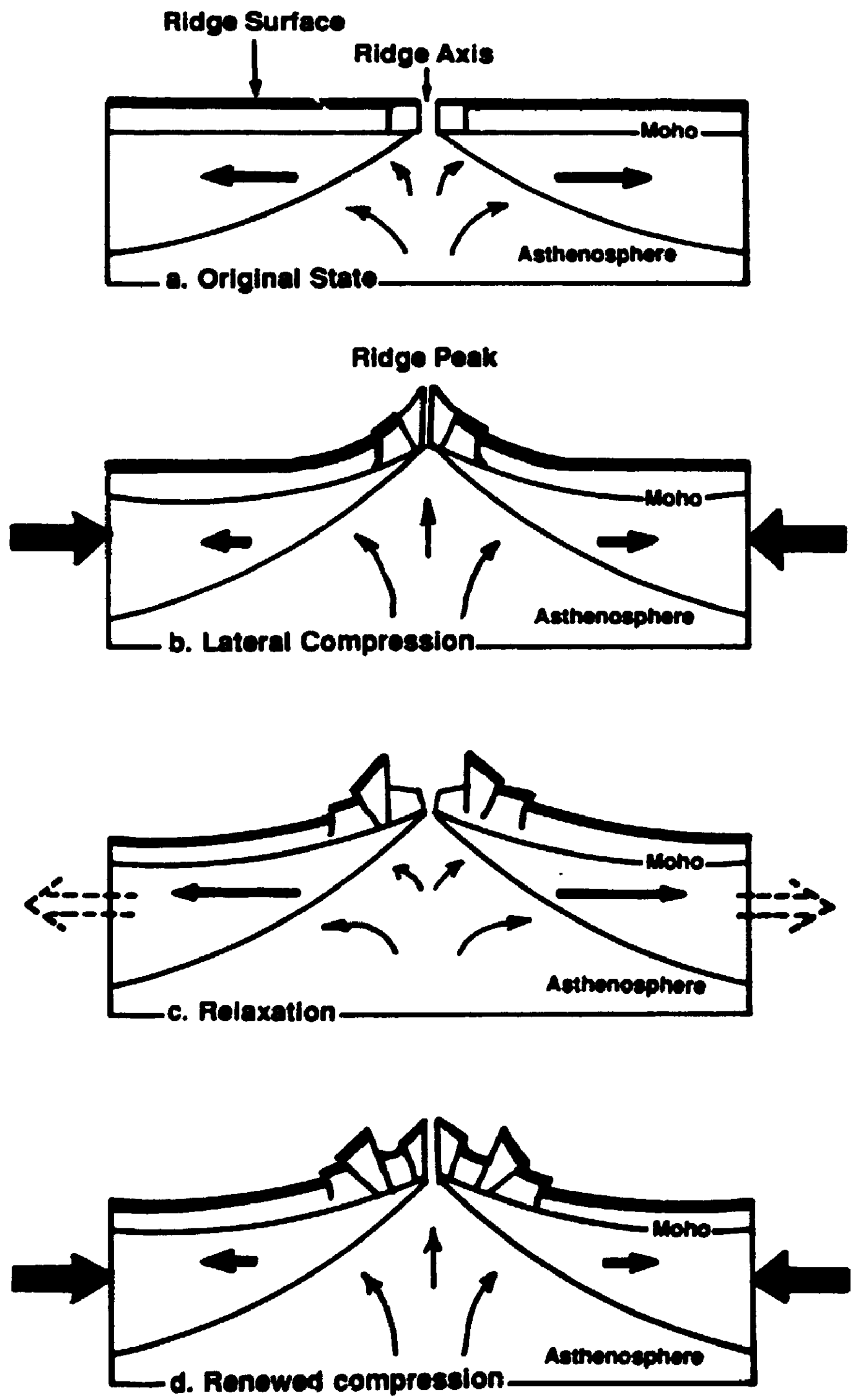
Ridge Surface
Ridge Axis
Moho
Asthenosphere
a. Original State
Ridge Peak
Moho
Asthenosphere
b. Lateral Compression
Moho
Asthenosphere
c. Relaxation
Moho
Asthenosphere
d. Renewed compression

the modeling results. Assuming the magma production rate to be nearly constant for periods of millions of years, the passive magma output forced by ice sheet stress largely exceeds its normal output rate (spreading rate) and thus exhausts the reservoir. Therefore, the magma output of the north Atlantic ridges in this scenario would not have enough pressure for upwelling onto the sea floor but to a depth lower than the sea floor, and form a new valley floor. Today, the observed topography at the north Atlantic ridges is characterized by a central deep valley and stepwise walls (cf. Mutter and Karson, 1992; Smith and Cann, 1993; Cannat, 1993; Tuchocky and Liu, 1994) This would most likely relate to the effect of multiple ice sheet loadings and discharges related to the glacial-interglacial fluctuations. Also, the slow spreading rate observed today at this ridge would have resulted from magma exhaustion due to the forced stretching, indicating that the magma reservoir underneath the north Atlantic ridge is still at the accumulation (recovery) stage. These relations are illustrated in Figure 7-11.

7.7. Magma Output at Mid-Ocean Ridges

7.7.1. Quasi-Instantaneous Output Related to Elastic Failure

With great ice sheet loading, the ocean ridges attain various values of elastic deformation at individual node pairs. As has been discussed, this deformation occurs at the same time as the failure point. is achieved. Therefore, failure displacement will occur immediately. Because the calculated magnitudes are the resultants of all forces including the drag force, there is no extra force to protect against the deformation. In other words, all forces agree to such a magnitude of the deformation at a node pair, which implies that the calculated displacement will be attained nearly instantaneously.

Figure 7-11. A conceptual model showing the influence of the ice sheet loading on the Northern Hemisphere continents upon North Atlantic Ocean ridges. a, A presumed original state as in Figure 7-10a. b, The forced extension by ice sheet loading. As the required extension largely exceeds its automatic spreading, the output magma is at a certain depth equilibrating with its upwelling pressure. Thus a central valley of the ridge axis is created. c, After the stretching force disappears, large scale crustal accretion at the central rift ceases. In this stage, magma is produced in small chambers and intermittently erupts on the valley floor mainly along the marginal faults. d, A new episode of forced extension driven by the next ice sheet loading. A new central valley floor is formed and the previous one becomes a terrace wall at the side of a new valley.

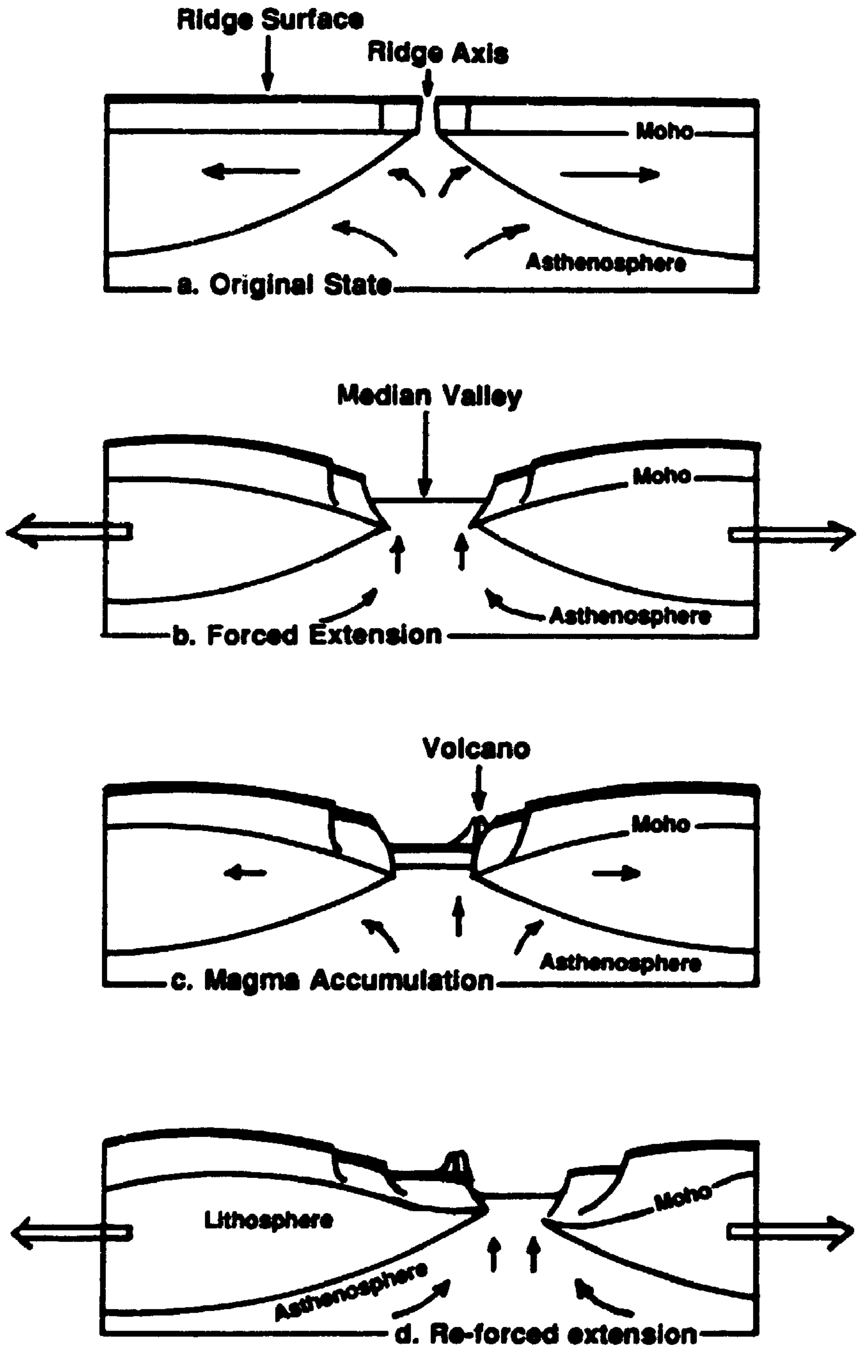
Ridge Surface
Ridge Axis
Moho
Asthenosphere
a. Original State
Median Valley
Moho
Asthenosphere
b. Forced Extension
Volcano
Moho
Asthenosphere
c. Magma Accumulation
Lithosphere
Moho
Asthenosphere
d. Re-forced extension

Using the displacement results listed in Appendix I, a minimum instantaneous magma output at mid-ocean ridges forced by the ice sheet load can be estimated. As the major displacements are located in the northern hemisphere, estimation is focused on the ridges in this range.

In the first step, the ridges are divided into sections according to displacement features and geographic distribution patterns. Following this, the length of each section is calculated. The quasi-instantaneous magma output is estimated as a minimum value of the ridge-crustal accretion volume forced by the failure extension.

In the Atlantic Ocean, the principal trend of the ridge axes above 17°N is longitudinal except for the transform faults. Therefore, we use the "v" component, the partial values in the y coordinate of the displacement vector (relative latitudinal displacement, see Appendix I for explanation) to approach the spreading value in the normal direction neglecting longitudinal and vertical translations. For the ridge section between 2 and 17°N, horizontal displacement is calculated and then converted to the normal direction of the ridge axis because the true spreading values cannot be simplified by substitution of any partial component of the three coordinates. The mean value for each ridge section is obtained by averaging the normal direction spreading values of all node pairs in that section. As an estimate, a uniform thickness of 5 km has been assumed for the new accreting crust. With the same treatment, the magma output at Juan de Fuca Ridge has been estimated. The output of magma in transform fault sections has not been taken into account. The total budget of the quasi-instantaneous magma output induced by the ice sheets loading is listed in Table 7.2.

Table 7-2. Quasi-instantaneous minimum magma output at mid-ocean ridges of the Northern Hemisphere induced by ice sheet loading (resulting from the elastic failure only) estimated from Model 3-1.

Ridge A A(long/lat)	Sections to B B(long/lat)	Latitude interval Δθ(degree)	Longitude interval Δφ(degree)	Length AB* (km)	Spreading magnitude mean (m)	Magma output (km³)
Atlantic	Ocean					
-10/83	10/77.6	5.6	20	783.990	(4.0)	(15.68)
10/77.6	9/75.4	2.2	1	246.107	20.5	25.23
9/75.4	-3/72	3.4	12	559.156	43.95	122.88
-3/72	-9/72	0	6	206.074	(36)	(37.09)
-9/72	-35/55	17	26	2531.347	33.1	415.96
-35/55	-28/49	6	7	839.604	22.69	95.25
-28/49	-30/41	8	2	904.819	16.57	74.96
-30/41	-45/29	13	15	2052.708	7.065	72.51
-45/29	-46/17	12	1	1337.908	2.701	18.07
-46/17	-28/2	15	18	2603.325	0.6	7.81
Subtotal				9438.713		832.67
						(885.44)
Pacific	Ocean					
-129/54.5	-130/45.5	9	1	1004.580	10.52	53.95
-126/44	-127/40.5	3.5	1	400.881	7.40	14.83
Subtotal				1405.461		68.78
Total						901.45
						(954.22)

*Note:

$$AB = \frac{2\pi R}{360}\sqrt{\Delta\theta^2 + \Delta\phi^2 \left(\frac{\cos\theta_A + \cos\theta_B}{2}\right)^2}$$

7.7.2. Perturbation of the Episodic Magma Output Related to Asthenosphere Deformation Flow

It is easily understood that the failure extension must stimulate massive magmatic eruptions at places where melt reservoirs have achieved certain pressures. A tentative and coarse estimate is presented here by using the available isostatic data. The total episodic magma output induced by the ice sheet loading is estimated below.

The total mass of the ice sheets is 4.2×10^{22} grams, using the equation

$$M_{ice\ sheets} = \Delta L A \rho_{water}.$$

Where the $M_{ice\ sheets}$ is the total mass of the world's ice sheets during the last glacial maximum. Taking the eustatic sea level lowering ΔL as 117 m (Denton and Hughes, 1981), the ocean area A as 361×10^6 km^2 (Judson et al., 1987), and the specific weight of water as 1.0 g/cm^3.

The complete depression in the Hudson Bay region is calculated by:

$$H_{depression} = H_{ice\ sheet} \times \rho_{ice}/\rho_{upper\ mantle}$$

where $H_{ice\ sheet}$ (the ice sheet height) is about 4000 m on average (cf. Denton and Hughes, 1981), the specific weight of the ice sheet ρ_{ice} is 0.9 and the specific weight of the upper mantle, $\rho_{upper\ mantle}$ is 3.5 g/cm^3. The complete depression for this region should be 1028 m.

The rebound value for the Hudson Bay region is observed to be about 300 m during the past 8 000 years (Peltier, 1985; Begin et al., 1993). Another 300 m of rebound between 14 000 to 8000 years B.P. has been extrapolated according to the exponential decrease of the rebound rate (cf. Peltier, 1985, Fig. 2). Obviously, there is 428 m rebound still missing, which correlates to a 42% loss of the ice sheet mass. This equals 1.76×10^{22} grams ($\sim 5 \times 10^{6}$ km^3) of magma output and 6.3×10^{24} calories of heat released to oceans.

To melt the total ice sheets (4.2×10^{22} grams), 3.36×10^{24} calories would have been needed (80 cal./g of the fusion heat of water). That means 2.94×10^{24} calories have been contributed to ocean warming. This amount is large enough to raise the seawater temperature about 2.2 °C assuming a modern ocean water volume of 1.32×10^{9} km^3 (cf. Judson et al., 1987).

7.8. Effects on Rapid Deglaciation and Global Warming

The following sections emphasize that the pulsative spreading and instantaneous heat release could powerfully stimulate a rapid deglaciation (termination) and global climate warming.

7.8.1. Instantaneous Heat Release

As discussed in section 7.6.1 and Table 7-2, the minimum forced quasi-instantaneous output of magma at mid-ocean ridges in the northern hemisphere is about 900 km^3. When exposed, the magma must cool and release heat to the ocean. The amount of the released heat is determined by the following equation with neglect of latent heat of crystallization:

$$Q = C\rho V\Delta T$$

where C is the specific heat of magma, about 0.3 cal./g.°C (cf. Anderson, 1989), ρ the density of solidified magma, assuming 3.5g/cm^3, V the volume of magma output, and ΔT the temperature difference between magma and deep ocean water, which is approximately 1200°C. The estimated minimum heat released from the magma to ocean water is 1.14 x 10^{21} calories. This is equivalent to 5% of the yearly amount of sunlight absorbed by the troposphere and ocean in the northern Atlantic basin.

The warming effect is closely related to the rate of the heat liberation. From previous observation, faulting is a very common phenomenon in the median valley of the North Atlantic Ridge (Smith and Cann, 1993). This must greatly enhance the permeability of the ridge crust and deep hydrothermal circulation, and thus accelerate magma cooling. Nevertheless, its climatic influence is much more than direct heating.

7.8.2. Stimulation for Deep Water Circulation

Studies by Lowell and Germanovitch (1995) and others (e.g., Baker et al., 1987, 1989) have pointed out that even as small amount as 0.01 km^3 of magma at an ocean ridge can generate a megaplume of ocean water mass in the order of 20 km in diameter. Over 800 km^3 of magma output in the northern Atlantic basin forced by the ice sheet loading must have caused chaotic perturbation in the ocean temperature gradient and density gradient, and therefore caused vigorous deep water circulation. During such an event, the exposed magma along the mid-ocean ridge axes heats the deep water just above the ridges. The heated water could form superplumes upflowing to certain heights.

Following this, the ambient cold water will form downflows migrating towards the hot ridges due to density gradient forcing. Because large extension of mid-ocean rifts is predicted in the region from the tropical Atlantic to the Arctic circle, the superplumes of hot water would influence almost the entire northern hemispheric Atlantic Ocean. Therefore, the induced vigorous massive deep water circulation must involve the whole Atlantic.

Many studies indicate that during glacial periods the North Atlantic deep water circulation was greatly weakened or even thought to have shut down (Broecker and Denton, 1989; Boyle et al., 1987, 1990; Bond et al., 1992). The polar ice front in the North Atlantic Ocean reached as far south as 40- 50°N (Ruddiman and McIntyre, 1981) during the last glacial maximum. The forced stretching of the mid-ocean ridges due to a critical volume of the ice sheets in the northern hemisphere, like a powerful engine, would have generated north Atlantic deep water circulation and forced world-wide ocean circulation, possibly flipping over the ocean-operation mode from glacial to interglacial.

7.8.3. Contribution to the Enhancement of Atmospheric CO_2 Levels

Greenhouse gases are an important factor in global warming. Observations of polar ice cores in both hemispheres show that the atmospheric CO_2 and methane (CH_4) fluctuate in phase with temperature (Dansgaard and Oschger, 1989; Barnola et al., 1987). The climate forcing of the change in CO_2 from 200 to 280 ppm is believed to be about 1.75 °C and the combined forcing of CO_2 and CH_4 could account for a 2.3 °C warming (Chappellaz et al., 1990; Lorius et al., 1990). But the mechanism of the rapid rise of these gases still remains a puzzle.

Massive magmatism at mid-ocean ridges has a positive effect on the enhancement of atmospheric CO_2 levels. Ocean water warming caused by magma output at ocean ridges must lower CO_2 solubility and drive more CO_2 from cold ocean regimes into the atmosphere. During magma eruptions, certain quantities of greenhouse gases will be liberated from the deep earth. In addition, the temperature rise near the ocean floor will intensify decomposition of organic matter in ocean sediments to produce more greenhouse gases. Taking all of these factors together, the episodic ocean ridge accretion, driven by the ice sheet loading, could greatly raise the atmospheric CO_2 from glacial to interglacial level within a rather short period.

7.9. Fluctuations in Spreading Rates of the Ocean Ridges and Glacial-Interglacial Oscillations

As illustrated in Figures 7-10 and 7-11, the mid-ocean ridge processes and the ice sheets are coupled together in the dynamic surficial environment of the planet Earth. In the previous section, the influence of ice sheet loading on ocean ridge process, and the spreading rate variation and topographic development was discussed. The following section will concentrate on how the mid-ocean ridge process might have an imprint on the pacing of secular climate change.

When the ice sheets reach a critical volume, enough to pass the elastic deformation threshold of the lithosphere at mid-ocean ridges, failure deformation must take place. Only massive magma output from mid-ocean ridges could provide the interior space to allow large scale isostatic depression of the crust underneath the ice sheets to occur, and hence lead to a complete collapse of the ice sheets by faulting and lowering the elevation (because the atmospheric temperature in the troposphere declines with elevation). Interlocked by this mechanism, the pulsative magmatism of the world mid-ocean ridges might in turn promote a complete deglaciation. Meanwhile, through direct heating, forcing deep ocean circulation and enhancing greenhouse gases levels of the atmosphere, the sudden exposure of a massive amount of magma from the mid-ocean ridges would lead to a world-ocean warming first and then a global climate warming, and force the climate into an interglacial period.

As mentioned above, the magma production in the deep earth is presumably constant on a time scale of millions of years. After excessive export of magma from the deep earth, the magma reservoir in these regions may become depleted. Therefore, the ocean ridges in the north Atlantic may have evolved into a relatively quiet stage of magma accumulation, during which small scale volcanism and slow spreading rates could only be observed. With less energy supplement from the earth's interior, the north Atlantic deep water circulation would decrease, and the global climate would become cooler and move into a glacial period of long-term ice-sheet growth.

The lithospheric thickness at mid-ocean ridge axes largely depends on magma flux, as indicated by the different thickness between the fast-spreading East Pacific Rise (Detrick et al., 1987; Harding et al., 1989; Vera et al., 1990) and the slow-spreading Mid-Atlantic Ridge (Huang et al., 1986; Bergman and Solomon, 1990; Kong et al., 1992). It is a direct expression of the ridge's thermal state, and should reflect the balance between heat loss through conductive and hydrothermal cooling, and heat supply from the asthenosphere (Cannat, 1993). Axial lithospheric thickening will enhance the strength of the ridge's lithosphere against ice-sheet- forced deformation and set up a new threshold of maximum volume of the ice sheets. Once this threshold of the ice sheets volume is achieved (which is determined by the fragile part of the lithosphere), a new episode of ocean ridge extension and deglaciation would re-occur. In this scenario, the ice sheet loading and ocean ridge processes could be coupled to produce the glacial-interglacial oscillations. Therefore, the secular climate oscillations very likely reflect the balance of a self-sustained system involving the earth's interior and the earth's surface rather than other exotic forcing mechanisms in the Quaternary.

7.10. Possible Link between Ocean Ridge Process and Ocean $^{87}Sr/^{86}Sr$ Changes on Glacial Cycle Scale

Strontium isotope studies in marine sediments indicate that $^{87}Sr/^{86}Sr$ ratios have been rising since the early Cenozoic (DePaolo and Ingram, 1985; Faure, 1986; Edmond, 1992; Paytan et al., 1993). This is attributed to plateau uplift, in particular of ›et (Ruddiman and Raymo, 1988; Ruddiman and Kutzbach, 1991; Raymo and Ruddiman, 1992; Edmond, 1992). It is believed that the Tibetan Plateau uplift has intensified the Indian monsoon and thus enhanced chemical weathering of the continental crust. However, this does not well explain the changes in $^{87}Sr/^{86}Sr$ ratios on the glacial cycle scale.

Short-term variations of the $^{87}Sr/^{86}Sr$ ratios in world oceans have been observed in recent years (Dia et al., 1992; Paytan et al., 1993; Clemens et al., 1993; Blum and Erel, 1995), but are not fully understood. As shown in Figure 7-12, Clemens et al. (1993) found that the $^{87}Sr/^{86}Sr$ variations follow a 100-kyr cycle more or less simultaneously with changes in ice volume (ocean $\delta^{18}O$) in the equatorial Indian Ocean

Figure 7-12. Seawater $^{87}Sr/^{86}Sr$ records compared to the SPECMAP $\delta^{18}O$ record of global ice volume (from Clemens et al., 1993) Indian Ocean site 758 (top) and Pacific Ocean V28-238 (bottom). Oxygen isotopic stages are labelled at the top (even numbers represent glacial intervals).

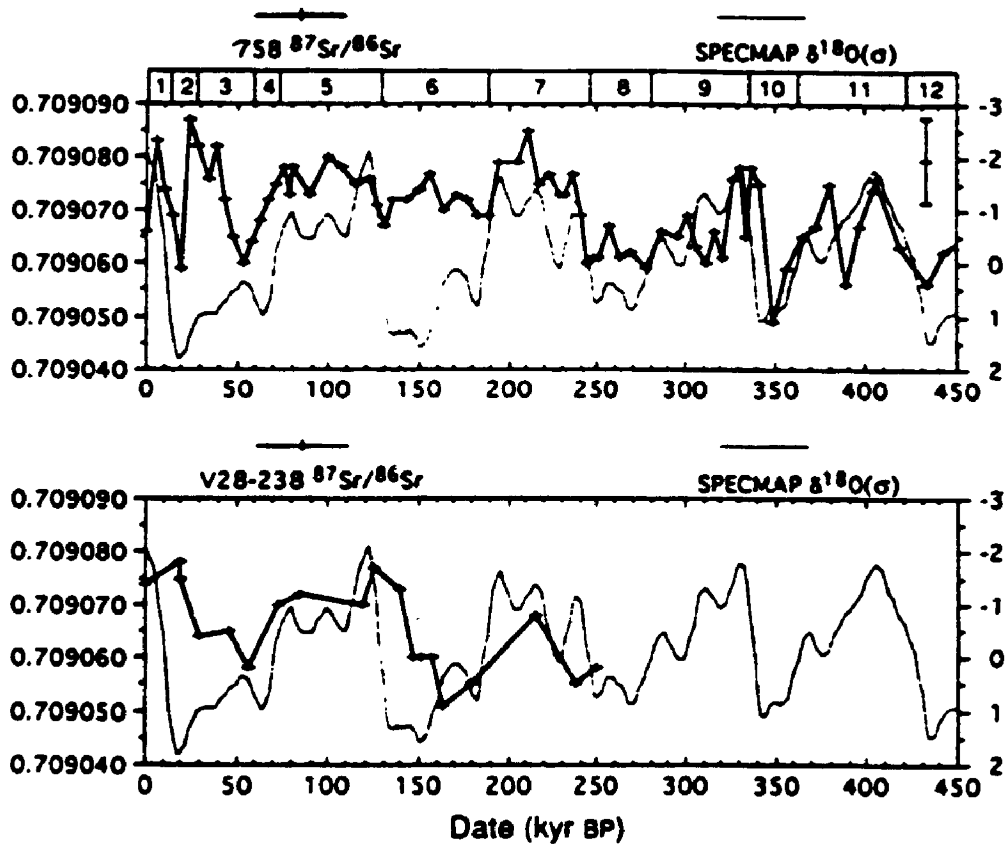
758 $^{87}Sr/^{86}Sr$
SPECMAP $\delta^{18}O(\sigma)$
1 2 3 4 5 6 7 8 9 10 11 12
0.709090
0.709080
0.709070
0.709060
0.709050
0.709040
-3
-2
-1
0
1
2
0 50 100 150 200 250 300 350 400 450
V28-238 $^{87}Sr/^{86}Sr$
SPECMAP $\delta^{18}O(\sigma)$
Date (kyr BP)

(actually leading the global ice-volume signal by a short period), and some thousand years ahead in the equatorial Pacific at deglaciations (Dia et al., 1992; Clemens et al., 1993). These phenomena could be better explained by the episodic extension of mid-ocean ridges. These magmas from ocean ridges with a typically low $^{87}Sr/^{86}Sr$ ratio of 0.7030 (cf. Faure, 1986) could release a great amount of strontium to the ocean by alteration with sea water. The observed low values of ocean $^{87}Sr/^{86}Sr$ ratios during deglaciations could be related to the pulsatory ocean ridge process. The continuous increase in the $^{87}Sr/^{86}Sr$ ratios of Cenozoic marine sediments is not fully explained by weathering factors alone because the great enhancement began much earlier than the plateau uplift-intensified weathering.

It should be stressed here that magma influx at mid-ocean ridges may be an important factor for ocean $^{87}Sr/^{86}Sr$ ratio change in the Cenozoic. The ocean $^{87}Sr/^{86}Sr$ ratio can be considered as a mixture of three isotopic varieties of strontium derived from young volcanic rocks, old sialic rocks of continental crust and marine carbonate rocks of Phanerozoic age. Therefore, the $^{87}Sr/^{86}Sr$ ratio of seawater is an indirect indicator of the kinds of rocks that are exposed to chemical weathering on the surface of continents and in ocean basins. The low intensity of magmatism in the Cenozoic suggests a reduced influence to the ocean $^{87}Sr/^{86}Sr$ signal than previously. Even though the chemical weathering of continental crust does not increase, the ocean $^{87}Sr/^{86}Sr$ can still increase. Likewise, an increase of magmatism will decrease the ratio, as observed for early geologic time (cf. Faure, 1986; Larson, 1991).

7.11. Support from Geologic Evidence

Sturchio et al. (1993) suggest that the geothermal activity in the Kenya rift valley regions corresponds to periods of high lake levels. Studies of the Younger Toba Tuff in Indonesia indicate that massive volcanism occurred during a climatic transition period, which has been attributed to rapid ice growth and global sea level falling (Rampino and Self, 1992, 1993). Due to discrepancies between the $^{87}Sr/^{86}Sr$ ratio in calcite shells of planktonic foraminifera, and the estimated chemical weathering influx for the past half million years, the possibility of pulsations of the seafloor hydrothermal fluxes has been proposed for future exploration (Froelich, 1993; Clemens et al., 1993).

More convincing evidence lies in the deep water temperature changes through glacial cycles. As shown in Figure 7-13, the deep ocean water temperatures rise simultaneously and abruptly with global ice volume waning. With the ice and melt water discharge to the ocean, the ocean would have become cooler at least in the deglaciation period if no deep heating had occurred. Obviously, the observed greater than 2 °C abrupt increase in the deep ocean water temperature cannot be explained by either orbital forcing or the ocean circulation mode switch. Furthermore, the temperature of the deep ocean water deceases and then is characterized by a long period of stability after a positive pulse until next maximum ice volume. This occurs independent of whether the climate is warm or cold.

Numerous studies on mid-ocean ridge processes provide useful information for the interpretation of the modeling results. The axial topography of mid-ocean ridges in the Atlantic ocean indicates a pulsative style of ridge process, as suggested by median ridge valleys constituted by stepwise walls and flat platforms (Smith and Cann, 1993; Karson et al., 1987; Pockalny et al., 1988; Detrick et al., 1990; Tucholke and Lin, 1994).

Figure 7-13. The marine oxygen-isotope records for the last glacial cycle (adopted from Broecker and Denton, 1990). The upper panel shows a smoothed version of the oxygen-isotope record for benthic foraminifera from eastern equatorial Pacific core V19-30. The middle panel shows the record after correction of 0.4‰ for a warming of deep water during the interglacial peaks after termination II and termination I. This corrected record is believed to closely represent changes in ice volume. The lower panel shows the impact on the benthic isotope record of changes in the temperature of deep Pacific water. For specific interpretation of the lower panel refer to the text.

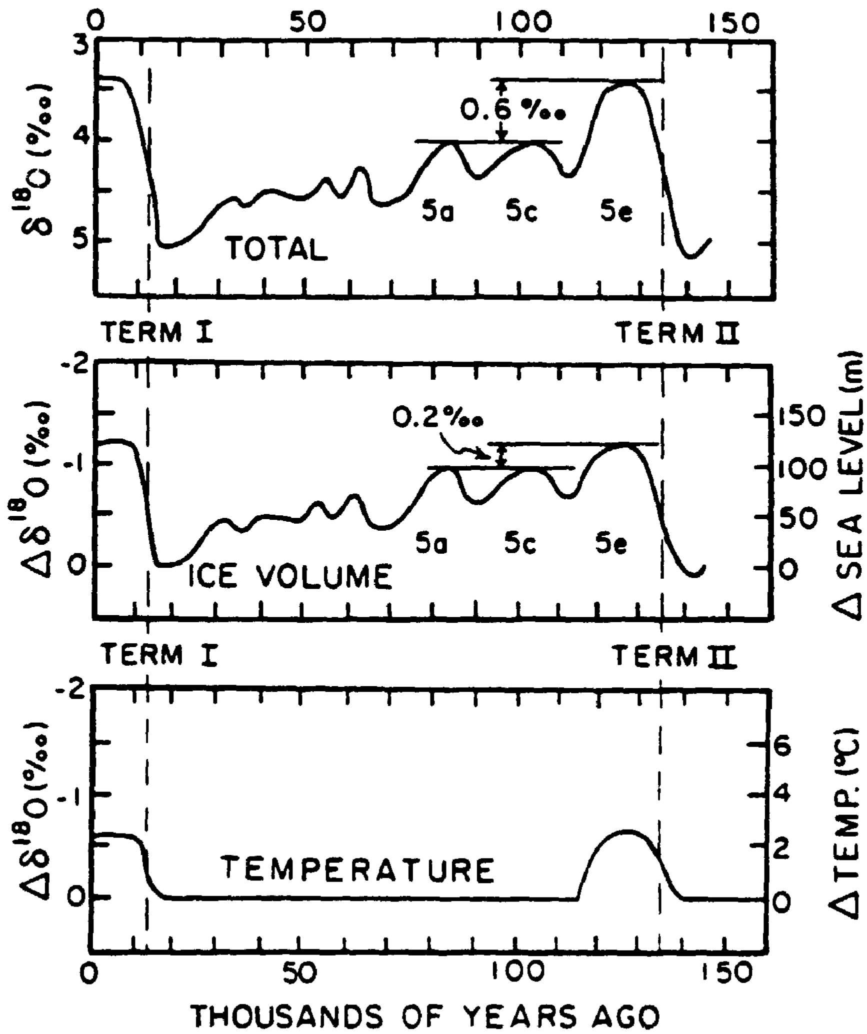
0
50
100
150
3
4
5
δ¹⁸O (‰)
0.6 ‰
5a
5c
5e
TOTAL
TERM I
TERM II
-2
-1
0
Δδ¹⁸O (‰)
0.2‰
150
100
50
0
Δ SEA LEVEL (m)
5a
5c
5e
ICE VOLUME
TERM I
TERM II
-2
-1
0
Δδ¹⁸O (‰)
6
4
2
0
Δ TEMP. (°C)
TEMPERATURE
0
50
100
150
THOUSANDS OF YEARS AGO

However, supporting evidence is still scanty for cyclicities at the 100 kyr scale. Possible explanations include the possibility that available bathymetric data do not have enough resolution power to detect these cycles because the calculated pulse extension is less than 100 m in width for most ridge sections. In addition, the topography of the ridges is complicated, highly developed normal faults are superimposed by multiple volcanic edifices and deformed by faulting segments between ridge domains. All of these factors greatly increase the difficulty for the use of bathymetric interpretation to identify the discontinuous and irregularly distributed extension in the order of about hundred meters or less. Therefore, more detailed measurements and systematic dating of central mid-ocean ridges are critical to support the hypothesis of this study and to provide substantial constraints for improving the existing models.

7.12. Comments on the Mid-Ocean Ridge Process-Link of the Quaternary Glacial Cyclicity

7.12.1. Magma Output and the Forced Mid-Ocean Ridge Extension

Under normal conditions, the output of magma at mid-ocean ridges represents a balance of the pressure in the melt chamber/ reservoir, the convection force of lower mantle, and the resistance of the plates against spreading. The axial high represents periods of waxing magmatism when crustal production rates exceed necking. The ridge troughs represent periods of waning magmatism when extensional tectonism is greater than constructional magmatism (Tuchocky and Liu, 1994). The latter case could be expected (from the modelling experiments) to occur most likely at the Atlantic ridges in the northern hemisphere where ridge-axial valleys are observed. However, for ridges characterized by axial highs which imply magma-rich reservoirs underneath, the magmatic flux must be far greater than the calculated horizontal displacement. Particularly, for some regions with giant melt regimes, even a small extensional force produced by ice sheet loading can trigger massive magmatism.

If we assume that the variation in $^{87}Sr/^{86}Sr$ ratios in ocean water during the transition period from last glacial maximum to deglaciation have been caused by mid-ocean ridge processing, it can be estimated that the magma output would cause the ratio to fall from 0.709087 to 0.709058 (cf. Clemens et al., 1993). The volume of ocean water during that period is obtained using today's value subtracting 130 m of sea level reduction. The riverine influx is neglected but compensated by using the modern ocean concentration of 7.7 ppm strontium. This manipulation is based on: (1) the riverine fluxes were greatly reduced for most areas of the world during the glacial maximum; (2) the duration of the change is less than 10 ka; and (3) the ocean water strontium concentration of the past is lower than today (cf. Blum and Erel, 1995). If 0.7035 of $^{87}Sr/^{86}Sr$ and 772 $\mu g/g$ of Sr concentration are adopted for average mid-ocean ridge basalts, 20,000 km^3 of hydrothermally altered magma is necessary. This counts for 0.4% of the estimated value (5×10^6 km^3).

The ice volume reconstruction for the Antarctic ice sheet raises a big discrepancy (Andrews, 1992; Colhoun et al., 1992). The construction with raised beach altitudes suggests an ice sheet during the last glacial which is much smaller than expected, and leads to 25 meters of the world ocean water in thickness missing (the reconstructed contribution of the deglaciation in the Antarctic to sea level rise at most 2.5 meters). This thesis proposes that it is possibly attributable to ocean ridge deformation and magma output induced by ice sheet loading. The amplitude of isostatic rebound could not be used for an estimate of ice sheet volume, but might provide a constraint for magma output from the world ocean ridge system.

For more accurate insight into the deformation forced by ice sheet loading, a refinement of model constructions is needed with the addition of updated geologic findings. Also, an ice sheet load in the Antarctic may need to be added to the model.

7.12.2. Ridge Processing and the Earth's Internal Dynamics

Paleoclimatic records both in marine and terrestrial sediments have revealed that the dominant glacial cycles are constant in each geomagnetic polarity Chron but different from others in other polarity intervals (see Figure 6-4 and Ruddiman and Raymo, 1988). As has been suggested, magnetic reversals are related to global heat flow, and thus to the internal dynamics (Larson, 1991; Larson and Olson, 1991). Although it is in contrast to the expected relation by Larson and Olson (1991), the geomagnetic paleo-intensities do show an inverse relation to global magmatic intensity (cf. Pick and Tauxe, 1993). The average geomagnetic intensity in the Matuyama chron is lower than in the Brunhes (cf. Valet and Meynadier, 1993). If the relation between magmatic and geomagnetic intensities is confirmed, the polarity reversal between the Matuyama and Brunhes would imply a major change in mantle dynamics, which could cause a change in crustal thickness of mid-ocean ridges and their mechanical strength. Therefore, a thinner crust of ridge axes in the Matuyama can be expected, which must result in an earlier failure extension, and implies a lower threshold of the ice sheet volume. In this case, a shorter periodicity of glacial cycle is produced. As observed in the Matuyama chron, the glacial cycles are obviously shorter than the 100 kyr cycle in the Brunhes.

7.12.3. Summary

Overall, evidence from a broad range of geo-observations and the modelling provide direct or indirect support for the hypothesis that the balance of exogenetic ice sheet growth and endogenetic dynamics through the most sensitive channel, the world mid-ocean ridge system, have paced the Quaternary glacial cycles. The mechanism was possibly first related to an amagmatic period which led to a global cooling, and thus the Quaternary glacial initiation. With ice sheet growth, magma accumulation, and the arrival of the ice volume threshold, failure deformation of the ocean ridges occurred, which induced massive magma output from the ridge system. Once this occurred, the massive magmatic process quickly destroyed the ice sheets through the evacuation of the earth's interior space for ice sheet depression which caused tectonic forcing on rapid collapse of the ice sheets (and also subjected the ice to high atmospheric temperature as mentioned earlier). By direct heating ocean water and the discharged ice, stimulating deep ocean circulation, and enhancing the atmospheric greenhouse gases levels, the massive magmatic process at ocean ridges produced a rapid global warming. After this process, the magma reservoirs became exhausted, the ocean ridges returned to a quiet stage with less magmatic activity, the world climate became cooler, and a new glacial period was resumed until another critical ice volume was attained (as illustrated in Figure 7-14).

It needs to be stressed that this study is just beginning. The establishment of the hypothesis must involve a large amount of additional work involving both collection of geologic evidence and model improvement.

Figure 7-14. Mid-ocean processes and the Quaternary glacial-interglacial oscillation-- A self-sustained Earth surfacial system.

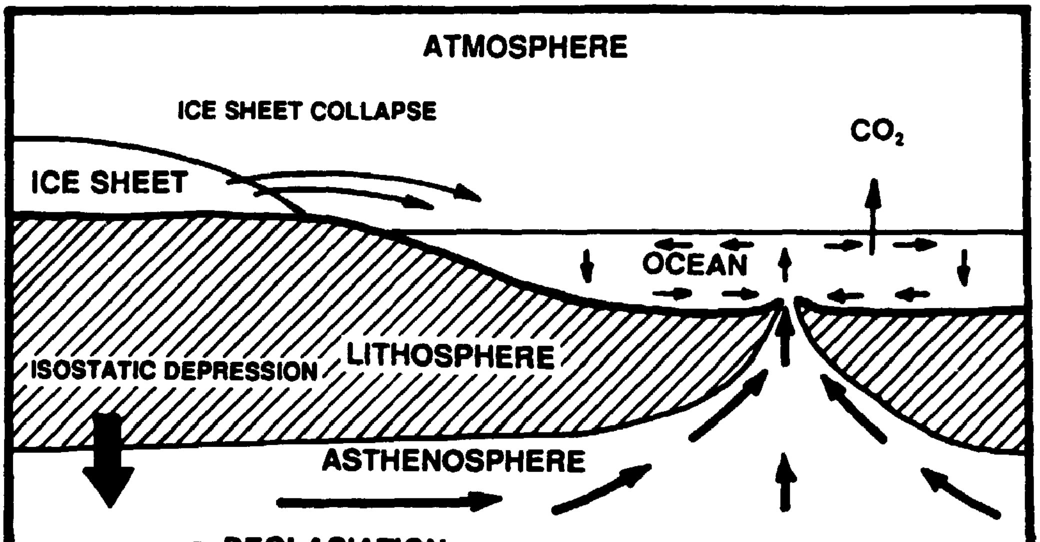

a. DEGLACIATION

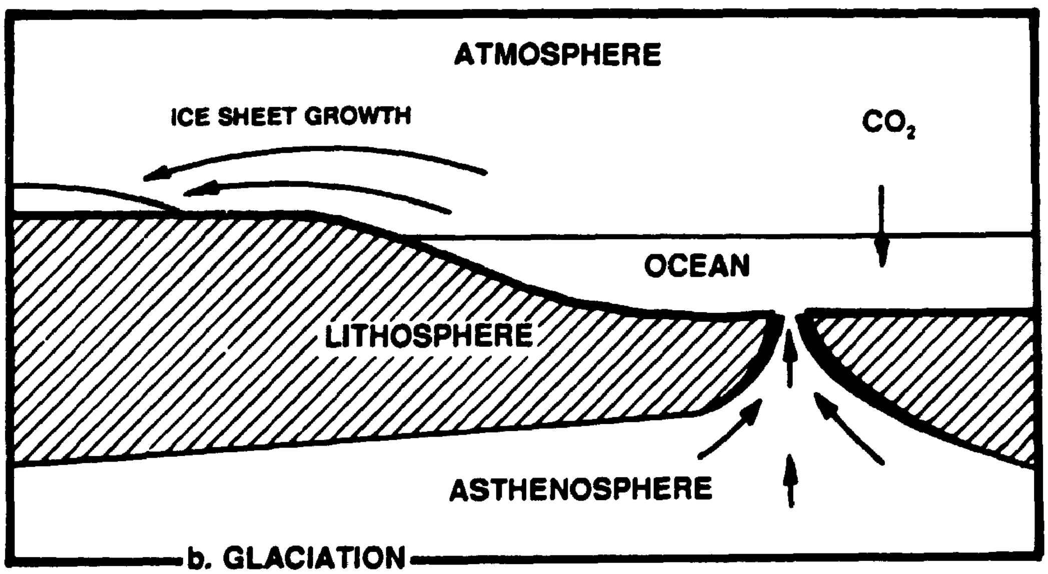

b. GLACIATION

CHAPTER 8

CONCLUSIONS AND FUTURE WORK

8.1. Conclusions

The major contributions and conclusions of this study are presented below.

1) By paleomagnetic investigation, the fluviolacustrine sequence in the Shijiawan section was determined to be in the period between 3.05 and 1.9 Ma B.P. Sedimentary analyses indicate that this sequence is mainly derived from river channel sand beds and floodplain deposits, reflecting a typical alluvial environment. The fine sediment layers are dominantly reworked red clay and loess, as was suggested by comparison of grain-size distribution, mineralogy, texture and colour. The last typical reworked red clay bed and the first typical reworked loess layer are respectively 2.7 and 2.61 Ma in age. After 1.9 Ma B.P., fluviolacustrine deposition in the Shijiawan section was replaced by a loess-paleosol accumulation, which shows an earlier termination of the hydrogenic environment in this area than in the central basin.

The upper part of the red clay formation in the Yanyu section correlates with the Gauss Chron. The smooth contacts suggest there is no significant hiatus between the red clay and the overlying loess. Therefore, it is considered as a continuous depositional sequence from red clay to loess in the Yanyu section, a similar conclusion to that obtained from the Lantian section and the Baoji section in the Guanzhong basin.

2) Stable carbon isotope studies of organic matter from the modern system reveal that the major floral species are C3 in type for both open forest and sage steppe. Only

a few non-arboreal species are C4. The related soils have $\delta^{13}C$ values close to the source floras. Systematic analyses through the soil profiles indicate that steppe flora has a major distribution depth within the upper 20 cm, much shallower than for the forest where the major distribution depth is more than 50 cm, consistent with field observations. This study provides a basis necessary for paleovegetational interpretation of the $\delta^{13}C$ signatures in paleosol profiles in the region.

3) Studies of the S5 unit, the best-developed paleosol in the Loess-paleosol sequence, demonstrate that the major pedogenic processes are decalcification and mechanical translocation of fine particles (clay illuviation). Except for calcareous carbonate, little change in chemical and mineral composition occurred during pedogenesis, suggesting a climate with slightly less precipitation than today. Stable carbon-isotopic evidence indicates a pronounced proportion of C4 plants and suggests that grasslands dominated the paleovegetation. Overall, evidence obtained from this study is not in agreement with the conventional conclusion that the S5 in the Guanzhong basin reflects a typical forest environment. For a more solid interpretation, better age control is required.

4) The Pliocene red clay formation shows great similarity in grain-size distribution, mineralogy, clay mineralogy, and chemical composition throughout individual profiles and between the Yanyu and Luochuan sections which are located in different basins hundreds of miles apart. Furthermore, the red clay is nearly identical to the overlying loess--paleosol sequence in grain-size, mineralogy, chemical composition and texture. The geographic distribution of the red clay coincides with the range of the loess. Therefore, an aeolian origin of the red clay is strongly suggested. This implies that

dust deposition from the deserts in central China started long before loess accumulation.

5) Studies of the Shijiawan fluviolacustrine sequence and the red clay formation in the Yanyu and Luochuan sections indicate that a stationary warm-dry climate in the Pliocene lasted until 2.7 Ma B.P. During that period, paleovegetation in the southern Guanzhong basin was dominated by a typical sage flora with little variability, indicative of drier conditions than in the early Quaternary interglacials and the present. This contrasts with a widely held opinion that the red clay formation was developed during a hot-wet climate.

6) The modern east Asian Monsoon climate shows a close relation to the distance from the west Pacific margin, the mean annual precipitation decreases inversely with the distance. This is supported by the evidence from sea level change, marginal migrations, and paleovegetational constructions for the last 18,000 years. Via the sea level-linked coastal migration and thus the change in distance from the Pacific margin, the Quaternary global glacial-interglacial signals were transmitted into the regional climate. Therefore, climate change recorded in the loess-paleosol sequence faithfully reflects global glacial climate change. From the distance-precipitation linkage, the loess plateau was located totally in the areas with a mean annual precipitation less than 150 mm during the last glacial maximum. This explains why the detrital calcite in loess layers remains essentially unaffected as commonly observed in the Malan loess in most regions. Also, the sea level-interlocked climate mechanism helps in the understanding of the climatic interpretation of the S5 from this study.

7) Evidence indicates a rather slow dust deposition through the red clay formation, reflecting the weakness of the Siberian cold high pressure cell during the Pliocene. Later

it was greatly intensified and this transition was completed in no more than 100 ka, as is constrained by the last typical reworked red clay bed and the first typical loess layer from 2.7 to 2.6 Ma B.P. Studies show that both a replacement of the regional climate system (which shows the demise of the Pliocene climate and gave way to the modern east Asian monsoon), and the advent of the Quaternary glacial-interglacial oscillations appeared with the transition. The time constraints for both changes critically challenges the previous tectonic forcing hypothesis for the Quaternary glacial initiation.

Nevertheless, the importance of the Tibetan Plateau and its accelerated uplift since late Pliocene associated with global cooling in the establishment of the modern east Asian monsoon and intensification of the Siberian cold high pressure centre cannot be ignored. Instead of total control by plateau uplift, this study stresses that it is the first global glaciation of the Quaternary that greatly and rapidly enhanced the blocking effect of the high Himalayas on the Indian Oceanic monsoon by creation of ice caps (or snow mantle) and glaciers. In this aspect, future work should involve precise dating constraints from inside the Tibetan Plateau and solid evidence for the amplitude of the uplift. Additional atmospheric general circulation modelling with robust boundary conditions obtained from geological study (e.g., ice caps and size, snowline, surface conditions such as vegetation, moisture, topography etc., elevation change both for high Himalayas and major Plateau, etc.) will be needed.

8) A preliminary elastic finite-element spheric model of the earth was established with the target to simulate the influence of the ice sheet loads on the deformation of the world mid-ocean ridge system. The modelling results with various parameter values (crustal thickness and stiffness coefficient of the springs) show that the distribution

patterns (the geographic positions of typical rifts and transform faults) and topography of both ridge axial high at the East Pacific Rise and ridge axial valley at northern Atlantic Ridges are closely related to the ice sheet-induced deformation. This suggests an influence of the great ice-sheets waning and waxing on shaping the world mid-ocean ridge system during the Quaternary.

9) Failure deformation of the mid-ocean ridges implies pulsative and massive magma output, which correlates with isostatic depression and leads to a complete collapse of the ice sheets. The total magma output contributed by elastic failure stretching and episodic magmatism related to the ice-loading could force asthenosphere deformation flow and cause a few degree warming of the world ocean in the first 2-3 ka after deglaciation. Furthermore, the ice sheet-loading induced magmatism at ocean ridges could employ all the positive factors to destroy the ice sheets and to force a global warming (by heat release, enhancement of atmospheric greenhouse gas levels, stimulation of deep ocean circulation and facilitation of isostatic depression to lower the ice sheet elevation).

10) Modelling experiments indicate that the maximum displacement of the mid-ocean ridges induced by the great ice sheets occurs in the northern North Atlantic ocean east of Greenland, with the magnitude slowly decreasing southward. This would suggest that the Atlantic Ocean ridges were more actively involved in the processes.

11) The pulsative magmatism (episodic spreading of the mid-ocean ridges) was first forced by massive ice sheet loading during glaciation. This in turn produced a decisive deglaciation and lead to an interglacial period. With the depletion of magma reservoirs underneath the ocean ridges after an massive episodic output, the mid-ocean ridge processing turned into an accumulation stage. With less heat supplement from the

Earth's interior, the world climate gradually entered into a long-term ice sheet build-up stage. Once a critical (maximum) volume of the ice sheets was attained, a failure deformation of the mid-ocean ridges occurred again, leading to a new episode of deglaciation and climate warming. By this mechanism, the world secular climate and the mid-ocean ridge processes coupled together, generating a self-sustained surfacial planet system, making a glacial-interglacial oscillated Quaternary climate.

8.2. Future Work

When the isostatic depression by ice sheet loading is considered as a critical factor for glaciation termination, the displacement at mid-ocean ridges should be at least equally taken into consideration, because the ocean ridge system is the most vulnerable part of the earth reflecting deformation. The primary modelling experiments show great potential for the examination of mid-ocean processes in the understanding of the Quaternary glacial-interglacial fluctuation. Future work will involve model refinement and geologic constraint. The former implies the need for extensive testing with large amounts of systematically various values of all the parameters employed. But it should be stressed, a substantial improvement depends largely on geoscience evidence. Episodic magmatism of the ridge processes at the glacial cycle scale ($10^4 \sim 10^5$ years) must be examined in the northern North Atlantic Ocean, which involves systematic sampling across the central rift in multiple ridge segments and accurate dating. In modern Quaternary studies, it has been evident that precise chronological dating is often decisive in resolving many of the major problems.

Appendix I

Displacements of the World Mid-Ocean Ridges Simulated by Model 3-1.

1) The coordinates x, y, and z are the radius of the earth, longitude, and latitude of the finite-element node, respectively. The longitudes are presented as 0 to 180° for 0-180°E, and 0 to -180° for 0-180°W. The latitudes are expressed as 0-90° for north latitude 0-90°N, and 0 to -90° for south latitudes 0-90°S.

2) The translations of each node along the x, y, and z axes are determined according to their original coordinates. The x, y, and z axes represent translations along longitudinal, latitudinal, and earth's radius directions respectively. The variables have been defined as x southwards, y eastwards, and z upwards as positive, and negative in their opposite directions. Values in the table are presented in metres.

3) u, v, and w are the 3 partial values of the displacement vector of each node pair in the x, y, and z coordinates, respectively. The node pairs are determined according to node positions in the finite-element network. A simple vector operation is employed for obtaining an absolute displacement. To calculate the absolute displacement of node A to node B for the node pair AB, for example, the following formulas are used:

$$u = x_A - x_B, \quad v = y_A - y_B, \quad w = z_A - z_B,$$

$$ABS(u) = \sqrt{(u^2 + v^2 + w^2)}$$

Where x, y, and z are the values of translations along x, y, and z coordinates, the denotations A and B indicate the values for nodes A and B respectively. The ABS(u) means absolute value of the vector displacement.

NODE NUMB	X-COORD	Y-COORD	Z-COORD	X-Translation	Y-Translation	Z-Translation	u	v	w	ABS(U)
1	6.37E+06	0	90	-712,02	-825 26	-596.83				
2	6.37E+06	-10	83.5	-1 6964	-778,91	-274.02	-7.3481	6.32	0.41	9 70
3	6.37E+06	-9.9	83.5	-9.0445	-772,59	-273.61				
13	6 37E+06	10	77.6	729.98	-260.69	41.07	4.07	20 63	-29.29	36.06
14	6.37E+06	10,1	77,7	734.05	-240,06	11,781				
24	6,37E+06	9	75,4	1209.5	-181,15	107.29	31.2	21 08	-3.04	37.78
25	6,37E+06	9,1	75,4	1240,7	-160,07	104 25				
52	6,37E+06	-9	72	399,91	-642,93	632.87	-63.36	66.6	-40.93	100 62
53	6,37E+06	-17,667	66,333	-276.07	-455,48	773.56	-26.79	33.62	-25.4	49 93
54	6,37E+06	-26,333	60,667	-401,12	-390,14	708.42	0.1	19.14	-10.4	21.78
55	6,37E+06	-35	55	-373,32	-534,19	694.52	-3,35	13,03	-1,86	13.58
56	6,37E+06	-8,9	71,9	336,55	-576,33	591,94				
57	6,37E+06	-17,567	66,267	-302,86	-421,86	748,16				
58	6,37E+06	-26,233	60,633	-401,02	-371	698,02				
59	6,37E+06	-34,9	55	-376,67	-521,16	692,66				
60	6,37E+06	-3	72	-480,64	-330,42	456,31	12,22	66,91	-19,47	70.75
61	6,37E+06	-2,9	71,9	-468,42	-263,51	438,84				
108	6,37E+06	-128,8	54,3	1953,1	1182,1	832,21	43,7	4,5	-10,94	45 27
109	6,37E+06	-129	54,5	1996,8	1186,6	821,27				
170	6,37E+06	-27,9	49,1	-204,39	-243,32	512,89	-3,56	-9,66	5,14	11.51
171	6,37E+06	-28	49	-207,95	-252,98	518,03				
183	6,37E+06	-129,4	50	-134,34	754,51	720,85	-27,47	-16,32	-34,1	46,73
184	6,37E+06	-129,5	50	-161,81	738,19	686,75				
247	6,37E+06	-130	45,5	-137,46	434,91	547,39	3,99	10,74	15,38	19.18
249	6,37E+06	-127	40,6	-56,298	262,75	494,21	-24,533	2,09	3,99	24 [illegible]
250	6,37E+06	-126	44	-77,898	403,7	635,68	-4,615	12,71	18,64	23 [illegible]
251	6,37E+06	-129,9	45,5	-133,47	445,65	562,77				
252	6,37E+06	-125,9	44	-82,513	416,41	654,32				
253	6,37E+06	-126,9	40,5	-80,831	264,84	498,2				
290	6,37E+06	-30	41	-79,061	-176,37	364	-2,647	6,91	-7,2	10.32
291	6,37E+06	-29,9	41	-81,708	-169,46	356,8				
425	6,37E+06	-45	29,1	-55,033	-112,14	256,26	1,714	4,78	-16,13	16.91
426	6,37E+06	-44,9	29	-53,319	-107,36	240,13				
427	6,37E+06	-38,8	33	-58,145	-129,39	273,42	-5,009	-6,8	14 86	17.09
429	6,37E+06	-39	33	-63,154	-136,19	288,28				
430	6,37E+06	-35	36,5	-29,154	-157,32	313,93	5,59	9,77	-17,94	21.18
431	6,37E+06	-34,8	36,5	-23,564	-147,55	295,99				
458	6,37E+06	32,1	31	-16,115	-27,888	159,2	-0,315	1,018	-0,17	1.08
460	6,37E+06	32	31	-16,43	-26,87	159,03				
548	6,37E+06	-107	24	-62,101	72,674	325,03	-2,722	0,106	0,96	2,89
549	6,37E+06	-106,8	23,9	-64,823	72,78	325,99				
550	6,37E+06	-106	20	-35,697	49,808	231	-0,356	-0,142	6,01	6.02
551	6,37E+06	-105,9	20	-36,053	49,666	237,01				
578	6,37E+06	-46	20	-19,809	-47,151	130,79	0,56	2,283	-3,52	4.23
579	6,37E+06	-45,5	25	-30,075	-74,53	187,47	0,647	1,964	-4,59	5,03
580	6,37E+06	-45,4	25	-29,428	-72,566	182,88				
581	6,37E+06	-45,9	20	-19,249	-44,868	127,27				

612	6.37E+06	38	20	-7.5998	-10.12	65.316	-0.0995	-0.466	0.918	1.03
613	6.37E+06	35	25	-15.184	-16.467	99.978	0.269	-0.739	0.722	1.07
614	6.37E+06	35.1	25	-14.915	-17.206	100.7				
617	6.37E+06	38.1	20	-7.6993	-10.586	66.234				
700	6.37E+06	-103.5	10	-19.005	19.183	108.71	0.089	-0.398	2.29	2.33
701	6.37E+06	-105	15	-29.013	31.861	159.88	0.516	-0.124	3.96	4.00
702	6.37E+06	-104.9	15	-28.497	31.737	163.84				
703	6.37E+06	-103.4	10	-18.916	18.785	111				
727	6.37E+06	-46	17	-14.773	-34.833	104.95	0.568	1.777	-0.67	1.98
728	6.37E+06	-45.9	17	-14.205	-33.056	104.28				
730	6.37E+06	-41.9	13.1	-12.265	-23.09	75.417	-0.348	0.669	-2.92	3.02
731	6.37E+06	-42	13	-12.613	-22.421	72.497				
732	6.37E+06	-38	10	-11.77	-16.147	59.067	-0.839	0.906	-2.094	2.43
733	6.37E+06	-37.9	10	-12.609	-15.241	56.973				
766	6.37E+06	42	12	-5.638	-5.3935	38.679	-0.1935	0.1396	1.224	1.25
767	6.37E+06	42.1	12.1	-5.8315	-5.2539	39.903				
770	6.37E+06	40	16	-2.8466	-7.227	48.411	-0.0118	0.0179	-0.528	0.53
771	6.37E+06	39.9	16	-2.8584	-7.2091	47.883				
775	6.37E+06	50	14	-7.3816	-7.3621	45.212	0.2533	0.4141	-2.27	2.32
776	6.37E+06	50	13.9	-7.1283	-6.948	42.942				
781	6.37E+06	56	14	-12.023	-7.8013	40.237	-0.465	-0.718	2.363	2.51
782	6.37E+06	56.1	14.1	-12.488	-8.5193	42.6				
784	6.37E+06	60	10	-5.5715	-5.1084	30.683	-0.0462	-0.343	1.285	1.33
785	6.37E+06	60.1	10.1	-5.6177	-5.4518	31.968				
866	6.37E+06	-101	0	-8.8261	6.1821	52.708	-0.1358	0.1592	0.196	0.29
867	6.37E+06	-101.9	5	-6.9514	10.104	69.086	-0.0335	-0.252	2.685	2.70
868	6.37E+06	-102	5.1	-7.1338	10.525	69.952	0.1599	-0.212	3.438	3.45
869	6.37E+06	-101.8	5.1	-6.9739	10.313	73.39				
870	6.37E+06	-101.7	5	-6.9849	9.8522	71.771				
871	6.37E+06	-100.9	0	-8.9619	6.3413	52.904				
873	6.37E+06	-95	4	-16.977	5.1487	79.423	-0.23	0.234	1.999	2.03
874	6.37E+06	-95	4.1	-17.207	5.3827	81.422				
875	6.37E+06	-90	4.1	-16.84	1.9128	83.526	0.217	0.1117	-2.17	2.18
876	6.37E+06	-90	4	-16.623	2.0245	81.356				
879	6.37E+06	-85	3	-13.572	-2.0912	81.001	-0.167	-0.205	1.969	1.99
880	6.37E+06	-85	3.1	-13.739	-2.2966	82.97				
881	6.37E+06	-80	3.1	-18.031	-6.9669	84.911	0.113	0.1199	-0.908	0.92
882	6.37E+06	-80	3	-17.918	-6.847	84.003				
904	6.37E+06	-33	5	-5.3182	-8.307	39.078	0.343	-0.607	1.511	1.66
905	6.37E+06	-32.9	5.1	-4.9752	-8.9142	40.589				
906	6.37E+06	-28	2.1	-6.9682	-5.9482	32.598	-0.3662	0.2797	-0.724	0.86
907	6.37E+06	-28	2	-7.3344	-5.6685	31.874				
908	6.37E+06	-20	1	-8.7449	-3.9391	32.222	0.1171	-0.205	0.668	0.71
909	6.37E+06	-20	1.1	-8.6278	-4.1442	32.89				
911	6.37E+06	-14	0	-9.1507	-3.3028	30.82	0.0623	0.0313	0.776	0.78
912	6.37E+06	-13.9	0.1	-9.0884	-3.2715	31.598				
944	6.37E+06	63	5	-3.6819	-3.1043	20.627	-0.0038	-0.1	0.246	0.27
945	6.37E+06	63.1	5	-3.6857	-3.2041	20.873				
947	6.37E+06	67	0	-2.5495	-1.9615	14.475	-0.0497	-0.011	0.192	0.20
948	6.37E+06	67.1	0	-2.5992	-1.9726	14.667				

1024	6,37E+06	-105	-5	-7,296	4,1421	34,862	0,1935	-0,268	-0,835	0,90
1025	6,37E+06	-104,9	-5	-7,1025	3,8745	34,027				
1026	6,37E+06	-107	-10	-4,0227	2,8802	24,302	-0,2178	0,0098	-0,307	0,38
1027	6,37E+06	-106,9	-10	-4,2405	2,89	23,995				
1065	6,37E+06	-14	-10	-2,9629	-1,3226	15,223	0,0406	0,1482	-0,039	0,16
1066	6,37E+06	-13,9	-10	-2,9223	-1,1744	15,184				
1067	6,37E+06	-14	-5	-4,5855	-1,9177	21,525	0,1226	0,1563	-0,04	0,20
1068	6,37E+06	-13,9	-5	-4,4629	-1,7614	21,485				
1099	6,37E+06	67	-5	-2,0783	-1,3181	10,291	0,1249	0,0858	-0,07	0,17
1100	6,37E+06	67,1	-5	-1,9534	-1,2323	10,221				
1101	6,37E+06	67,5	-10	-1,6066	-0,99853	7,1724	0,0621	0,0837	-0,038	0,11
1102	6,37E+06	67,6	-10	-1,5445	-0,91484	7,1348				
1176	6,37E+06	-110	-15	-2,4706	2,3679	15,622	0,0749	-0,059	-0,445	0,46
1177	6,37E+06	-110	-15,2	-2,3957	2,3092	15,177				
1178	6,37E+06	-112	-19	-2,2388	1,8393	11,905	-0,0384	0,089	-0,09	0,13
1179	6,37E+06	-111,9	-19	-2,2772	1,9283	11,815				
1217	6,37E+06	-15	-15	-2,4063	-1,0584	10,867	0,0538	0,1309	-0,071	0,16
1218	6,37E+06	-14,9	-15	-2,3525	-0,92746	10,796				
1219	6,37E+06	-15	-20	-1,8432	-0,85005	7,8668	0,0079	0,11	0,039	0,12
1220	6,37E+06	-14,9	-20	-1,8353	-0,74002	7,9056				
1253	6,37E+06	66,5	-15	-0,90257	-0,81326	5,0081	0,01221	0,0746	-0,052	0,09
1254	6,37E+06	66,6	-15	-0,89036	-0,73864	4,9562				
1256	6,37E+06	67	-20	-0,54533	-0,58288	3,4026	0,0068	0,0562	0,019	0,06
1257	6,37E+06	67,1	-20	-0,53853	-0,52671	3,422				
1333	6,37E+06	-112	-25	-1,585	1,3614	7,7959	-0,0574	0,0825	0,083	0,13
1334	6,37E+06	-111,9	-25	-1,6424	1,4439	7,8792				
1335	6,37E+06	-112	-30	-1,1602	1,0447	5,4257	-0,0178	0,0687	0,064	0,10
1336	6,37E+06	-111,9	-30	-1,178	1,1134	5,4896				
1372	6,37E+06	-14	-27	-1,2228	-0,64866	4,9492	0,0065	0,08	0,022	0,08
1373	6,37E+06	-13,9	-27	-1,2163	-0,56864	4,9708				
1374	6,37E+06	-15	-30	-0,87143	-0,63735	4,065	0,01469	0,067	-0,03	0,07
1375	6,37E+06	-14,9	-30	-0,85674	-0,57038	4,0346				
1405	6,37E+06	60	-30	-0,42755	-0,72478	2,2103	0,02088	0,053	-0,072	0,09
1406	6,37E+06	60,2	-30	-0,40667	-0,6718	2,1387				
1408	6,37E+06	65	-26,6	-0,46249	-0,58056	2,274	-0,0101	-0,023	0,087	0,09
1409	6,37E+06	65	-26,5	-0,47255	-0,60317	2,3612				
1411	6,37E+06	68	-24,1	-0,18627	-0,46727	2,4594	-0,0199	0,0835	0,019	0,09
1412	6,37E+06	68,1	-24	-0,20614	-0,38377	2,4779				
1413	6,37E+06	68,1	-24,2	-0,169	-0,40456	2,3692	-0,0283	0,0308	0,116	0,12
1414	6,37E+06	68,2	-24,1	-0,19725	-0,3738	2,4851				
1416	6,37E+06	75	-30	-0,47452	-0,16728	1,9041	-0,0084	0,0138	0,045	0,05
1417	6,37E+06	75,1	-30	-0,48095	-0,15344	1,9488				
1493	6,37E+06	-111	-36,1	-0,81019	0,70984	3,4253	-0,0405	0,0759	0,134	0,16
1494	6,37E+06	-110,9	-36	-0,85064	0,78572	3,5591				
1496	6,37E+06	-107	-40	-0,40992	0,37833	2,3396	-0,0117	0,0138	-0,012	0,02
1497	6,37E+06	-106,9	-40	-0,42162	0,39217	2,3275				
1498	6,37E+06	-105,1	-37,2	-0,17149	0,54855	2,8419	-0,0227	-0,048	-7E-04	0,05
1499	6,37E+06	-104,9	-37,3	-0,1942	0,50019	2,8412				
1500	6,37E+06	-105	-37	-0,24423	0,59026	3,2146	0,05601	-0,007	-0,042	0,07
1501	6,37E+06	-104,9	-37,1	-0,18622	0,58319	3,1723				

1504	6.37E+06	-100	-37 5	-0 44159	0 58169	3 5464	0.02238	-0 043	-0 193	0 20
1505	6.37E+06	-100	-37 6	-0 41921	0 53838	3 3536				
1508	6.37E+06	-95	-38.1	-0 59968	0.49003	3 6037	-0 0453	0.0351	0.181	0 19
1509	6.37E+06	-95	-38	-0.64498	0 52514	3 7851				
1510	6.37E+06	-92	-38	-0 88893	0 50555	4 0058	0 05898	-0 044	-0 159	0 18
1511	6 37E+06	-92	-38.1	-0 82995	0.46165	3 8467				
1514	6 37E+06	-87	-40	-0.74468	0 46652	3 9126	-0.0028	0 0066	0 064	0 06
1515	6 37E+06	-86 9	-40	-0 74743	0.47309	3.9762				
1543	6 37E+06	-16	-37	-0 66713	-0 52278	2.5586	-0 0076	0.0481	-0 023	0 05
1544	6 37E+06	-15.9	-37	-0 67473	-0.47472	2.5355				
1545	6.37E+06	-16	-40	-0 42171	-0.45766	2.0467	-0 005	0 0385	-0.004	0 04
1546	6.37E+06	-15 9	-40	-0.42671	-0 41913	2 0428				
1571	6.37E+06	45	-40	-0.29871	-0.63154	1 7054	0.00213	0 0234	-0.013	0 03
1572	6 37E+06	45.1	-40	-0 29658	-0.60817	1 692				
1574	6.37E+06	50	-36.1	-0 4382	-0.72944	1 92	-0.0176	-0 008	0.084	0 09
1575	6.37E+06	50	-36	-0 45576	-0.73769	2.0036				
1576	6.37E+06	55	-33	-0.4017	-0.74952	2.091	0.00064	0 0236	-0 074	0 08
1577	6.37E+06	55	-33.1	-0.40106	-0 7259	2.017				
1585	6 37E+06	77	-35	-0 28422	-0.12663	1.2814	0.00573	0 0189	0 017	0 03
1586	6 37E+06	77.1	-35	-0 27849	-0 10774	1 298				
1588	6.37E+06	78.5	-40	-0.11627	-0.09774	0 80861	-0.0013	0.0098	0.003	0 01
1589	6 37E+06	78.6	-40	-0 11761	-0 087959	0 81184				
1596	6.37E+06	95	-43	-0.10996	-0.059966	0.74862	0.0003	0 0019	-0 039	0 04
1597	6.37E+06	95	-43.1	-0.109[illegible]6	-0 058108	0 70996				
1600	6.37E+06	100	-44 1	-0.13362	-0 05219	0.64932	-0.0019	-0.002	0 032	0 03
1601	6 37E+06	100	-44	-0.13554	-0.054346	0 68104				
1602	6.37E+06	105	-45	-0.16364	-0 044648	0 6861	0.00585	0.0045	-0.04	0 04
1603	6 37E+06	105	-45.1	-0.15779	-0.040176	0 64614				
1606	6 37E+06	110	-46.1	-0 12675	-0 026938	0.55802	-0.0068	-0.002	0 031	0 03
1607	6.37E+06	110	-46	-0.13355	-0.028885	0 58877				
1609	6 37E+06	118	-48	-0.044632	-0.005992	0.43905	0.00082	0 0005	-0.025	0 03
1610	6.37E+06	117 9	-48.1	-0.043811	-0 005445	0 41386				
1613	6 37E+06	120	-48.1	-0 039808	-0 000898	0 40441	-0.0041	0 0006	0.023	0 02
1614	6 37E+06	120	-48	-0.043913	-0.000343	0.42693				
1617	6 37E+06	125	-48.3	-0.051489	0.013578	0.42915	0.00289	-2E-04	-0.029	0 03
1618	6 37E+06	125	-48.4	-0.048601	0 013419	0 40005				
1621	6.37E+06	130	-48.7	-0.05[illegible]925	0 029264	0 39384	-0 0029	0 0006	0.029	0 03
1622	6.37E+06	130	-48.6	-0 054776	0.02989	0.4231				
1625	6.37E+06	135	-48.8	-0.062762	0.04922	0.42624	0.00358	-0.001	-0.03	0.03
1626	6.37E+06	135	-48.9	-0 059184	0.047873	0.3965				
1628	6.37E+06	141	-50	-0.047121	0 082841	0.37669	0.00043	0.0038	0 008	0 01
1629	6.37E+06	141.1	-50	-0.04669	0 086595	0.38459				
1630	6.37E+06	140	-49.1	-0.07784	0.073286	0.39522	-0.0057	-5E-04	0.028	0 03
1631	6.37E+06	140.1	-49	-0.083558	0.072798	0.42342				
1674	6.37E+06	-115	-50	-0.21927	0 11375	1.162	-0.0008	0.0104	-0 008	0 01
1675	6.37E+06	-114.9	-50	-0 22002	0.12412	1.1543				
1677	6.37E+06	-110	-44.1	-0.25883	0 27861	1.8497	-0.0089	-0.009	0 029	0 03
1678	6.37E+06	-110	-44	-0.26569	0.26966	1.8787				
1691	6.37E+06	-80	-44.1	-0 4664	0.32643	3.2047	-0.0117	-0 018	0.147	0 15
1692	6.37E+06	-80	-44	-0.47811	0 30795	3.3516				

1693	6,37E+06	-75,9	-46	-0,78815	0 26292	3.1263	0,03101	0,0016	-0,049	0 06
1694	6,37E+06	-76	-46,1	-0,75714	0,26451	3.0769				
1720	6 37E+06	-15	-45,1	-0 35584	-0,32083	1,4357	0 00498	0,0359	0,017	0 04
1721	6,37E+06	-14,9	-45	-0 35086	-0 28493	1,4525				
1724	6,37E+06	-10	-48,1	-0,15565	-0,15534	1,0378	-0,0038	-0,02	0 044	0 05
1725	6,37E+06	-10	-48	-0,15944	-0,17496	1,0816				
1728	6 37E+06	-6,9	-50	-0,19506	-0,12815	0 94802	0 00584	0,0193	-0 073	0 08
1729	6,37E+06	-7	-50	-0,18922	-0,10886	0,87465				
1742	6,37E+06	30	-50	-0,13221	-0,24419	1,0349	0,00348	-0 004	-0,041	0,04
1743	6,37E+06	30,1	-50	-0,12873	-0,24776	0,99354				
1745	6,37E+06	35	-46,1	-0,2677	-0,39593	1,3141	-0,0143	0,0056	0,059	0 06
1746	6,37E+06	35	-46	-0,28196	-0 39031	1,3728				
1748	6,37E+06	40	-43	-0,27685	-0,51862	1,5585	0,00307	0,0097	-0,061	0 06
1749	6,37E+06	40	-43,1	-0,27378	-0,50888	1,4979				
1766	6,37E+06	79	-42,1	-0,086422	-0,09368	0,67771	-0,0035	-0,002	0 023	0,02
1767	6,37E+06	79,1	-42	-0,089896	-0,096143	0,70068				
1772	6,37E+06	85	-42,1	-0,081056	-0,065065	0,69421	-0,0034	0,0046	0,031	0 03
1773	6,37E+06	85	-42	-0,084441	-0,060475	0,72519				
1774	6,37E+06	88	-41,5	-0,11408	-0,05789	0,78664	0,00718	-0,005	-0,036	0,04
1775	6,37E+06	88	-41,6	-0,1069	-0,063339	0,75105				
1801	6,37E+06	150	-54	-0,082089	0,13255	0,34583	-0,0023	0,0112	0,019	0 02
1802	6,37E+06	150,1	-53,9	-0,084345	0,14373	0,36449				
1804	6,37E+06	145	-52,5	-0,050874	0,11268	0,34453	-0,0001	-0,007	-0,016	0,02
1805	6,37E+06	152,1	-59	-0,058472	0,12734	0,26845	4,3E-05	-0,01	-0,013	0,02
1806	6,37E+06	152	-59,1	-0,058429	0,11696	0,25512				
1807	6,37E+06	159,8	-60	-0,059796	0,13223	0,31688	-0,0004	0,0039	0,006	0,01
1808	6,37E+06	160	-60	-0,06022	0,13613	0,32285				
1829	6,37E+06	-155	-60	-0,062927	-0,023757	0,51211	-0,0004	0,0009	-0,008	0,01
1830	6,37E+06	-154,9	-60	-0,063306	-0,022816	0,50403				
1833	6,37E+06	-150	-58	-0,045649	0,0019088	0,55559	0,00147	0,0064	-0,024	0,02
1834	6,37E+06	-150	-58,1	-0,044181	0,0083516	0,53204				
1837	6,37E+06	-144,9	-56,1	-0,1005	0,042097	0,5993	0,00193	-0,003	0,023	0,02
1838	6,37E+06	-145	-56	-0,098572	0,03921	0,62253				
1841	6,37E+06	-140	-56	-0,091743	0,064822	0,61248	-0,0007	-0,003	-0,016	0,02
1842	6,37E+06	-140	-56,1	-0,092424	0,062127	0,59689				
1845	6,37E+06	-135	-55,6	-0,086574	0,08261	0,63342	-0,0007	0,0054	0,019	0,02
1846	6,37E+06	-135	-55,5	-0,087231	0,088012	0,6526				
1848	6,37E+06	-130	-55,5	-0,12559	0,10029	0,69359	0,00564	-0,005	-0,023	0,02
1849	6,37E+06	-130	-55,6	-0,11995	0,095652	0,67085				
1852	6,37E+06	-125	-55,6	-0,16109	0,10533	0,69629	-0,0036	0,0032	0,023	0,02
1853	6,37E+06	-125	-55,5	-0,16472	0,10853	0,7197				
1854	6,37E+06	-120	-55	-0,16723	0,11821	0,77824	0,003	0,0145	-0,027	0,03
1855	6,37E+06	-119,9	-55,1	-0,16423	0,13272	0,75163				
1882	6,37E+06	-60	-60	-0,23117	-0,11222	1,1051	0,16477	-0,049	-0,601	0,63
1900	6,37E+06	-10	-57	-0,066397	-0,16119	0,50362				
1903	6,37E+06	-5	-55	-0,046452	-0,1239	0,56253	-0,0028	0,0075	-0,025	0,03
1904	6 37E+06	-5	-55,1	-0,049285	-0,11645	0,5379				
1907	6,37E+06	0	-54,2	-0,077809	-0,087415	0,60343	0,01564	-0,002	0,02	0,03
1908	6,37E+06	-0,1	-54,1	-0,062166	-0,089121	0,6238				
1909	6,37E+06	0	-54	-0,068204	-0,07954	0,64854	-0,0166	-0,007	-0,033	0,04

1910	6,37E+06	0,1	-54,1	-0,084824	-0,086903	0,61529				
1911	6,37E+06	5	-53	-0,20807	-0,090884	0,76385	-0,0073	-0,007	-0,013	0,02
1912	6,37E+06	5	-53,1	-0,21533	-0,097513	0,7506				
1916	6,37E+06	10	-53,1	-0,1525	-0,097113	0,78606	0,00515	0,004	0,014	0,02
1917	6,37E+06	10	-53	-0,14735	-0,093112	0,80051				
1918	6,37E+06	15	-52	-0,14454	-0,10359	0,88443	-0,0078	0,0023	-0,021	0,02
1919	6,37E+06	15	-52,1	-0,15229	-0,10128	0,86377				
1922	6,37E+06	20	-52,6	-0,16212	-0,10997	0,8346	0,00297	-0,005	0,025	0,03
1923	6,37E+06	20	-52,5	-0,15915	-0,11478	0,85918				
1924	6,37E+06	26	-53	-0,13601	-0,1532	0,81683	-0,0054	0,0132	-0,047	0,05
1925	6,37E+06	26	-53,1	-0,14143	-0,14005	0,76953				
1953	6,37E+06	145	-52,6	-0,050992	0,10551	0,32897				
1956	6,37E+06	-16,9	-59,1	-0,054993	-0,18347	0,48317	-0,0011	-0,004	0,009	0,01
1957	6,37E+06	-17	-59	-0,056138	-0,18771	0,49202				
1959	6,37E+06	-14	-58	-0,031352	-0,17771	0,49221	0,00498	0,0106	-0,021	0,02
1960	6,37E+06	-14	-58,1	-0,026372	-0,16714	0,47104				
1963	6,37E+06	-10	-57,1	-0,063671	-0,1489	0,48189	0,01888	0,2767	-0,149	0,31
1981	6,37E+06	165	-61,5	-0,04479	0,12784	0,33273				
1987	6,37E+06	170	-62,1	-0,035946	0,10672	0,40044	-4E-05	0,0206	0,014	0,02
1988	6,37E+06	170	-62	-0,035983	0,1273	0,41417				
1989	6,37E+06	180	-63	-0,24133	-0,032873	0,68778	-0,0033	-0,008	-0,004	0,01
1990	6,37E+06	180	-63,1	-0,24462	-0,040412	0,6837				
1995	6,37E+06	-173	-64,1	-0,3806	-0,096345	0,72684	0,00442	0,0113	0,008	0,01
1996	6,37E+06	-173	-64	-0,37618	-0,085077	0,73519				
1997	6,37E+06	-165	-62,5	-0,033984	-0,055[illegible]31	0,5211	-0,0019	-0,007	-0,013	0,01
199[illegible]	6,37E+06	-165	-62,6	-0,035841	-0,06[illegible]2	0,50847				
1999	6,37E+06	-160	-61	-0,054765	-0,024413	0,51194	-0,0009	0,0002	-0,015	0,01
2000	6,37E+06	-160	-61,1	-0,055703	-0,024229	0,49739				

Appendix II

Node Coordinates of the discretized finite elements.

Node#	Z-Coord. (m)	X-Coord. (degree)	Y-Coord. (degree)
1	6371000	0	90
2	6371000	350	83.5
3	6371000	350.1	83.5
4	6371000	355	83.5
5	6371000	60	85
6	6371000	110	85
7	6371000	170	85
8	6371000	230	85
9	6371000	270	85
10	6371000	325	85
11	6371000	341	82
12	6371000	345	83
13	6371000	10	77.6
14	6371000	10.1	77.7
15	6371000	15	78
16	6371000	60	80
17	6371000	93	80
18	6371000	110	79
19	6371000	168	78
20	6371000	238	81
21	6371000	288	80
22	6371000	339	76.5
23	6371000	1	77
24	6371000	9	75.4
25	6371000	9.1	75.4
26	6371000	15	75.3
27	6371000	58	70.5
28	6371000	80	75
29	6371000	116	76
30	6371000	170	70
31	6371000	175	70.5
32	6371000	190	75
33	6371000	189	66.5
34	6371000	193	65
35	6371000	195	68
36	6371000	203	74.5
37	6371000	203	72
38	6371000	218	72.5
39	6371000	215	70
40	6371000	231	72.5
41	6371000	230	69.5
42	6371000	258	68.5
43	6371000	281	73
44	6371000	300	69.5
45	6371000	312	59
46	6371000	338	71.5
47	6371000	359	75.5
48	6371000	347	72.5
49	6371000	336	68
50	6371000	323	62
51	6371000	311	52
52	6371000	351	72
55	6371000	325	55
56	6371000	351.1	71.9
59	6371000	325.1	56
60	6371000	357	72
61	6371000	357.1	71.9
62	6371000	4	70
63	6371000	358	70
64	6371000	350	65
65	6371000	343	60
66	6371000	338	54
67	6371000	3.5	62
68	6371000	353	58
69	6371000	24	71
70	6371000	15	67
71	6371000	4	60.5
72	6371000	30	65
73	6371000	46	67.5
74	6371000	44	65
75	6371000	58.5	69
76	6371000	60	65
77	6371000	90	70
78	6371000	80	68
79	6371000	74	65
80	6371000	90	65
81	6371000	110	70
82	6371000	100	65
83	6371000	120	65
84	6371000	140	70
85	6371000	140	65
86	6371000	160	65
87	6371000	180	64
88	6371000	197	60.5
89	6371000	212	61
90	6371000	223	60
91	6371000	230	60
92	6371000	240	68.5
93	6371000	240	60
94	6371000	250	60
95	6371000	260	60
96	6371000	270	60
97	6371000	290	67
98	6371000	280	60
99	6371000	297	60
100	6371000	300	55
101	6371000	290	60
102	6371000	290	55
103	6371000	280	55
104	6371000	270	55
105	6371000	260	55
106	6371000	250	55
107	6371000	240	55
108	6371000	231.2	54.3
109	6371000	231	54.5
110	6371000	229	56
111	6371000	220	56.5
112	6371000	210	56
113	6371000	200.5	56
114	6371000	190	55
115	6371000	180	60
116	6371000	180	53
117	6371000	167	58.5
118	6371000	170	50
119	6371000	158	58
120	6371000	158	54
121	6371000	160	49
122	6371000	149	60.5
123	6371000	140	60
124	6371000	138	55
125	6371000	145	53.5
126	6371000	145	46
127	6371000	130	50
128	6371000	130	55
129	6371000	130	60
130	6371000	120	60
131	6371000	120	56
132	6371000	120	50
133	6371000	110	50
134	6371000	110	55
135	6371000	110	60
136	6371000	100	60
137	6371000	100	55
138	6371000	100	50
139	6371000	90	50
140	6371000	80	50
141	6371000	80	55
142	6371000	80	60
143	6371000	70	60
144	6371000	70	55
145	6371000	70	50
146	6371000	60	50
147	6371000	60	55
148	6371000	60	60
149	6371000	50	60
150	6371000	50	55
151	6371000	50	50
152	6371000	40	60
153	6371000	40	55
154	6371000	40	50
155	6371000	30	50
156	6371000	30	55
157	6371000	30	60
158	6371000	20	60
159	6371000	20	55
160	6371000	20	50
161	6371000	10	50
162	6371000	10	55
163	6371000	10	60
164	6371000	5	55
165	6371000	0	50
166	6371000	357	55
167	6371000	350	50
168	6371000	350	55
169	6371000	339	50
170	6371000	332.1	49.1
171	6371000	332	49
172	6371000	320	45
173	6371000	311	42
174	6371000	305	50
175	6371000	300	50
176	6371000	290	50
177	6371000	280	50
178	6371000	270	50
179	6371000	260	50
180	6371000	250	50
181	6371000	240	50
182	6371000	235	50
183	6371000	230.6	50
184	6371000	230.5	50
185	6371000	220	54
186	6371000	220	50
187	6371000	210	53
188	6371000	210	50
189	6371000	200	52
190	6371000	200	50
191	6371000	190	51
192	6371000	190	50
193	6371000	180	50
194	6371000	142	48
195	6371000	90	60
196	6371000	90	55
197	6371000	95	45

198	6371000	95	40
199	6371000	100	45
200	6371000	100	40
201	6371000	105	40
202	6371000	105	45
203	6371000	110	45
204	6371000	110	40
205	6371000	115	40
206	6371000	115	45
207	6371000	120	45
208	6371000	120	40
209	6371000	130	45
210	6371000	127	40
211	6371000	135	40
212	6371000	137	44
213	6371000	140	40
214	6371000	145	40
215	6371000	150	45
216	6371000	150	40
217	6371000	155	40
218	6371000	155	45
219	6371000	160	45
220	6371000	160	40
221	6371000	165	40
222	6371000	165	45
223	6371000	170	45
224	6371000	170	40
225	6371000	175	40
226	6371000	175	45
227	6371000	180	45
228	6371000	180	40
229	6371000	185	40
230	6371000	185	45
231	6371000	190	45
232	6371000	190	40
233	6371000	195	40
234	6371000	195	45
235	6371000	200	45
236	6371000	200	40
237	6371000	205	45
238	6371000	205	40
239	6371000	210	40
240	6371000	210	45
241	6371000	215	45
242	6371000	215	40
243	6371000	220	45
244	6371000	220	40
245	6371000	225	40
246	6371000	225	45
247	6371000	230	45.5
248	6371000	230	40
249	6371000	233	40.6
250	6371000	234	44
251	6371000	230.1	45.5
252	6371000	234.1	44
253	6371000	233.1	40.5
254	6371000	238	35
255	6371000	237	46
256	6371000	240	45
257	6371000	238	40
258	6371000	245	40
259	6371000	245	45
260	6371000	250	45
261	6371000	250	40
262	6371000	256	40
263	6371000	255	45
264	6371000	260	45
265	6371000	260	40
266	6371000	265	40
267	6371000	265	45
268	6371000	270	45
269	6371000	270	40
270	6371000	275	45
271	6371000	275	40
272	6371000	280	40
273	6371000	280	45
274	6371000	285	45
275	6371000	285	40
276	6371000	291.5	40
277	6371000	290	45
278	6371000	295	45
279	6371000	295	43
280	6371000	295	40
281	6371000	300	40
282	6371000	300	46
283	6371000	305	45
284	6371000	305	40
285	6371000	310	40
286	6371000	315	40
287	6371000	320	40
288	6371000	325	44
289	6371000	325	40
290	6371000	330	41
291	6371000	330.1	41
292	6371000	335	40
293	6371000	340	45
294	6371000	342	40
295	6371000	345	40
296	6371000	345	45
297	6371000	350	45
298	6371000	352	41
299	6371000	355	45
300	6371000	355	40
301	6371000	0	45
302	6371000	1	40
303	6371000	3	43
304	6371000	12	45
305	6371000	10	40
306	6371000	19	42
307	6371000	20	45
308	6371000	25	45
309	6371000	25	40
310	6371000	30	40
311	6371000	30	45
312	6371000	35	45
313	6371000	35	40
314	6371000	40	40
315	6371000	40	45
316	6371000	45	45
317	6371000	45	40
318	6371000	50	40
319	6371000	50	45
320	6371000	55	45
321	6371000	55	40
322	6371000	60	40
323	6371000	60	45
324	6371000	65	45
325	6371000	65	40
326	6371000	70	40
327	6371000	70	45
328	6371000	75	45
329	6371000	75	40
330	6371000	80	40
331	6371000	80	45
332	6371000	85	45
333	6371000	85	40
334	6371000	90	40
335	6371000	90	45
336	6371000	95	35
337	6371000	95	30
338	6371000	100	35
339	6371000	100	30
340	6371000	105	30
341	6371000	105	35
342	6371000	110	35
343	6371000	110	30
344	6371000	115	30
345	6371000	115	35
346	6371000	120	35
347	6371000	120	30
348	6371000	123	30
349	6371000	125	35
350	6371000	130	35
351	6371000	129	30
352	6371000	135	30
353	6371000	135	35
354	6371000	140	35
355	6371000	140	30
356	6371000	145	30
357	6371000	145	35
358	6371000	150	35
359	6371000	150	30
360	6371000	155	30
361	6371000	155	35
362	6371000	160	35
363	6371000	160	30
364	6371000	165	30
365	6371000	165	35
366	6371000	170	35
367	6371000	170	30
368	6371000	175	30
369	6371000	175	35
370	6371000	180	35
371	6371000	180	30
372	6371000	185	30
373	6371000	185	35
374	6371000	190	35
375	6371000	190	30
376	6371000	195	30
377	6371000	195	35
378	6371000	200	35
379	6371000	200	30
380	6371000	205	30
381	6371000	205	35
382	6371000	210	35
383	6371000	210	30
384	6371000	215	30
385	6371000	215	35
386	6371000	220	35
387	6371000	220	30
388	6371000	225	30
389	6371000	225	35
390	6371000	230	35
391	6371000	230	30
392	6371000	235	35

393	6371000	235	30
394	6371000	240	30
395	6371000	246	30
396	6371000	246	35
397	6371000	250	35
398	6371000	250	30
399	6371000	255	30
400	6371000	255	35
401	6371000	260	35
402	6371000	260	30
403	6371000	265	30
404	6371000	265	35
405	6371000	270	35
406	6371000	270	30
407	6371000	275	32
408	6371000	275	35
409	6371000	275	30
410	6371000	280	30
411	6371000	280	34
412	6371000	284	34.5
413	6371000	285	30
414	6371000	290	30
415	6371000	290	32 5
416	6371000	295	35
417	6371000	295	30
418	6371000	300	30
419	6371000	300	37
420	6371000	305	35
421	6371000	305	30
422	6371000	310	30
423	6371000	310	35
424	6371000	315	35
425	6371000	315	29.1
426	6371000	315.1	29
427	6371000	321 2	33
428	6371000	325	30
429	6371000	321	33
430	6371000	325	36 5
431	6371000	325.2	36 5
432	6371000	330	35
433	6371000	330	30
434	6371000	335	30
435	6371000	335	35
436	6371000	343	36
437	6371000	344	33
438	6371000	345	30
439	6371000	350	30
440	6371000	350	35
441	6371000	352	36
442	6371000	354	34
443	6371000	355	30
444	6371000	0	30
445	6371000	0	35
446	6371000	358	37
447	6371000	8	35
448	6371000	5	30
449	6371000	14	31
450	6371000	15	35
451	6371000	20	38
452	6371000	22	34
453	6371000	20	32.5
454	6371000	30	32
455	6371000	30	35
456	6371000	35	36
457	6371000	33	32
458	6371000	32 1	31
459	6371000	40	30
460	6371000	32	31
461	6371000	40	35
462	6371000	42	37
463	6371000	50	36
464	6371000	50	32
465	6371000	47	30
466	6371000	52 5	30
467	6371000	55	35
468	6371000	60	35
469	6371000	60	30
470	6371000	65	30
471	6371000	65	35
472	6371000	70	35
473	6371000	70	30
474	6371000	75	30
475	6371000	75	35
476	6371000	80	35
477	6371000	80	30
478	6371000	85	30
479	6371000	85	35
480	6371000	90	35
481	6371000	90	30
482	6371000	95	25
483	6371000	95	20
484	6371000	100	25
485	6371000	100	20
486	6371000	105	25
487	6371000	105	20
488	6371000	110	25
489	6371000	108	20
490	6371000	114	17
491	6371000	117	20
492	6371000	115	23
493	6371000	115	25
494	6371000	120	26
495	6371000	123	25
496	6371000	125	20
497	6371000	130	20
498	6371000	130	25
499	6371000	135	25
500	6371000	135	20
501	6371000	140	20
502	6371000	140	25
503	6371000	145	25
504	6371000	145	20
505	6371000	150	20
506	6371000	150	25
507	6371000	155	25
508	6371000	155	20
509	6371000	160	20
510	6371000	160	25
511	6371000	165	25
512	6371000	165	20
513	6371000	170	20
514	6371000	170	25
515	6371000	175	25
516	6371000	175	20
517	6371000	180	20
518	6371000	180	25
519	6371000	186	25
520	6371000	186	20
521	6371000	190	20
522	6371000	190	25
523	6371000	195	25
524	6371000	195	20
525	6371000	200	20
526	6371000	200	25
527	6371000	205	25
528	6371000	206	20
529	6371000	210	20
530	6371000	210	25
531	6371000	215	25
532	6371000	215	20
533	6371000	220	20
534	6371000	220	25
535	6371000	225	25
536	6371000	225	20
537	6371000	230	20
538	6371000	230	25
539	6371000	235	25
540	6371000	235	20
541	6371000	240	20
542	6371000	240	25
543	6371000	245	25
544	6371000	245	20
545	6371000	250	20
546	6371000	250	25
547	6371000	250	27
548	6371000	253	24
549	6371000	253 2	23 9
550	6371000	254	20
551	6371000	254.1	20
552	6371000	258	20
553	6371000	260	18
554	6371000	264	19
555	6371000	262	23
556	6371000	260	27
557	6371000	265	28
558	6371000	265	25
559	6371000	270	20
560	6371000	270	25
561	6371000	271	22
562	6371000	277	20
563	6371000	276	25
564	6371000	280	27
565	6371000	280	19
566	6371000	286	17 5
567	6371000	285	25
568	6371000	290	25
569	6371000	290	20
570	6371000	295	20
571	6371000	295	25
572	6371000	300	25
573	6371000	300	20
574	6371000	305	20
575	6371000	305	25
576	6371000	310	25
577	6371000	310	20
578	6371000	314	20
579	6371000	314 5	25
580	6371000	314.6	25
581	6371000	314.1	20
582	6371000	320	20
583	6371000	320	25
584	6371000	325	25
585	6371000	325	20
586	6371000	332	20
587	6371000	332	25

588	6371000	332	28
589	6371000	338	25
590	6371000	338	20
591	6371000	343	20
592	6371000	345	26
593	6371000	350	25
594	6371000	350	20
595	6371000	355	20
596	6371000	355	25
597	6371000	0	25
598	6371000	0	20
599	6371000	5	20
600	6371000	5	25
601	6371000	10	25
602	6371000	10	20
603	6371000	15	20
604	6371000	15	25
605	6371000	20	25
606	6371000	20	20
607	6371000	25	20
608	6371000	25	25
609	6371000	33	25
610	6371000	30	20
611	6371000	36	20
612	6371000	38	20
613	6371000	35	25
614	6371000	35.1	25
615	6371000	37	25
616	6371000	40	25
617	6371000	38.1	20
618	6371000	40	20
619	6371000	45	20
620	6371000	45	25
621	6371000	50	27
622	6371000	50	20
623	6371000	58	20
624	6371000	60	26
625	6371000	65	26
626	6371000	65	20
627	6371000	74	20
628	6371000	71	26
629	6371000	75	25
630	6371000	80	25
631	6371000	80	20
632	6371000	85	25
633	6371000	86	20
634	6371000	88	23
635	6371000	90	20
636	6371000	90	25
637	6371000	95	13.5
638	6371000	95	10
639	6371000	99	8
640	6371000	100	15
641	6371000	103.5	10
642	6371000	105	15
643	6371000	109	13
644	6371000	110	10
645	6371000	116	10
646	6371000	120	15
647	6371000	120	10
648	6371000	125	10
649	6371000	125	15
650	6371000	130	15
651	6371000	130	10
652	6371000	135	10
653	6371000	135	15
654	6371000	140	15
655	6371000	140	10
656	6371000	145	10
657	6371000	145	15
658	6371000	150	15
659	6371000	150	10
660	6371000	155	10
661	6371000	155	15
662	6371000	160	15
663	6371000	160	10
664	6371000	165	10
665	6371000	165	15
666	6371000	170	15
667	6371000	170	10
668	6371000	175	10
669	6371000	175	15
670	6371000	180	15
671	6371000	180	10
672	6371000	185	10
673	6371000	185	15
674	6371000	190	15
675	6371000	190	10
676	6371000	195	10
677	6371000	195	15
678	6371000	200	15
679	6371000	200	10
680	6371000	205	10
681	6371000	205	15
682	6371000	210	15
683	6371000	210	10
684	6371000	215	10
685	6371000	215	15
686	6371000	220	15
687	6371000	220	10
688	6371000	225	10
689	6371000	225	15
690	6371000	230	15
691	6371000	230	10
692	6371000	235	10
693	6371000	235	15
694	6371000	240	15
695	6371000	240	10
696	6371000	245	10
697	6371000	245	15
698	6371000	250	15
699	6371000	250	10
700	6371000	256.5	10
701	6371000	255	15
702	6371000	255.1	15
703	6371000	256.6	10
704	6371000	260	10
705	6371000	260	15
706	6371000	266	15
707	6371000	265	10
708	6371000	270	10
709	6371000	270	13
710	6371000	270	17
711	6371000	275	15
712	6371000	276	10
713	6371000	279	8
714	6371000	281	12
715	6371000	286	12
716	6371000	292	12
717	6371000	290	17
718	6371000	295	15
719	6371000	301	14
720	6371000	296	10
721	6371000	300	10
722	6371000	306	10
723	6371000	305	15
724	6371000	310	15
725	6371000	310	10
726	6371000	315	10
727	6371000	314	17
728	6371000	314.1	17
729	6371000	320	16
730	6371000	318.1	13.1
731	6371000	318	13
732	6371000	322	10
733	6371000	322.1	10
734	6371000	325	15
735	6371000	328	15
736	6371000	328	10
737	6371000	332	8
738	6371000	332	15
739	6371000	336	15
740	6371000	336	10
741	6371000	341	10
742	6371000	342	15
743	6371000	346	15
744	6371000	345	10
745	6371000	350	10
746	6371000	350	15
747	6371000	355	15
748	6371000	355	10
749	6371000	0	10
750	6371000	0	15
751	6371000	5	15
752	6371000	5	10
753	6371000	10	10
754	6371000	10	15
755	6371000	15	15
756	6371000	15	10
757	6371000	20	10
758	6371000	20	15
759	6371000	25	15
760	6371000	25	10
761	6371000	30	10
762	6371000	30	15
763	6371000	35	15
764	6371000	35	10
765	6371000	41	11
766	6371000	42	12
767	6371000	42.1	12.1
768	6371000	43	14
769	6371000	42	17
770	6371000	40	16
771	6371000	39.9	16
772	6371000	38	15
773	6371000	46	17
774	6371000	50	16
775	6371000	50	14
776	6371000	50	13.9
777	6371000	50	12.5
778	6371000	48	10
779	6371000	54	10
780	6371000	56	13
781	6371000	56	14
782	6371000	56.1	14.1

783	6371000	60	18
784	6371000	60	10
785	6371000	60.1	10.1
786	6371000	63.5	14
787	6371000	66	16
788	6371000	70	15
789	6371000	67	10
790	6371000	70	10
791	6371000	75	10
792	6371000	77	15
793	6371000	80	15
794	6371000	80	10
795	6371000	83	15
796	6371000	90	15
797	6371000	90	12
798	6371000	92	10
799	6371000	85	6
800	6371000	95	7
801	6371000	95	0
802	6371000	100	0
803	6371000	100	4
804	6371000	105	5
805	6371000	105	0
806	6371000	110	0
807	6371000	110	5
808	6371000	118	.
809	6371000	115	0
810	6371000	120	0
811	6371000	120	6
812	6371000	125	5
813	6371000	125	0
814	6371000	130	0
815	6371000	130	4
816	6371000	135	3
817	6371000	135	0
818	6371000	140	0
819	6371000	140	2
820	6371000	145	5
821	6371000	145	0
822	6371000	150	0
823	6371000	150	5
824	6371000	155	5
825	6371000	155	0
826	6371000	160	0
827	6371000	160	5
828	6371000	165	5
829	6371000	165	0
830	6371000	170	0
831	6371000	170	5
832	6371000	175	5
833	6371000	175	0
834	6371000	180	0
835	6371000	180	5
836	6371000	185	5
837	6371000	185	0
838	6371000	190	0
839	6371000	190	5
840	6371000	195	5
841	6371000	195	0
842	6371000	200	0
843	6371000	200	5
844	6371000	205	5
845	6371000	205	0
846	6371000	210	0
847	6371000	210	5
848	6371000	215	5
849	6371000	215	0
850	6371000	220	0
851	6371000	220	5
852	6371000	225	5
853	6371000	225	0
854	6371000	230	0
855	6371000	230	5
856	6371000	235	5
857	6371000	235	0
858	6371000	240	0
859	6371000	240	5
860	6371000	245	5
861	6371000	245	0
862	6371000	250	0
863	6371000	250	5
864	6371000	255	5
865	6371000	255	0
866	6371000	259	0
867	6371000	258.1	5
868	6371000	258	5.1
869	6371000	258.2	5.1
870	6371000	258.3	5
871	6371000	259.1	0
872	6371000	265	0
873	6371000	265	4
874	6371000	265	4.1
875	6371000	270	4.1
876	6371000	270	4
877	6371000	270	0
878	6371000	275	0
879	6371000	275	3
880	6371000	275	3.1
881	6371000	280	3.1
882	6371000	280	3
883	6371000	280	0
884	6371000	285	0
885	6371000	285	4
886	6371000	290	5
887	6371000	290	0
888	6371000	295	0
889	6371000	295	5
890	6371000	300	7
891	6371000	300	4
892	6371000	300	0
893	6371000	305	0
894	6371000	305	5
895	6371000	310	7
896	6371000	310	3
897	6371000	310	0
898	6371000	314	0
899	6371000	315	5
900	6371000	320	5
901	6371000	325	5
902	6371000	322	0
903	6371000	330	0
904	6371000	327	5
905	6371000	327.1	5.1
906	6371000	332	2.1
907	6371000	332	2
908	6371000	340	1
909	6371000	340	1.1
910	6371000	340	5
911	6371000	346	0
912	6371000	346.1	0.1
913	6371000	349	1
914	6371000	350	5
915	6371000	355	5
916	6371000	355	0
917	6371000	0	0
918	6371000	0	4
919	6371000	8	4
920	6371000	10	5
921	6371000	10	0
922	6371000	15	0
923	6371000	15	5
924	6371000	20	5
925	6371000	20	0
926	6371000	25	0
927	6371000	25	5
928	6371000	30	5
929	6371000	30	0
930	6371000	35	0
931	6371000	35	5
932	6371000	40	5
933	6371000	40	0
934	6371000	43	0
935	6371000	48	6
936	6371000	50	5
937	6371000	48	0
938	6371000	50	0
939	6371000	55	0
940	6371000	55	5
941	6371000	60	5
942	6371000	60	0
943	6371000	63	0
944	6371000	63	5
945	6371000	63.1	5
946	6371000	66	5
947	6371000	67	0
948	6371000	67.1	0
949	6371000	70	0
950	6371000	71	6
951	6371000	75	6
952	6371000	75	0
953	6371000	80	0
954	6371000	80	6
955	6371000	85	0
956	6371000	90	0
957	6371000	90	5
958	6371000	95	-5
959	6371000	95	-10
960	6371000	100	-10
961	6371000	100	-5
962	6371000	105	-5
963	6371000	105	-10
964	6371000	110	-10
965	6371000	110	-5
966	6371000	115	-4
967	6371000	115	-10
968	6371000	119	-9
969	6371000	120	-5
970	6371000	125	-5
971	6371000	125	-10
972	6371000	130	-10
973	6371000	130	-5
974	6371000	135	-5
975	6371000	135	-9.5
976	6371000	140	-10
977	6371000	140	-5

978	6371000	145	-5
979	6371000	146	-10
980	6371000	150	-10
981	6371000	150	-5
982	6371000	150	-2
983	6371000	155	-3
984	6371000	155	-5
985	6371000	155	-10
986	6371000	160	-10
987	6371000	161	-4
988	6371000	165	-5
989	6371000	165	-10
990	6371000	170	-10
991	6371000	170	-5
992	6371000	175	-5
993	6371000	175	-10
994	6371000	180	-10
995	6371000	180	-5
996	6371000	185	-5
997	6371000	185	-10
998	6371000	190	-10
999	6371000	190	-5
F1000	6371000	195	-5
F1001	6371000	195	-10
F1002	6371000	200	-10
F1003	6371000	200	-5
F1004	6371000	205	-5
F1005	6371000	205	-10
F1006	6371000	210	-10
F1007	6371000	210	-5
F1008	6371000	215	-5
F1009	6371000	215	-10
F1010	6371000	220	-10
F1011	6371000	220	-5
F1012	6371000	225	-5
F1013	6371000	225	-10
F1014	6371000	230	-10
F1015	6371000	230	-5
F1016	6371000	235	-5
F1017	6371000	235	-10
F1018	6371000	240	-10
F1019	6371000	240	-5
F1020	6371000	245	-5
F1021	6371000	245	-10
F1022	6371000	250	-10
F1023	6371000	250	-5
F1024	6371000	255	-5
F1025	6371000	255.1	-5
F1026	6371000	253	-10
F1027	6371000	253.1	-10
F1028	6371000	260	-10
F1029	6371000	260	-5
F1030	6371000	265	-5
F1031	6371000	265	-10
F1032	6371000	270	-10
F1033	6371000	270	-5
F1034	6371000	275	-5
F1035	6371000	275	-10
F1036	6371000	280	-10
F1037	6371000	280	-8
F1038	6371000	282	-10
F1039	6371000	286	-10
F1040	6371000	286	-5
F1041	6371000	290	-5
F1042	6371000	290	-10

F1043	6371000	295	-10
F1044	6371000	295	-5
F1045	6371000	300	-5
F1046	6371000	300	-10
F1047	6371000	305	-10
F1048	6371000	305	-5
F1049	6371000	310	-5
F1050	6371000	310	-10
F1051	6371000	315	-10
F1052	6371000	315	-5
F1053	6371000	320	-3
F1054	6371000	320	-6
F1055	6371000	320	-10
F1056	6371000	326	-11
F1057	6371000	325	-5
F1058	6371000	328	-3.5
F1059	6371000	331	-5
F1060	6371000	331	-10
F1061	6371000	335	-10
F1062	6371000	335	-5
F1063	6371000	340	-5
F1064	6371000	340	-10
F1065	6371000	346	-10
F1066	6371000	346.1	-10
F1067	6371000	346	-5
F1068	6371000	346.1	-5
F1069	6371000	350	-5
F1070	6371000	350	-10
F1071	6371000	356	-10
F1072	6371000	356	-5
F1073	6371000	1	-5
F1074	6371000	1.5	-10
F1075	6371000	5	-10
F1076	6371000	5	-5
F1077	6371000	10	-5
F1078	6371000	10	-10
F1079	6371000	14	-10
F1080	6371000	14	-8
F1081	6371000	20	-5
F1082	6371000	20	-10
F1083	6371000	25	-10
F1084	6371000	25	-5
F1085	6371000	30	-5
F1086	6371000	30	-10
F1087	6371000	35	-10
F1088	6371000	35	-5
F1089	6371000	38	-2
F1090	6371000	39	-10
F1091	6371000	46	-10
F1092	6371000	46.5	-5
F1093	6371000	50	-5
F1094	6371000	50	-10
F1095	6371000	56	-5
F1096	6371000	56	-10
F1097	6371000	60	-10
F1098	6371000	60	-5
F1099	6371000	67	-5
F1100	6371000	67.1	-5
F1101	6371000	67.5	-10
F1102	6371000	67.6	-10
F1103	6371000	70	-10
F1104	6371000	70	-5
F1105	6371000	75	-5
F1106	6371000	75	-10
F1107	6371000	80	-10

F1108	6371000	80	-5
F1109	6371000	85	-5
F1110	6371000	85	-10
F1111	6371000	90	-10
F1112	6371000	90	-5
F1113	6371000	95	-15
F1114	6371000	95	-20
F1115	6371000	100	-20
F1116	6371000	100	-15
F1117	6371000	105	-15
F1118	6371000	105	-20
F1119	6371000	110	-20
F1120	6371000	110	-15
F1121	6371000	115	-15
F1122	6371000	112	-22
F1123	6371000	115	-21.5
F1124	6371000	120	-20
F1125	6371000	120	-18
F1126	6371000	120	-14
F1127	6371000	125	-16
F1128	6371000	125	-20
F1129	6371000	130	-13
F1130	6371000	130	-20
F1131	6371000	135	-20
F1132	6371000	135	-15
F1133	6371000	140	-14
F1134	6371000	140	-20
F1135	6371000	145	-20
F1136	6371000	144	-13.5
F1137	6371000	150	-17
F1138	6371000	152	-20
F1139	6371000	155	-15
F1140	6371000	160	-15
F1141	6371000	160	-20
F1142	6371000	165	-20
F1143	6371000	166	-15
F1144	6371000	170	-15
F1145	6371000	170	-20
F1146	6371000	175	-20
F1147	6371000	175	-15
F1148	6371000	180	-15
F1149	6371000	180	-20
F1150	6371000	186	-20
F1151	6371000	185	-15
F1152	6371000	190	-15
F1153	6371000	190	-20
F1154	6371000	195	-20
F1155	6371000	195	-15
F1156	6371000	200	-15
F1157	6371000	200	-20
F1158	6371000	205	-20
F1159	6371000	205	-15
F1160	6371000	210	-15
F1161	6371000	210	-20
F1162	6371000	215	-20
F1163	6371000	215	-15
F1164	6371000	220	-15
F1165	6371000	220	-20
F1166	6371000	225	-20
F1167	6371000	225	-15
F1168	6371000	230	-15
F1169	6371000	230	-20
F1170	6371000	236	-20
F1171	6371000	235	-15
F1172	6371000	240	-15

F1173	6371000	240	-20
F1174	6371000	245	-20
F1175	6371000	245	-15
F1176	6371000	250	-15
F1177	6371000	250	-15 2
F1178	6371000	248	-19
F1179	6371000	248.1	-19
F1180	6371000	255	-20
F1181	6371000	255	-15
F1182	6371000	260	-15
F1183	6371000	260	-20
F1184	6371000	265	-20
F1185	6371000	265	-15
F1186	6371000	270	-15
F1187	6371000	270	-20
F1188	6371000	275	-20
F1189	6371000	275	-15
F1190	6371000	280	-15
F1191	6371000	280	-20
F1192	6371000	285	-20
F1193	6371000	285	-14
F1194	6371000	290	-18
F1195	6371000	290	-20
F1196	6371000	295	-20
F1197	6371000	295	-15
F1198	6371000	300	-15
F1199	6371000	300	-20
F1200	6371000	305	-20
F1201	6371000	305	-15
F1202	6371000	310	-15
F1203	6371000	310	-20
F1204	6371000	315	-20
F1205	6371000	315	-15
F1206	6371000	320	-15
F1207	6371000	320	-18
F1208	6371000	323	-15
F1209	6371000	325	-15
F1210	6371000	325	-20
F1211	6371000	331	-20
F1212	6371000	331	-15
F1213	6371000	335	-15
F1214	6371000	335	-20
F1215	6371000	340	-20
F1216	6371000	340	-15
F1217	6371000	345	-15
F1218	6371000	345.1	-15
F1219	6371000	345	-20
F1220	6371000	345.1	-20
F1221	6371000	350	-20
F1222	6371000	350	-15
F1223	6371000	356	-15
F1224	6371000	356	-20
F1225	6371000	0	-20
F1226	6371000	3	-15
F1227	6371000	4	-20
F1228	6371000	6	-15
F1229	6371000	10	-15
F1230	6371000	10	-20
F1231	6371000	13	-20
F1232	6371000	12	-17
F1233	6371000	20	-15
F1234	6371000	20	-20
F1235	6371000	25	-20
F1236	6371000	25	-15
F1237	6371000	30	-15
F1238	6371000	30	-20
F1239	6371000	35	-20
F1240	6371000	35	-15
F1241	6371000	39	-13
F1242	6371000	40	-20
F1243	6371000	45	-20
F1244	6371000	45	-17
F1245	6371000	50	-16
F1246	6371000	50	-20
F1247	6371000	55	-20
F1248	6371000	55	-15
F1249	6371000	60	-15
F1250	6371000	60	-20
F1251	6371000	65	-20
F1252	6371000	64	-15
F1253	6371000	66.5	-15
F1254	6371000	66.6	-15
F1255	6371000	70	-15
F1256	6371000	67	-20
F1257	6371000	67 1	-20
F1258	6371000	70	-20
F1259	6371000	75	-20
F1260	6371000	75	-15
F1261	6371000	80	-15
F1262	6371000	80	-20
F1263	6371000	85	-20
F1264	6371000	85	-15
F1265	6371000	90	-15
F1266	6371000	90	-20
F1267	6371000	95	-25
F1268	6371000	95	-30
F1269	6371000	100	-30
F1270	6371000	100	-25
F1271	6371000	105	-25
F1272	6371000	105	-30
F1273	6371000	110	-30
F1274	6371000	110	-25
F1275	6371000	113	-25
F1276	6371000	114	-30
F1277	6371000	117	-30
F1278	6371000	116	-25
F1279	6371000	120	-25
F1280	6371000	121	-30
F1281	6371000	125	-30
F1282	6371000	125	-25
F1283	6371000	130	-25
F1284	6371000	130	-30
F1285	6371000	135	-30
F1286	6371000	135	-25
F1287	6371000	140	-25
F1288	6371000	140	-30
F1289	6371000	145	-30
F1290	6371000	145	-25
F1291	6371000	150	-25
F1292	6371000	150	-30
F1293	6371000	155	-30
F1294	6371000	157	-30
F1295	6371000	156	-28
F1296	6371000	154	-25
F1297	6371000	160	-25
F1298	6371000	160	-30
F1299	6371000	165	-30
F1300	6371000	165	-25
F1301	6371000	170	-25
F1302	6371000	170	-30
F1303	6371000	175	-30
F1304	6371000	173	-25
F1305	6371000	180	-25
F1306	6371000	180	-30
F1307	6371000	185	-30
F1308	6371000	185	-25
F1309	6371000	190	-25
F1310	6371000	190	-30
F1311	6371000	195	-30
F1312	6371000	195	-25
F1313	6371000	200	-25
F1314	6371000	200	-30
F1315	6371000	205	-30
F1316	6371000	205	-25
F1317	6371000	210	-25
F1318	6371000	210	-30
F1319	6371000	215	-30
F1320	6371000	215	-25
F1321	6371000	220	-25
F1322	6371000	220	-30
F1323	6371000	225	-30
F1324	6371000	225	-25
F1325	6371000	230	-25
F1326	6371000	230	-30
F1327	6371000	235	-30
F1328	6371000	235	-25
F1329	6371000	240	-25
F1330	6371000	240	-30
F1331	6371000	245	-30
F1332	6371000	245	-25
F1333	6371000	248	-25
F1334	6371000	248 1	-25
F1335	6371000	248	-30
F1336	6371000	248 1	-30
F1337	6371000	254	-30
F1338	6371000	254	-25
F1339	6371000	260	-25
F1340	6371000	260	-30
F1341	6371000	265	-30
F1342	6371000	265	-25
F1343	6371000	270	-25
F1344	6371000	270	-30
F1345	6371000	275	-30
F1346	6371000	275	-25
F1347	6371000	280	-25
F1348	6371000	280	-30
F1349	6371000	288	-30
F1350	6371000	285	-25
F1351	6371000	289	-25
F1352	6371000	295	-25
F1353	6371000	295	-30
F1354	6371000	300	-30
F1355	6371000	300	-25
F1356	6371000	305	-25
F1357	6371000	305	-30
F1358	6371000	310	-30
F1359	6371000	310	-25
F1360	6371000	315	-25
F1361	6371000	315	-30
F1362	6371000	320	-30
F1363	6371000	320	-25
F1364	6371000	325	-25
F1365	6371000	326	-30
F1366	6371000	330	-30
F1367	6371000	328	-26

F1368	6371000	335	-25
F1369	6371000	335	-30
F1370	6371000	340	-30
F1371	6371000	340	-25
F1372	6371000	346	-27
F1373	6371000	346.1	-27
F1374	6371000	345	-30
F1375	6371000	345.1	-30
F1376	6371000	350	-30
F1377	6371000	350	-25
F1378	6371000	355	-25
F1379	6371000	355	-30
F1380	6371000	0	-30
F1381	6371000	0	-25
F1382	6371000	6	-28
F1383	6371000	5	-30
F1384	6371000	10	-31
F1385	6371000	10	-25
F1386	6371000	16	-25
F1387	6371000	15	-30
F1388	6371000	19	-30
F1389	6371000	22	-30
F1390	6371000	20	-25
F1391	6371000	25	-25
F1392	6371000	27	-30
F1393	6371000	33	-30
F1394	6371000	33	-27
F1395	6371000	30	-24
F1396	6371000	37	-30
F1397	6371000	40	-30
F1398	6371000	40	-25
F1399	6371000	45	-25
F1400	6371000	45	-30
F1401	6371000	50	-30
F1402	6371000	50	-25
F1403	6371000	55	-25
F1404	6371000	55	-30
F1405	6371000	60	-30
F1406	6371000	60.2	-30
F1407	6371000	65	-30
F1408	6371000	65	-26.6
F1409	6371000	66	-26.5
F1410	6371000	60	-25
F1411	6371000	68	-24.1
F1412	6371000	68.1	-24
F1413	6371000	68.1	-24.2
F1414	6371000	68.2	-24.1
F1415	6371000	70	-30
F1416	6371000	75	-30
F1417	6371000	75.1	-30
F1418	6371000	73	-25
F1419	6371000	80	-25
F1420	6371000	80	-30
F1421	6371000	85	-30
F1422	6371000	85	-25
F1423	6371000	90	-25
F1424	6371000	90	-30
F1425	6371000	331	-22
F1426	6371000	95	-35
F1427	6371000	95	-40
F1428	6371000	100	-40
F1429	6371000	100	-35
F1430	6371000	105	-35
F1431	6371000	105	-40
F1432	6371000	110	-40
F1433	6371000	110	-35
F1434	6371000	113	-34
F1435	6371000	115	-40
F1436	6371000	120	-40
F1437	6371000	117	-34
F1438	6371000	120	-33.5
F1439	6371000	125	-33
F1440	6371000	125	-36
F1441	6371000	125	-40
F1442	6371000	130	-40
F1443	6371000	130	-36
F1444	6371000	130	-32.5
F1445	6371000	133	-32
F1446	6371000	135	-36
F1447	6371000	135	-40
F1448	6371000	140	-40
F1449	6371000	140	-34
F1450	6371000	144	-36
F1451	6371000	145	-40
F1452	6371000	150	-40
F1453	6371000	150	-36
F1454	6371000	155	-35
F1455	6371000	155	-40
F1456	6371000	161	-40
F1457	6371000	160	-37
F1458	6371000	165	-35
F1459	6371000	166	-40
F1460	6371000	170	-40
F1461	6371000	170	-35
F1462	6371000	177.5	-35
F1463	6371000	175	-40
F1464	6371000	180	-40
F1465	6371000	180	-37.5
F1466	6371000	180	-34
F1467	6371000	185	-35
F1468	6371000	185	-40
F1469	6371000	190	-40
F1470	6371000	190	-35
F1471	6371000	195	-35
F1472	6371000	195	-40
F1473	6371000	200	-35
F1474	6371000	200	-40
F1475	6371000	205	-40
F1476	6371000	205	-35
F1477	6371000	210	-35
F1478	6371000	210	-40
F1479	6371000	215	-40
F1480	6371000	215	-35
F1481	6371000	220	-35
F1482	6371000	220	-40
F1483	6371000	225	-40
F1484	6371000	225	-35
F1485	6371000	230	-35
F1486	6371000	230	-40
F1487	6371000	235	-40
F1488	6371000	235	-35
F1489	6371000	240	-35
F1490	6371000	240	-40
F1491	6371000	245	-40
F1492	6371000	245	-35
F1493	6371000	249	-36.1
F1494	6371000	249.1	-36
F1495	6371000	250	-40
F1496	6371000	253	-40
F1497	6371000	253.1	-40
F1498	6371000	254 9	-37 2
F1499	6371000	255.1	-37 3
F1500	6371000	255	-37
F1501	6371000	255 1	-37 1
F1502	6371000	255	-35
F1503	6371000	260	-35
F1504	6371000	260	-37 5
F1505	6371000	260	-37 6
F1506	6371000	260	-40
F1507	6371000	265	-40
F1508	6371000	265	-38.1
F1509	6371000	265	-38
F1510	6371000	268	-38
F1511	6371000	268	-38.1
F1512	6371000	270	-35
F1513	6371000	275	-35
F1514	6371000	273	-40
F1515	6371000	273.1	-40
F1516	6371000	280	-40
F1517	6371000	280	-35
F1518	6371000	287	-34
F1519	6371000	286	-40
F1520	6371000	290	-40
F1521	6371000	290	-35
F1522	6371000	295	-35
F1523	6371000	295	-40
F1524	6371000	302	-40
F1525	6371000	300	-35
F1526	6371000	305	-35
F1527	6371000	305	-40
F1528	6371000	310	-40
F1529	6371000	310	-35
F1530	6371000	315	-35
F1531	6371000	315	-40
F1532	6371000	318	-40
F1533	6371000	320	-38
F1534	6371000	320	-34
F1535	6371000	323	-34
F1536	6371000	325	-40
F1537	6371000	330	-40
F1538	6371000	330	-35
F1539	6371000	335	-35
F1540	6371000	335	-40
F1541	6371000	340	-40
F1542	6371000	340	-35
F1543	6371000	344	-37
F1544	6371000	344.1	-37
F1545	6371000	344	-40
F1546	6371000	344.1	-40
F1547	6371000	350	-40
F1548	6371000	350	-35
F1549	6371000	355	-35
F1550	6371000	355	-40
F1551	6371000	0	-40
F1552	6371000	0	-35
F1553	6372000	5	-35
F1554	6371000	5	-40
F1556	6371000	10	40
F1556	6371000	10	-35
F1557	6371000	17	-36
F1558	6371000	15	-40
F1559	6371000	20	-40
F1560	6371000	20	-36
F1561	6371000	20	-33
F1562	6371000	25	-36

F1563	6371000	25	-40
F1564	6371000	30	-40
F1565	6371000	30	-35.5
F1566	6371000	34	-35
F1567	6371000	35	-40
F1568	6371000	40	-40
F1569	6371000	40	-35
F1570	6371000	45	-35
F1571	6371000	45	-40
F1572	6371000	45.1	-40
F1573	6371000	50	-40
F1574	6371000	50	-36.1
F1575	6371000	50	-36
F1576	6371000	55	-33
F1577	6371000	55	-33.1
F1578	6371000	55	-40
F1579	6371000	60	-40
F1580	6371000	60	-35
F1581	6371000	65	-35
F1582	6371000	65	-40
F1583	6371000	70	-40
F1584	6371000	70	-35
F1585	6371000	77	-35
F1586	6371000	77.1	-35
F1587	6371000	75	-40
F1588	6371000	78.5	-40
F1589	6371000	78.6	-40
F1590	6371000	80	-40
F1591	6371000	80	-35
F1592	6371000	85	-35
F1593	6371000	85	-40
F1594	6371000	90	-40
F1595	6371000	90	-35
F1596	6371000	95	-43
F1597	6371000	95	-43.1
F1598	6371000	95	-50
F1599	6371000	100	-50
F1600	6371000	100	-44.1
F1601	6371000	100	-44
F1602	6371000	105	-45
F1603	6371000	105	-45.1
F1604	6371000	105	-50
F1605	6371000	110	-50
F1606	6371000	110	-46.1
F1607	6371000	110	-46
F1608	6371000	115	-45
F1609	6371000	118	-48
F1610	6371000	117.9	-48.1
F1611	6371000	115	-50
F1612	6371000	120	-50
F1613	6371000	120	-48.1
F1614	6371000	120	-48
F1615	6371000	120	-45
F1616	6371000	125	-45
F1617	6371000	125	-48.3
F1618	6371000	125	-48.4
F1619	6371000	125	-50
F1620	6371000	130	-50
F1621	6371000	130	-48.7
F1622	6371000	130	-48.6
F1623	6371000	130	-45
F1624	6371000	135	-45
F1625	6371000	135	-48.8
F1626	6371000	135	-48.9
F1627	6371000	135	-50
F1628	6371000	141	-50
F1629	6371000	141.1	-50
F1630	6371000	140	-49.1
F1631	6371000	140.1	-49
F1632	6371000	140	-45
F1633	6371000	145	-45
F1634	6371000	145	-50
F1635	6371000	150	-50
F1636	6371000	150	-45
F1637	6371000	155	-45
F1638	6371000	155	-50
F1639	6371000	160	-50
F1640	6371000	160	-45
F1641	6371000	162	-45
F1642	6371000	164	-50
F1643	6371000	165	-45
F1644	6371000	170	-45
F1645	6371000	170	-50
F1646	6371000	175	-50
F1647	6371000	175	-45
F1648	6371000	180	-45
F1649	6371000	180	-50
F1650	6371000	186	-50
F1651	6371000	183	-45
F1652	6371000	190	-45
F1653	6371000	190	-50
F1654	6371000	195	-50
F1655	6371000	195	-45
F1656	6371000	200	-45
F1657	6371000	200	-50
F1658	6371000	205	-50
F1659	6371000	205	-45
F1660	6371000	210	-45
F1661	6371000	210	-50
F1662	6371000	215	-50
F1663	6371000	215	-45
F1664	6371000	220	-45
F1665	6371000	220	-50
F1666	6371000	225	-50
F1667	6371000	225	-45
F1668	6371000	230	-45
F1669	6371000	230	-50
F1670	6371000	235	-50
F1671	6371000	235	-45
F1672	6371000	240	-45
F1673	6371000	240	-50
F1674	6371000	245	-50
F1675	6371000	245.1	-50
F1676	6371000	250	-50
F1677	6371000	250	-44.1
F1678	6371000	250	-44
F1679	6371000	245	-45
F1680	6371000	255	-45
F1681	6371000	255	-50
F1682	6371000	260	-50
F1683	6371000	260	-45
F1684	6371000	265	-45
F1685	6371000	265	-50
F1686	6371000	270	-50
F1687	6371000	270	-45
F1688	6371000	275	-45
F1689	6371000	275	-50
F1690	6371000	280	-50
F1691	6371000	280	-44.1
F1692	6371000	280	-44
F1693	6371000	284.1	-46
F1694	6371000	284	-46.1
F1695	6371000	283	-50
F1696	6371000	290	-50
F1697	6371000	290	-45
F1698	6371000	294	-47
F1699	6371000	295	-50
F1700	63710[illegible]	[illegible]0	-50
F1701	6371000	300	-45
F1702	6371000	306	-45
F1703	6371000	305	-50
F1704	6371000	310	-50
F1705	6371000	310	-45
F1706	6371000	315	-44
F1707	6371000	312	-46
F1708	6371000	313	-50
F1709	6371000	317	-50
F1710	6371000	320	-50
F1711	6371000	320	-45
F1712	6371000	325	-45
F1713	6371000	325	-50
F1714	6371000	330	-50
F1715	6371000	330	-45
F1716	6371000	335	-45
F1717	6371000	335	-50
F1718	6371000	340	-50
F1719	6371000	340	-45
F1720	6371000	345	-45.1
F1721	6371000	345.1	-45
F1722	6371000	345	-50
F1723	6371000	350	-50
F1724	6371000	350	-48.1
F1725	6371000	350	-48
F1726	6371000	350	-44
F1727	6371000	355	-45
F1728	6371000	353.1	-50
F1729	6371000	353	-50
F1730	6371000	0	-50
F1731	6371000	0	-45
F1732	6371000	5	-45
F1733	6371000	5	-50
F1734	6371000	10	-50
F1735	6371000	10	-45
F1736	6371000	15	-45
F1737	6371000	15	-50
F1738	6371000	20	-50
F1739	6371000	20	-45
F1740	6371000	25	-45
F1741	6371000	25	-50
F1742	6371000	30	-50
F1743	6371000	30.1	-50
F1744	6371000	35	-50
F1745	6371000	35	-46.1
F1746	6371000	35	-46
F1747	6371000	30	-45
F1748	6371000	40	-43
F1749	6371000	40	-43.1
F1750	6371000	40	-50
F1751	6371000	45	-50
F1752	6371000	45	-45
F1753	6371000	50	-45
F1754	6371000	50	-50
F1755	6371000	55	-50
F1756	6371000	55	-45
F1757	6371000	60	-45

F1758	6371000	60	-50
F1759	6371000	65	-50
F1760	6371000	67	-47
F1761	6371000	65	-44
F1762	6371000	70	-45
F1763	6371000	70	-50
F1764	6371000	75	-50
F1765	6371000	75	-45
F1766	6371000	79	-42.1
F1767	6371000	79.1	-42
F1768	6371000	80	-45
F1769	6371000	80	-50
F1770	6371000	85	-50
F1771	6371000	85	-45
F1772	6371000	85	-42.1
F1773	6371000	85	-42
F1774	6371000	88	-41.5
F1775	6371000	88	-41.6
F1776	6371000	90	-45
F1777	6371000	90	-50
F1778	6371000	95	-55
F1779	6371000	95	-59
F1780	6371000	100	-59.5
F1781	6371000	100	-55
F1782	6371000	105	-55
F1783	6371000	105	-60
F1784	6371000	110	-60
F1785	6371000	110	-55
F1786	6371000	115	-55
F1787	6371000	115	-60
F1788	6371000	120	-60
F1789	6371000	120	-55
F1790	6371000	125	-55
F1791	6371000	125	-59.5
F1792	6371000	130	-59
F1793	6371000	130	-55
F1794	6371000	135	-55
F1795	6371000	135	-60
F1796	6371000	140	-60
F1797	6371000	140	-55
F1798	6371000	145	-56
F1799	6371000	145	-60
F1800	6371000	150	-60
F1801	6371000	150	-54
F1802	6371000	150.1	-53.9
F1803	6371000	155	-55
F1804	6371000	145	-52.5
F1805	6371000	152.1	-59
F1806	6371000	152	-59.1
F1807	6371000	159.8	-60
F1808	6371000	160	-60
F1809	6371000	160	-55
F1810	6371000	166	-55
F1811	6371000	167	-57
F1812	6371000	165	-60
F1813	6371000	170	-60
F1814	6371000	170	-57
F1815	6371000	170	-54
F1816	6371000	175	-55
F1817	6371000	175	-60
F1818	6371000	180	-60
F1819	6371000	180	-56
F1820	6371000	180	-53
F1821	6371000	185	-55
F1822	6371000	190	-55
F1823	6371000	185	-60
F1824	6371000	190	-60
F1825	6371000	195	-60
F1826	6371000	195	-55
F1827	6371000	200	-55
F1828	6371000	200	-60
F1829	6371000	205	-60
F1830	6371000	205.1	-60
F1831	6371000	205	-55
F1832	6371000	210	-55
F1833	6371000	210	-58
F1834	6371000	210	-58.1
F1835	6371000	210	-60
F1836	6371000	215	-60
F1837	6371000	215.1	-56.1
F1838	6371000	215	-56
F1839	6371000	215	-53
F1840	6371000	220	-53
F1841	6371000	220	-56
F1842	6371000	220	-56.1
F1843	6371000	220	-60
F1844	6371000	225	-60
F1845	6371000	225	-55.6
F1846	6371000	225	-55.5
F1847	6371000	225	-53
F1848	6371000	230	-55.5
F1849	6371000	230	-55.6
F1850	6371000	230	-60
F1851	6371000	235	-60
F1852	6371000	235	-55.6
F1853	6371000	235	-55.5
F1854	6371000	240	-55
F1855	6371000	240.1	-55.1
F1856	6371000	240	-60
F1857	6371000	245	-60
F1858	6371000	245	-55
F1859	6371000	250	-55
F1860	6371000	250	-60
F1861	6371000	255	-60
F1862	6371000	256	-55
F1863	6371000	260	-56
F1864	6371000	260	-60
F1865	6371000	265	-60
F1866	6371000	265	-55
F1867	6371000	270	-55
F1868	6371000	270	-60
F1869	6371000	275	-60
F1870	6371000	275	-55
F1871	6371000	280	-56
F1872	6371000	280	-60
F1873	6371000	285	-60
F1874	6371000	285	-55
F1875	6371000	290	-55
F1876	6371000	290	-60
F1877	6371000	295	-60
F1878	6371000	295	-57
F1879	6371000	295	-53
F1880	6371000	300	-53
F1881	6371000	300	-57
F1882	6371000	300	-60
F1883	6371000	305	-60
F1884	6371000	305	-57
F1885	6371000	305	-53
F1886	6371000	310	-53
F1887	6371000	310	-56.5
F1888	6371000	310	-60
F1889	6371000	315	-60
F1890	6371000	313	-56
F1891	6371000	320	-55
F1892	6371000	320	-60
F1893	6371000	325	-60
F1894	6371000	325	-55
F1895	6371000	330	-55
F1896	6371000	330	-60
F1897	6371000	335	-60
F1898	6371000	335	-55
F1899	6371000	340	-55
F1900	6371000	350	-57
F1901	6371000	350	-54
F1902	6371000	354	-54
F1903	6371000	355	-55
F1904	6371000	355	-55.1
F1905	6371000	355	-60
F1906	6371000	0	-60
F1907	6371000	0	-54.2
F1908	6371000	359.9	-54.1
F1909	6371000	0	-54
F1910	6371000	0.1	-54.1
F1911	6371000	5	-53
F1912	6371000	5	-53.1
F1913	6371000	5	-60
F1914	6371000	10	-60
F1915	6371000	12	-60
F1916	6371000	10	-53.1
F1917	6371000	10	-53
F1918	6371000	15	-52
F1919	6371000	15	-52.1
F1920	6371000	15	-60
F1921	6371000	20	-60
F1922	6371000	20	-52.6
F1923	6371000	20	-52.5
F1924	6371000	26	-53
F1925	6371000	26	-53.1
F1926	6371000	25	-60
F1927	6371000	30	-60
F1928	6371000	30	-55
F1929	6371000	35	-55
F1930	6371000	35	-60
F1931	6371000	40	-60
F1932	6371000	40	-55
F1933	6371000	45	-55
F1934	6371000	45	-60
F1935	6371000	50	-59.5
F1936	6371000	50	-55
F1937	6371000	55	-55
F1938	6371000	58	-59
F1939	6371000	60	-60
F1940	6371000	60	-56
F1941	6371000	65	-55
F1942	6371000	65	-60
F1943	6371000	70	-60
F1944	6371000	70	-55
F1945	6371000	75	-52.5
F1946	6371000	75	-55
F1947	6371000	75	-60
F1948	6371000	80	-60
F1949	6371000	80	-55
F1950	6371000	85	-55
F1951	6371000	90	-55
F1952	6371000	90	-59

F1953	6371000	145	-52.6
F1954	6371000	340	-59
F1955	6371000	340	-60
F1956	6371000	343.1	-59.1
F1957	6371000	343	-59
F1958	6371000	345	-55
F1959	6371000	346	-58
F1960	6371000	346	-58.1
F1961	6371000	346	-60
F1962	6371000	350	-60
F1963	6371000	350	-57 1
F1964	6371000	95	-65
F1965	6371000	98	-70
F1966	6371000	99	-67
F1967	6371000	110	-67
F1968	6371000	110	-70
F1969	6371000	120	-70
F1970	6371000	120	-67
F1971	6371000	130	-67
F1972	6371000	130	-70
F1973	6371000	140	-70
F1974	6371000	138 5	-66 5
F1975	6371000	139	-64
F1976	6371000	145	-65
F1977	6371000	145	-67
F1978	6371000	150	-70
F1979	6371000	150	-68 5
F1980	6371000	150	-65 5
F1981	6371000	165	-61 5
F1982	6371000	165	-61 6
F1983	6371000	160	-66
F1984	6371000	163	-70
F1985	6371000	170	-71
F1986	6371000	170	-67
F1987	6371000	170	-62 1
F1988	6371000	170	-62
F1989	6371000	180	-63
F1990	6371000	180	-63 1
F1991	6371000	180	-68
F1992	6371000	180	-71 5
F1993	6371000	190	-73
F1994	6371000	190	-69
F1995	6371000	187	-64 1
F1996	6371000	187	-64
F1997	6371000	195	-62 5
F1998	6371000	195	-62 6
F1999	6371000	200	-61
F2000	6371000	200	-61.1
F2001	6371000	203	-70
F2002	6371000	200	-75
F2003	6371000	210	-74
F2004	6371000	210	-68
F2005	6371000	220	-65.5
F2006	6371000	220	-73
F2007	6371000	225	-64
F2008	6371000	227	-72
F2009	6371000	230	-70
F2010	6371000	230	-64 5
F2011	6371000	240	-65
F2012	6371000	240	-73
F2013	6371000	250	-73 5
F2014	6371000	250	-65.5
F2015	6371000	260	-66
F2016	6371000	260	-74
F2017	6371000	270	-75
F2018	6371000	270	-66
F2019	6371000	280	-66
F2020	6371000	280	-75
F2021	6371000	289	-76
F2022	6371000	292	-66
F2023	6371000	296	-66
F2024	6371000	300	-66
F2025	6371000	300	-80
F2026	6381000	310	-81
F2027	6371000	310	-66
F2028	6371000	320	-65
F2029	6371000	290	-70
F2030	6371000	297 5	-70
F2031	6371000	300	-72
F2032	6371000	310	-72
F2033	6371000	320	-72
F2034	6371000	320	-81
F2035	6371000	330	-81
F2036	6371000	330	-73
F2037	6371000	329	-65
F2038	6371000	340	-67
F2039	6371000	340	-73
F2040	6371000	339	-80
F2041	6371000	350	-75
F2042	6371000	354	-72
F2043	6371000	350	-67
F2044	6371000	0	-63
F2045	6371000	0	-70
F2046	6371000	8	-73
F2047	6371000	10	-70
F2048	6371000	10	-65
F2049	6371000	7	-62
F2050	6371000	20	-65
F2051	6371000	20	-70
F2052	6371000	20	-71 5
F2053	6371000	33	-70
F2054	6371000	30	-65
F2055	6371000	40	-65
F2056	6371000	40	-70
F2057	6371000	44	-70
F2058	6371000	55	-70
F2059	6371000	52	-66
F2060	6371000	60	-65
F2061	6371000	62	-70
F2062	6371000	70	-70
F2063	6371000	70	-65
F2064	6371000	80	-65
F2065	6371000	80	-70
F2066	6371000	90	-70
F2067	6371000	90	-65
F2068	6371000	346	-68
F2069	6371000	95	-70
F2070	6371000	135	-61 6
F2071	6371000	100	-75
F2072	6371000	110	-75
F2073	6371000	120	-75
F2074	6371000	130	-75
F2075	6371000	140	-75
F2076	6371000	150	-75
F2077	6371000	160	-75
F2078	6371000	170	-75
F2079	6371000	180	-75
F2080	6371000	190	-75
F2081	6371000	200	-80
F2082	6371000	210	-80
F2083	6371000	230	-80
F2084	6371000	250	-80
F2085	6371000	270	-80
F2086	6371000	290	-80
F2087	6371000	220	-75
F2088	6371000	0	-80
F2089	6371000	20	-80
F2090	6371000	10	-75
F2091	6371000	20	-75
F2092	6371000	30	-75
F2093	6371000	50	-75
F2094	6371000	40	-80
F2095	6371000	60	-80
F2096	6371000	55	-75
F2097	6371000	60	-75
F2098	6371000	70	-75
F2099	6371000	80	-75
F2100	6371000	80	-80
F2101	6371000	90	-75
F2102	6371000	100	-80
F2103	6371000	120	-80
F2104	6371000	140	-80
F2105	6371000	155	-80
F2106	6371000	155	-82
F2107	6371000	180	-85
F2108	6371000	180	-80
F2109	6371000	200	-83
F2110	6371000	220	-85
F2111	6371000	260	-85
F2112	6371000	300	-85
F2113	6371000	320	-85
F2114	6371000	340	-85
F2115	6371000	20	-85
F2116	6371000	60	-85
F2117	6371000	100	-85
F2118	6371000	140	-85
F2119	6371000	180	-87 5
F2120	6371000	270	-87 5
F2121	6371000	0	-87 5
F2122	6371000	90	-87 5

Appendix III

Discretized Elements with Crustal Thickness and Ice Load (Presented in thickness (m)).

1) There are 15 groups and the elements are independently numbered in each group.

2) The elements include triangles (3 nodes) and quadrilaterals (4 nodes). In the triangle element entries the digits from the fifth columns should be moved forward to refer to their meanings. Abbreviations in the table are explained below:

Nod#/crust, node number or crustal thickness in this column;

matrl/grad, the elastic properties in material mechanical classification;

crust/thics, crustal thickness;

ice/thics, mean ice sheet thickness in the element.

3) The crustal thicknesses were converted to lithospheric thicknesses during calculation, as exemplified in the following.

e.g.,

2.5 km → 20 km
5.0 km → 35 km
20 km → 70 km
35 km → 105 km.

15(groups)	0	0	1 00				
6	43	1	3 00	0			
1	0	2 94E+04	0 00		0	0	
1 21E+11	0 258			1			
0	0	0	0.00	0			
0	0	0	0 00	0			
elem.#	node #	node #	node #	ncd#/crst	matrl/grad	crst/thics.	ice/thics.
0	0	0	0 00	2.50E+03			
1	1	2	3.00	5.00E+03			
2	1	3	4.00	2.00E+04			
3	1	4	5.00	2.00E+04			
4	1	5	6.00	2.00E+04			
5	1	6	7.00	5.00E+03			
6	1	7	8.00	2.00E+04			
7	1	8	9.00	2.00E+04			
8	1	9	10 00	12			
9	1	10	11.00	5.00E+03	2 00E+04		
10	1	12	2 00	14			
11	3	2	13.00	15	1	0	2 50E+03
12	4	3	14.00	16	1	0	5 00E+03
13	5	4	15 00	17	1	2.00E+04	
14	6	5	16.00	18	1	2.00E+04	
15	7	6	17.00	19	1	2.00E+04	
16	7	18	29.00	20	1	2.00E+04	
17	8	7	19.00	21	1	5 00E+03	
18	9	8	20 00	1	1	2 00E+04	
19	10	9	21 00	22	2 00E+04	1 00E+03	
20	11	10	21.00	23	1	3 50E+04	2.50E+03
21	12	11	22 00	13	1	2 00E+04	
22	2	12	23 00	25	1	5 00E+03	
23	14	13	24 00	26	1	2.50E+03	
24	15	14	25 00	27	1	5.00E+03	
25	16	15	26 00	1	1	2 00E+04	2 50E+03
26	17	16	27 00	1	2.00E+04	2 50E+03	
27	17	27	28 00	29	3 50E+04	2 80E+03	
28	18	17	28 00	31	1	3.50E+04	2 00E+03
29	19	29	30.00	33	1	2 00E+04	
30	32	19	31 00	35	1	2 00E+04	

31	32	33	34 00	37	1	2.00E+04	
32	36	32	35.00	39	1	2 00E+04	
33	38	36	37 00	41	1	2 00E+04	
34	40	38	39.00	36	1	2 00E+04	
35	20	19	32 00	40	1	5 00E+03	
36	20	36	38 00	43	1	5.00E+03	
37	20	40	42 00	44	1	2 00E+04	2 00E+03
38	21	20	43.00	1	1	2 00E+04	1 50E+03
39	44	43	97.00	46	2.00E+04		
40	22	21	44.00	1	1	3 50E+04	3.00E+03
41	44	45	46.00	47	3.50E+04	2.00E+03	
42	23	22	46.00	24	1	2.00E+04	
43	13	23	47.00		1	5.00E+03	
6	162	1	3.00	0			
1	0	2 94E+04	0.00		0	0	
1 21E+11	0.258			1			
0	0	0	0.00	0			
0	0	0	0.00	0			
0	0	0	0.00	0			
0	0	0	0.00	1			
1	47	46	48.00	1	2.00E+04		
2	48	46	49.00	50	2.00E+04		
3	49	46	45.00	1	1	2.00E+04	
4	50	45	51.00	55	2.00E+04		
5	54	50	51.00	54	1	5.00E+03	
6	53	49	50 00	53	1	5 00E+03	
7	52	48	49.00	1	1	5 00E+03	
8	47	48	52.00	60	5.00E+03		
9	24	47	52 00	61	1	5.00E+03	
10	25	24	60.00	56	1	2 50E+03	
11	61	60	52 00	57	1	2.50E+03	
12	56	52	53.00	58	1	2 50E+03	
13	57	53	54.00	59	1	2.50E+03	
14	58	54	55.00	62	1	2 50E+03	
15	26	25	61.00	63	1	5 00E+03	
16	62	61	56.00	64	1	5 00E+03	
17	63	56	57.00	65	1	5 00E+03	
18	64	57	58 00	66	1	5 00E+03	
19	65	58	59 00	1	1	5.00E+03	
20	27	26	69 00	75	2 00E+04	2 50E+03	
21	27	69	73.00	1	1	2 00E+04	2 00E+03

22	69	26	62.00	67	2.00E+04		
23	62	63	64.00	70	1	2.00E+04	
24	69	62	67.00	68	1	2.00E+04	1.00E+03
25	67	64	65.00	71	1	2.00E+04	
26	70	67	68.00	1	1	2.00E+04	1.50E+03
27	68	65	66.00	72	2.00E+04		
28	73	69	70.00	1	1	3.50E+04	2.50E+03
29	73	72	74.00	76	3.50E+04	2.20E+03	
30	75	73	74.00	1	1	3.50E+04	2.00E+03
31	28	27	77.00	78	3.50E+04	2.50E+03	
32	77	27	75.00	79	1	3.50E+04	2.00E+03
33	78	75	76.00	81	1	3.50E+04	2.50E+03
34	29	28	77.00	80	1	3.50E+04	1.60E+03
35	77	78	79.00	82	1	3.50E+04	1.00E+03
36	81	77	80.00	1	1	3.50E+04	1.50E+03
37	29	81	84.00	1	3.50E+04		
38	81	82	83.00	85	3.50E+04		
39	84	81	83.00	1	1	3.50E+04	
40	29	84	30.00	86	3.50E+04		
41	30	84	85.00	87	1	3.50E+04	
42	33	30	86.00	1	1	3.50E+04	
43	31	30	33.00	1	3.50E+04		
44	33	87	34.00	1	2.00E+04		
45	34	87	88.00	89	2.00E+04		
46	37	35	34.00	1	1	3.50E+04	
47	34	88	89.00	90	3.50E+04		
48	39	37	89.00	91	1	3.50E+04	
49	41	39	90.00	42	1	3.50E+04	1.00E+03
50	40	41	92.00	93	1	2.00E+04	5.00E+02
51	92	41	91.00	94	1	3.50E+04	2.50E+03
52	42	92	93.00	1	1	3.50E+04	3.50E+03
53	42	94	95.00	96	3.50E+04	4.00E+03	
54	43	42	95.00	98	1	3.50E+04	4.00E+03
55	97	43	96.00	1	1	3.50E+04	3.70E+03
56	97	98	101.00	99	3.50E+04	4.00E+03	
57	45	44	97.00	1	1	2.00E+04	5.00E+02
58	97	101	99.00	51	3.50E+04	2.00E+03	
59	45	99	100.00	1	1	2.00E+04	
60	51	100	174.00	1	2.00E+04	1.50E+03	
61	100	175	174.00	102	3.50E+04	2.00E+03	
62	100	99	101.00	175	1	3.50E+04	2.00E+03

63	100	102	176.00	102	1	3.50E+04	2.50E+03
64	101	98	103.00	176	1	3.50E+04	4.00E+03
65	102	103	177.00	103	1	3.50E+04	4.00E+03
66	98	96	104.00	176	1	3.50E+04	4.60E+03
67	103	104	178.00	104	1	3.50E+04	4.10E+03
68	96	95	105.00	178	1	3.50E+04	4.50E+03
69	104	105	179.00	105	1	3.50E+04	4.00E+03
70	95	94	106.00	179	1	3.50E+04	4.20E+03
71	105	106	180.00	106	1	3.50E+04	3.20E+03
72	94	93	107.00	180	1	3.50E+04	3.50E+03
73	106	107	181.00	107	1	3.50E+04	3.00E+03
74	93	91	110.00	1	1	3.50E+04	2.50E+03
75	107	110	109.00	181	3.50E+04	2.50E+03	
76	107	109	108.00	1	1	3.50E+04	2.50E+03
77	181	108	182.00	1	3.50E+04	2.50E+03	
78	108	183	182.00	183	5.00E+03		
79	108	109	184.00	1	1	2.50E+03	
80	91	90	110.00	1	3.50E+04		
81	90	111	110.00	109	2.00E+04		
82	110	111	185.00	184	1	5.00E+03	
83	109	185	186.00	111	1	5.00E+03	
84	90	89	112.00	185	1	2.00E+04	
85	111	112	187.00	186	1	5.00E+03	
86	185	187	188.00	1	1	5.00E+03	
87	89	88	113.00	1	3.50E+04		
88	89	113	112.00	187	2.00E+04		
89	11[illegible]	113	189.00	188	1	5.00E+03	
90	107	189	190.00	88	1	5.00E+03	
91	34	87	115.00	113	1	2.00E+04	
92	88	115	114.00	189	1	2.00E+04	
93	113	114	191.00	190	1	5.00E+03	
94	189	191	192.00	1	1	5.00E+03	
95	87	86	117.00	1	3.50E+04		
[illegible]	87	117	115.00	116	2.00E+04		
97	115	117	118.00	1	1	2.00E+04	
98	114	115	116.00	191	2.00E+04		
99	114	116	193.00	1	1	5.00E+03	
100	191	193	192.00	1	5.00E+03		
101	116	118	193.00	117	5.00E+03		
102	86	122	119.00	118	1	3.50E+04	
103	117	119	120.00	1	1	2.00E+04	

104	118	120	121 00	122	2 00E+04		
105	86	85	123 00	1	1	3 50E+04	
106	122	123	124 00	125	3 50E+04		
107	119	122	124.00	1	1	2 00E+04	
108	119	125	120.00	121	2 00E+04		
109	120	125	126.00	1	1	2 00E+04	
110	125	194	126.00	1	2 00E+04		
111	125	124	194.00	123	3 50E+04		
112	85	83	129.00	124	1	3 50E+04	
113	123	129	128.00	194	1	3.50E+04	
114	124	128	127.00	1	1	3.50E+04	
115	83	130	129.00	128	3.50E+04		
116	129	130	131.00	127	1	3 50E+04	
117	128	131	132.00	130	1	3.50E+04	
118	83	82	135.00	131	1	3 50E+04	
119	130	135	134 00	132	1	3 50E+04	
120	131	134	133 00	1	1	3 50E+04	
121	82	136	135.00	134	3.50E+04		
122	135	136	137 00	133	1	3.50E+04	
123	134	137	138.00	136	1	3 50E+04	
124	82	80	195.00	137	1	3.50E+04	
125	136	195	196.00	138	1	3 50E+04	
126	137	196	139 00	195	1	3 50E+04	
127	80	79	142.00	196	1	3.50E+04	
128	195	142	141.00	139	1	3.50E+04	
129	196	141	140.00	1	1	3.50E+04	
130	79	143	142.00	141	3.50E+04		
131	142	143	144.00	140	1	3 50E+04	
132	141	144	145 00	143	1	3 50E+04	
133	79	76	148 00	144	1	3 50E+04	
134	143	148	147.00	145	1	3 50E+04	
135	144	147	146.00	148	1	3 50E+04	
136	76	74	149 00	147	1	3 50E+04	
137	148	149	150 00	146	1	3 50E+04	
138	147	150	151.00	1	1	3 50E+04	
139	74	152	149 00	150	3 50E+04		
140	149	152	153 00	151	1	3 50E+04	
141	150	153	154.00	152	1	3 50E+04	
142	74	72	157 00	153	1	3 50E+04	2 50E+03
143	152	157	156.00	154	1	3 50E+04	2 00E+03
144	153	156	155 00	1	1	3 50E+04	

145	72	158	157 00	156	3.50E+04	3.00E+03	
146	157	158	159.00	155	1	3 50E+04	2.50E+03
147	156	159	160 00	158	1	3 50E+04	
148	72	70	163 00	159	1	3 50E+04	3 50E+03
149	158	163	162.00	160	1	3 50E+04	2.50E+03
150	159	162	161 00	1	1	3.50E+04	2.00E+03
151	70	71	163.00	162	3.50E+04	1.50E+03	
152	163	71	164 00	161	1	3 50E+04	1 50E+03
153	162	164	165 00	164	1	3 50E+04	5.00E+02
154	71	68	166.00	165	1	2.00E+04	1.80E+03
155	164	166	167 00	166	1	2.00E+04	5.00E+02
156	68	168	167.00	168	1	2.00E+04	1.30E+03
157	68	65	66 00	168	1	2.00E+04	
158	66	169	167 00	169	1	2.00E+04	
159	66	59	170.00	170	1	5.00E+03	
160	59	55	171.00	171	1	2.50E+03	
161	55	51	172.00	1	1	5.00E+03	
162	172	51	173 00		5.00E+03		
6	146	1	3 00	0			
1	0	2.94E+04	0.00		0	0	
1 21E+11	0 258			1			
0	0	0	0.00	0			
0	0	0	0 00	0			
0	0	0	0 00	0			
0	0	0	0 00	199			
1	138	139	197 00	200	1	3.50E+04	
2	199	197	198 00	1	1	3.50E+04	
3	138	199	202.00	201	3 50E+04		
4	202	199	200.00	203	1	3 50E+04	
5	133	138	202.00	204	1	3.50E+04	
6	203	202	201.00	1	1	3.50E+04	
7	133	203	206.00	205	3 50E+04		
8	206	203	204.00	207	1	3 50E+04	
9	132	133	206 00	208	1	3.50E+04	
10	207	206	205 00	209	1	3 50E+04	
11	127	132	207.00	210	1	3 50E+04	
12	209	207	208 00	212	1	3 50E+04	
13	194	127	209.00	1	1	3 50E+04	
14	209	210	212 00	1	3.50E+04		
15	212	210	211 00	1	2.00E+04		
16	212	211	213 00	213	2 00E+04		

17	126	194	212.00	214	1	2.00E+04	
18	215	126	213.00	1	1	5.00E+03	
19	215	214	216.00	218	5.00E+03		
20	121	126	215.00	217	1	5.00E+03	
21	218	215	216.00	1	1	5.00E+03	
22	121	218	219.00	220	5.00E+03		
23	219	218	217.00	1	1	5.00E+03	
24	121	219	222.00	221	5.00E+03		
25	222	219	220.00	223	1	5.00E+03	
26	118	121	222.00	224	1	5.00E+03	
27	223	222	221.00	1	1	5.00E+03	
28	118	223	226.00	225	5.00E+03		
29	226	223	224.00	227	1	5.00E+03	
30	193	118	226.00	228	1	5.00E+03	
31	227	226	225.00	1	1	5.00E+03	
32	193	227	230.00	229	5.00E+03		
33	230	227	228.00	231	1	5.00E+03	
34	192	193	230.00	232	1	5.00E+03	
35	231	230	229.00	1	1	5.00E+03	
36	192	231	234.00	233	5.00E+03		
37	234	231	232.00	235	1	5.00E+03	
38	190	192	234.00	236	1	5.00E+03	
39	235	234	233.00	1	1	5.00E+03	
40	190	235	237.00	238	5.00E+03		
41	237	235	236.00	240	1	5.00E+03	
42	188	190	237.00	239	1	5.00E+03	
43	240	237	238.00	1	1	5.00E+03	
44	188	240	241.00	242	5.00E+03		
45	241	240	239.00	243	1	5.00E+03	
46	186	188	241.00	244	1	5.00E+03	
47	243	241	242.00	1	1	5.00E+03	
48	186	243	246.00	245	5.00E+03		
49	246	243	244.00	247	1	5.00E+03	
50	184	186	246.00	248	1	5.00E+03	
51	247	246	245.00	249	1	5.00E+03	
52	250	247	248.00	251	1	5.00E+03	
53	183	184	247.00	252	1	2.50E+03	
54	251	247	250.00	253	1	2.50E+03	
55	252	250	249.00	1	1	2.50E+03	
56	182	183	251.00	255	5.00E+03		
57	182	251	252.00	257	1	5.00E+03	

58	255	252	253.00	256	1	5.00E+03	
59	181	182	255.00	1	1	3.50E+04	1.50E+03
60	256	255	257.00	1	3.50E+04		
61	181	256	259.00	258	3.50E+04	5.00E+02	
62	259	256	257.00	260	1	3.50E+04	
63	180	181	259.00	261	1	3.50E+04	5.00E+02
64	260	259	258.00	1	1	3.50E+04	
65	180	260	263.00	262	3.50E+04	5.00E+02	
66	263	260	261.00	264	1	3.50E+04	
67	179	180	263.00	265	1	3.50E+04	5.00E+02
68	264	263	262.00	1	1	3.50E+04	
69	179	264	267.00	266	3.50E+04	3.00E+03	
70	267	264	265.00	268	1	3.50E+04	5.00E+02
71	178	179	267.00	269	1	3.50E+04	3.00E+03
72	268	267	266.00	1	1	3.50E+04	5.00E+02
73	178	268	270.00	271	3.50E+04	3.50E+03	
74	270	268	269.00	273	1	3.50E+04	2.50E+03
75	177	178	270.00	272	1	3.50E+04	3.50E+03
76	273	270	271.00	1	1	3.50E+04	2.50E+03
77	177	273	274.00	275	3.50E+04	3.50E+03	
78	274	273	272.00	277	1	3.50E+04	2.00E+03
79	176	177	274.00	276	1	3.50E+04	3.50E+03
80	277	274	275.00	1	1	3.50E+04	2.00E+03
81	176	277	278.00	279	3.50E+04	3.00E+03	
82	278	277	276.00	1	1	3.50E+04	1.50E+03
83	279	276	280.00	282	2.00E+04		
84	175	176	278.00	1	1	3.50E+04	3.00E+03
85	282	278	279.00	281	3.50E+04	1.50E+03	
86	282	279	280.00	1	1	2.00E+04	
87	174	175	282.00	1	3.50E+04	1.50E+03	
88	174	282	283.00	284	2.00E+04		
89	283	282	281.00	173	1	2.00E+04	
90	51	174	283.00	1	1	2.00E+04	
91	173	283	284.00	1	2.00E+04		
92	173	284	285.00	1	5.00E+03		
93	173	285	286.00	287	5.00E+03		
94	172	173	286.00	[illegible]	1	5.00E+03	
95	171	172	288.00	289	5.00E+03		
96	288	172	287.00	290	1	5.00E+03	
97	171	288	289.00	291	1	5.00E+03	
98	170	171	290.00	1	1	2.50E+03	

99	169	170	293.00	293	5.00E+03		
100	170	291	292.00	1	1	5.00E+03	
101	293	292	294.00	296	5.00E+03		
102	167	169	293.00	295	1	2.00E+04	
103	296	293	294.00	1	1	2.00E+04	
104	167	296	297.00	298	2.00E+04		
105	297	296	295.00	299	1	2.00E+04	
106	165	167	297.00	1	1	2.00E+04	
107	299	297	298.00	1	2.00E+04		
108	165	299	301.00	300	3.50E+04		
109	301	299	298.00	303	1	3.50E+04	
110	161	165	301.00	302	1	3.50E+04	
111	303	301	300.00	1	1	3.50E+04	
112	161	303	304.00	305	3.50E+04		
113	304	303	302.00	307	1	2.00E+04	
114	160	161	304.00	1	1	3.50E+04	
115	307	304	306.00	1	3.50E+04		
116	304	305	306.00	308	2.00E+04		
117	155	160	307.00	309	1	3.50E+04	
118	308	307	306.00	1	1	3.50E+04	
119	155	308	311.00	310	3.50E+04		
120	311	308	309.00	1	1	3.50E+04	
121	155	311	312.00	313	3.50E+04		
122	312	311	310.00	315	1	3.50E+04	
123	154	155	312.00	314	1	3.50E+04	
124	315	312	313.00	1	1	3.50E+04	
125	154	315	316.00	317	3.50E+04		
126	316	315	314.00	319	1	3.50E+04	
127	151	154	316.00	318	1	3.50E+04	
128	319	316	317.00	1	1	3.50E+04	
129	151	319	320.00	321	3.50E+04		
130	320	319	318.00	323	1	3.50E+04	
131	146	151	320.00	322	1	3.50E+04	
132	323	320	321.00	1	1	3.50E+04	
133	146	323	324.00	325	3.50E+04		
134	324	323	322.00	327	1	3.50E+04	
135	145	146	324.00	326	1	3.50E+04	
136	327	324	325.00	1	1	3.50E+04	
137	145	327	328.00	329	3.50E+04		
138	328	327	326.00	331	1	3.50E+04	
139	140	145	328.00	330	1	3.50E+04	

140	331	328	329.00	1	1	3.50E+04	
141	140	331	332.00	333	3.50E+04		
142	332	331	330.00	335	1	3.50E+04	
143	139	140	332.00	334	1	3.50E+04	
144	335	332	333.00	1	1	3.50E+04	
145	139	335	197.00	198	3.50E+04		
146	197	335	334.00		1	3.50E+04	
6	163	1	3.00	0			
1	0	2.94E+04	0.00		0	0	
1.21E+11	0.258			1			
0	0	0	0.00	0			
0	0	0	0.00	0			
0	0	0	0.00	0			
0	0	0	0.00	338			
1	336	337	339.00	338	1	3.50E+04	
2	200	198	336.00	341	1	3.50E+04	
3	201	200	338.00	340	1	3.50E+04	
4	341	338	339.00	342	1	3.50E+04	
5	204	201	341.00	343	1	3.50E+04	
6	342	341	340.00	345	1	3.50E+04	
7	205	204	342.00	344	1	3.50E+04	
8	345	342	343.00	346	1	3.50E+04	
9	208	205	345.00	347	1	3.50E+04	
10	346	345	344.00	349	1	3.50E+04	
11	210	208	346.00	348	1	3.50E+04	
12	349	346	347.00	1	1	3.50E+04	
13	210	349	350.00	351	2.00E+04		
14	350	349	348.00	353	1	2.00E+04	
15	211	210	350.00	1	1	2.00E+04	
16	353	350	351.00	1	2.00E+04		
17	353	351	352.00	1	5.00E+03		
18	213	211	353.00	1	2.00E+04		
19	213	353	354.00	355	5.00E+03		
20	354	353	352.00	357	1	5.00E+03	
21	214	213	354.00	356	1	5.00E+03	
22	357	354	355.00	358	1	5.00E+03	
23	216	214	357.00	359	1	5.00E+03	
24	358	357	356.00	361	1	5.00E+03	
25	217	216	358.00	360	1	5.00E+03	
26	361	358	359.00	362	1	5.00E+03	
27	220	217	361.00	363	1	5.00E+03	

	28	362	361	360.00	365	1	5.00E+03	
	29	221	220	362.00	364	1	5.00E+03	
	30	365	362	363.00	366	1	5.00E+03	
	31	224	221	365.00	367	1	5.00E+03	
	32	366	365	364.00	369	1	5.00E+03	
	33	225	224	366.00	368	1	5.00E+03	
	34	369	366	367.00	370	1	5.00E+03	
	35	228	225	369.00	371	1	5.00E+03	
	36	370	369	368.00	373	1	5.00E+03	
	37	229	228	370.00	372	1	5.00E+03	
	38	373	370	371.00	374	1	5.00E+03	
	39	232	229	373.00	375	1	5.00E+03	
	40	374	373	372.00	377	1	5.00E+03	
	41	233	232	374.00	376	1	5.00E+03	
	42	377	374	375.00	378	1	5.00E+03	
	43	236	233	377.00	379	1	5.00E+03	
	44	378	377	376.00	381	1	5.00E+03	
	45	238	236	378.00	380	1	5.00E+03	
	46	381	378	379.00	382	1	5.00E+03	
	47	239	238	381.00	383	1	5.00E+03	
	48	382	381	380.00	385	1	5.00E+03	
	49	242	239	382.00	384	1	5.00E+03	
	50	385	382	383.00	386	1	5.00E+03	
	51	244	242	385.00	387	1	5.00E+03	
	52	386	385	384.00	389	1	5.00E+03	
	53	245	244	386.00	388	1	5.00E+03	
	54	389	386	387.00	390	1	5.00E+03	
	55	248	245	389.00	391	1	5.00E+03	
	56	390	389	388.00	392	1	5.00E+03	
	57	249	248	390.00	393	1	5.00E+03	
	58	392	390	391.00	1	1	5.00E+03	
	59	253	249	392.00	254	5.00E+03		
	60	257	253	392.00	394	1	5.00E+03	
	61	254	392	393.00	396	1	5.00E+03	
	62	258	257	254.00	1	1	3.50E+04	
	63	396	254	395.00	1	3.50E+04		
	64	254	394	395.00	397	5.00E+03		
	65	261	258	396.00	398	1	3.50E+04	
	66	397	396	395.00	400	1	3.50E+04	
	67	262	261	397.00	399	1	3.50E+04	
	68	400	397	398.00	401	1	3.50E+04	

	69	265	262	400.00	402	1	3.50E+04	
	70	401	400	399.00	404	1	3.50E+04	
	71	266	265	401.00	403	1	3.50E+04	
	72	404	401	402.00	405	1	3.50E+04	
	73	269	266	404.00	406	1	3.50E+04	
	74	405	404	403.00	408	1	3.50E+04	
	75	271	269	405.00	407	1	3.50E+04	
	76	408	405	406.00	1	1	3.50E+04	
	77	407	406	409.00	411	2.00E+04		
	78	272	271	408.00	1	1	3.50E+04	
	79	411	408	407.00	410	3.50E+04		
	80	411	407	409.00	412	1	2.00E+04	
	81	275	272	411.00	413	1	3.50E+04	
	82	412	411	410.00	1	1	2.00E+04	
	83	276	275	412.00	1	3.50E+04		
	84	412	413	415.00	1	2.00E+04		
	85	415	413	414.00	416	5.00E+03		
	86	276	412	415.00	417	1	2.00E+04	
	87	416	415	414.00	1	1	5.00E+03	
	88	280	276	416.00	419	2.00E+04		
	89	281	280	416.00	418	1	2.00E+04	
	90	419	416	417.00	1	1	5.00E+03	
	91	284	281	419.00	1	2.00E+04		
	92	284	419	420.00	421	5.00E+03		
	93	420	419	418.00	423	1	5.00E+03	
	94	285	284	420.00	422	1	5.00E+03	
	95	423	420	421.00	424	1	5.00E+03	
	96	286	285	423.00	425	1	5.00E+03	
	97	424	423	422.00	429	1	5.00E+03	
	98	287	286	424.00	1	1	5.00E+03	
	99	429	424	425.00	426	5.00E+03		
	100	427	429	425.00	430	1	2.50E+03	
	101	289	287	429.00	431	1	5.00E+03	
	102	430	429	427.00	432	1	2.50E+03	
	103	431	427	428.00	1	1	5.00E+03	
	104	290	289	430.00	431	5.00E+03		
	105	291	290	430.00	1	1	2.50E+03	
	106	291	431	432.00	1	5.00E+03		
	107	432	428	433.00	435	5.00E+03		
	108	292	291	432.00	434	1	5.00E+03	
	109	435	432	433.00	436	1	5.00E+03	

110	294	292	435.00	437	1	5.00E+03	
111	436	435	434.00	1	1	5.00E+03	
112	437	434	438.00	440	2.00E+04		
113	295	294	436.00	1	1	2.00E+04	
114	440	436	437.00	439	2.00E+04		
115	440	437	438.00	441	1	2.00E+04	
116	298	295	440.00	442	1	2.00E+04	
117	441	440	439.00	1	1	2.00E+04	
118	442	439	443.00	446	3.50E+04		
119	300	298	441.00	1	1	3.50E+04	
120	302	300	446.00	445	3.50E+04		
121	446	441	442.00	444	1	2.00E+04	
122	445	442	443.00	1	1	3.50E+04	
123	305	302	447.00	447	2.00E+04		
124	302	446	445.00	448	1	2.00E+04	
125	447	445	444.00	1	1	3.50E+04	
126	305	447	450.00	1	2.00E+04		
127	450	447	449.00	1	2.00E+04		
128	449	447	448.00	451	3.50E+04		
129	306	305	450.00	452	1	2.00E+04	
130	451	450	453.00	1	1	2.00E+04	
131	450	449	453.00	1	2.00E+04		
132	309	306	451.00	455	3.50E+04		
133	309	451	452.00	454	1	3.50E+04	
134	455	452	453.00	1	1	2.00E+04	
135	310	309	455.00	456	3.50E+04		
136	313	310	455.00	457	1	3.50E+04	
137	456	455	454.00	458	1	2.00E+04	
138	457	454	460.00	462	1	5.00E+03	
139	314	313	456.00	461	1	3.50E+04	
140	462	456	457.00	1	1	2.00E+04	
141	317	314	462.00	1	3.50E+04		
142	461	459	465.00	463	3.50E+04		
143	318	317	462.00	1	1	3.50E+04	
144	463	462	464.00	465	3.50E+04		
145	464	462	461.00	467	1	2.00E+04	
146	321	318	463.00	466	1	3.50E+04	
147	467	463	464.00	468	1	3.50E+04	
148	322	321	467.00	469	1	3.50E+04	
149	468	467	466.00	471	1	3.50E+04	
150	325	322	468.00	470	1	3.50E+04	

151	471	468	469.00	472	1	3.50E+04	
152	326	325	471.00	473	1	3.50E+04	
153	472	471	470.00	475	1	3.50E+04	
154	329	326	472.00	474	1	3.50E+04	
155	475	472	473.00	476	1	3.50E+04	
156	330	329	475.00	477	1	3.50E+04	
157	476	475	474.00	479	1	3.50E+04	
158	333	330	476.00	478	1	3.50E+04	
159	479	476	477.00	480	1	3.50E+04	
160	334	333	479.00	481	1	3.50E+04	
161	480	479	478.00	336	1	3.50E+04	
162	198	334	480.00	337	1	3.50E+04	
163	336	480	481.00		1	3.50E+04	
6	170	1	3.00	0			
1	0	2.94E+04	0.00		0	0	
1.21E+11	0.258			1			
0	0	0	0.00	0			
0	0	0	0.00	0			
0	0	0	0.00	0			
0	0	0	0.00	484			
1	339	337	482.00	485	1	3.50E+04	
2	484	482	483.00	486	1	3.50E+04	
3	340	339	484.00	487	1	3.50E+04	
4	486	484	485.00	488	1	3.50E+04	
5	343	340	486.00	489	1	3.50E+04	
6	488	486	487.00	493	1	3.50E+04	
7	344	343	488.00	492	1	3.50E+04	
8	493	488	489.00	491	1	3.50E+04	
9	492	489	490.00	494	1	2.00E+04	
10	347	344	493.00	1	1	3.50E+04	
11	494	493	492.00	495	3.50E+04		
12	494	492	491.00	1	1	2.00E+04	
13	495	491	496.00	1	5.00E+03		
14	348	347	494.00	495	3.50E+04		
15	351	348	494.00	1	1	2.00E+04	
16	351	495	498.00	497	5.00E+03		
17	498	495	496.00	499	1	5.00E+03	
18	352	351	498.00	500	1	5.00E+03	
19	499	498	497.00	502	1	5.00E+03	
20	355	352	499.00	501	1	5.00E+03	
21	502	499	500.00	503	1	5.00E+03	

22	356	355	502.00	504	1	5.00E+03	
23	503	502	501.00	506	1	5.00E+03	
24	359	356	503.00	505	1	5.00E+03	
25	506	503	504.00	507	1	5.00E+03	
26	360	359	506.00	508	1	5.00E+03	
27	507	506	505.00	510	1	5.00E+03	
28	363	360	507.00	509	1	5.00E+03	
29	510	507	508.00	511	1	5.00E+03	
30	364	363	510.00	512	1	5.00E+03	
31	511	510	509.00	514	1	5.00E+03	
32	367	364	511.00	513	1	5.00E+03	
33	514	511	512.00	515	1	5.00E+03	
34	368	367	514.00	516	1	5.00E+03	
35	515	514	513.00	518	1	5.00E+03	
36	371	368	515.00	517	1	5.00E+03	
37	518	515	516.00	519	1	5.00E+03	
38	372	371	518.00	520	1	5.00E+03	
39	519	518	517.00	522	1	5.00E+03	
40	375	372	519.00	521	1	5.00E+03	
41	522	519	520.00	523	1	5.00E+03	
42	376	375	522.00	524	1	5.00E+03	
43	523	522	521.00	526	1	5.00E+03	
44	379	376	523.00	525	1	5.00E+03	
45	526	523	524.00	527	1	5.00E+03	
46	380	379	526.00	528	1	5.00E+03	
47	527	526	525.00	530	1	5.00E+03	
48	383	380	527.00	529	1	5.00E+03	
49	530	527	528.00	531	1	5.00E+03	
50	384	383	530.00	532	1	5.00E+03	
51	531	530	529.00	534	1	5.00E+03	
52	387	384	531.00	533	1	5.00E+03	
53	534	531	532.00	535	1	5.00E+03	
54	388	387	534.00	536	1	5.00E+03	
55	535	534	533.00	538	1	5.00E+03	
56	391	388	535.00	537	1	5.00E+03	
57	538	535	536.00	539	1	5.00E+03	
58	393	391	538.00	540	1	5.00E+03	
59	539	538	537.00	542	1	5.00E+03	
60	394	393	539.00	541	1	5.00E+03	
61	542	539	540.00	543	1	5.00E+03	
32	395	394	542.00	544	1	5.00E+03	

63	543	542	541.00	1	1	5.00E+03	
64	398	395	547.00	546	3.50E+04		
65	547	395	543.00	545	1	5.00E+03	
66	546	543	544.00	548	1	5.00E+03	
67	399	398	547.00	1	1	3.50E+04	
68	548	547	346.00	550	5.00E+03		
69	548	546	545.00	1	1	5.00E+03	
70	402	399	556.00	556	3.50E+04		
71	399	548	549.00	551	1	3.50E+04	
72	549	548	550.00	1	1	2.50E+03	
73	549	551	552.00	555	5.00E+03		
74	556	549	552.00	554	1	3.50E+04	
75	555	552	553.00	557	1	3.50E+04	
76	403	402	556.00	558	1	3.50E+04	
77	557	556	555.00	559	1	2.00E+04	
78	558	555	554.00	1	1	2.00E+04	
79	406	403	557.00	560	3.50E+04		
80	406	557	558.00	561	1	2.00E+04	
81	560	558	559.00	563	1	2.00E+04	
82	409	406	560.00	1	1	2.00E+04	
83	563	560	561.00	1	2.00E+04		
84	563	561	562.00	564	5.00E+03		
85	410	409	563.00	565	1	2.00E+04	
86	564	563	562.00	1	1	5.00E+03	
87	413	410	564.00	1	2.00E+04		
88	413	564	567.00	566	5.00E+03		
89	567	564	565.00	568	1	5.00E+03	
90	414	413	567.00	569	1	5.00E+03	
91	568	567	566.00	571	1	5.00E+03	
92	417	414	568.00	570	1	5.00E+03	
93	571	568	569.00	572	1	5.00E+03	
94	418	417	571.00	573	1	5.00E+03	
95	572	571	570.00	575	1	5.00E+03	
96	421	418	572.00	574	1	5.00E+03	
97	575	572	573.00	576	1	5.00E+03	
98	422	421	575.00	577	1	5.00E+03	
99	576	575	574.00	579	1	5.00E+03	
100	425	422	576.00	578	1	5.00E+03	
101	579	576	577.00	580	1	5.00E+03	
102	426	425	579.00	581	1	2.50E+03	
103	580	579	578.00	1	1	2.50E+03	

104	426	580	583.00	582	5.00E+03		
105	583	580	581.00	583	1	5.00E+03	
106	428	427	426.00	1	1	5.00E+03	
107	428	583	584.00	585	5.00E+03		
108	584	583	582.00	584	1	5.00E+03	
109	433	432	428.00	588	1	5.00E+03	
110	433	584	587.00	586	1	5.00E+03	
111	587	584	585.00	1	1	5.00E+03	
112	434	433	588.00	589	5.00E+03		
113	434	588	587.00	590	1	2.00E+04	
114	589	587	586.00	592	1	2.00E+04	
115	438	434	589.00	591	1	2.00E+04	
116	592	589	590.00	1	1	2.00E+04	
117	439	438	592.00	1	2.00E+04		
118	439	592	593.00	594	3.50E+04		
119	593	592	591.00	596	1	3.50E+04	
120	443	439	593.00	595	1	3.50E+04	
121	596	593	594.00	597	1	3.50E+04	
122	444	443	596.00	598	1	3.50E+04	
123	597	596	595.00	600	1	3.50E+04	
124	448	444	597.00	599	1	3.50E+04	
125	600	597	598.00	601	1	3.50E+04	
126	449	448	600.00	602	1	3.50E+04	
127	601	600	599.00	1	1	3.50E+04	
128	449	601	604.00	603	3.50E+04		
129	604	601	602.00	605	1	3.50E+04	
130	453	449	604.00	606	1	3.50E+04	
131	605	604	603.00	608	1	3.50E+04	
132	454	453	605.00	607	1	3.50E+04	
133	608	605	606.00	1	1	3.50E+04	
134	454	608	609.00	610	3.50E+04		
135	609	608	607.00	1	1	3.50E+04	
136	609	610	611.00	613	3.50E+04		
137	460	454	609.00	612	1	5.00E+03	
138	613	609	611.00	614	1	5.00E+03	
139	458	460	613.00	617	1	2.50E+03	
140	614	613	612.00	615	1	2.50E+03	
141	457	458	614.00	618	1	5.00E+03	
142	615	614	617.00	459	1	5.00E+03	
143	461	457	615.00	1	1	3.50E+04	
144	459	615	616.00	1	3.50E+04		

145	616	615	618.00	620	3.50E+04		
146	465	459	616.00	619	1	3.50E+04	
147	620	616	618.00	1	1	3.50E+04	
148	465	620	621.00	622	3.50E+04		
149	621	620	619.00	1	1	3.50E+04	
150	621	622	623.00	621	3.50E+04		
151	466	464	465.00	624	1	2.00E+04	
152	466	621	623.00	1	1	2.00E+04	
153	469	466	624.00	625	3.50E+04		
154	470	469	624.00	626	1	3.50E+04	
155	625	624	623.00	628	1	2.00E+04	
156	473	470	625.00	627	1	3.50E+04	
157	628	625	626.00	629	1	2.00E+04	
158	474	473	628.00	1	1	3.50E+04	
159	629	628	627.00	630	3.50E+04		
160	477	474	629.00	631	1	3.50E+04	
161	630	629	627.00	632	1	3.50E+04	
162	478	477	630.00	633	1	3.50E+04	
163	632	630	631.00	636	1	3.50E+04	
164	481	478	632.00	1	1	3.50E+04	
165	636	632	634.00	1	3.50E+04		
166	632	633	634.00	1	3.50E+04		
167	636	634	635.00	1	3.50E+04		
168	634	633	635.00	482	2.00E+04		
169	337	481	636.00	483	1	3.50E+04	
170	482	636	635.00		1	3.50E+04	
6	180	1	3.00	0			
1	0	2.94E+04	0.00		0	0	
1.21E+1?	0.258			1			
0	0	0	0.00	0			
0	0	0	0.00	0			
0	0	0	0.00	0			
0	0	0	0.00	640			
1	485	483	637.00	641	1	3.50E+04	
2	640	637	639.00	1	1	3.50E+04	
3	637	638	639.00	642	2.00E+04		
4	487	485	640.00	643	1	3.50E+04	
5	642	640	641.00	1	1	3.50E+04	
6	643	641	644.00	643	2.00E+04		
7	489	487	641.00	1	1	3.50E+04	
8	490	489	643.00	645	2.00E+04		

9	490	643	644.00	1	1	2.00E+04	
10	491	490	646.00	647	5.00E+03		
11	646	490	645.00	649	1	5.00E+03	
12	496	491	646.00	648	1	5.00E+03	
13	649	646	647.00	650	1	5.00E+03	
14	497	496	649.00	65'	1	5.00E+03	
15	650	649	648.00	653	1	5.00E+03	
16	500	497	650.00	652	1	5.00E+03	
17	653	650	651.00	654	1	5.00E+03	
18	501	500	653.00	655	1	5.00E+03	
19	654	653	652.00	657	1	5.00E+03	
20	504	501	654.00	656	1	5.00E+03	
21	657	654	655.00	658	1	5.00E+03	
22	505	504	657.00	659	1	5.00E+03	
23	658	657	656.00	561	1	5.00E+03	
24	508	505	658.00	660	1	5.00E+03	
25	661	658	659.00	662	1	5.00E+03	
26	509	508	661.00	663	1	5.00E+03	
27	662	661	660.00	665	1	5.00E+03	
28	512	509	662.00	664	1	5.00E+03	
29	665	662	663.00	666	1	5.00E+03	
30	513	512	665.00	667	1	5.00E+03	
31	666	665	664.00	669	1	5.00E+03	
32	516	513	666.00	668	1	5.00E+03	
33	669	666	667.00	670	1	5.00E+03	
34	517	516	669.00	671	1	5.00E+03	
35	670	669	668.00	673	1	5.00E+03	
36	520	517	670.00	672	1	5.00E+03	
37	673	670	671.00	674	1	5.00E+03	
38	521	520	673.00	675	1	5.00E+03	
39	674	673	672.00	677	1	5.00E+03	
40	524	521	674.00	676	1	5.00E+03	
41	677	674	675.00	678	1	5.00E+03	
42	525	524	677.00	679	1	5.00E+03	
43	678	677	676.00	681	1	5.00E+03	
44	528	525	678.00	680	1	5.00E+03	
45	681	678	679.00	682	1	5.00E+03	
46	529	528	681.00	683	1	5.00E+03	
47	682	681	680.00	685	1	5.00E+03	
48	532	529	682.00	684	1	5.00E+03	
49	685	682	683.00	686	1	5.00E+03	
50	533	532	685.00	687	1	5.00E+03	
51	686	685	684.00	689	1	5.00E+03	
52	536	533	686.00	688	1	5.00E+03	
53	689	686	687.00	690	1	5.00E+03	
54	537	536	689.00	691	1	5.00E+03	
55	690	689	688.00	693	1	5.00E+03	
56	540	537	690.00	692	1	5.00E+03	
57	693	690	691.00	694	1	5.00E+03	
58	541	540	693.00	695	1	5.00E+03	
59	694	693	692.00	697	1	5.00E+03	
60	544	541	694.00	696	1	5.00E+03	
61	697	694	695.00	698	1	5.00E+03	
62	545	544	697.00	699	1	5.00E+03	
63	698	697	696.00	701	1	5.00E+03	
64	550	545	698.00	700	1	5.00E+03	
65	701	698	699.00	702	1	5.00E+03	
66	551	550	701.00	703	1	2.50E+03	
67	702	701	700.00	702	1	2.50E+03	
68	553	552	551.00	1	1	5.00E+03	
69	553	702	705.00	704	5.00E+03		
70	705	702	703.00	1	1	5.00E+03	
71	553	705	706.00	707	5.00E+03		
72	706	705	704.00	1	1	5.00E+03	
73	559	554	710.00	706	2.00E+04		
74	710	554	553.00	1	1	3.50E+04	
75	710	706	709.00	708	3.50E+04		
76	709	706	707.00	711	1	5.00E+03	
77	562	559	710.00	712	1	2.00E+04	
78	711	710	709.00	1	1	3.50E+04	
79	712	709	708.00	714	5.00E+03		
80	565	562	711.00	713	1	2.00E+04	
81	714	711	712.00	715	1	3.50E+04	
82	566	565	714.00	1	1	2.00E+04	
83	715	714	713.00	1	3.50E+04		
84	569	566	717.00	716	5.00E+03		
85	717	566	715.00	718	1	2.00E+04	
86	570	569	717.00	1	1	5.00E+03	
87	718	717	716.00	719	2.00E+04		
88	573	570	718.00	720	1	5.00E+03	
89	719	718	716.00	1	1	2.00E+04	
90	719	720	721.00	723	2.00E+04		

91	574	573	719.00	1	1	5.00E+03	
92	723	719	722.00	1	5.00E+03		
93	722	719	721.00	724	2.00E+04		
94	577	574	723.00	725	1	5.00E+03	
95	724	723	722.00	727	1	5.00E+03	
96	578	577	724.00	726	1	5.00E+03	
97	727	724	725.00	1	1	5.00E+03	
98	727	726	731.00	1	5.00E+03		
99	731	726	732.00	728	5.00E+03		
100	581	578	727.00	730	1	2.50E+03	
101	728	727	731.00	733	1	2.50E+03	
102	730	731	732.00	729	1	2.50E+03	
103	582	581	728.00	1	1	5.00E+03	
104	729	728	730.00	734	5.00E+03		
105	585	582	729.00	733	1	5.00E+03	
106	734	729	730.00	735	1	5.00E+03	
107	586	585	734.00	736	1	5.00E+03	
108	735	734	733.00	1	1	5.00E+03	
109	586	735	738.00	737	5.00E+03		
110	738	735	736.00	739	1	5.00E+03	
111	590	586	738.00	740	1	2.00E+04	
112	739	738	737.00	742	1	2.00E+04	
113	591	590	739.00	741	1	2.00E+04	
114	742	739	740.00	1	1	2.00E+04	
115	591	742	743.00	744	3.50E+04		
116	743	742	741.00	746	1	3.50E+04	
117	594	591	743.00	745	1	3.50E+04	
118	746	743	744.00	747	1	3.50E+04	
119	595	594	746.00	748	1	3.50E+04	
120	747	746	745.00	750	1	3.50E+04	
121	598	595	747.00	749	1	3.50E+04	
122	750	747	748.00	751	1	3.50E+04	
123	599	598	750.00	752	1	3.50E+04	
124	751	750	749.00	754	1	3.50E+04	
125	602	599	751.00	753	1	3.50E+04	
126	754	751	752.00	755	1	3.50E+04	
127	603	602	754.00	756	1	3.50E+04	
128	755	754	753.00	758	1	3.50E+04	
129	606	603	755.00	757	1	3.50E+04	
130	758	755	756.00	759	1	3.50E+04	
131	607	606	758.00	760	1	3.50E+04	

132	759	758	757.00	762	1	3.50E+04	
133	610	607	759.00	761	1	3.50E+04	
134	762	759	760.00	763	1	3.50E+04	
135	611	610	762.00	764	1	3.50E+04	
136	763	762	761.00	1	1	3.50E+04	
137	611	763	772.00	765	3.50E+04		
138	772	763	764.00	771	1	3.50E+04	
139	612	611	772.00	766	1	5.00E+03	
140	771	772	765.00	770	1	5.00E+03	
141	617	612	771.00	767	1	2.50E+03	
142	770	771	766.00	769	1	2.50E+03	
143	618	617	770.00	768	1	5.00E+03	
144	769	770	767.00	773	1	5.00E+03	
145	619	618	769.00	774	1	3.50E+04	
146	773	769	768.00	775	1	3.50E+04	
147	774	768	767.00	776	1	5.00E+03	
148	775	767	766.00	777	1	2.50E+03	
149	776	766	765.00	1	1	5.00E+03	
150	777	765	778.00	774	2.00E+04		
151	622	619	773.00	783	1	3.50E+04	
152	623	622	774.00	782	1	3.50E+04	
153	783	774	775.00	781	1	5.00E+03	
154	782	775	776.00	780	1	2.50E+03	
155	781	776	777.00	779	1	5.00E+03	
156	780	777	778.00	786	1	2.00E+04	
157	783	782	785.00	785	1	5.00E+03	
158	782	781	784.00	1	1	2.50E+03	
159	781	780	784.00	1	5.00E+03		
160	780	779	784.00	1	5.00E+03		
161	786	785	789.00	1	5.00E+03		
162	626	623	783.00	787	2.00E+04		
163	626	783	786.00	1	1	2.00E+04	
164	787	786	789.00	788	2.00E+04		
165	627	626	787.00	790	1	2.00E+04	
166	788	787	789.00	1	1	2.00E+04	
167	627	788	792 [illegible]	791	2.00E+04		
168	792	788	790.00	1	1	2.00E+04	
169	792	791	794.00	793	2.00E+04		
170	631	627	792.00	1	1	3.50E+04	
171	793	792	794.00	795	3.50E+04		
172	633	631	793.00	1	1	3.50E+04	

173	795	793	794.00	796	3.50E+04		
174	635	633	795.00	1	1	2.00E+04	
175	796	795	797.00	799	2.00E+04		
176	797	795	794.00	1	1	2.00E+04	
177	635	796	637.00	798	2.00E+04		
178	637	796	797.00	1	1	2.00E+04	
179	483	635	637.00	1	3.50E+04		
180	637	798	638.00		2.00E+04		
6	172	1	1.00	0			
1	0	2.94E[illegible]	0.00		0	0	
1.21E+11	0.258			1			
0	0	0	0.00	0			
0	0	0	0.00	0			
0	0	0	0.00	0			
0	0	0	0.00	803			
1	639	638	800.00	802	1	2.00E+04	
2	803	800	801.00	804	1	5.00E+03	
3	641	639	803.00	1	1	2.00E+04	
4	804	803	805.00	[illegible]	2.00E+04		
5	805	803	802.00	[illegible]	[illegible]		
6	644	641	804.00	[illegible]	1	2.00E+04	
7	807	804	805.00	[illegible]	1	2.00E+04	
8	645	644	807.00	[illegible]	1	2.00E+04	
9	808	607	806.00	811	1	2.00E+04	
10	647	645	808.00	810	1	5.00E+03	
11	811	808	809.00	812	1	2.00E+04	
12	648	647	811.00	813	1	5.00E+03	
13	812	811	810.00	815	1	2.00E+04	
14	651	648	[illegible]	814	1	5.00E+03	
15	815	812	813.00	816	1	2.00E+04	
16	652	651	815.00	817	1	5.00E+03	
17	816	815	814.00	819	1	2.00E+04	
18	655	652	816.00	818	1	5.00E+03	
19	819	816	817.00	820	1	2.00E+04	
20	656	655	819.00	1	1	5.00E+03	
21	820	819	821.00	1	5.00E+03		
22	821	819	818.00	823	2.00E+04		
23	659	656	820.00	822	1	5.00E+03	
24	823	820	821.00	824	1	5.00E+03	
25	660	659	823.00	825	1	5.00E+03	
26	824	823	822.00	827	1	5.00E+03	

27	663	660	824.00	826	1	5.00E+03	
28	827	824	825.00	828	1	5.00E+03	
29	664	663	827.00	829	1	5.00E+03	
30	828	827	826.00	831	1	5.00E+03	
31	667	664	828.00	830	1	5.00E+03	
32	831	828	829.00	832	1	5.00E+03	
33	668	667	831.00	833	1	5.00E+03	
34	832	831	830.00	835	1	5.00E+03	
35	671	668	832.00	834	1	5.00E+03	
36	835	832	833.00	836	1	5.00E+03	
37	672	671	835.00	837	1	5.00E+03	
38	836	835	834.00	839	1	5.00E+03	
39	675	672	836.00	838	1	5.00E+03	
40	839	836	837.00	840	1	5.00E+03	
41	676	675	839.00	841	1	5.00E+03	
42	840	839	838.00	843	1	5.00E+03	
43	679	676	840.00	842	1	5.00E+03	
44	843	840	841.00	844	1	5.00E+03	
45	680	679	843.00	845	1	5.00E+03	
46	844	843	842.00	847	1	5.00E+03	
47	683	680	844.00	846	1	5.00E+03	
48	847	844	845.00	848	1	5.00E+03	
49	684	683	847.00	849	1	5.00E+03	
50	848	847	846.00	851	1	5.00E+03	
51	687	684	848.00	850	1	5.00E+03	
52	851	848	849.00	852	1	5.00E+03	
53	688	687	851.00	853	1	5.00E+03	
54	852	851	850.00	855	1	5.00E+03	
55	691	688	852.00	854	1	5.00E+03	
56	855	852	853.00	856	1	5.00E+03	
57	692	691	855.00	857	1	5.00E+03	
58	856	855	854.00	859	1	5.00E+03	
59	695	692	856.00	858	1	5.00E+03	
60	859	856	[illegible]	860	1	5.00E+03	
61	696	695	859.00	861	1	5.00E+03	
62	860	859	858.00	863	1	5.00E+03	
63	699	696	860.00	862	1	5.00E+03	
64	863	860	861.00	864	1	5.00E+03	
65	700	699	863.00	865	1	5.00E+03	
66	864	863	862.00	1	1	5.00E+03	
67	700	864	868.00	867	5.00E+03		

68	868	864	865 00	1	1	5 00E+03	
69	867	865	866 00	869	5 00E+03		
70	703	700	868 00	870	1	2 50E+03	
71	869	868	867 00	871	1	2 50E+03	
72	870	867	866 00	1	1	2 50E+03	
73	704	703	869 00	874	5 00E+03		
74	707	704	869 00	873	1	5 00E+03	
75	874	869	870 00	87[illegible]	1	2 50E+03	
76	873	870	871.00	875	1	5 00E+03	
77	708	707	874.00	876	1	5 00E+03	
78	875	874	873.00	877	1	2 50E+03	
79	876	873	872.00	880	1	5 00E+03	
80	712	708	875.00	879	1	5 00E+03	
81	880	875	876 00	878	1	2 50E+03	
82	879	876	877 00	881	1	5 00E+03	
83	713	712	880 00	882	1	5 00E+03	
84	881	880	879 00	883	1	2 50E+03	
85	882	879	878 00	885	1	2 50E+03	
86	715	713	881 00	884	1	3 50E+04	
87	885	881	882.00	1	1	3 50E+04	
88	884	882	883 00	886	3 50E+04		
89	716	715	885 00	887	1	3 50E+04	
90	886	885	884 00	889	1	3 50E+04	
91	720	716	886 00	888	1	3 50E+04	
92	889	886	887 00	1	1	3 50E+04	
93	721	720	890 00	891	2 00E+04		
94	890	720	889 00	892	1	3 50E+04	
95	891	889	888 00	894	1	3 50E+04	
96	722	721	890 00	1	1	2 00E+04	
97	894	890	891 00	893	3 50E+04		
98	894	891	892 00	1	1	3 50E+04	
99	[illegible]	722	895 00	896	5 00E+03		
100	895	722	894 00	897	1	2 00E+04	
101	896	894	893 00	899	1	3 50E+04	
102	726	725	895 00	898	1	5 00E+03	
103	899	895	896 00	1	1	2 00E+04	
104	896	897	898 00	900	3 50E+04		
105	732	726	899 00	1	1	5 00E+03	
106	900	899	902 00	1	5 00E+03		
107	902	899	898 00	904	2 00E+04		
108	732	900	901 00	903	1	5 00E+03	
109	904	901	902 00	1	1	5 00E+03	
110	904	903	907.00	1	5 00E+03		
111	907	903	908 00	905	5 00E+03		
112	733	732	904 00	906	1	2 50E+03	
113	905	904	907.00	737	1	2 50E+03	
114	736	733	905 00	910	1	5 00E+03	
115	737	905	906.00	1	1	5 00E+03	
116	910	906	909 00	908	5.00E+03		
117	909	906	907.00	910	1	2 50E+03	
118	741	740	737.00	1	1	2.00E+04	
119	744	741	914.00	1	3.50E+04		
120	745	744	914.00	913	3.50E+04		
121	914	741	910.00	912	1	2 00E+04	
122	913	910	909.00	911	1	5.00E+03	
123	912	909	908.00	915	1	2.50E+03	
124	748	745	914 00	916	1	3.50E+04	
125	915	914	913.00	918	1	2.00E+04	
126	749	748	915.00	917	1	3 50E+04	
127	918	915	916.00	919	1	2.00E+04	
128	752	749	918.00	921	1	3 50E+04	
129	919	918	917.00	920	1	2.00E+04	
130	753	752	919 00	1	1	3.50E+04	
131	920	919	921.00	923	3 50E+04		
132	756	753	920.00	922	1	3 50E+04	
133	923	920	921.00	924	1	3 50E+04	
134	757	756	923.00	925	1	3 50E+04	
135	924	923	922.00	927	1	3 50E+04	
136	760	757	924 00	926	1	3 50E+04	
137	927	924	925.00	928	1	3 50E+04	
138	761	760	927.00	929	1	3 50E+04	
139	928	927	926.00	931	1	3 50E+04	
140	764	761	928 00	930	1	3 50E+04	
141	931	928	929 00	932	1	3 50E+04	
142	765	764	931 00	933	1	3 50E+04	
143	932	331	930 00	935	1	3 50E+04	
144	778	765	932 00	934	1	3.50E+04	
145	935	932	933 00	936	1	3 50E+04	
146	779	778	935.00	937	1	2 00E+04	
147	936	935	934 00	1	1	2 00E+04	
148	779	936	940 00	939	5 00E+03		
149	940	936	938 00	1	1	5 00E+03	

150	936	937	938.00	941	5.00E+03		
151	784	779	940.00	942	1	5.00E+03	
152	941	940	939.00	1	1	5.00E+03	
153	784	941	944.00	943	5.00E+03		
154	944	941	942.00	1	1	5.00E+03	
155	944	943	947.00	945	5.00E+03		
156	785	784	944.00	948	1	2.50E+03	
157	945	944	947.00	946	1	2.50E+03	
158	789	785	945.00	1	1	5.00E+03	
159	946	945	948.00	1	5.00E+03		
160	789	946	950.00	949	5.00E+03		
161	950	946	948.00	1	1	5.00E+03	
162	790	789	950.00	951	2.00E+04		
163	791	790	950.00	952	1	2.00E+04	
164	951	950	949.00	954	1	5.00E+03	
165	794	791	951.00	953	1	2.00E+04	
166	954	951	952.00	1	1	5.00E+03	
167	794	954	799.00	955	2.00E+04		
168	[illegible]	954	953.00	957	1	5.00E+03	
169	798	797	799.00	956	1	5.00E+03	
170	957	799	955.00	1	1	5.00E+03	
171	798	957	800.00	801	5.00E+03		
172	800	957	956.00		1	5.00E+03	
6	164	1	3.00	0			
1	0	2.94E+04	0.00		0	0	
1.21E+11	0.258			1			
0	0	0	0.00	0			
0	0	0	0.00	0			
0	0	0	0.00	0			
0	0	0	0.00	961			
1	802	801	958.00	960	1	5.00E+03	
2	961	958	959.00	962	1	5.00E+03	
3	805	802	961.00	963	1	5.00E+03	
4	962	961	960.00	1	1	5.00E+03	
5	806	805	965.00	1	2.00E+04		
6	805	962	965.00	964	5.00E+03		
7	965	962	963.00	966	1	5.00E+03	
8	809	806	[illegible]	967	1	2.00E+04	
9	966	965	964.00	969	1	5.00E+03	
10	810	809	966.00	1	1	2.00E+04	
11	969	966	968.00	1	2.00E+04		

12	968	966	967.00	970	5.00E+03		
13	813	810	969.00	971	1	2.00E+04	
14	970	969	968.00	973	1	2.00E+04	
15	814	813	970.00	972	1	2.00E+04	
16	973	970	971.00	974	1	2.00E+04	
17	817	814	973.00	975	1	2.00E+04	
18	974	973	972.00	977	1	2.00E+04	
19	818	817	974.00	976	1	2.00E+04	
20	977	974	975.00	978	1	2.00E+04	
21	821	818	977.00	979	1	2.00E+04	
22	978	977	976.00	1	1	2.00E+04	
23	822	821	982.00	981	5.00E+03		
24	982	821	978.00	980	1	2.00E+04	
25	981	978	979.00	983	1	2.00E+04	
26	825	822	982.00	984	1	5.00E+03	
27	983	982	981.00	985	1	2.00E+04	
28	984	981	980.00	987	1	2.00E+04	
29	826	825	983.00	1	1	5.00E+03	
30	987	983	984.00	986	2.00E+04		
31	987	984	985.00	988	1	2.00E+04	
32	829	826	987.00	1	1	5.00E+03	
33	988	987	989.00	1	5.00E+03		
34	989	987	986.00	991	2.00E+04		
35	830	829	988.00	990	1	5.00E+03	
36	991	988	[illegible]	[illegible]	1	5.00E+03	
37	833	830	991.00	993	1	5.00E+03	
38	992	991	990.00	995	1	5.00E+03	
39	834	833	992.00	994	1	5.00E+03	
40	995	992	993.00	996	1	5.00E+03	
41	837	834	995.00	997	1	5.00E+03	
42	996	995	994.00	999	1	5.00E+03	
43	838	837	996.00	998	1	5.00E+03	
44	999	996	997.00	1000	1	5.00E+03	
45	841	838	999.00	1001	1	5.00E+03	
46	1000	999	998.00	1003	1	5.00E+03	
47	842	841	1000.00	1002	1	5.00E+03	
48	1003	1000	1001.00	1004	1	5.00E+03	
49	845	842	1003.00	1005	1	5.00E+03	
50	1004	1003	1002.00	1007	1	5.00E+03	
51	846	845	1004.00	1006	1	5.00E+03	
52	1007	1004	1005.00	1008	1	5.00E+03	

53	849	846	1007 00	1009	1	5 00E+03	
54	1008	1007	1006 00	1011	1	5 00E+03	
55	850	849	1008.00	1010	1	5 00E+03	
56	1011	1008	1009 00	1012	1	5 00E+03	
57	853	850	1011 00	1013	1	5.00E+03	
58	1012	1011	1010 00	1015	1	5 00E+03	
59	854	853	1012.00	1014	1	5 00E+03	
60	1015	1012	1013 00	1016	1	5 00E+03	
61	857	854	1015 00	1017	1	5 00E+03	
62	1016	1015	1014 00	1019	1	5 00E+03	
63	858	857	1016.00	1018	1	5 00E+03	
64	1019	1016	1017 00	1020	1	5 00E+03	
65	861	859	1019 00	1021	1	5 00E+03	
66	1020	1019	1018.00	1023	1	5 00E+03	
67	862	861	1020.00	1022	1	5 00E+03	
68	1023	1020	1021 00	1024	1	5 00E+03	
69	865	862	1023 00	1026	1	5.00E+03	
70	1024	1023	1022 00	1	1	5.00E+03	
71	866	865	1024 00	1025	5 00E+03		
72	871	866	1024 00	1027	1	2 50E+03	
73	1025	1024	1026 00	1	1	2.50E+03	
74	871	1025	1029.00	1028	2 50E+03		
75	1029	1025	1027.00	1030	1	5 00E+03	
76	872	871	1029 00	1031	1	5 00E+03	
77	1030	1029	1028 00	1033	1	5 00E+03	
78	877	872	1030.00	1032	1	5 00E+03	
79	1033	1030	1031 00	1034	1	5.00E+03	
80	878	[illegible]	1033 00	1035	1	5.00E+03	
81	1034	1033	1032.00	1037	1	5 00E+03	
82	883	878	1034 00	1036	1	5 00E+03	
83	1037	1034	1035 00	1	1	5 00E+03	
84	1037	1036	1038.00	1040	5.00E+03		
85	884	883	1037.00	1039	1	3.50E+04	
86	1040	1037	1038 00	1041	1	3 50E+04	
87	887	884	1040 00	1042	1	3 50E+04	
88	1041	1040	1039.00	1044	1	3 50E+04	
89	888	887	1041 00	1043	1	3 50E+04	
90	1044	1041	1042 00	1045	1	3 50E+04	
91	892	888	1044 00	1046	1	3 50E+04	
92	1045	1044	1043 00	1048	1	3 50E+04	
93	893	892	1045.00	1047	1	3 50E+04	
94	1048	1045	1046 00	1049	1	3 50E+04	
95	897	893	1048 00	1050	1	3 50E+04	
96	1049	1048	1047.00	1052	1	3.50E+04	
97	898	897	1049 00	1051	1	3 50E+04	
98	1052	1049	1050.00	1053	1	3 50E+04	
99	902	899	898.00	1054	1	2 00E+04	
100	1053	898	1052.00	1055	1	3 50E+04	
101	1054	1052	1051.00	1	1	3 50E+04	
102	903	902	1058.00	1057	5.00E+03		
103	1058	902	1053.00	1	1	2.00E+04	
104	1057	1053	1054.00	1056	3.50E+04		
105	1057	1054	1055.00	1059	1	3.50E+04	
106	1062	907	1058.00	1056	1	5 00E+03	
107	1059	1058	1057.00	1	1	2.00E+04	
108	1059	1056	1060.00	1061	2.00E+04		
109	1062	1059	1060.00	1063	1	5.00E+03	
110	908	907	1062.00	1064	1	5.00E+03	
111	1063	1062	1061.00	1067	1	5.00E+03	
112	911	908	1063.00	1065	1	5.00E+03	
113	1067	1063	1064.00	1068	1	5.00E+03	
114	912	911	1067.00	1066	1	2.50E+03	
115	1068	1067	1065.00	1069	1	2.50E+03	
116	913	912	1068.00	1070	1	5.00E+03	
117	1069	1068	1066.00	1072	1	5 00E+03	
118	916	913	1069.00	1071	1	5 00E+03	
119	1072	1069	1070.00	1073	1	5.00E+03	
120	917	916	1072.00	1074	1	5 00E+03	
121	1073	1072	1071.00	1076	1	5.00E+03	
122	921	917	1073.00	1075	1	2 00E+04	
123	1076	1073	1074.00	1	1	2.00E+04	
124	921	1076	1077 00	1078	2.00E+04		
125	1077	1076	1075.00	1	1	2 00E+04	
126	922	921	1080.00	1	3.50E+04		
127	921	1077	1080.00	1079	2.00E+04		
128	1080	1077	1078.00	1081	1	2 00E+04	
129	925	922	1080 00	1082	1	3.50E+04	
130	1081	1080	1079 00	1084	1	3.50E+04	
131	926	925	1081 00	1083	1	3.50E+04	
132	1064	1081	1082.00	1085	1	3.50E+04	
133	929	926	1084 00	1086	1	3 50E+04	
134	1085	1084	1063.00	1088	1	3 50E+04	

135	930	929	1085.00	1087	1	3.50E+04	
136	1088	1085	1086.00	1089	1	3.50E+04	
137	933	930	1088.00	1090	1	3.50E+04	
138	1089	1088	1087.00	1	1	3.50E+04	
139	934	933	1089.00	1092	3.50E+04		
140	937	934	1089.00	1091	1	2.00E+04	
141	1092	1089	1090.00	1093	1	2.00E+04	
142	938	937	1092.00	1094	1	5.00E+03	
143	1093	1092	1091.00	1095	1	5.00E+03	
144	939	938	1093.00	1096	1	5.00E+03	
145	1095	1093	1094.00	1098	1	5.00E+03	
146	942	939	1095.00	1097	1	5.00E+03	
147	1098	1095	1096.00	1099	1	5.00E+03	
148	943	942	1098.00	1101	1	5.00E+03	
149	1099	1098	1097.00	1	1	5.00E+03	
150	947	943	1099.00	1100	5.00E+03		
151	948	947	1099.00	1102	1	2.50E+03	
152	1100	1099	1101.00	1104	1	2.50E+03	
153	949	948	1100.00	1103	1	5.00E+03	
154	1104	1100	1102.00	1105	1	5.00E+03	
155	952	949	1104.00	1106	1	5.00E+03	
156	1105	1104	1103.00	1108	1	5.00E+03	
157	953	952	1105.00	1107	1	5.00E+03	
158	1108	1105	1106.00	1109	1	5.00E+03	
159	955	953	1108.00	1110	1	5.00E+03	
160	1109	1108	1107.00	1112	1	5.00E+03	
161	956	955	1109.00	1111	1	5.00E+03	
162	1112	1109	1110.00	958	1	5.00E+03	
163	801	956	1112.00	959	1	5.00E+03	
164	958	1112	1111.00		1	5.00E+03	
6	163	1	3.00	0			
1	0	2.94E+04	0.00		0	0	
1.21E+11	0.258			1			
0	0	0	0.00	0			
0	0	0	0.00	0			
0	0	0	0.00	0			
0	0	0	0.00	1116			
1	960	959	1113.00	1115	1	5.00E+03	
2	1116	1113	1114.00	1117	1	5.00E+03	
3	963	960	1116.00	1118	1	5.00E+03	
4	1117	1116	1115.00	1120	1	5.00E+03	

5	964	963	1117.00	1119	1	5.00E+03	
6	1120	1117	1118.00	1121	1	5.00E+03	
7	967	964	1120.00	1122	1	5.00E+03	
8	1121	1120	1119.00	1	1	5.00E+03	
9	968	967	1121.00	1	5.00E+03		
10	1121	1122	1123.00	1126	2.00E+04		
11	971	968	1121.00	1125	1	2.00E+04	
12	1126	1121	1123.00	1	1	2.00E+04	
13	1125	1123	1124.00	1127	5.00E+03		
14	971	1126	1125.00	1128	1	2.00E+04	
15	1127	1125	1124.00	1129	1	3.50E+04	
16	972	971	1127.00	1130	1	2.00E+04	
17	1129	1127	1128.00	1	1	3.50E+04	
18	975	972	1129.00	1133	2.00E+04		
19	975	1129	1132.00	1131	1	3.50E+04	
20	1132	1129	1130.00	1134	1	3.50E+04	
21	1133	1132	1131.00	1	1	3.50E+04	
22	976	975	1133.00	1136	2.00E+04		
23	979	976	1133.00	1135	1	3.50E+04	
24	1136	1133	1134.00	1137	1	3.50E+04	
25	979	1136	1135.00	1	1	3.50E+04	
26	1137	1135	1138.00	1	3.50E+04		
27	980	979	1137.00	1139	2.00E+04		
28	985	980	1137.00	1	1	2.00E+04	
29	1139	1137	1138.00	1140	2.00E+04		
30	986	985	1139.00	1141	1	2.00E+04	
31	1140	1139	1138.00	1143	1	2.00E+04	
32	989	986	1140.00	1142	1	2.00E+04	
33	1143	1140	1141.00	1144	1	2.00E+04	
34	990	989	1143.00	1	1	5.00E+03	
35	1144	1143	1145.00	1	5.00E+03		
36	1145	1143	1142.00	1147	2.00E+04		
37	993	990	1144.00	1146	1	5.00E+03	
38	1147	1144	1145.00	1148	1	5.00E+03	
39	994	993	1147.00	1149	1	5.00E+03	
40	1148	1147	1146.00	1151	1	5.00E+03	
41	997	994	1148.00	1150	1	5.00E+03	
42	1151	1148	1149.00	1152	1	5.00E+03	
43	998	997	1151.00	1153	1	5.00E+03	
44	1152	1151	1150.00	1155	1	5.00E+03	
45	1001	998	1152.00	1154	1	5.00E+03	

46	1155	1152	1153.00	1156	1	5.00E+03	
47	1002	1001	1155.00	1157	1	5.00E+03	
48	1156	1155	1154.00	1159	1	5.00E+03	
49	1005	1002	1156.00	1158	1	5.00E+03	
50	1159	1156	1157.00	1160	1	5.00E+03	
51	1006	1005	1159.00	1161	1	5.00E+03	
52	1160	1159	1158.00	1163	1	5.00E+03	
53	1009	1006	1160.00	1162	1	5.00E+03	
54	1163	1160	1161.00	1164	1	5.00E+03	
55	1010	1009	1163.00	1165	1	5.00E+03	
56	1164	1163	1162.00	1167	1	5.00E+03	
57	1013	1010	1164.00	1166	1	5.00E+03	
58	1167	1164	1165.00	1168	1	5.00E+03	
59	1014	1013	1167.00	1169	1	5.00E+03	
60	1168	1167	1166.00	1171	1	5.00E+03	
61	1017	1014	1168.00	1170	1	5.00E+03	
62	1171	1168	1169.00	1172	1	5.00E+03	
63	1018	1017	1171.00	1173	1	5.00E+03	
64	1172	1171	1170.00	1175	1	5.00E+03	
65	1021	1018	1172.00	1174	[illegible]	5.00E+03	
66	1175	1172	1173.00	1176	1	5.00E+03	
67	1022	1021	1175.00	1178	1	5.00E+03	
68	1176	1175	1174.00	1177	1	5.00E+03	
69	1027	1026	1176.00	1179	1	2.50E+03	
70	1177	1176	1178.00	1	1	2.50E+03	
71	1027	1177	1181.00	1180	5.00E+03		
72	1181	1177	1179.00	1182	1	5.00E+03	
73	1028	1027	1181.00	1183	1	5.00E+03	
74	1182	1181	1180.00	1185	1	5.00E+03	
75	1031	1028	1182.00	1184	1	5.00E+03	
76	1185	1182	1183.00	1186	1	5.00E+03	
77	1032	1031	1185.00	1187	1	5.00E+03	
78	1186	1185	1184.00	1189	1	5.00E+03	
79	1035	1032	1186.00	1188	1	5.00E+03	
80	1189	1186	1187.00	1190	1	5.00E+03	
81	1036	1035	1189.00	1191	1	5.00E+03	
82	1190	1189	1188.00	1193	1	5.00E+03	
83	1038	1036	1190.00	1192	1	5.00E+03	
84	1193	1190	1191.00	1	1	5.00E+03	
85	1039	1038	1193.00	1194	3.50E+04		
86	1042	1039	1193.00	1195	1	3.50E+04	
87	1194	1193	1192.00	1197	1	5.00E+03	
88	1043	1042	1194.00	1196	1	3.50E+04	
89	1197	1194	1195.00	1198	1	3.50E+04	
90	1046	1043	1197.00	1199	1	3.50E+04	
91	1196	1197	1196.00	1201	1	3.50E+04	
92	1047	1046	1198.00	1200	1	3.50E+04	
93	1201	1198	1199.00	1202	1	3.50E+04	
94	1050	1047	1201.00	1203	1	3.50E+04	
95	1202	1201	1200.00	1205	1	3.50E+04	
96	1051	1050	1202.00	1204	1	3.50E+04	
97	1205	1202	1203.00	1206	1	3.50E+04	
98	1055	1051	1205.00	1207	1	3.50E+04	
99	1206	1205	1204.00	1208	1	3.50E+04	
100	1056	1055	1206.00	1	1	3.50E+04	
101	1208	1206	1207.00	1	3.50E+04		
102	1056	1208	1209.00	1210	2.00E+04		
103	1209	1208	1207.00	1212	1	2.00E+04	
104	1060	1056	1209.00	1211	1	2.00E+04	
105	1212	1209	1210.00	1213	1	2.00E+04	
106	1061	1060	1212.00	1214	1	5.00E+03	
107	1213	1212	1211.00	1216	1	5.00E+03	
108	1064	1061	1213.00	1215	1	5.00E+03	
109	1216	1213	1214.00	1217	1	5.00E+03	
110	1065	1064	1216.00	1219	1	5.00E+03	
111	1217	1216	1215.00	1218	1	5.00E+03	
112	1066	1065	1217.00	1220	1	2.50E+03	
113	1218	1217	1219.00	1222	1	2.50E+03	
114	1070	1066	1218.00	1221	1	5.00E+03	
115	1222	1218	1220.00	1223	1	5.00E+03	
116	1071	1070	1222.00	1224	1	5.00E+03	
117	1223	1222	1221.00	1226	1	5.00E+03	
118	1074	1071	1223.00	1225	1	5.00E+03	
119	1226	1223	1224.00	1228	1	5.00E+03	
120	1075	1074	1226.00	1	1	2.00E+04	
121	1228	1226	1227.00	1	2.00E+04		
122	1226	1225	1227.00	1229	5.00E+03		
123	1078	1075	1228.00	1230	1	2.00E+04	
124	1229	1228	1227.00	1232	1	2.00E+04	
125	1079	1078	1229.00	1231	1	2.00E+04	
126	1232	1229	1230.00	1233	1	2.00E+04	
127	1082	1079	1232.00	1234	1	3.50E+04	

128	1233	1232	1231.00	1236	1	3.50E+04	
129	1083	1082	1233.00	1235	1	3.50E+04	
130	1236	1233	1234.00	1237	1	3.50E+04	
131	1086	1083	1236.00	1238	1	3.50E+04	
132	1237	1236	1235.00	1240	1	3.50E+04	
133	1087	1086	1237.00	1239	1	3.50E+04	
134	1240	1237	1238.00	1241	1	3.50E+04	
135	1090	1087	1240.00	1	1	3.50E+04	
136	1241	1240	1239.00	1244	3.50E+04		
137	1091	1090	1241.00	1243	1	2.00E+04	
138	1244	1241	1242.00	1	1	2.00E+04	
139	1241	1239	1242.00	1245	2.00E+04		
140	1094	1091	1244.00	1246	1	5.00E+03	
141	1245	1244	1243.00	1248	1	5.00E+03	
142	1096	1094	1245.00	1247	1	5.00E+03	
143	1248	1245	1246.00	1249	1	5.00E+03	
144	1097	1096	1248.00	1250	1	5.00E+03	
145	1249	1248	1247.00	1252	1	5.00E+03	
146	1101	1097	1249.00	1251	1	5.00E+03	
147	1252	1249	1250.00	1	1	5.00E+03	
148	1101	1252	1253.00	1256	5.00E+03		
149	1253	1252	1251.00	1254	1	5.00E+03	
150	1102	1101	1253.00	1257	1	2.50E+03	
151	1254	1253	1256.00	1255	1	2.50E+03	
152	1103	1102	1254.00	1258	1	5.00E+03	
153	1255	1254	1257.00	1260	1	5.00E+03	
154	1106	1103	1255.00	1259	1	5.00E+03	
155	1260	1255	1258.00	1261	1	5.00E+03	
156	1107	1106	1260.00	1262	1	5.00E+03	
157	1261	1260	1259.00	1264	1	5.00E+03	
158	1110	1107	1261.00	1263	1	5.00E+03	
159	1264	1261	1262.00	1265	1	5.00E+03	
160	1111	1110	1264.00	1266	1	5.00E+03	
161	1265	1264	1263.00	1113	1	5.00E+03	
162	959	1111	1265.00	1114	1	5.00E+03	
163	1113	1265	1266.00		1	5.00E+03	
6	173	1	3.00	0			
1	0	2.94E+04	0.00		0	0	
1.21E+11	0.258			1			
0	0	0	0.00	0			
0	0	0	0.00	0			

0	0	0	0.00	0			
0	0	0	0.00	1270			
1	1115	1114	1267.00	1269	1	5.00E+03	
2	1270	1267	1268.00	1271	1	5.00E+03	
3	1118	1115	1270.00	1272	1	5.00E+03	
4	1271	1270	1269.00	1274	1	5.00E+03	
5	1119	1118	1271.00	1273	1	5.00E+03	
6	1274	1271	1272.00	1275	1	5.00E+03	
7	1122	1119	1274.00	1276	1	5.00E+03	
8	1275	1274	1273.00	1278	1	5.00E+03	
9	1123	1122	1275.00	1277	1	2.00E+04	
10	1278	1275	1276.00	1279	1	2.00E+04	
11	1124	1123	1278.00	1280	1	3.50E+04	
12	1279	1278	1277.00	1282	1	3.50E+04	
13	1128	1124	1279.00	1281	1	3.50E+04	
14	1282	1279	1280.00	1283	1	3.50E+04	
15	1130	1128	1282.00	1284	1	3.50E+04	
16	1283	1282	1281.00	1286	1	3.50E+04	
17	1131	1130	1283.00	1285	1	3.50E+04	
18	1286	1283	1284.00	1287	1	3.50E+04	
19	1134	1131	1286.00	1288	1	3.50E+04	
20	1287	1286	1285.00	1290	1	3.50E+04	
21	1135	1134	1287.00	1289	1	3.50E+04	
22	1290	1287	1288.00	1291	1	3.50E+04	
23	1137	1135	1290.00	1292	1	3.50E+04	
24	1291	1290	1289.00	1	1	3.50E+04	
25	1137	1291	1138.00	1296	3.50E+04		
26	1138	1291	1292.00	1295	1	3.50E+04	
27	1296	1292	1293.00	1	1	3.50E+04	
28	1295	1293	1294.00	1297	3.50E+04		
29	1141	1138	1296.00	1	1	2.00E+04	
30	1297	1296	1295.00	1298	2.00E+04		
31	1297	1295	1294.00	1	1	2.00E+04	
32	1295	1293	1294.00	1300	5.00E+03		
33	1142	1141	1297.00	1299	1	2.00E+04	
34	1300	1297	1298.00	1301	1	2.00E+04	
35	1145	1142	1300.00	1302	1	2.00E+04	
36	1301	1300	1299.00	1	1	2.00E+04	
37	1145	1301	1304.00	1303	2.00E+04		
38	1304	1301	1302.00	1	1	2.00E+04	
39	1146	1145	1304.00	1305	5.00E+03		

40	1149	1146	1304.00	1306	1	5.00E+03	
41	1305	1304	1303.00	1308	1	5.00E+03	
42	1150	1149	1305.00	1307	1	5.00E+03	
43	1308	1305	1306.00	1309	1	5.00E+03	
44	1153	1150	1308.00	1310	1	5.00E+03	
45	1309	1308	1307.00	1312	1	5.00E+03	
46	1154	1153	1309.00	1311	1	5.00E+03	
47	1312	1309	1310.00	1313	1	5.00E+03	
48	1157	1154	1312.00	1314	1	5.00E+03	
49	1313	1312	1311.00	1316	1	5.00E+03	
50	1158	1157	1313.00	1315	1	5.00E+03	
51	1316	1313	1314.00	1317	1	5.00E+03	
52	1161	1158	1316.00	1318	1	5.00E+03	
53	1317	1316	1315.00	1320	1	5.00E+03	
54	1162	1161	1317.00	1319	1	5.00E+03	
55	1320	1317	1318.00	1321	1	5.00E+03	
56	1165	1162	1320.00	1322	1	5.00E+03	
57	1321	1320	1319.00	1324	1	5.00E+03	
58	1166	1165	1321.00	1323	1	5.00E+03	
59	1324	1321	1322.00	1325	1	5.00E+03	
60	1169	1166	1324.00	1326	1	5.00E+03	
61	1325	1324	1323.00	1328	1	5.00E+03	
62	1170	1169	1325.00	1327	1	5.00E+03	
63	1328	1325	1326.00	1329	1	5.00E+03	
64	1173	1170	1328.00	1330	1	5.00E+03	
65	1329	1328	1327.00	1332	1	5.00E+03	
66	1174	1173	1329.00	1331	1	5.00E+03	
67	1332	1329	1330.00	1333	1	5.00E+03	
68	1178	1174	1332.00	1335	1	5.00E+03	
69	1333	1332	1331.00	1334	1	5.00E+03	
70	1179	1178	1333.00	1336	1	2.50E+03	
71	1334	1333	1335.00	1338	1	2.50E+03	
72	1180	1179	1334.00	1337	1	5.00E+03	
73	1338	1334	1336.00	1339	1	5.00E+03	
74	1183	1180	1338.00	1340	1	5.00E+03	
75	1339	1338	1337.00	1342	1	5.00E+03	
76	1184	1183	1339.00	1341	1	5.00E+03	
77	1342	1339	1340.00	1343	1	5.00E+03	
78	1187	1184	1342.00	1344	1	5.00E+03	
79	1343	1342	1341.00	1346	1	5.00E+03	
80	1188	1187	1343.00	1345	1	5.00E+03	

81	1346	1343	1344.00	1347	1	5.00E+03	
82	1191	1188	1346.00	1348	1	5.00E+03	
83	1347	1346	1345.00	1350	1	5.00E+03	
84	1192	1191	1347.00	1349	1	5.00E+03	
85	1350	1347	1348.00	1351	1	5.00E+03	
86	1195	1192	1350.00	1	1	5.00E+03	
87	1351	1350	1349.00	1352	5.00E+03		
88	1196	1195	1351.00	1353	1	3.50E+04	
89	1352	1351	1349.00	1355	1	3.50E+04	
90	1199	1196	1352.00	1354	1	3.50E+04	
91	1355	1352	1353.00	1356	1	3.50E+04	
93	1200	1199	1355.00	1357	1	3.50E+04	
94	1356	1355	1354.00	1359	1	3.50E+04	
95	1203	1200	1356.00	1358	1	3.50E+04	
96	1359	1356	1357.00	1360	1	3.50E+04	
97	1204	1203	1359.00	1	1	3.50E+04	
98	1360	1359	1358.00	1	3.50E+04		
99	1207	1204	1360.00	1	3.50E+04		
100	1360	1358	1361.00	1	2.00E+04		
101	1207	1360	1363.00	1362	2.00E+04		
102	1363	1360	1361.00	1364	1	2.00E+04	
103	1210	1207	1363.00	1365	1	2.00E+04	
104	1364	1363	1362.00	1425	1	2.00E+04	
105	1211	1210	1364.00	1	1	2.00E+04	
106	1425	1364	1367.00	1	2.00E+04		
107	1367	1364	1365.00	1368	2.00E+04		
108	1214	1211	1425.00	1369	1	5.00E+03	
109	1368	1425	1367.00	1	1	5.00E+03	
110	1369	1367	1366.00	1	5.00E+03		
111	1366	1367	1365.00	1371	5.00E+03		
112	1215	1214	1368.00	1370	1	5.00E+03	
113	1371	1368	1369.00	1372	1	5.00E+03	
114	1219	1215	1371.00	1374	1	5.00E+03	
115	1372	1371	1370.00	1373	1	5.00E+03	
116	1220	1219	1372.00	1375	1	2.50E+03	
117	1373	1372	1374.00	1377	1	2.50E+03	
118	1221	1220	1373.00	1376	1	5.00E+03	
119	1377	1373	1375.00	1378	1	5.00E+03	
120	1224	1221	1377.00	1379	1	5.00E+03	
121	1378	1377	1376.00	1381	1	5.00E+03	
122	1225	1224	1378.00	1380	1	5.00E+03	

123	1381	1378	1379.00	1382	1	5.00E+03	
124	1227	1225	1381.00	1383	1	5.00E+03	
125	1382	1381	1380.00	1385	1	5.00E+03	
126	1230	1227	1382.00	1	1	2.00E+04	
127	1385	1382	1384.00	1	2.00E+04		
128	1384	1382	1383.00	1386	5.00E+03		
129	1231	1230	1385.00	1387	1	2.00E+04	
130	1386	1385	1384.00	1390	1	2.00E+04	
131	1234	1231	1386.00	1389	1	3.50E+04	
132	1390	1386	1388.00	1	1	3.50E+04	
133	1386	1387	1388.00	1391	2.00E+04		
134	1235	1234	1390.00	1392	1	3.50E+04	
135	1391	1390	1389.00	1395	1	3.50E+04	
136	1238	1235	1391.00	1394	1	3.50E+04	
137	1395	1391	1392.00	1	1	3.50E+04	
138	1394	1392	1393.00	1394	2.00E+04		
139	1239	1238	1395.00	1398	1	3.50E+04	
140	1242	1239	1394.00	1396	1	2.00E+04	
141	1398	1394	1393.00	1	1	2.00E+04	
142	1243	1242	1398.00	1	2.00E+04		
143	1398	1396	1397.00	1	5.00E+03		
144	1243	1398	1399.00	1400	5.00E+03		
145	1399	1398	1397.00	1402	1	5.00E+03	
146	1246	1243	1399.00	1401	1	5.00E+03	
147	1402	1399	1400.00	1403	1	5.00E+03	
148	1247	1246	1402.00	1404	1	5.00E+03	
149	1403	[illegible]	1401.00	1410	1	5.00E+03	
150	1250	1247	1403.00	1405	1	5.00E+03	
151	1410	1403	1404.00	1409	1	5.00E+03	
152	1251	1250	1410.00	1	1	5.00E+03	
153	1409	1410	1405.00	1408	5.00E+03		
154	1409	1405	1406.00	1	1	2.50E+03	
155	1408	1406	1407.00	1411	5.00E+03		
156	1256	1251	1409.00	1413	1	5.00E+03	
157	1411	1409	1408.00	1415	1	2.50E+03	
158	1413	1408	1407.00	1412	1	5.00E+03	
159	1257	1256	1411.00	1414	1	[illegible]	
160	1412	1411	1413.00	1417	1	2.50E+03	
161	1414	1413	1416.00	1	1	2.50E+03	
162	1413	1415	1416.00	1414	5.00E+03		
163	1258	1257	1412.00	1418	1	5.00E+03	

164	1259	1258	1414.00	1	1	5.00E+03	
165	1418	1414	1417.00	1419	5.00E+03		
166	1262	1259	1418.00	1420	1	5.00E+03	
167	1419	1418	1417.00	1422	1	5.00E+03	
168	1263	1262	1419.00	1421	1	5.00E+03	
169	1422	1419	1420.00	1423	1	5.00E+03	
170	1266	1263	1422.00	1424	1	5.00E+03	
171	1423	1422	1421.00	1267	1	5.00E+03	
172	1114	1266	1423.00	1268	1	5.00E+03	
173	1267	1423	1424.00		1	5.00E+03	
6	188	1	3.00	0			
1	0	2.94E+04	0.00		0	0	
1.21E+11	0.258			1			
0	0	0	0.00	0			
0	0	0	0.00	0			
0	0	0	0.00	0			
0	0	0	0.00	1429			
1	1269	1268	1426.00	1428	1	5.00E+03	
2	1429	1426	1427.00	1430	1	5.00E+03	
3	1272	1269	1429.00	1431	1	5.00E+03	
4	1430	1429	1428.00	1433	1	5.00E+03	
5	1273	1272	1430.00	1432	1	5.00E+03	
6	1433	1430	1431.00	1434	1	5.00E+03	
7	1276	1273	1433.00	1435	1	5.00E+03	
8	1434	1433	1432.00	1437	1	5.00E+03	
9	1277	1276	1434.00	1436	1	2.00E+04	
10	1437	1434	1435.00	1438	1	5.00E+03	
11	1280	1277	1437.00	1	1	3.50E+04	
12	1438	1437	1436.00	1439	5.00E+03		
[illegible]	[illegible]	1280	1438.00	1	1	3.50E+04	
14	1439	1438	1440.00	1441	5.00E+03		
15	1440	1438	1436.00	1444	1	5.00E+03	
16	1284	1281	1439.00	1443	1	3.50E+04	
17	1444	1439	1440.00	1442	1	5.00E+03	
18	1443	1440	1441.00	1445	1	5.00E+03	
19	1285	1284	1444.00	1446	1	3.50E+04	
20	1445	1444	1443.00	1447	1	5.00E+03	
21	1446	1443	1442.00	1449	1	5.00E+03	
22	1288	1285	1445.00	1	1	3.50E+04	
23	1449	1445	1446.00	1448	5.00E+03		
24	1449	1445	1447.00	1450	1	5.00E+03	

25	1289	1288	1449.00	1451	1	3.50E+04	
26	1450	1449	1448.00	1453	1	5.00E+03	
27	1292	1289	1450.00	1452	1	3.50E+04	
28	1453	1450	1451.00	1	1	5.00E+03	
29	1293	1292	1453.00	1	3.50E+04		
30	1293	1453	1454.00	1455	5.00E+03		
31	1454	1453	1452.00	1	1	5.00E+03	
32	1294	1454	1457.00	1456	5.00E+03		
33	1457	1454	1455.00	1	1	5.00E+03	
34	1298	1294	1457.00	1458	2.00E+04		
35	1299	1298	1457.00	1459	1	2.00E+04	
36	1458	1457	1456.00	1461	1	2.00E+04	
37	1302	1299	1458.00	1460	1	2.00E+04	
38	1461	1458	1459.00	1462	1	2.00E+04	
39	1303	1302	1461.00	1463	1	2.00E+04	
40	1462	1461	1460.00	1	1	2.00E+04	
41	1462	1463	1465.00	1	2.00E+04		
42	1465	1463	1464.00	1466	2.00E+04		
43	1306	1303	1462.00	1	1	5.00E+03	
44	1466	1462	1465.00	1	5.00E+03		
45	1465	1464	1468.00	1467	5.00E+03		
46	1307	1306	1466.00	1468	1	5.00E+03	
47	1467	1466	1465.00	1470	1	5.00E+03	
48	1310	1307	1467.00	1469	1	5.00E+03	
49	1470	1467	1468.00	1471	1	5.00E+03	
50	1311	1310	1470.00	1472	1	5.00E+03	
51	1471	1470	1469.00	1473	1	5.00E+03	
52	1314	1311	1471.00	1474	1	5.00E+03	
53	1473	1471	1472.00	1476	1	5.00E+03	
54	1315	1314	1473.00	1475	1	5.00E+03	
55	1476	1473	1474.00	1477	1	5.00E+03	
56	1318	1315	1476.00	1478	1	5.00E+03	
57	1477	1476	1475.00	1480	1	5.00E+03	
58	1319	1318	1477.00	1479	1	5.00E+03	
59	1480	1477	1478.00	1481	1	5.00E+03	
60	1322	1319	1480.00	1482	1	5.00E+03	
61	1481	1480	1479.00	1484	1	5.00E+03	
62	1323	1322	1481.00	1483	1	5.00E+03	
63	1484	1481	1482.00	1485	1	5.00E+03	
64	1326	1323	1484.00	1486	1	5.00E+03	
65	1485	1484	1483.00	1488	1	5.00E+03	

66	1327	1326	1485.00	1487	1	5.00E+03	
67	1488	1485	1486.00	1489	1	5.00E+03	
68	1330	1327	1488.00	1490	1	5.00E+03	
69	1489	1488	1487.00	1492	1	5.00E+03	
70	1331	1330	1489.00	1491	1	5.00E+03	
71	1492	1489	1490.00	1493	1	5.00E+03	
72	1335	1331	1492.00	1495	1	5.00E+03	
73	1493	1492	1491.00	1494	1	5.00E+03	
74	1336	1335	1493.00	1502	1	2.50E+03	
75	1337	1336	1494.00	1	1	5.00E+03	
76	1502	1494	1500.00	1498	5.00E+03		
77	1500	1494	1493.00	1496	1	2.50E+03	
78	1498	1493	1495.00	1503	1	5.00E+03	
79	1340	1337	1502.00	1501	1	5.00E+03	
80	1503	1502	1500.00	1499	1	5.00E+03	
81	1501	1500	1498.00	1497	1	2.50E+03	
82	1499	1498	1496.00	1	1	2.50E+03	
83	1503	1501	1504.00	1505	5.00E+03		
84	1504	1501	1499.00	1506	1	2.50E+03	
85	1505	1499	1497.00	1509	1	5.00E+03	
86	1341	1340	1503.00	1	1	5.00E+03	
87	1509	1503	1504.00	1508	5.00E+03		
88	1509	1504	1505.00	1507	1	2.50E+03	
89	1508	1505	1506.00	1510	1	5.00E+03	
90	1344	1341	1509.00	1511	1	5.00E+03	
91	1510	1509	1508.00	1514	1	2.50E+03	
92	1511	1508	1507.00	1	1	5.00E+03	
93	1344	1510	1512.00	1513	5.00E+03		
94	1345	1344	1512.00	1515	1	5.00E+03	
95	1513	1512	1510.00	1514	1	5.00E+03	
96	1515	1510	1511.00	1517	1	2.50E+03	
97	1348	1345	1513.00	1516	1	5.00E+03	
98	1517	1513	1515.00	1518	1	5.00E+03	
99	1349	1348	1517.00	1519	1	5.00E+03	
100	1518	1517	1516.00	1	1	5.00E+03	
101	1349	1518	1521.00	1520	3.50E+04		
102	1521	1518	1519.00	1522	1	3.50E+04	
103	1353	1349	1521.00	1523	1	3.50E+04	
104	1522	1521	1520.00	1525	1	3.50E+04	
105	1354	1353	1522.00	1524	1	3.50E+04	
106	1525	1522	1523.00	1526	1	3.50E+04	

107	1357	1354	1525.00	1	1	3.50E+04	
108	1526	1525	1524.00	1	3.50E+04		
109	1358	1357	1526.00	1	3.50E+04		
110	1526	1524	1527.00	1	2.00E+04		
111	1358	1526	1529.00	1528	2.00E+04		
112	1529	1526	1527.00	1530	1	2.00E+04	
113	1361	1358	1529.00	1531	1	2.00E+04	
114	1530	1529	1528.00	1	1	2.00E+04	
115	1530	1531	1532.00	1534	2.00E+04		
116	1362	1361	1530.00	1533	1	2.00E+04	
117	1534	1530	1532.00	1533	1	2.00E+04	
118	1365	1362	1534.00	1	1	2.00E+04	
119	1535	1534	1533.00	1	2.00E+04		
120	1535	1533	1536.00	1	5.00E+03		
121	1536	1533	1532.00	1538	5.00E+03		
122	1366	1365	1535.00	1537	1	5.00E+03	
123	1538	1535	1536.00	1539	1	5.00E+03	
124	1369	1366	1538.00	1540	1	5.00E+03	
125	1539	1538	1537.00	1542	1	5.00E+03	
127	1370	1369	1539.00	1541	1	5.00E+03	
128	1542	1539	1540.00	1543	1	5.00E+03	
129	1374	1370	1542.00	1545	1	5.00E+03	
130	1543	1542	1541.00	1544	1	5.00E+03	
131	1375	1374	1543.00	1546	1	2.50E+03	
132	1544	1543	1545.00	1548	1	2.50E+03	
133	1376	1375	1544.00	1547	1	5.00E+03	
134	1548	1544	1546.00	1549	1	5.00E+03	
135	1379	1376	1548.00	1550	1	5.00E+03	
136	1549	1548	1547.00	1552	1	5.00E+03	
137	1380	1379	1549.00	1551	1	5.00E+03	
138	1552	1549	1550.00	1553	1	5.00E+03	
139	1383	1380	1552.00	1554	1	5.00E+03	
140	1553	1552	1551.00	1556	1	5.00E+03	
141	1384	1383	1553.00	1555	1	5.00E+03	
142	1556	1553	1554.00	1	1	5.00E+03	
143	1387	1384	1557.00	1	2.00E+04		
144	1557	1384	1556.00	1558	5.00E+03		
145	1557	1556	1555.00	1561	1	5.00E+03	
146	1388	1387	1557.00	1	1	2.00E+04	
147	1561	1557	1560.00	1559	2.00E+04		
148	1562	1557	1558.00	1	1	5.00E+03	

149	1389	1388	1561.00	1	3.50E+04		
150	1392	1389	1561.00	1562	3.50E+04		
151	1392	1561	1560.00	1563	1	2.00E+04	
152	1562	1560	1559.00	1565	1	5.00E+03	
153	1393	1392	1562.00	1564	1	2.00E+04	
154	1565	1562	1563.00	1566	1	5.00E+03	
155	1396	1393	1565.00	1567	1	2.00E+04	
156	1566	1565	1564.00	1569	1	5.00E+03	
157	1397	1396	1566.00	1568	1	5.00E+03	
158	1569	1566	1567.00	1570	1	5.00E+03	
159	1400	1397	1569.00	1571	1	5.00E+03	
160	1570	1569	1568.00	1575	1	5.00E+03	
161	1401	1400	1570.00	1	1	5.00E+03	
162	1575	1570	1571.00	1574	5.00E+03		
163	1575	1571	1572.00	1	1	2.50E+03	
164	1574	1572	1573.00	1576	5.00E+03		
165	1404	1401	1575.00	1577	1	5.00E+03	
166	1576	1575	1574.00	1578	1	2.50E+03	
167	1577	1574	1573.00	1	1	5.00E+03	
168	1405	1404	1576.00	1406	5.00E+03		
169	1405	1576	1577.00	1	1	2.50E+03	
170	1406	1577	1580.00	1579	5.00E+03		
171	1580	1577	1578.00	1581	1	5.00E+03	
172	1407	1406	1580.00	1582	1	5.00E+03	
173	1581	1580	1579.00	1584	1	5.00E+03	
174	1415	1407	1581.00	1583	1	5.00E+03	
175	1584	1581	1582.00	1585	1	5.00E+03	
176	1416	1415	1584.00	1587	1	5.00E+03	
177	1585	1584	1583.00	1	1	5.00E+03	
178	1585	1587	1588.00	1586	5.00E+03		
179	1417	1416	1585.00	1589	1	2.50E+03	
180	1586	1585	1588.00	1591	1	2.50E+03	
181	1420	1417	1586.00	1590	1	5.00E+03	
182	1591	1586	1589.00	1592	1	5.00E+03	
183	1421	1420	1591.00	1593	1	5.00E+03	
184	1592	1591	1590.00	1595	1	5.00E+03	
185	1424	1421	1592.00	1594	1	5.00E+03	
186	1595	1592	1593.00	1426	1	5.00E+03	
187	1268	1424	1595.00	1427	1	5.00E+03	
188	1426	1595	1594.00		1	5.00E+03	
6	195	1	3.00	0			

1	0	2.94E+04	0.00		0	0	
1.21E+11	0.258			1			
0	0	0	0.00	0			
0	0	0	0.00	0			
0	0	0	0.00	0			
0	0	0	0.00	1601			
1	1428	1427	1596.00	1600	1	5.00E+03	
2	1601	1596	1597.00	1599	1	2.50E+03	
3	1600	1597	1598.00	1602	1	5.00E+03	
4	1432	1428	1601.00	1603	1	5.00E+03	
5	1602	1601	1600.00	1604	1	2.50E+03	
6	1603	1600	1599.00	1607	1	5.00E+03	
7	1432	1431	1602.00	1606	1	5.00E+03	
8	1607	1602	1603.00	1605	1	2.50E+03	
9	1606	1603	1604.00	1608	1	5.00E+03	
10	1435	1432	1607.00	1	1	5.00E+03	
11	1608	1607	1609.00	1610	5.00E+03		
12	1609	1607	1606.00	1611	1	2.50E+03	
13	1610	1606	1605.00	1615	1	5.00E+03	
14	1436	1435	1608.00	1614	1	5.00E+03	
15	1615	1608	1609.00	1613	1	5.00E+03	
16	1614	1609	1610.00	1612	1	2.50E+03	
17	1613	1610	1611.00	1616	1	5.00E+03	
18	1441	1436	1615.00	1617	1	5.00E+03	
19	1616	1615	1614.00	1618	1	5.00E+03	
20	1617	1614	1613.00	1619	1	2.50E+03	
21	1616	1613	1612.00	1623	1	5.00E+03	
22	1442	1441	1616.00	1622	1	5.00E+03	
23	1623	1616	1617.00	1621	1	5.00E+03	
24	1622	1617	1618.00	1620	1	2.50E+03	
25	1621	1618	1619.00	1624	1	5.00E+03	
26	1447	1442	1623.00	1625	1	5.00E+03	
27	1624	1623	1622.00	1626	1	5.00E+03	
28	1625	1622	1621.00	1627	1	2.50E+03	
29	1626	1621	1620.00	1632	1	5.00E+03	
30	1448	1447	1624.00	1631	1	5.00E+03	
31	1632	1624	1625.00	1630	1	5.00E+03	
32	1631	1625	1626.00	1628	1	2.50E+03	
33	1630	1626	1627.00	1633	1	5.00E+03	
34	1451	1448	1632.00	1634	1	5.00E+03	
35	1633	1632	1631.00	1	1	5.00E+03	

36	1634	1631	1629.00	1628	5.00E+03		
37	1629	1631	1630.00	1636	1	2.50E+03	
38	1452	1451	1633.00	1635	1	5.00E+03	
39	1636	1633	1634.00	1637	1	5.00E+03	
40	1455	1452	1636.00	1638	1	5.00E+03	
41	1637	1636	1635.00	1640	1	5.00E+03	
42	1456	1455	1637.00	1639	1	5.00E+03	
43	1640	1637	1638.00	1	1	5.00E+03	
44	1456	1640	1641.00	1642	5.00E+03		
45	1641	1640	1639.00	1643	1	5.00E+03	
46	1459	1456	1641.00	1	1	2.00E+04	
47	1643	1641	1642.00	1644	2.00E+04		
48	1460	1459	1643.00	1645	1	2.00E+04	
49	1644	1643	1642.00	1647	1	2.00E+04	
50	1463	1460	1644.00	1646	1	2.00E+04	
51	1647	1644	1645.00	1648	1	2.00E+04	
52	1464	1463	1647.00	1649	1	2.00E+04	
53	1648	1647	1646.00	1	1	2.00E+04	
54	1464	1648	1651.00	1650	2.00E+04		
55	1651	1648	1649.00	1	1	2.00E+04	
56	1468	1464	1651.00	1652	5.00E+03		
57	1469	1468	1651.00	1653	1	5.00E+03	
58	1652	1651	1650.00	1655	1	5.00E+03	
59	1472	1469	1652.00	1654	1	5.00E+03	
60	1655	1652	1653.00	1656	1	5.00E+03	
61	1474	1472	1655.00	1657	1	5.00E+03	
62	1656	1655	1654.00	1659	1	5.00E+03	
63	1475	1474	1656.00	1658	1	5.00E+03	
64	1659	1656	1657.00	1660	1	5.00E+03	
65	1478	1475	1659.00	1661	1	5.00E+03	
66	1660	1659	1658.00	1663	1	5.00E+03	
67	1479	1478	1660.00	1662	1	5.00E+03	
68	1663	1660	1661.00	1664	1	5.00E+03	
69	1482	1479	1663.00	1665	1	5.00E+03	
70	1664	1663	1662.00	1667	1	5.00E+03	
71	1483	1482	1664.00	1666	1	5.00E+03	
72	1667	1664	1665.00	1668	1	5.00E+03	
73	1486	1483	1667.00	1669	1	5.00E+03	
74	1668	1667	1666.00	1671	1	5.00E+03	
75	1487	1486	1668.00	1670	1	5.00E+03	
76	1671	1668	1669.00	1672	1	5.00E+03	

77	1490	1487	1671.00	1673	1	5.00E+03	
78	1672	1671	1670.00	1679	1	5.00E+03	
79	1491	1490	1672.00	1674	1	5.00E+03	
80	1679	1672	1673.00	1678	1	5.00E+03	
81	1495	1491	1679.00	1	1	5.00E+03	
82	1678	1679	1674.00	1	5.00E+03		
83	1496	1495	1678.00	1677	5.00E+03		
84	1497	1496	1678.00	1675	1	2.50E+03	
85	1677	1678	1674.00	1	1	2.50E+03	
86	1497	1677	1680.00	1681	5.00E+03		
87	1680	1677	1676.00	1683	1	5.00E+03	
88	1506	1497	1680.00	1682	1	5.00E+03	
89	1683	1680	1681.00	1684	1	5.00E+03	
90	1507	1506	1683.00	1685	1	5.00E+03	
91	1684	1683	1682.00	1687	1	5.00E+03	
92	1514	1507	1684.00	1686	1	5.00E+03	
93	1687	1684	1685.00	1	1	5.00E+03	
94	1514	1687	1688.00	1689	5.00E+03		
95	1688	1687	1686.00	1	1	5.00E+03	
96	1516	1515	1692.00	1691	5.00E+03		
97	1692	1515	1514.00	1	1	2.50E+03	
98	1691	1514	1688.00	1690	5.00E+03		
99	1691	1688	1689.00	1693	1	5.00E+03	
100	1519	1516	1692.00	1694	1	5.00E+03	
101	1693	1692	1691.00	1695	1	2.50E+03	
102	1694	1691	1690.00	1697	1	5.00E+03	
103	1520	1519	1693.00	1696	1	3.50E+04	
104	1697	1693	1694.00	1	1	3.50E+04	
105	1694	1695	1696.00	1698	3.50E+04		
106	1523	1520	1697.00	1699	1	3.50E+04	
107	1698	1697	1696.00	1	1	3.50E+04	
108	1524	1523	1698.00	1	3.50E+04		
109	1524	1698	1701.00	1700	2.00E+04		
110	1701	1698	1699.00	1702	1	2.00E+04	
111	1527	1524	1701.00	1703	1	2.00E+04	
112	1702	1701	1700.00	1705	1	2.00E+04	
113	1528	1527	1702.00	1704	1	2.00E+04	
114	1705	1702	1703.00	1706	1	2.00E+04	
115	1531	1528	1705.00	1	1	2.00E+04	
116	1706	1705	1707.00	1708	2.00E+04		
117	1707	1705	1704.00	1709	1	2.00E+04	

118	1706	1707	1708.00	1	1	5.00E+03	
119	1532	1706	1711.00	1710	5.00E+03		
120	1711	1706	1709.00	1712	1	5.00E+03	
121	1536	1532	1711.00	1713	1	5.00E+03	
122	1712	1711	1710.00	1715	1	5.00E+03	
123	1537	1536	1712.00	1714	1	5.00E+03	
124	1715	1712	1713.00	1716	1	5.00E+03	
125	1540	1537	1715.00	1717	1	5.00E+03	
126	1716	1715	1714.00	1719	1	5.00E+03	
127	1541	1540	1716.00	1718	1	5.00E+03	
128	1719	1716	1717.00	1720	1	5.00E+03	
129	1545	1541	1719.00	1722	1	5.00E+03	
130	1720	1719	1718.00	1724	1	5.00E+03	
131	1720	1722	1723.00	1721	1	5.00E+03	
132	1546	1545	1720.00	1725	1	2.50E+03	
133	1721	1720	1724.00	1728	1	2.50E+03	
134	1725	1724	1729.00	1	1	2.50E+03	
135	1724	1723	1729.00	1726	5.00E+03		
136	1547	1546	1721.00	1	1	5.00E+03	
137	1726	1721	1725.00	1727	5.00E+03		
138	1550	1547	1726.00	1728	1	5.00E+03	
139	1727	1726	1725.00	1731	1	5.00E+03	
140	1551	1550	1727.00	1730	1	5.00E+03	
141	1731	1727	1728.00	1732	1	5.00E+03	
142	1554	1551	1731.00	1733	1	5.00E+03	
143	1732	1731	1730.00	1735	1	5.00E+03	
144	1555	1554	1732.00	1734	1	5.00E+03	
145	1735	1732	1733.00	1736	1	5.00E+03	
146	1558	1555	1735.00	1737	1	5.00E+03	
147	1736	1735	1734.00	1739	1	5.00E+03	
148	1559	1558	1736.00	1738	1	5.00E+03	
149	1739	1736	1737.00	1740	1	5.00E+03	
150	1563	1559	1739.00	1741	1	5.00E+03	
151	1740	1739	1738.00	1747	1	5.00E+03	
152	1564	1563	1740.00	1742	1	5.00E+03	
153	1747	1740	1741.00	1746	1	5.00E+03	
154	1567	1564	1747.00	1	1	5.00E+03	
155	1746	1747	1742.00	1745	5.00E+03		
156	1746	1742	1743.00	1	1	2.50E+03	
157	1745	1743	1744.00	1748	5.00E+03		
158	1568	1567	1746.00	1749	1	5.00E+03	

159	1748	1746	1745.00	1750	1	2.50E+03	
160	1749	1745	1744.00	1	1	5.00E+03	
161	1571	1568	1748.00	1572	5.00E+03		
162	1571	1748	1749.00	1	1	2.50E+03	
163	1572	1749	1752.00	1751	5.00E+03		
164	1752	1749	1750.00	1753	1	5.00E+03	
165	1573	1572	1752.00	1754	1	5.00E+03	
166	1753	1752	1751.00	1756	1	5.00E+03	
167	1578	1573	1753.00	1755	1	5.00E+03	
168	1756	1753	1754.00	1757	1	5.00E+03	
169	1579	1578	1756.00	1758	1	5.00E+03	
170	1757	1756	1755.00	1761	1	5.00E+03	
171	1582	1579	1757.00	1760	1	5.00E+03	
172	1761	1757	1758.00	1	1	5.00E+03	
173	1760	1758	1759.00	1762	5.00E+03		
174	1583	1582	1761.00	1763	1	5.00E+03	
175	1762	1761	1760.00	1	1	5.00E+03	
176	1760	1759	1763.00	1765	2.00E+04		
177	1587	1583	1762.00	1764	1	5.00E+03	
178	1765	1762	1763.00	1	1	5.00E+03	
179	1588	1587	1766.00	1768	5.00E+03		
180	1766	1587	1765.00	1769	1	5.00E+03	
181	1768	1765	1764.00	1767	1	5.00E+03	
182	1589	1588	1766.00	1	1	2.50E+03	
183	1590	1589	1767.00	1773	5.00E+03		
184	1593	1590	1767.00	1772	1	5.00E+03	
185	1773	1767	1766.00	1771	1	2.50E+03	
186	1772	1766	1768.00	1770	1	5.00E+03	
187	1771	1768	1769.00	1774	1	5.00E+03	
188	1594	1593	1773.00	1775	1	5.00E+03	
189	1774	1773	1772.00	1776	1	2.50E+03	
190	1775	1772	1771.00	1777	1	5.00E+03	
191	1776	1771	1770.00	1596	1	5.00E+03	
192	1427	1594	1774.00	1597	1	5.00E+03	
193	1596	1774	1775.00	1	1	2.50E+03	
194	1597	1775	1776.00	1598	5.00E+03		
195	1597	1776	1777.00		1	5.00E+03	
6	207	1	3.00	0			
1	0	2.94E+04	0.00		0	0	
1.21E+11	0.258			1			
0	0	0	0.00	0			

0	0	0	0.00	0			
0	0	0	0.00	0			
0	0	0	0.00	1781			
1	1599	1598	1778.00	1780	1	5.00E+03	
2	1781	1778	1779.00	1782	1	5.00E+03	
3	1604	1599	1781.00	1783	1	5.00E+03	
4	1782	1781	1780.00	1785	1	5.00E+03	
5	1605	1604	1782.00	1784	1	5.00E+03	
6	1785	1782	1783.00	1786	1	5.00E+03	
7	1611	1605	1785.00	1787	1	5.00E+03	
8	1786	1785	1784.00	1789	1	5.00E+03	
9	1612	1611	1786.00	1788	1	5.00E+03	
10	1789	1786	1787.00	1790	1	5.00E+03	
11	1619	1612	[illegible]	1791	1	5.00E+03	
12	1790	1789	1788.00	1793	1	5.00E+03	
13	1620	1619	1790.00	1792	1	5.00E+03	
14	1793	1790	1791.00	1794	1	5.00E+03	
15	1627	1620	1793.00	1795	1	5.00E+03	
16	1794	1793	1792.00	1797	1	5.00E+03	
17	1628	1627	1794.00	1796	1	5.00E+03	
18	1797	1794	1795.00	1	1	5.00E+03	
19	1634	1629	1804.00	1953	5.00E+03		
20	1804	1629	1628.00	1798	1	2.50E+03	
21	1953	1628	1797.00	1799	1	5.00E+03	
22	1798	1797	1796.00	1802	1	5.00E+03	
23	1635	1634	1804.00	1801	1	5.00E+03	
24	1802	1804	1953.00	1	1	2.50E+03	
25	1801	1953	1798.00	1800	5.00E+03		
26	1801	1798	[illegible]	1803	1	5.00E+03	
27	1638	1635	1802.00	1	1	5.00E+03	
28	1803	1802	1805.00	1806	5.00E+03		
29	1805	1802	1801.00	1	1	2.50E+03	
30	1806	1801	1800.00	1809	5.00E+03		
31	1639	1638	1803.00	1808	1	5.00E+03	
32	1809	1803	1805.00	1807	1	5.00E+03	
33	1808	1805	1806.00	1	1	2.50E+03	
34	1807	1806	1800.00	1810	5.00E+03		
35	1642	1639	1809.00	1811	1	5.00E+03	
36	1810	1809	1808.00	1	1	5.00E+03	
37	1811	1808	1812.00	1815	5.00E+03		
38	1645	1642	1810.00	1814	1	2.00E+04	

39	1815	1810	1811.00	1813	1	2.00E+04	
40	1814	1811	1812.00	1816	1	5.00E+03	
41	1646	1645	1815.00	1	1	2.00E+04	
42	1816	1815	1814.00	1817	2.00E+04		
43	1816	1814	1813.00	1820	1	5.00E+03	
44	1649	1646	1816.00	1819	1	2.00E+04	
45	1820	1816	1817.00	1	1	5.00E+03	
46	1650	1649	1820.00	1821	2.00E+04		
47	1650	1820	1819.00	1	1	5.00E+03	
48	1819	1817	1818.00	1823	5.00E+03		
49	1821	1819	1818.00	1822	1	5.00E+03	
50	1653	1650	1821.00	1824	1	5.00E+03	
51	1822	1821	1823.00	1826	1	5.00E+03	
52	1654	1653	1822.00	1825	1	5.00E+03	
53	1826	1822	1824.00	1827	1	5.00E+03	
54	1657	1654	1826.00	1828	1	5.00E+03	
55	1827	1826	1825.00	1831	1	5.00E+03	
56	1658	1657	1827.00	1829	1	5.00E+03	
57	1831	1827	1828.00	1832	1	5.00E+03	
58	1661	1658	1831.00	1833	1	5.00E+03	
59	1832	1831	1829.00	1834	1	5.00E+03	
60	1833	1829	1830.00	1	1	2.50E+03	
61	1834	1830	1835.00	1839	5.00E+03		
62	1662	1661	1832.00	1838	1	5.00E+03	
63	1839	1832	1833.00	1837	1	5.00E+03	
64	1838	1833	1834.00	1836	1	2.50E+03	
65	1837	1834	1835.00	1840	1	5.00E+03	
66	1665	1662	1839.00	1841	1	5.00E+03	
67	1840	1839	1838.00	1842	1	5.00E+03	
68	1841	1838	1837.00	1843	1	2.50E+03	
69	1842	1837	1836.00	1847	1	5.00E+03	
70	1666	1665	1840.00	1846	1	5.00E+03	
71	1847	1840	1841.00	1845	1	5.00E+03	
72	1846	1841	1842.00	1844	1	2.50E+03	
73	1845	1842	1843.00	1848	1	5.00E+03	
74	1669	1666	1847.00	1	1	5.00E+03	
75	1847	1846	1848.00	1849	5.00E+03		
76	1848	1846	1845.00	1850	1	2.50E+03	
77	1849	1845	1844.00	1853	1	5.00E+03	
78	1670	1669	1848.00	1852	1	5.00E+03	
79	1853	1848	1849.00	1851	1	2.50E+03	

80	1852	1849	1850.00	1854	1	5.00E+03	
81	1673	1670	1853.00	1855	1	5.00E+03	
82	1854	1853	1852.00	1856	1	2.50E+03	
83	1855	1852	1851.00	1	1	5.00E+03	
84	1674	1673	1854.00	1675	5.00E+03		
85	1674	1854	1855.00	1	1	2.50E+03	
86	1675	1855	1858.00	1857	5.00E+03		
87	1858	1855	1856.00	1859	1	5.00E+03	
88	1676	1675	1858.00	1860	1	5.00E+03	
89	1859	1858	1857.00	1862	1	5.00E+03	
90	1681	1676	1859.00	1861	1	5.00E+03	
91	1862	1859	1860.00	1863	1	5.00E+03	
92	1682	1681	1862.00	1864	1	5.00E+03	
93	1863	1862	1861.00	1866	1	5.00E+03	
94	1685	1682	1863.00	1865	1	5.00E+03	
95	1866	1863	1864.00	1867	1	5.00E+03	
96	1686	1685	1866.00	1868	1	5.00E+03	
97	1867	1866	1865.00	1870	1	5.00E+03	
98	1689	1686	1867.00	1869	1	5.00E+03	
99	1870	1867	1868.00	1871	1	5.00E+03	
100	1690	1689	1870.00	1872	1	5.00E+03	
101	1871	1870	1869.00	1874	1	5.00E+03	
102	1695	1690	1871.00	1873	1	5.00E+03	
103	1874	1871	1872.00	1	1	5.00E+03	
104	1696	1695	1875.00	1	3.50E+04		
105	1875	1695	1874.00	1876	5.00E+03		
106	1875	1874	1873.00	1879	1	5.00E+03	
107	1699	1696	1875.00	1	1	3.50E+04	
108	1879	1875	1878.00	1877	3.50E+04		
109	1878	1875	1876.00	1880	1	5.00E+03	
110	1700	1699	1879.00	1881	1	2.00E+04	
111	1880	1879	1878.00	1882	1	2.00E+04	
112	1881	1878	1877.00	1885	1	5.00E+03	
113	1703	1700	1880.00	1884	1	2.00E+04	
114	1885	1880	1881.00	1883	1	2.00E+04	
115	1884	1881	1882.00	1886	1	5.00E+03	
116	1704	1703	1885.00	1887	1	2.00E+04	
117	1886	1885	1884.00	1888	1	2.00E+04	
118	1887	1884	1883.00	1890	1	5.00E+03	
119	1708	1704	1886.00	1	1	2.00E+04	
120	1890	1886	1887.00	1889	2.00E+04		

121	1890	1887	1888.00	1891	1	5.00E+03	
122	1709	1708	1890.00	1892	1	5.00E+03	
123	1891	1890	1889.00	1	1	5.00E+03	
124	1710	1709	1891.00	1894	5.00E+03		
125	1713	1710	1891.00	1893	1	5.00E+03	
126	1894	1891	1892.00	1895	1	5.00E+03	
127	1714	1713	1894.00	1896	1	5.00E+03	
128	1895	1894	1893.00	1898	1	5.00E+03	
129	1717	1714	1895.00	1897	1	5.00E+03	
130	1898	1895	1896.00	1899	1	5.00E+03	
131	1718	1717	1898.00	1954	1	5.00E+03	
132	1899	1898	1897.00	1	1	5.00E+03	
133	1954	1897	1955.00	1	5.00E+03		
134	1899	1954	1957.00	1956	5.00E+03		
135	1957	1954	1955.00	1	1	5.00E+03	
136	1956	1955	1961.00	1958	5.00E+03		
137	1722	1718	1899.00	1959	1	5.00E+03	
138	1958	1899	1957.00	1960	1	5.00E+03	
139	1959	1957	1956.00	1	1	2.50E+03	
140	1960	1956	1961.00	1901	5.00E+03		
141	1723	1722	1958.00	1900	1	5.00E+03	
142	1901	1958	1959.00	1963	1	5.00E+03	
143	1900	1959	1960.00	1962	1	2.50E+03	
144	1963	1960	1961.00	1902	1	5.00E+03	
145	1729	1723	1901.00	1903	1	5.00E+03	
146	1902	1901	1900.00	1904	1	5.00E+03	
147	1903	1900	1963.00	1905	1	2.50E+03	
148	1904	1963	1962.00	1	1	5.00E+03	
149	1729	1902	1908.00	1	5.00E+03		
150	1908	1902	1903.00	1907	5.00E+03		
151	1908	1903	1904.00	1906	1	2.50E+03	
152	1907	1904	1905.00	1909	1	5.00E+03	
153	1726	1729	1908.00	1910	1	2.50E+03	
154	1909	1908	1907.00	1913	1	2.50E+03	
155	1910	1907	1906.00	1	1	5.00E+03	
156	1730	1728	1909.00	1911	5.00E+03		
157	1733	1730	1909.00	1912	1	5.00E+03	
158	1911	1909	1910.00	1	1	2.50E+03	
159	1912	1910	1913.00	1917	5.00E+03		
160	1734	1733	1911.00	1916	1	5.00E+03	
161	1917	1911	1912.00	1914	1	2.50E+03	

162	1916	1912	1913.00	1	1	5.00E+03	
163	1916	1914	1915.00	1918	5.00E+03		
164	1737	1734	1917.00	1919	1	5.00E+03	
165	1918	1917	1916.00	1920	1	2.50E+03	
166	1919	1916	1915.00	1923	1	5.00E+03	
167	1738	1737	1918.00	1922	1	5.00E+03	
168	1923	1918	1919.00	1921	1	2.50E+03	
169	1922	1919	1920.00	1924	1	5.00E+03	
170	1741	1738	1923.00	1925	1	5.00E+03	
171	1924	1923	1922.00	1926	1	2.50E+03	
172	1925	1922	1921.00	1	1	5.00E+03	
173	1742	1741	1924.00	1743	5.00E+03		
174	1742	1924	1925.00	1	1	2.40E+03	
175	1743	1925	1928.00	1927	5.00E+03		
176	1928	1925	1926.00	1929	1	5.00E+03	
177	1744	1743	1928.00	1930	1	5.00E+03	
178	1929	1928	1927.00	1932	1	5.00E+03	
179	1750	1744	1929.00	1931	1	5.00E+03	
180	1932	1929	1930.00	1933	1	5.00E+03	
181	1751	1750	1932.00	1934	1	5.00E+03	
182	1933	1932	1931.00	1936	1	5.00E+03	
183	1754	1751	1933.00	1935	1	5.00E+03	
184	1936	1933	1934.00	1937	1	5.00E+03	
185	1755	1754	1936.00	1938	1	5.00E+03	
186	1937	1936	1935.00	1940	1	5.00E+03	
187	1758	1755	1937.00	1	1	5.00E+03	
188	1940	1937	1938.00	1	5.00E+03		
189	1940	1938	1939.00	1	2.00E+04		
190	1759	1758	1940.00	1	5.00E+03		
191	1759	1940	1941.00	1942	2.00E+04		
192	1941	1940	1939.00	1944	1	2.00E+04	
193	1763	1759	1941.00	1943	1	2.00E+04	
194	1944	1941	1942.00	1	1	2.00E+04	
195	1764	1763	1945.00	1946	5.00E+03		
196	1945	1763	1944.00	1947	1	2.00E+04	
197	1946	1944	1943.00	1949	1	2.00E+04	
198	1769	1764	1945.00	1	1	5.00E+03	
199	1945	1946	1949.00	1948	2.00E+04		
200	1949	1946	1947.00	1950	1	2.00E+04	
201	1770	1769	1949.00	1	1	2.00E+04	
202	1950	1949	1952.00	1	5.00E+03		

4 of/de 4

PM-1 3½"x4" PHOTOGRAPHIC MICROCOPY TARGET
NBS 1010a ANSI/ISO #2 EQUIVALENT

203	1949	1948	1952 00	1951	2 00E+04		
204	1777	1770	1950 00	1	1	5 00E+03	
205	1951	1950	1952 00	1778	5 00E+03		
206	1598	1777	1951 00	1779	1	5 00E+03	
207	1778	1951	195[illegible] 00		1	5 00E+03	
6	144	1	3 00	0			
1	0	2 94E+04	0 00		0	0	
1 21E+11	0 258			1			
0	0	0	0 00	0			
0	0	0	0 00	0			
0	0	0	0 00	0			
0	0	0	0 00	1966			
1	1780	1779	1964 00	1965	1	2 00E+04	
2	1966	1964	2069 00	1	1	2 00E+04	
3	1783	1780	1966 00	1967	2 00E+04		
4	1784	1783	1966 00	1968	1	2 00E+04	
5	1967	1966	1965 00	1	1	3 50E+04	
6	1787	1784	1967 00	1970	2 00E+04		
7	1788	1787	1967 00	1969	1	2 00E+04	
8	1970	1967	1968 00	1	1	3 50E+04	
9	1791	1788	1970 00	1971	2 00E+04		
10	1792	1791	1970 00	1972	1	2 00E+04	
11	1971	1970	1969 00	1	1	3 50E+04	
12	1795	1792	2070 00	1	5 00E+03		
13	2070	1792	1971 00	1975	2 00E+04		
14	1796	1795	2070 00	1974	1	5 00E+03	
15	1975	2070	1971 00	1973	1	2 00E+04	
16	1974	1971	1972 00	1976	1	3 50E+04	
17	1799	1796	1975 00	1977	1	5 00E+03	
18	1976	1975	1974 00	1	1	2 00E+04	
19	1977	1974	1973 00	1980	3 50E+04		
20	1800	1799	1976 00	1979	1	5 00E+03	
21	1980	1976	1977 00	1978	1	2 00E+04	
22	1979	1977	1973 00	1	1	3 50E+04	
23	1807	1800	1980 00	1	5 00E+03		
24	1812	1808	1981 00	1982	5 00E+03		
25	1981	1808	1807 00	1983	1	2 50E+03	
26	1982	1807	1980 00	1984	1	5 00E+03	
27	1983	1980	1979 00	1	1	2 00E+04	
28	1984	1979	1978 00	1988	3 50E+04		
29	1813	1812	1981 00	1987	1	5 00E+03	

30	1988	1981	1982 00	1986	1	2 50E+03	
31	1987	1982	1983 00	1985	1	5 00E+03	
32	1986	1983	1984 00	1	1	2 00E+04	
33	1817	1813	1988 00	1989	5.00E+03		
34	1818	1817	1988 00	1990	1	5 00E+03	
35	1989	1988	1987.00	1991	1	2 50E+03	
36	1990	1987	1986.00	1992	1	5 00E+03	
37	1991	1986	1985 00	1996	1	2 00E+04	
38	1823	1818	1989 00	1995	1	5 00E+03	
39	1996	1985	1990.00	1	1	2 50E+03	
40	1995	1990	1991 00	1	5 00E+03		
41	1824	1823	1996.00	1997	5.00E+03		
42	1825	1824	1996.00	1998	1	5 00E+03	
43	1997	1996	1995.00	1934	1	2 50E+03	
44	1998	1995	1991.00	1993	1	5 00E+03	
45	1994	1991	1992.00	1999	1	2 00E+04	
46	1828	1825	1997 00	2000	1	5 00E+03	
47	1999	1997	1998 00	2001	1	2 50E+03	
48	2000	1998	1994.00	2002	1	5 00E+03	
49	2001	1994	1993 00	1	1	2 00E+04	
50	1829	1828	1999 00	1830	5.00E+03		
51	1829	1999	2000.00	1	1	2 50E+03	
52	1830	2000	2001.00	2004	5 00E+03		
53	1835	1830	2001 00	2003	1	5 00E+03	
54	2004	2001	2002.00	2005	1	2 00E+04	
55	1836	1835	2004.00	2006	1	5 00E+03	
56	2005	2004	2003 00	1	1	2 00E+04	
57	1843	1836	2005.00	2007	5 00E+03		
58	1844	1843	2005.00	2008	1	5 00E+03	
59	2007	2005	2006 00	2010	1	2 00E+04	
60	1850	1844	2007.00	2009	1	5 00E+03	
61	2010	2007	2008.00	1	1	2 00E+04	
62	1851	1850	2010 00	2011	5 00E+03		
63	1856	1851	2010 00	2012	1	5 00E+03	
64	2011	2010	2009 00	1	1	2 00E+04	
65	1857	1856	2011.00	2014	5 00E+03		
66	1860	1857	2011 00	2013	1	5 00E+03	
67	2014	2011	2012 00	1	1	2 00E+04	
68	1861	1860	2014 00	2015	5 00E+03		
69	1864	1861	2014 00	2016	1	5 00E+03	
70	2015	2014	2013 00	1	1	2 00E+04	

71	1865	1864	2015 00	2018	5 00E+03		
72	1868	1865	2015 00	2017	1	5 00E+03	
73	2018	2015	2016 00	1	1	2.00E+04	
74	1869	1868	2018 00	2019	5 00E+03		
75	1872	1869	2018 00	2020	1	5 00E+03	
76	2019	2018	2017.00	1	1	2 00E+04	
77	1873	1872	2019.00	2022	5 00E+03		
78	1876	1873	2019 00	1	1	5 00E+03	
79	2022	2019	2029.00	2021	2 00E+04		
80	2029	2019	2020.00	2023	1	2.00E+04	
81	1877	1876	2022.00	2030	1	5 00E+03	
82	2023	2022	2029.00	2025	1	3.50E+04	
83	2030	2029	2021.00	2024	1	3.50E+04	
84	1882	1877	2023.00	2031	1	5 00E+03	
85	2024	2023	2030.00	1	1	2 00E+04	
86	2031	2030	2025.00	1	2 00E+04		
87	1883	1882	2024.00	2027	5.00E+03		
88	1888	1883	2024.00	2032	1	5 00E+03	
89	2027	2024	2031.00	2026	1	2.00E+04	
90	2032	2031	2025.00	1	1	2.00E+04	
91	1889	1888	2027.00	2028	5.00E+03		
92	1892	1889	2027.00	2033	1	5.00E+03	
93	2028	2027	2032.00	2034	1	2.00E+04	
94	2033	2032	2026 00	1	1	2 00E+04	
95	1893	1892	2028.00	2037	5 00E+03		
96	1896	1893	2028.00	2036	1	5 00E+03	
97	2037	2028	2033.00	2035	1	2.00E+04	
98	2036	2033	2034 00	1	1	2.00E+04	
99	1897	1896	2037.00	2038	5.00E+03		
100	1955	1897	2037.00	2039	1	5 00E+C3	
101	2038	2037	2036.00	2040	1	2 00E+04	
102	2039	2036	2035.00	2068	1	2 00E+04	
103	1961	1955	2038 00	2041	1	5 00E+03	
104	2068	2038	2039 00	1	1	2 00E+04	
105	2041	2039	2040 00	2043	2 00E+04		
106	1962	1961	2068 00	2042	1	5 00E+03	
107	2043	2068	2041 00	2044	1	2 00E+04	
108	1905	1962	2043 00	2045	1	5 00E+03	
109	2044	2043	2042 00	1	1	2 00E+04	
110	1906	1905	2044 00	2049	5 00E+03		
111	1913	1906	2044 00	1915	1	5 00E+03	

112	1914	1913	2049 00	2048	1	5 00E+03	
113	1920	1915	2049 00	1	1	2 00E+04	
114	2049	2044	2048 00	2047	2 00E+04		
115	2048	2044	2045.00	2046	1	2 00E+04	
116	2047	2045	2042.00	2050	1	2.00E+04	
117	1921	1920	2048 00	2051	1	2 00E+04	
118	2050	2048	2047.00	2052	1	2 00E+04	
119	2051	2047	2046.00	2054	1	2.00E+04	
120	1926	1921	2050.00	2053	1	2.00E+04	
121	2054	2050	2051.00	1	1	2.00E+04	
122	2053	2051	2052.00	1	2.00E+04		
123	1927	1926	2054.00	1	2.00E+04		
124	1930	1927	2054.00	2055	2.00E+04		
125	1931	1930	2054.00	2056	1	2 00E+04	
126	2055	2054	2053.00	1	1	2.00E+04	
127	1934	1931	2055.00	2059	2 00E+04		
128	1935	1934	2055.00	2057	1	2.00E+04	
129	2059	2055	2056.00	1	1	2.00E+04	
130	1938	1935	2059.00	2060	2.00E+04		
131	1939	1938	2059.00	1	1	2.00E+04	
132	2060	2059	2061.00	1	2.00E+04		
133	2061	2059	2058.00	1	3.50E+04		
134	2059	2057	2058.00	2063	3.50E+04		
135	1942	1939	2060.00	2062	1	2 00E+04	
136	2063	2060	2061.00	1	1	2 00E+04	
137	1943	1942	2063.00	2064	2.00E+04		
138	1947	1943	2063 00	2065	1	2.00E+04	
139	2064	2063	2062.00	1	1	2 00E+04	
140	1948	1947	2064.00	2067	2 00E+04		
141	1952	1948	2064.00	2066	1	2.00E+04	
142	2067	2064	2065.00	1964	1	2 00E+04	
143	1779	1952	2067.00	2069	1	2 00E+04	
144	1964	2067	2066 00		1	2 00E+04	
6	85	1	3.00	0			
1	0	2 94E+04	0 00		0		
1 21E+11	0 258			1			
0	0	0	0 00	0			
0	0	0	0 00	0			
0	0	0	0 00	0			
0	0	0	0 00	1			
1	1965	2069	2071 00	2072	3 50E+04		

2	1968	1965	2071 00	2103	1	3 50E+04	
3	2072	2071	2102 00	1	1	3 50E+04	
4	2103	2102	2117 00	2073	3 50E+04		
5	1969	1968	2072 00	1	1	3 50E+04	
6	2073	2072	2103 00	2074	3 50E+04		
7	1972	1969	2073 00	2104	1	3 50E+04	
8	2074	2073	2103 00	2118	1	3 50E+04	
9	2104	2103	2117 00	2119	1	3 50E+04	
10	2118	2117	2122.00	2075	1	3 50E+04	
11	1973	1972	2074 00	1	1	3 50E+04	
12	2075	2074	2104.00	2076	3 50E+04		
13	1978	1973	2075 00	2105	1	3 50E+04	
14	2076	2075	2104 00	2106	1	3 50E+04	
15	2105	2104	2118 00	2107	1	3 50E+04	
16	2106	2118	2119 00	2077	1	3 50E+04	
17	1984	1978	2076 00	1	1	3 50E+04	
18	2077	2076	2105 00	2078	3 50E+04		
19	1985	1984	2077 00	2108	1	2 00E+04	
20	2078	2077	2105 00	2107	1	2 00E+04	
21	2108	2105	2106 00	2079	1	2 00E+04	
22	1992	1985	2078.00	1	1	2 00E+04	
23	2079	2078	2108 00	2080	2.00E+04		
24	1993	1992	2079 00	1	1	2 00E+04	
25	2080	2079	2108 00	1	2[illegible]+04		
26	1993	2080	2002 00	2081	2 00E+04		
27	2002	2080	2108 00	2109	1	2 00E+04	
28	2081	2108	2107.00	2082	1	2 00E+04	
29	2003	2002	2081 00	1	1	3 50E+04	
30	2082	2081	2109 00	1	3.50E+04		
31	2006	2003	2087 00	2083	3 50E+04		
32	2087	2003	2082 00	2110	1	3 50E+04	
33	2083	2082	2109 00	2119	1	3 50E+04	
34	2110	2109	2107 00	2009	1	3 50E+04	
35	2008	2006	2087 00	2012	1	3 50E+04	
36	2009	2087	2083 00	2084	1	3 50E+04	
37	2013	2012	2083 00	2111	1	3 50E+04	
38	2084	2083	2110 00	2120	1	3 50E+04	
39	2111	2110	2119 00	2085	1	3 50E+04	
40	2016	2013	2084 00	1	1	3.50E+04	
41	2085	2084	2111 00	1	3 50E+04		
42	2017	2016	2085 00	1	3 50E+04		

43	2020	2017	2085 00	2086	3 50E+04		
44	2021	2020	2085 00	2112	1	3 50E+04	
45	2086	2085	2111 00	1	1	3 50E+04	
46	2112	2111	2120.00	1	3 50E+04		
47	2021	2086	2025.00	1	3.50E+04		
48	2025	2086	2112 00	2113	3 50E+04		
49	2026	2025	2112 00	2121	1	3 50E+04	
50	2113	2112	2120 00	1	1	3 50E+04	
51	2034	2026	2113 00	2114	3.50E+04		
52	2035	2034	2113 00	1	1	3 50E+04	
53	2114	2113	2121.00	1	3 50E+04		
54	2040	2035	2114.00	2090	3.50E+04		
55	2046	2042	2041 00	2088	1	3 50E+04	
56	2090	2041	2040 00	2115	1	3 50E+04	
57	2088	2040	2114.00	1	1	3 50E+04	
58	2115	2114	2121 00	2091	3.50E+04		
59	2052	2046	2090.00	2089	1	3 50E+04	
60	2091	2090	2088 00	1	1	3 50E+04	
61	2089	2088	2115.00	2092	3 50E+04		
62	2053	2052	2091 00	2094	1	3 50E+04	
63	2092	2091	2089 00	2116	1	3 50E+04	
64	2094	2089	2115 00	2122	1	3 50E+04	
65	2116	2115	2121 00	2093	1	3 50E+04	
66	2056	2053	2092.00	1	1	3 50E+04	
67	2093	2092	2094 00	1	3.50E+04		
68	2057	2056	2093.00	2096	3 50E+04		
69	2058	2057	2093.00	2095	1	3 50E+04	
70	2096	2093	2094 00	1	1	3.50E+04	
71	2095	2094	2116.00	2097	3 50E+04		
72	2061	2058	2096.00	1	1	3 50E+04	
73	2097	2096	2095 00	2098	3 50E+04		
74	2062	2061	2097 00	2100	1	3 50E+04	
75	2098	2097	2095 00	1	1	3 50E+04	
76	2100	2095	2116 00	2099	3 50E+04		
77	2065	2062	2098 00	1	1	3 50E+04	
78	2099	2098	2100.00	2101	3 50E+04		
79	2066	2065	2099 00	2102	1	3 50E+04	
80	2101	2099	2100 00	2117	1	3 50E+04	
81	2102	2100	2116 00	1	1	3 50E+04	
82	2117	2116	2122 00	2071	3 50E+04		
83	2069	2066	2101 00	1	1	3 50E+04	

84	2071	2101	2102.00	2122	3 50E+04		
85	2119	2120	2121 00		1	3.50E+04	
1							
				0			
1	0	0	0 00		8 00E+14		
0	0	0					

REFERENCES

Agrawal, D.P. (1985) Cenozoic climatic changes in Kashmir: The multidisciplinary data. In: **Climate and Geology of Kashmir** (Agrawal, D.P., Kusumgar, S., and Krishnamurthy, R.V., eds.), Today and Tomorrow, New Delhi, 1-12.

Agrawal, D.P., Dodia, B.S., Kottla, B.S., Razdan, H., and Sahni, A. (1989) The Plio-Pleistocene geologic and climatic record of the Kashmir valley, India: A review and new data. **Palaeogeography, Palaeoclimatology, Palaeoecology 73**, 267-286.

Ambrose, S.H. and Sikes, N.E. (1991) Soil carbon isotope evidence for Holocene habitat change in the Kenya Rift Valley. **Science 253**, 1402-1405.

An, Z.S. and Wei, L.Y. (1980) The fifth layer paleosol in the Lishi loess and its paleoclimatic significance. **Acta Pedological Sinica 17**, 1-12 (in Chinese).

An, Z.S., Kukla, G.J., Porter, S.C., and Xiao, J.L. (1991) Magnetic susceptibility evidence of monsoon variation on the loess plateau of central China during the last 130,000 years. **Quaternary Research 36**, 29-36.

An, Z.S., Porter, S.C., Zhou, W.J., Lu, Y.C., Donahue, D.J., Head, M.J., Wu, X.H., Ren, J.Z., and Zheng H.B. (1993) Episode of strengthened summer monsoon climate of Younger Dryas age on the loess plateau of central China. **Quaternary Research 39**, 45-54.

Anderson, D.L. (1989) **Theory of the Earth**. Blackwell Scientific Publications.

Anderson, J.G. (1923) Essays on the Cenozoic of Northern China. **Memoirs of Geological Survey of China Series A 3**, 1-52.

Andrews, J.T. (1992) A case of missing water. **Nature 358**, pp281.

Bake, V.R. (1983) Late-Pleistocene fluvial system. In: Porter, S.C. (ed), **Late Quaternary Environments of the United States**, Minneapolis, University of Minnesota Press, **1**, 115-129.

Baker, E.T., Levelle, J.W., Feely, R.A., Massoth, G.J., Walker, S.L., and Lupton, J.E. (1989) Episodic venting of hydrothermal fluids from the Juan de Fuca Ridge. **Journal of Geophysical Research, 94**, 9237

Balesdent, J., Mariotti, A., and Guillet, B. (1987) Natural ^{13}C abundance as a tracer for studies of soil organic matter dynamics. **Soil Biology and Biochemistry 19**, 25-30.

Barnett, T.P., Dumenil, L., Schlese, U., Roeckner, E., and Latif, M. (1991) The Asian snow cover-monsoon-ENSO connection. In: **Teleconnections Linking Worldwide Climate Anomalies: Scientific Basis and Societal Impact**. Cambridge University Press, 101-225.

Barnola, J.M., Raynaud, D., Korotkevich, Y.S., and Lorius, C. (1987) Vostok ice core provides 160,000-year record of atmospheric CO^2. **Nature, 329**, 408-414.

Barrell, J. (1919a) The nature and bearings of isostasy. **American Journal of Science, 48**, 281-290.

Barrell, J. (1919b) The status of the theory of isostasy. **American Journal of Science, 48**, 291-338.

Barron, V. and Torrent, J. (1986) Use of the Kubelka-Munk theory to study the influence of iron oxides on soil colour. **Journal of Soil Science 37**, 499-510.

Becker-Heidmann, P. and Scharpenseel, H-W. (1986) Thin layer $\delta^{13}C$ and $D^{14}C$ monitoring of "lessive" soil profiles. **Radiocarbon 28**, 383-390.

Beer, J., Shen, C.D., Heller, F., Liu, T.S., Bonani, G., Dittrich, B., Suter, M., Kubik, P.W. (1993) ^{10}Be and magnetic susceptibility in Chinese loess. **Geophysical Research Letter 20**, 57-60.

Begin, Y., Berube, D., and Gregoire, M. (1993) Downward migration of coastal conifers as a response to recent land emergence in east Hudson Bay, Quebec. **Quaternary Research, 40**, 81-88.

Bender, M.M. (1971) Variations in the $^{13}C/^{12}C$ ratios of plants in relation to the pathway of photosynthetic carbon dioxide fixation. **Photochemistry 10**, 1239-1244.

Bender, M.M., Rouhani, I., Vines, H.M., and Black, C.C. (1973) $^{13}C/^{12}C$ ratio changes in crassulacean acid metabolism. **Plant Physiology 52**, 427-430.

Berger, A.L. (1976) Obliquity and procession for the last 5,000,000 years. **Astronomy and Astrophysics, 51**, 127-135.

Berger, A.L. (1984) Accuracy and frequency stability of the earth's orbital elements during the Quaternary. In: Berger, A.L., Imbrie, J., Hays, J., Kukla, G. and Saltzman, B. (eds.), **Milankovitch and Climate**, Boston: D. Reidel, 3-39.

Berger, A. and Loutre, M.F. (1991) Insolation values for the climate of the last 10 million years. **Quaternary Science Review, 10**, 297-317.

Berger, A.L., Imbrie., J., Hays, J., Kukla, G., and Saltzman, B. (1984) **Milankovitch and Climate** (eds). Boston, D. Reidel.

Berger, W.H., Killingly, J.S. and Vincent, E. (1987) Time scale of the Wisconsin/Holocene transition: Oxygen isotope record in the western equatorial Pacific.

Quaternary Research, 28, 295-306.

Bergman, E.A. and Solomon, S.C. (1990) Earthquake swarms on the Mid-Atlantic Ridge: Products of magmatism or extensional tectonics? **Journal of Geophysical Research, 95**, 4943-4965.

Enatia, T.T. and Kapoor, K.C. (1982) Petrographic and sedimentation of Siwalik Arenites of Panjab and Himachal Padesh. In: **Recent Researches of Geology 8** (Kupta, V.J., ed.), Hindustan Publishing Corp., 188-195.

Birchfield, G.E. (1985) Ice sheet dynamics and the Pleistocene ice ages. In: Nicolis, C. and Nicolis, G. (eds.), **Irreversible Phenomena and Dynamical Systems Analysis in Geosciences**, 381-398.

Birchfield, G.E., Weertman, J. and Lunde, A.T. (1981) A paleo-climate model of Northern Hemisphere ice sheets **Quaternary Research, 15**, 126-142.

Birkeland, P.W. (1974) **Pedology, Weathering, and Geomorphological Research**. Oxford University Press, Inc. 103-124.

Blanchon, P. and Shaw, J. (1995) Reef drowning during the last deglaciation: evidence for catastrophic sea-level rise and ice-sheet collapse. **Geology, 23**, 4-8.

Blum, J.D. and Erel, Y. (1995) A silicate weathering mechanism linking increases in marine $^{87}Sr/^{86}Sr$ with global glaciation. **Nature, 373**, 415-418.

Blumenthal, M.B. (1990) Effects on west African air humidity on Atlantic sea surface temperature. In: **Greenhouse Effect, Sea Level and Drought**, Klumer, 21-40.

Bond, G., Heinrich, H., Broecker, W., Labeyrie, L., McManus, J., Andrews, J., Huon, S., Jantschik, R., Clasen, S., Simet, C., Tedesco, K., Klas, M., Bonan, G., and Ivy, S. (1992) Evidence for massive discharges of icebergs into the North Atlantic ocean during the last glacial period. **Nature, 360**, 245-249.

Boyle, E.A. (1988) Cadmium chemical tracer of deepwater. **Paleoceanography, 3(4)**, 471-489.

Boyle, E.A. (1988a) The role of vertical chemical fractionation in controlling late Quaternary atmospheric carbon dioxide. **Journal of Geophysical Research, 93**, 15701-15714.

Boyle, E.A. and Keigwin, L. (1985/1986) Comparison of Atlantic and Pacific paleochemical records for the last 215,000 years: changes in deep ocean circulation and chemical inventories. **Earth and Planetary Science Letters 76**, 135-150.

Boyle, E.A. and Keigwin, L. (1987) North Atlantic thermohaline circulation during the past 20,000 years linked to high latitude surface temperature. **Nature, 330**, 35-40.

Broccoli, A.J. and Manabe, S. (1987) The influence of continental ice, atmospheric CO_2 and land albedo on the climate of the last glacial maximum. **Climate Dynamics, 1**, 87-99.

Broecker, W.S. (1994) Massive iceberg discharges as triggers for global climate change. **Nature, 372**, 421-424.

Broecker, W.S. and van Donk. J. (1970) Insolation changes, ice volumes and the O^{18} record in deep-sea cores. **Reviews of Geophysics and Space Physics 8**, 169-197.

Broecker, W.S. and Denton, G.H. (1990) The role of ocean-atmosphere reorganizations in glacial cycles. **Quaternary Science Reviews, 9**, 305-341.

Broecker, W.S., Peng, T.-H., Jouzel, J. and Russell, G. (1990) The magnitude of global fresh-water transports of importance to ocean circulation. **Climate Dynamics, 4**, 73-79.

Browning, K. (1992) Clouding: The issue. **Science and Present Affairs, Spring 1992**, 35-42.

Burbank, D.W., Derry, L.A., and France-Lanord, C. (1993) Reduced Himalayan sediment production 8 Myr ago despite an intensified monsoon. **Nature, 364**, 48-50.

Calhoun, E.A. (1985) Glaciations of the West Coast Range, Tasmania. **Quaternary Research, 24**, 39-59.

Cannat, M. (1993) Emplacement of mantle rocks in the seafloor at mid-ocean ridges. **Journal of Geophysical Research, 98(B3)**, 4163-4172

Cao, B.X., Liu, S.R., Zhao, B.Y., and Guan, K.N. (1966) A primary study of the Cenozoic in You-he region, Weinan, Shaanxi. In: **Proceedings of Symposium on the Cenozoic of Lantian, Shaanxi.** Science Press (in Chinese), 121-124.

Catt, J.A. (1990) Paleopedology manual, chapter 1. **Quaternary International 6**, 2-20.

Cerling, T.E. and Hay, R.L. (1986) An isotopic study of paleosol carbonates from Olduvai Gorge. **Quaternary Research 25**, 63-78.

Cerling, T.E., Quade, J., Wang, Y., and Bowman, J.R. (1989) Carbon isotopes in soils and palaeosols as ecology and palaeoecology indicators. **Nature 341**, 138-139.

Cerling, T.E., Wang, Y., and Quade, J. (1993) Expansion of C4 ecosystems as an indicator of global ecological change in the late Miocene. **Nature 361**, 344-345.

Chappell, J. and Shackleton, N.J. (1986) Oxygen isotopes and sea level. **Nature, 324**, 137-140.

Chappellaz, J., Barnola, J.M., Raynaud, D., Korotkevich, Y.S. and Lorius, C. (1990) Ice-core record of atmospheric methane over the past 160,000 years. **Nature, 345**, 127-131.

Chaudhri, R.S. (1982) Petrology of the Siwalik Group of Nepal Himalaya. In: **Recent Researches of Geology 8** (Kupta, V.J., ed.), 424-468. Hindustan Publishing Corp.

Chen, X. (1994) Stratigraphy and large mammals of the "Jinglean" stage, Shanxi, China. **Quaternary Sciences 1994 (4)**, 339-353.

China Map Press (1984) Vegetations in China. *In* "**Atlas of the People's Republic of China**", pp.15, China Map Press, Beijing, China (in Chinese).

Chinese Academy of Geology (1974) **Atlas of Provincial Geological Map of the People's Republic of China**. China Geological Map Press (in Chinese).

Clemens, S.C., Farrell, J.W., and Gromet, L.P. (1993) Synchronous changes in seawater strontium isotope composition and global climate. **Nature, 363**, 607-610.

CLIMAP Project Members (1981) Seasonal reconstruction of the Earth's surface at the last glacial maximum. **Geological Society of America, Map and Chart Series 36.**

Clough, R.W. and Filippa, C.A. (1968) A refined quadrilateral element for analysis of plate bending. **Proc. 2nd Conf. on Matrix Methods in Structural Mechanics, Wright Patterson, AFB, OH**.

Coblentz, D.D. and Sandiford, M. (1994) Tectonic stresses in the African plate: constraints on the ambient lithospheric stress state. **Geology, 22**, 831-834.

Coleman, M. and Hodges, K. (1995) Evidence for Tibetan plateau uplift before 14 Myr ago from a new minimum age for east-west extension. **Nature, 374**, 49-52.

Colhoun, E.A., Mabin, M.C.G., Adamson, D.A., and Kirk, R.M. (1992) Antarctic ice volume and contribution to sea-level fall at 20,000 yr BP from raised beaches. **Nature 358**, 316-319.

Craig, H. (1957) Isotopic standards for carbon and oxygen and correction factors for mass-spectrometric analysis of carbon dioxide. **Geochimica et Cosmochimica Acta 12**, 133-149.

Croll, J. (1875) **Climate and Time**. New York, Appleton and Co., 388p.

Crowley, T.J. and Kim, K.-Y. (1994) Milankovitch forcing of the last interglacial sea level. **Science, 265**, 1566-1568.

Cui, Z.J. and Zheng, B.X. (1975) Scientific Expedition Report on the Mt. Everest Region: **Modern Glaciers and Geomorphology**. 169-179. Science Press, Beijing.

Dansgaard, W. and Oeschger, H. (1985) Past Environmental long-term records from the Arctic. In: Oeschger, H. and Langway, C.C.Jr. (eds.), **The Environmental Record in Glaciers and Ice Sheets**, 287-318. John Wiley & Sons.

Dansgaard, W., White, J.W.C and Johnson, S.J. (1989) The abrupt termination of the Younger Dryas climate event. **Nature, 339**, 532-533.

De Decker, P., Correge, T. and Head, J. (1991) Late Pleistocene record of cyclic eolian activity from tropical Australia suggesting the Younger Dryas is not an unusual climatic event. **Geology, 19**, 602-605.

Deines, P. (1980) The isotopic composition of reduced organic carbon. *In* "**Handbook of Environmental Isotope Geochemistry; 1. The Terrestrial Environment**" (A.P. Fritz and J.Ch. Fontes, Eds.), Elsevier, Amsterdam, 329-406.

DeLaune, R.D. (1986) The use of $\delta^{13}C$ signature of C-3 and C-4 plants in determining past depositional environments in rapidly accreting marshes of the Mississippi river deltaic plain, Louisiana, U.S.A. **Chemical Geology (Isotope Geoscience Section) 59**, 315-320.

Denton, G.H. and Hughes, T.J. (1981) **The Last Great Ice Sheets** (eds.). John Wiley & Sons, New York.

Denton, G.H. and Hughes, T.J. (1983) Milankovitch theory of ice ages: Hypothesis of ice-sheet linkage between regional insolation and global climate. **Quaternary Research, 20**, 125-144.

Denton, G.H., Hughes, T.J. and Karlen, W. (1986) Global ice-sheet system interlocked by sea level. **Quaternary Research, 26**, 3-26.

Detrick, R.S., Buhl, P., Vera, E., Mutter, J., Orcutt, J., Madsen, J., and Brocher, T. (1987) Multichannel seismic imaging of a crustal magma chamber along the East Pacific Rise between 9°N and 13°N. **Nature, 326**, 35-41.

Detrick, R.S., Mutter, J.C., Buhl, P., and Kim, I.I. (1990) No evidence from multichannel reflection data for a crustal magma chamber in the MARK area on the Mid-Atlantic Ridge. **Nature, 347**, 61-63.

Dia, A.N., Cohen, A.S., O'Nions, R.K., and Shackleton, N.J. (1992) Seawater Sr isotope variation over the past 300 kyr and influence of global climate cycles. **Nature, 356**, 786-788.

Ding, Z.L. (1988) Investigation and division of pedostratigraphy and climatostratigraphy on the China loess. Ph.D. Thesis. Institute of Geology, Chinese Academy of Sciences, Beijing.

Ding, Z.L., Liu, T.S., Liu, X.M., Chen, M.Y., and An, Z.S. (1990) Thirty-seven climatic cycles in the last 2.5 Ma. **Chinese Science Bulletin 35**, 667-671.

Ding, Z.L., Rutter, N., Liu, T.S., Evans, M.E., and Wang, Y. (1991) Climatic correlation between Chinese loess and deep-sea cores: A structural approach. In: **Loess, Environment and Global Change** (Liu, T.S., ed.), Science Press, Beijing, China. 168-186.

Ding, Z.L., Rutter, N., Han, J., and Liu, T.S. (1992) A coupled environmental system formed at about 2.5 Ma in East Asia. **Palaeogeography, Palaeoclimatology, Palaeoecology 94**, 223-242.

Dorn, R.I., DeNiro, M.J., and Ajie, H.O. (1987) Isotopic evidence for climatic influence on alluvial-fan development in Death Valley, California. **Geology 15**, 108-110.

Dreimanis, A. (1962) Quantitative gasometric determination of calcite and dolomite by using chittick apparatus. **Journal of Sedimentary Petrology 32**, 520-529.

Duplessy, J.C., Shackleton, N.J., Fairbank, R.G., Labeyrie, L., Oppo, D. and Kallel, N. (1988) Deepwater source variations during the last climatic cycle and their impact on the global deepwater circulation. **Paleoceanography, 3(3)**, 343-360.

Edmond, J.M. (1992) Himalayan tectonics, weathering processes, and the strontium isotope record in marine limestones. **Science, 258**, 1594-1597.

Emiliani, C. (1955) Pleistocene temperatures. **Journal of Geology, 63**, 538-578.

Erickson, S.G. (1993) Sedimentary loading, lithospheric flexure, and subduction initiation at passive margins. **Geology, 21**, 125-128.

Evans, L.J. (1992) Alteration products at the earth's surface-- the clay minerals. In: **Weathering, Soils & Paleosols** (Martini, I.P. and Chesworth, W. eds.), Chapter 5, Elsevier Science Publishers B.V., Amterdam. 107-125.

Evans, M.E., Wang, Y., Rutter, N., and Ding, Z. (1991) Preliminary magnetostratigraphy of the red clay underlying the loess sequence at Baoji, China. **Geophysical Research Letters 18**, 1409-1412.

Fægri, K. and Iversen, J. (1989) **Textbook of Pollen Analysis**, IV Edition. John Willey & Sons, Chichester. 1-163.

Faure, G. (1986) **Principles of Isotope Geology, 2nd Ed**. New York; Toronto, Wiley. 183-238.

Fichefet, T., Hovine, S., and Duplessy, J.C. (1994) A model study of the Atlantic thermohaline circulation during the last glacial maximum. **Nature, 372**, 252-255.

First Institute of Oceanography, State Oceanic Administration. (1984) **Topographic Map of Bohai and Huanghai Seas**, China Map Press, Shanghai.

Flint, R.F. (1971) **Glacial and Quaternary Geology**. John Wiley and Sons, New York.

Froelich, P.N. (1993) Ruling in the improbable. **Nature, 363**, 585-587.

Gardner, R and Pye, K. (1981) Nature, origin and paleoenvironmental significance of red coastal and desert dune sands. **Progress in Physical Geography 5**, 514-534.

Garrett, W.E. (1985) **Earth's Dynamic Crust** (ed.). The Cartographic Division, National Geographic Society, Washington, D.C.

Goodfriend, G.A. (1990) Rainfall in the Negev Desert during the middle Holocene, based on ^{13}C of organic matter in land snail shells. **Quaternary Research 34**, 186-197.

Guillet, B. and Souchier, B. (1982) Amorphous and crystalline oxyhydroxides and oxides in soils (iron, aluminium, manganese, silicon). In: Bonneau, M. and Souchier, B. (eds.), **Constituents and Properties of Soils** (tran. Farmer, V.C.), Academic Press, London. 21-42.

Guillet, B., Faivre, P., Mariotti, A., and Khobzi, J. (1988) The ^{14}C dates and $^{13}C/^{12}C$ ratios of soil organic matter as a means of studying the past vegetation in intertropical regions: examples from Colombia (South America). **Palaeogeography, Palaeoclimatology, Palaeoecology 65**, 51-58.

Guo, Z.T., Fedoroff, N., and An, Z.S. (1991) Genetic types of the Holocene soil and the Pleistocene paleosols in the Xifeng loess section in central China. In: Liu, T.S. (ed.) **Loess, Environment and Global Change**. 93-111. Science Press, Beijing, China.

Guo, Z.T., Liu, T.S., and An, Z.S. (1994) Paleosols of the last 0.15 Ma in the Weinan loess section and their paleoclimatic significance. **Quaternary Sciences 1994(3)**, 256-269 (in Chinese with English abstract).

Hammer, C.U. Clausen, H.B., Dansgaard, W., Neftel, A., Kristinsdottir, P., and Johnson, E. (1985) Continuous impurity analysis along the Dye 3 deep core. In: Langway, C.C., Oeschger, H., and Dansgaard, W. (eds.), **Greenland Ice Core: Geophysics, Geochemistry and the Environment, Amer. Geophys. Union Mon., 33**, 90-94.

Han, J. (1987) A study of the loess in Penglai District, Shandong Province. In: **Aspects of Loess Research** (Liu, T.S., ed.), China Ocean Press, Beijing. 76-84.

Han, J. (1988a) Sporopollen assemblage features of some sections in Mt. Naimona'nyi region and their paleogeographic significance. In: **Proceedings of Sino-Japanese Joint Scientific Symposium on Tibetan Plateau Vol.I** (Shidei, T., ed.). Kyoto, Japan. 23-37.

Han, J. (1988b) A preliminary study on clay minerals of Quaternary sediments in Mt. Naimonan'yi region. In: **Proceedings of Sino-Japanese Joint Scientific Symposium on Tibetan Plateau Vol.I** (Shidei, T., ed.), Kyoto, Japan. 13-22.

Harding, A.J., Orcutt, J.A., Kappus, M.E., Vera, E.E., Mutter, J.C., Buhl, P., Detrick, R.S., and Brocher, T.M. (1989) Structure of young oceanic crust at 13°N on the East Pacific Rise from expanding spread profiles. **Journal of Geophysical Research, 94**, 12163-12196.

Harrison, T.M., Copeland, P., Kidd, W.S.F., and Yin, A. (1992) Raising Tibet. **Science, 255**, 1663-1670.

Haskell, N.A. (1935) The motion of a viscous fluid under a surface load. **Physics, 6**, 265-269.

Haskell, N.A. (1936) The motion of a viscous fluid under a surface load. 2. **Physics, 7**, 56-61.

Hattersley, P.W. (1983) The distribution of C3 and C4 grasses in Australia in relation to climate. **Oecologia (Berlin) 57**, 113-128.

Hays, J.D., Imbrie, J., and Shackleton, N.J. (1976) Variations in the Earth's orbit: pacemaker of the ice ages. **Science, 194**, 1121-1132.

He, P.Y., Liu, L.S., and Yu, Q.H. (1984) Approach on the age and environmental change of the "Sanmen Sequence" from the Dongpogou Section of Sanmen Gorge. **Geological Reviews 30(2)**. (in Chinese).

Heezen, B.C. and Tharp, M. (1970) **Major Topographic Division of the Continental Margins**. Source of Data: Office of the Geographer, Department of State.

Heller, F. and Liu, T.S. (1982) Magnetostratigraphical dating of loess deposits in China. **Nature, 300**, 431-433.

Heller, F. and Liu, T.S. (1984) Magnetism of Chinese loess deposits. **Geophysical Journal of the Royal Astronomical Society 77**, 125-141.

Heller, F. and Liu, T.S. (1986) Paleoclimatic and sedimentary history from magnetic susceptibility of loess in China. **Geophysical Research Letters 13**, 1169-1172.

Heller, F., Meili, B., Wang, J.D., Li, H.M., and Liu, T.S. (1987) Magnetization and sedimentation history of loess in the central Loess Plateau of China. In: **Aspects of Loess**

Research (Liu, T.S. ed.), China Ocean Press, Beijing. 147-163.

Heller, F., Shen, C.D., Beer, J., Liu, X.M., Liu, T.S., Bronger, A., Suter, M., and Bonani, G. (1993) Quantitative estimates of pedogenic ferromagnetic mineral formation in Chinese loess and palaeoclimatic implications. **Earth and Planetary Science Letters 114**, 385-390.

Heller, F. and Evans, M.E. (1995) Loess magnetism. **Reviews of Geophysics 33**(2), 211-240

Hou, X.Y. (1979) **Vegetation Map of China**. Institute of Botany, Academia Sinica (ed.). Map Publisher of China, Beijing.

Houghton, J. (1991) The predictability of weather and climate. **Philosophical Transaction of the R. Society of London A 337**, 521-572.

Hsu, J. (1978) On the paleobotanical evidence for continental drift and Himalayan uplift. **Paleobotany 25**, 131-142.

Hsu, J., Tao, J.Y., and Sun, X.J. (1973) On the discovery of *Quercus Semicarpifolia* bed in Mount Shisha Pangma and its significance in botany and geology. **Acta Botanica Sinica 15(1)**, 103-119.

Huang, P.Y., Solomon, S.C., Bergman, E.A., and Nabelek, J.L. (1986) Focal depths and mechanisms of Mid-Atlantic Ridge earthquakes from body waveform inversion. **Journal of Geophysical Research, 91**, 579-598.

Huang, S.S., Yang, X.Q., and Xie, Q. (1992) the effects of the arctic sea ice on the variations of atmospheric general circulation and climate. **Acta Meteorologica Sinica 6**, 1-14.

Hughes, T. (1987) Ice dynamics and deglaciation models when ice sheets collapsed. In Ruddiman, W.F., and Wright, H.E.,Jr., (eds), **North America and Adjacent Oceans during the Last Deglaciation, The Geology of North America, K-3**, 183-220.

Hughes, T.J., Denton, G.H., Andersen, B.G., Schilling, D.H., Fastook, J.L., and Lingle, G.S. (1981) The last great ice sheets: a global view. In: Denton, G.H. and Hughes, T.J. (eds.), **The Last Great Ice Sheets**, John Wiley & Sons, New York. 263-317.

Hyde, W.T. and Peltier, W.R. (1985) Sensitivity experiments with a model of the ice age cycle: the response to harmonic forcing. **Journal of Atmospheric Science 42**, 2170-2188.

Imbrie, J. (1985) A theoretical framework for the Pleistocene ice ages. **Journal of Geological Society (London), 142**, 417-432.

Imbrie, J. and Imbrie, K.P. (1979) **Ice Ages**. Enslow Publishers, Short Hills, New Jersey, 61-161.

Imbrie, J. and Imbrie, J.Z. (1980) Modelling the climatic response to orbital variations. **Science, 207**, 943-953.

Imbrie, J., Hays, J.D., Martinson, D., McIntyre, A., Mix, A., Morley, J., Pisias, N., Prell, W., and Shackleton, N.J. (1984) The orbital theory of Pleistocene climate: support from a revised chronology of marine $\delta^{18}O$ record. In: Berger, A.L., Imbrie, J., Hays, J., Kukla, G. and Saltzman, B. (eds), **Milankovitch and Climate**, Boston, D. Reidel. 269-305.

Institute of Botany, Academia Sinica (1960) **Vegetational Distribution Divisions of China**. Science Press, Beijing, (in Chinese). 7-55.

Ji, H.X., Huang, W.P., Chen W.Y., Wu, Q.Q., and Zheng, S.H. (1981) The discovery of the Hipparion faunas in Tibet and its significance on the problem of the uplift of the Plateau. In: **Studies on the Period, Amplitude and Type of the Uplift of the Tibetan Plateau** (CSEQXP, Academia Sinica, eds.), 19-25. Science Press, Beijing.

Jouzel, J., Barkov, N.I., Barnola, J.M., Genson, C., Korotkevitch, Y.S., Kotlyakov, V.M., Legrand, M., Lorius, C., Petit, J.P., Petrov, V.N., Raisbeck, G., Raynaud, D., Ritz, C. and Yiou, F. (1989) Global change over the last climatic cycle from the Vostok ice core record (Antarctica). **Quaternary International, 2**, 15-24.

Jouzel, J., Lorius, C., Petit, J.R., Genthon, C., Barkov, N.I., Kotlyakov, V.M. and Petrov, √.M. (1987) Vostok ice core: A continuous isotope temperature record over the last climatic cycle (160,000 years) **Nature, 329**, 403-408.

Judson, S., Kauffman, M.E., and Leet, L.D. (1987) **Physical Geology Seventh Edition**, Prentice-Hall, Inc., Englewood Cliffs, New Jersey. 1-484.

Karson, J.A., Thompson, G., Humphries, S.E., Edmond, J.M., Bryan, W.B., Brown, J.R., Winters, A.T., Pockalny, R.A., Casey, J.F., Campbell, A.C., Klinkhammer, G., Palmer, M.R., Kinzler, R.J., and Sulanowska, M.M. (1987) Along axis variations in seafloor spreading in the MARK area. **Nature, 328**, 681-685.

Keeling, C.D., Mook, W.G. and Tans, P.P. (1979) Recent trends in the $^{13}C/^{12}C$ ratio of atmospheric carbon dioxide. **Nature 277**, 121-123.

Kemp, R.A. (1985) The cause of redness in some buried and non-buried soils in eastern England. **Journal of Soil Science 36**, 329-334.

Kong, L.S., Solomon, S.C., and Purdy, G.M. (1992) Microearthquake characteristics of a mid-ocean ridge along-axis high. **Journal of Geophysical Research, 97**, 1659-1685.

Krishnamurthy, R.V., DeNiro, M.J., and Pant, R.K. (1982) Isotope evidence for Pleistocene climatic changes in Kashmir, India. **Nature 298**, 640-641.

Krishnamurthy, R.V. and Bhattacharya, S.K. (1989) Paleovegetational history in the Kashmir basin, India, derived from $^{13}C/^{12}C$ ratio in paleosols. **Earth and Planetary Science Letters 95**, 291-296.

Kudrass, R.H., Erlenkeuser, H., Vollbrech, R. and Weiss, W. (1991) Global nature of the Younger Dryas cooling event inferred from oxygen isotope data from Sulu Sea cores. **Nature, 349**, 406-408.

Kukla, G. (1987) Loess stratigraphy in central China. **Quaternary Science Reviews 6**, 191-219.

Kukla, G., Heller, F., Liu, X.M., Xu, T.C., Liu, T.C., and An, Z.S. (1988) Climates in China dated by magnetic susceptibility. **Geology 16**, 811-814.

Kukla, G. and An, Z. (1989) Loess stratigraphy in Central China. **Paleogeography Paleoclimatology Paleoecology 72**, 203-225.

Kutzbach, J.E. and Guetter, P.J. (1986) The influence of changing orbital parameters and surface boundary conditions on climate simulations for the past 18,000 years. **Journal of Atmospheric Science 43**, 1726-1759.

Kutzbach, J.E., Guetter, P.J., Behling, P.J., and Selin, R. (1993) Simulated climatic changes: Results of the COHMAP climate-model experiments. In: **Global Climates Since the Last Glacial Maximum** (Wright, H.E.Jr., Kutzbach, J.E., Webb III, T., Ruddiman, W.F., Street-Perrott, F.A., and Bartlein. P.J., eds.), University of Minnesota Press, Minneapolis, London. 24-93.

Lamb, H.H. (1972) **Climate: Present, Past and Future**. Vol. 1. Methuan & Co., London.

Ladyman, S.J. and Harkness,D.D. (1980) Carbon isotope measurement as an index of soil development. **Radiocarbon 22**, 885-891.

Larson, R.L. (1991) Latest pulse of Earth: Evidence for a mid-Cretaceous superplume. **Geology, 19**, 547-550.

Larson, R.L. and Olson, P. (1991) Mantle plumes control magnetic reversal frequency. **Earth and Planetary Science Letters, 107**, 437-447.

Legrand, M.R., Delmas, R.J. and Charlson, R.J. (1988) Climate forcing implications from Vostok ice-core sulphate data. **Nature, 334**, 418-420.

Lehman, S.J. and Keigwin, L.D. (1992) Sudden changes in North Atlantic circulation during the last deglaciation. **Nature, 356**, 757-762.

Leavitt, S.W., and Long, A. (1982) Evidence for $^{13}C/^{12}C$ fractionation between tree leaves and wood. **Nature 298**, 742-744.

Li, C.K., Wu, W.Y., and Qiu, Z.D. (1984) A preliminary subdivision and comparison of the Neogene terrestrial deposits in China. **Vertebrate Paleontology Sinica 22**, 163-178. (in Chinese).

Li, J.J., Wen, S.X., Zhang, Q.S., Wang, F.B., Zheng, B.X., and Li, B.Y. (1979) The age, amplitude and type of the Qinghai-Xizang Plateau uplift. **Scientia Sinica 6**, 608-616.

Li, W.Y. (1983) Sporopollen assemblages from some localities of southern Qinghai-Xizang Plateau in the Pliocene and their paleogeographic significance. In: **Quaternary Geology in Xizang** (Tibet), Science Press, Beijing. 162-178.

Li, W.Y. (1985) Studies on vegetation and paleogeography from late Tertiary to early Quaternary in China. **Quaternaria Sinica 6(2)**, 77-82.

Lin, B., Liu, R., and An, Z. (1991) Preliminary research on stable isotopic compositions of Chinese loess. *In* "**Loess, Environment and Global Change**" (Liu, T.S., Ed.), Science Press, Beijing, China. 124-131.

Linsley, B.K. and Thunell, R.C. (1990) The record of deglaciation in the Sulu Sea: Evidence for the Younger Dryas event in the tropical western Pacific. **Paleoceanography** 5, 1025-1039.

Liu, J.Q., Chen, T.M., Nie, G.Z., Song, C.Y., Guo, Z.T., Li, K., Gao, S.J., Qiao, Y.L., and Ma, Z.B. (1994) Datings and reconstruction of the high resolution time series in the Weinan loess section of the last 150000 years. **Quaternary Sciences 1994(3)**, 193-202 (in Chinese with English Abstract).

Liu, T.S. (1959) Younger loess and older loess. **Journal of Geology 5**, 22-25 (in Chinese).

Liu, T.S. (1964) **The Loess along the Middle Reaches of the Huanghe (Yellow) River**. Science Press, Beijing (in Chinese).

Liu, T.S. (1965) **The Loess Deposits of China**. Science Press, Beijing (in Chinese).

Liu, T.S. (1966) **The Composition and Texture of Loess**. Science Press, Beijing (in Chinese).

Liu, T.S. Chen, M.Y., and Li, X.F. (1981) A satellite images study on the dust storm at Beijing on April 17-21, 1980. In: **Quaternary Geology and Environment of China** (Liu, T.S. ed.), China Ocean Press, Beijing, 48-52.

Liu, T.S. and Yuan, B.Y. (1982) Quaternary climatic fluctuation: A correlation of records in loess with that of deep sea core V28-238. In: **Geological Research 1** (Institute of Geology, Academia Sinica ed.), Science Press, Beijing. 93-101.

Liu, T.S. (1985) **Loess and the Environment**. China Science Press (in Chinese).

Liu, T.S. (1987) **Aspects of Loess Research (ed.)**. China Ocean Press, Beijing.

Liu, T.S. and Yuan, B.Y. (1987) Paleoclimatic cycles in northern China: Luochuan loess section and its environmental implications. In: **Aspects of Loess Research** (Liu, T.S. ed.). China Ocean Press, Beijing. 3-26.

Liu, T.S. and Han, J. (1988) The role of Qinghai-Xizang Plateau uplift in the shift of the monsoon patterns over China. In: **Proceedings of Sino-Japanese Joint Scientific Symposium on Tibetan Plateau Vol.I** (Shidei, T., ed.), Kyoto, Japan. 39-48.

Liu, T.S. (1991) **Loess, Environment and Global Change** (ed.) Science Press, Beijing, China.

Liu, T.S., Ding, Z.L., Chen, M.Y., and An, Z.S. (1989) The global surface energy system and the geological role of wind stress. **Quaternary International, 2**, 43-54.

Liu, T.S., Ding, Z.L., Yu, Z., and Rutter, N. (1993) Susceptibility time series of the Baoji section and the bearings on paleoclimatic periodicities in the last 2.5 Ma. **Quaternary International, 17**, 33-38.

Liu, W.M. (1990) SSIAP-A computer program for static and dynamic soil-structure interaction analysis. Unpublished technical report.

Liu, X.M., Liu, T.S., Xu, T.C., Liu, C., and Chen, M.Y. (1988) The primary study on magnetostratigraphy of a loess profile in Xifeng area, Gansu province. **Geophysical Journal of the Royal Astronomical Society 92**, 345-348.

Liu, X.M., Liu, T.S., Shaw, J., Heller, F., Xu, T.C., and Yuan, B.Y. (1991) Paleomagnetic and paleoclimatic studies of Chinese loess. In: **Loess, Environment and Global Change** (Liu, T.S., ed.). 61-81. Science Press, Beijing, China.

Liu, X.M., Rolph, T., Bloemendal, J., Shaw, J., and Liu, T.S. (1995) Quantitative estimates of palaeoprecipitation at Xifeng, in the Loess Plateau of China. **Palaeogeography, Palaeoclimatology, Palaeoecology 113**, 243-248.

Livingstone, D.A. and Clayton, W.D. (1980) An altitudinal cline in tropical African grass floras and its paleoecological significance. **Quaternary Research 13**, 392-402.

Loper, D.E. (1992) On the correlation between mantle plume flux and the frequency of reversals of the geomagnetic field. **Geophysical Research Letters, 19**, 25-28.

Lorius, C., Jouzel, J., Raynaud, D., Hansen, J. and Le Treut, H. (1990) The ice-core record: climate sensitivity and future greenhouse warming. **Nature, 347**, 139-145.

Lowell, R.P. and Germanovich, L.N. (1995) Dike injection and the formation of megaplumes at ocean ridges. **Science, 267**, 1804-1807.

Lu, Y.C. and An, Z.S. (1979) The natural environment change of the Loess Plateau during about the last 700,000 years. **Science Bulletin 24**, 221-224 (in Chinese).

Lydolph, P.E. (1985) **The Climate of the Earth**. Rowman & Allanheld. pp386.

Maher, B.A. and Taylor, R.M. (1988) Formation of ultrafine-grained magnetite in soils. **Nature 336**, 368-370.

Maher, B.A. and Thompson, R. (1991) Mineral magnetic record of the Chinese loess and paleosols. **Geology 19**, 3-6.

Maher, B.A. and Thompson, R. (1992) Paleoclimatic significance of the mineral magnetic record of the Chinese loess and paleosols. **Quaternary Research 37**, 155-170.

Maher, B.A., Thompson, R., and Zhou, L.P. (1994) Spatial and temporal reconstructions of changes in the Asian palaeomonsoon: A new mineral magnetic approach. **Earth and Planetary Science Letters 125**, 461-471.

Manaba, S. and Terpstra, T.B. (1974) The effects of mountains on the general circulation of the atmosphere as identified by numerical experiments. **Journal of Atmospheric Science 31**, 3-42.

Manaba, S. and Broccoli, A.J. (1985) The influence of continental ice sheets on the climate of an ice age. **Journal of Geophysical Research 90**, 2167-2190.

Manabe, S. and Stauffer, R.J. (1988) Two stable equilibria of a coupled ocean-atmosphere model. **Journal of Climate, 1**, 841-866.

Mankinen, E.A. and Darmple, G.B. (1979) Revised geomagnetic polarity time scales of the interval 0-5 m.y. B.P. **Journal of Geophysical Research 84**, 615-626.

Martin, A., Mariotti, A., Balesdent, J., Lavelle, P. and Vuattoux, R. (1990) Estimate of organic matter turnover rate in a savanna soil by ^{13}C natural abundance measurements. **Soil Biology and Biochemistry 22**, 517-523.

Masukenkichi and Todatatsu (1944) Loess distribution in North China. In: **Mongolic Institute of East Asia, 8** (in Japanese).

Matsushima, Y. (1976) the alluvial deposits in the southern part of the Miura Peninsula, Kanagawa Prefecture. **Bulletin of Natural Science of the Kanagawa Prefectural**

Museum 9, 87-162.

McConnell, R.K. (1965) Isostatic adjustment in a layered earth. **Journal of Geophysical Research, 70**, 5171-5188.

Mercer, J.H. (1984) Simultaneous climatic change in both hemispheres and similar bipolar interglacial wanning: evidence and implications. In: Hansen, H. and Takahashi, T. (eds.), **Climate Process and Climate Sensitivity, Ewing, M. (ed.), American Geophysical Union Geophysical Monograph 5**, 307-313.

Milankovitch, M.M. (1941) Canon of insolation and the ice-age problem. **Royal serb. Acad. Spec. Publ., 133, Belgrade**. English translation published in 1969 by Israel Program for Scientific Translations, U.S. Dept. of Commerce and Nat. Sci. Fdn., Washington, D.C.

Mix, A C. (1987) The oxygen-isotope record of glaciation. In Ruddiman, W.F., and Wright, H.E., Jr., (eds), **North America and Adjacent Oceans during the Last Deglaciation, The Geology of North America, K-3**, 111-136.

Mix, A.C. and Ruddiman, W.F. (1985) Structure and timing of the last deglaciation, Oxygen-isotope evidence. **Quaternary Sci. Rev., 4**, 58-108.

Mo, D.W. and Derbyshire, E. (1991) The depositional environment of the late Pliocene "red clay", Jing-Le basin, Shanxi Province, China. **Sedimentary Geology 70**, 33-40.

Moor, P.D. (1994) High hopes for C4 plants. **Nature 367**, 322-323.

Morley, J.J. and B.A. (1991) Evolving Pliocene-Pleistocene climate: A north Pacific perspective. **Quaternary Science Reviews 10**, 225-237.

Mutter, J.C. and Karson, J.A. (1992) Structural processes at slow-spreading ridges. **Science, 257**, 627-634.

Nelson, C.S.,Hendy, C.H., Jarrett, G.R., and Cuthbertson, A.M. (1985) Near-synchroneity of New Zealand alpine glaciations and Northern Hemisphere continental glaciations during the past 750 kyr. **Nature, 318**, 361-363.

Nesbit, H.W. and Young, G.M. (1982) Early Proterozoic climates and plate motions inferred from major element chemistry of lutites. **Nature 299**, 715-717.

Ni, Y.Q. and Qian, Y.F. (1991) The effects of sea surface temperature anomalies over the mid-latitude western Pacific on the Asian summer monsoon. **Acta Meteorologica Sinica 5**, 28-39.

Oerlemans, J. (1980) Model experiments on the 100,000-yr glacial cycle. **Nature, 287**, 430-432.

O'Leary, M.H. (1981) Carbon isotope fractionation in plants. **Photochemistry 20**, 553-567.

O'Leary, M.H (1988) Carbon isotopes in photosynthesis. **Bioscience 38**, 325-326.

Paterson, W.S.B. and Hammer, C.U. (1987) Ice core and other glaciological data. In Ruddiman, W.F., and Wright, H.E., Jr., (eds), **North America and Adjacent Oceans during the Last Deglaciation, The Geology of North America, K-3**, 91-110.

Paytan, A., Kastner, M., Martin, E.E., Macdougall, J.D., and Herbert, T (1993) Marine barite as a monitor of seawater strontium isotope composition. **Nature, 366**, 445-449.

Pei, W.Z., Zhou, M.Z., and Zheng, J.J. (1963) **Cenozoic of China**. Science Press (in Chinese).

Pei, W.Z. and Huang W.P. (1959) Some opinions on the Sanmen Series. In: **Proceedings of the Symposium on Quaternary Geology of the Sanmen Gorge**. Science Press. 3-20 (in Chinese).

Peltier, W.R. (1982) Dynamics of the ice age Earth. **Advances in Geophysics, 24**, 1-146.

Peltier, W.R. (1985) relaxation oscillator model of the ice age cycle. In: Nicolis, C. and Nicolis, G. (eds.), **Irreversible Phenomena and Dynamical Systems Analysis in Geosciences**, 399-416.

Peltier, W.R. (1987) Glacial isostasy, mantle viscosity, and Pleistocene climatic change. In: Ruddiman, W.F., and Wright, H.E., Jr., (eds), **North America and Adjacent Oceans during the Last Deglaciation, The Geology of North America, K-3**, 155-182.

Peltier, W.R. (1988) Lithospheric thickness, Antarctic deglaciation history, and ocean basin discretization effects in a global model of postglacial sea level change: A summary of some sources of nonuniqueness. **Quaternary Research 29**, 93-112.

Peltier, W.R. and Hyde, W. (1984) A model of the ice age cycle. In: Berger, A.L., Imbrie, J., Hays, J., Kukla, G. and Saltzman, B. (eds), **Milankovitch and Climate, Part II**, 565-580.

Pick, T. and Tauxe, L. (1993) Geomagnetic palaeointensities during the Cretaceous normal superchron measured using submarine basaltic glass. **Nature, 366**, 238-242.

PiPujol, M.D. and Buurman, P. (1994) The distinction between ground-water gley and surface-water gley phenomena in Tertiary paleosols of the Ebro basin, NE Spain. **Palaeogeography, Palaeoclimatology, Palaeoecology 110**, 103-113.

Pockalny, R.A., Detrick, R.S., and Fox, P.J. (1988) Morphology and tectonics of the Kane Transform from Sea Beam bathymetry data. **Journal of Geophysical Research, 93**, 3179-3193.

Pollard, D. (1982) A simple ice sheet model yields realistic 100 kyr Glacial cycles. **Nature, 296**, 334-338.

Pollard, D. (1983) Ice-age simulations with a calving ice-sheet model. **Quaternary Research, 20**, 30-48.

Pollard, D. (1984) Some ice-age aspects of a calving ice sheet model. In: Berger, A.L. et al. (eds.), **Milankovitch and Climate**, Boston, D. Reidel (NATO ASI Series). 564-591.

Pollard, D. Ingersoll, A.P. and Lockwood, J.G. (1980) Response of a zonal climate-ice sheet model to the orbital perturbations during the Quaternary ice ages. **Tellus, 32**, 301-319.

Porter, S.C. (1975) Equilibrium-line altitudes of late Quaternary glaciers in the Southern Alps, New Zealand. **Quaternary Research, 5**, 27-47.

Porter, S.C. (1981a) Pleistocene glaciation in the southern Lake District of Chile. **Quaternary Research, 16**, 263-292.

Porter, S.C. (1981b) Glaciation evidence of Holocene climatic change. In: Wigley, T.M., Ingram, M.J., and Farmere, G. (eds.), **Climate and History**, Cambridge University Press. 82-110.

Porter, S.C. (1988) Landscapes of the last ice age in North America. **Americans Before Columbus (Carlise, R.C., ed.) Ethnology Mon., 12**, dept. of Anthropology, University Pittsburgh. 1-24.

Porter, S.C. and An, Z.S. (1995) Correlation between climate events in the North Atlantic and China during the last glaciation. **Nature 375**, 305-308.

Qin, Y.S. and Zhao, S.L. (1991) New progress in study of sedimentation model of Chinese shelf area. In: **Quaternary Coastline Changes in China** (Qin, Y.S. and Zhao, S.L., eds.), China Ocean Press, Beijing. 1-20.

Quade, J., Cerling, T.E., and Bowman, J.R. (1989) Systematic variations in the carbon and oxygen isotopic composition of pedogenic carbonate along elevation transects in the southern Great Basin, United States. **Geological Society of America Bulletin 101**, 464-475.

Rahmstorf, S. (1994) Rapid climate transitions in a coupled ocean-atmosphere model. **Nature, 372**, 82-85.

Rampino, M.R. and Self, S. (1992) Volcanic winter and accelerated glaciation following the Toba super-eruption. **Nature, 359**, 50-52.

Rampino, M.R. and Self, S. (1993) Climate-volcanism feedback and the Toba eruption of ~74,000 years ago. **Quaternary Research, 40**, 269-280.

Raymo, M.E. and Ruddiman, W.F. (1992) Tectonic forcing of late Cenozoic climate. **Nature, 359**, 117-122.

Ren, M.E. (1985) An Outline of China's Physical Geography. **China Knowledge Series**. Foreign Languages Press, Beijing.

Richardson, R.M., Solomon, S.C., and Sleep, N.H. (1979) Tectonic stress in the plates. **Reviews of Geophysics and Space Physics, 17**, 981-1019.

Richardson, S.M. and McSween, H.Y., Jr. (1989) **Geochemistry Pathways and Processes**, Prentice Hall, Englewood Cliffs, New Jersey. 166-207.

Richthofen, F.V. (1877) **China 1**. Berlin.

Richthofen, F.V. (1882) On the mode of origin of the loess. **Geological Magazine, 9 (ser. 2)**, 293-305.

Rind, D., Peteet, D. and Kukla, G. (1989) Can Milankovitch orbital variations initiate the growth of ice sheets in a general circulation model? **Journal of Geophysical Research, 94**, 12851-12871.

Robinson, J.M. (1994) Atmospheric CO_2 and plants. **Nature 368**, 105-106.

Ross, G.J. (1975) Experimental alteration of chlorites into vermiculites by chemical oxidation. **Nature 255**, 133-134.

Ross, G.J. and Kodama, H. (1970) Differential release of potassium from interstratified mica clay minerals as related to probable differences in their mica layer components. **Clays and Clay Minerals 18**, 151-156.

Ross, G.J. and Kodama, H. (1976) Experimental alteration of a chlorite into a regular interstratified chlorite-vermiculite by chemical oxidation. **Clays and Clay Minerals 24**, 183-190.

Royer, A., DeAngelis, M., and Petit, J.R. (1983) A 30,000 year record of physical and optical properties of microparticles from an East Antarctic ice core and implications for paleoclimate reconstruction models. **Climatic Change, 5**, 381-412.

Ruddiman, W.F. (1987) Synthesis: The ocean ice/sheet record. In: Ruddiman, W.F. and Wright, H.E. Jr. (eds), **North America and Adjacent Oceans during the Last**

Deglaciation. Geological Society of America, Geology of North America, **K-3**. 463-478.

Ruddiman, W.F. and McIntyre, A. (1981) The North Atlantic Ocean during the last deglaciation. **Paleogeography Paleoclimatology Paleoecology 35**, 145-214.

Ruddiman, W.F., Raymo, M., and McIntyre, A. (1986) Matuyama 41,000 years cycles: North Atlantic Ocean and Northern Hemisphere ice sheets. **Earth and Planetary Science Letters, 80**, 117-129.

Ruddiman, W.F. and Raymo, M.E. (1988) Northern Hemisphere climate regimes during the past 3 Ma: Possible tectonic connections. **Philosophical Transaction of the Royal Society of London B 318**, 411-430.

Ruddiman, W.F. an Kutzbach, J.E. (1991) Plateau uplift and climatic change. **Scientific American, March, 1991**, 66-75.

Salinger, M.J. (1990) New Zealand climate: Trends since the Last Glacial Maximum. In: Donnelly, T. and Wasson, R.J. (eds), **Proceedings of the 3rd Symposium on Late Quaternary Climatic History of Australia** (Melbourne University, November 28-29, 1987), Canberra, Commonwealth Scientific Research Organization, Water Resources, 100-106.

Sasajima, S. and Wang, Y. (1984) **The Recent Research of Loess in China** (eds.). Kyoto Institute of Natural History.

Schilling, D.H. and Hollin, J.T. (1981) Numerical reconstruction of valley glaciers and small ice caps. In: Denton, G.H. and Hughes, T.J. (eds.), **The Last Great Ice Sheets**, John Wiley & Sons, New York. 207-220.

Schwartz, D., Mariotti, A., Lanfranchi, R., and Guillet, B. (1986) $^{13}C/^{12}C$ ratios of soil organic matter as indicators of vegetation changes in the Congo. **Geoderma 39**, 97-103.

Schwertmann, U., Murad, E, and Schulze, D.G. (1982) Is there Holocene reddening (haematite formation) in soils of axenic temperate areas? **Geoderma 27**, 209-223.

Shackleton, N.J. (1967) Oxygen isotope analyses and Pleistocene temperatures, reassessed. **Nature, 215**, 15-17.

Shackleton, N.J. (1987) Oxygen isotope, ice volume and sea level. **Quaternary Science Reviews 6**, 183-190.

Shackleton, N.J. (1988) Oxygen isotopes, ice volume, and sea level. **Quaternary Science Reviews 6**, 183-190.

Shackleton, N.J. and Opdyke, N.D. (1973) Oxygen isotope and paleomagnetic stratigraphy of equatorial Pacific core V28-238: Oxygen isotope temperatures and ice volumes on a 10^5 and 10^6 year scale. **Quaternary Research 3**, 39-55.

Shackleton, N.J., Imbrie, J., and Piasias, N.G. (1988) The evolution of oceanic oxygen-isotopic variability in the North Atlantic over the past three million years. **Philosophical Transaction of the Royal Society of London, B318**, 679-688.

Shen, C.D., Beer, J., Liu, T.S., Oschger, H., Bonani, G., Suter, M., and Wolfli, W. (1992) ^{10}Be in Chinese Loess. **Earth and Planetary Science Letters 109**, 169-177.

Shen, C.D., Yi, W.C., Liu, T.S., Beer, J., Heller, F., Bonani, G., Dittrich, B., Kubik, W., and Suter, M. (1994) ^{10}Be-susceptibility model and the quantitative estimates of pedogenic ferromagnetic material flux in Chinese loess. **Quaternary Sciences 1994**(1), 75-86.

Shi, Y.C. (1958) Loess and its origin in western Shanxi Province. **Quaternaria Sinica 1(1)**, 252-253 (in Chinese).

Skinner, B.J. and Porter, S.C. (1987) **Physical Geology**. J. Wiley & Sons.

Smith, B.N. and Epstein, S. (1971) Two categories of $^{13}C/^{12}C$ ratios for higher plants. **Plant Physiology 47**, 380-384.

Smith, D.K. and Cann, J.R. (1993) Building the crust at the Mid-Atlantic Ridge. **Nature, 365**, 707-715.

Stacey, F.D. (1977) **Physics of the Earth, Second Edition**. pp90, 292. John Willey & Sons, New York.

Sturchio, N.C., Dunkley, P.N., and Smith, M. (1993) Climate-driven variations in geothermal activity in the northern Kenya rift valley. **Nature, 362**, 233-234.

Suggate, R.P. (1978) **The Geology of New Zealand, Volumes 1 and 2**. E.C. Keating, Wellington.

Sukumar, R., Ramesh, R., Pant, R.K., and Rajagopalan, G. (1993) A $\delta^{13}C$ record of late Quaternary climate change from tropical peats in southern India. **Nature 364**, 703-706.

Sun, J.Z. (1987) New Paleomagnetic data on the Wujiapu section, Weinan, Shaanxi. In: **The Collected Papers of the IV National Quaternary Meeting, 87'Beijing**. (in Chinese).

Sun, J.Z., Zhao, J.B., Sun, X.Y., Wei, M.J., Li, H.M., and Zhou, Z.B. (1985) Loess even older in Liujiapo. In: **Proceedings of the International Symposium on Loess Research, Oct. 5-16, Xi'an**, 14 pp.

Sun, X.J. (1989) Re-investigation on the late Pleistocene vegetation in Beizhuang of

Weinan, Shaanxi. **Quaternary Sciences 1989(2)**, 177-190.

Tan, K.H. (1994) **Environmental Soil Science**. Marcel Dekker, Inc., New York, 43-44.

Tang, K.L. (1981) Micromorphology and genesis of the paleosols in loess, Wugong, Shaanxi. **Science Bulletin 26**, 177-179 (in Chinese).

Tarling, D.H. (1981) The crust of the earth. In: **The Cambridge Encyclopedia of Earth Sciences** (Smith, D.G., eds.), 164-188. Cambridge University Press, Cambridge, London.

Teachers College of Northwest China (1984) **Maps of the Natural Geography of China**. Special Publications Map Office, Beijing.

Tedford, R.H., Flynn, L.J., Qiu, Z.X., Opdyke, N.D., and Downs, W.R. (1991) Yushe Basin, China: Paleomagnetically calibrated mammalian biostratigraphic standard for the late Neogene of eastern Asia. **Journal of Vertebrate Paleontology 11(4)**, 519-526.

Teeri, J. and Stowe, L.G. (1976) Climatic patterns and the distribution of C-4 grasses in North America. **Oecologia 23**, 1-12.

Teilhard de Chardin, P. and Young, C.C. (1930) Preliminary observations on the preloessic and post-Pontian formations in Western Shansi and Northern Shensi. **Memoirs of Geological Survy of China Series A 8**, 1-54.

Teilhard de Chardin, P. and Young, C.C. (1931) Fossil mammals from the late Cenozoic of northern China. **Paleontologica Sinica Series C, 9**, 1-42.

Teller, J.T. (1985) Glacial Lake Agassiz and its influence on the Great Lakes. In: Karrow, P.F. and Calkin, P.E. (eds), **Quaternary Evolution of the Great Lakes, Geological Association Canada Special Papers 30**, 1-16.

Tieszen, L.L., Senyimbia, M.M., Imbamra, S.K., and Troughton, J.H. (1979) The distribution of C-3 and C-4 grasses and carbon isotope discrimination along an altitudinal and moisture gradient in Kenya. **Oecologia 37**, 337-350.

Dikinson, R.E. (1992) Land surface. In: **Climate System Modeling** (Trenberth, K.E., ed.), Cambridge University Press, Butler & Tanner, Frome and London. 149-172.

Tucholke, B.E. and Lin, J. (1994) A geological model for the structure of ridge segments in slow spreading ocean crust. **Journal of Geophysical Research, 99(B6)** 11937-11958.

Valet, J.-P. and Meynadier, L. (1993) Geomagnetic field intensity and reversals during the past four million years. **Nature, 366**, 234-238.

Venum, T., Jansen, E., Arnold, M., Beyer, I., and Duplessy, J.-C. (1992) Water mass exchange between the North Atlantic and the Norwegian Sea during the past 28,000 years. **Nature, 356**, 783-785.

Vera, E.E., Mutter, J.C., Buhl, P., Orcutt, J.A., Harding, A.J., Kappus, M.E., Detrick, R.S., and Brocher, T.M. (1990) The structure of 0- to 0.2-m.y.-old oceanic crust at 9°N on the East Pacific Rise from expanded spread profiles. **Journal of Geophysical Research, 95**, 15529-15556.

Verosub, K.L., Fine, P., Singer, M.J., and Tenpas, J. (1993) Pedogenesis and paleoclimate: Interpretation of the magnetic susceptibility record of Chinese loess-paleosol sequences. **Geology 21**, 1011-1014.

Wang, F.B. and Li, B.Y. (1985) The lower boundary of the Quaternary in the Himalaya region in China. In: **Quaternary Geology and Environment of China** (Liu, T.S., ed.), China Ocean Press, Beijing. 18-26.

Wang, P.X. (1992) A paleoceanographic comparison of west Pacific marginal seas during the last glaciation. In: **Paleoceanography of the South China Sea in the Late-Quaternary**. Qingdao University of Oceanography Press, Qingdao. 308-321.

Wang, P.X. (1995) The role of west Pacific marginal seas in glacial aridification of China: A preliminary study. **Quaternary Sciences 1995**(1), 32-42.

Wang, Y., Evans, M.E., Rutter, N., and Ding, Z. (1990) Magnetic susceptibility of Chinese loess and its bearing on paleoclimate. **Geophysical Research Letters 17 (12)**,2449-2451.

Weertman, J. (1976) Milankovitch solar radiation variations and ice age ice sheet sizes. **Nature, 261**, 17-20.

Williams, D.F., Thunell, R.C., Tappa, E., Rio, D., and Raffi, I. (1988) Chronology of the Pleistocene oxygen isotope record: 0-1.88 m.y. B.P. **Palaeogeography, Palaeoclimatology, Palaeoecology 64**, 221-240.

Winkler, M.G. and Wang, P.K. (1993) The late-Quaternary vegetation and climate of China. In: **Global Climates Since the Last Glacial Maximum** (Wright, H.E.Jr., Kutzbach, J.E., Webb III, T., Ruddiman, W.F., Street-Perrott, F.A., and Bartlein, P.J., eds.). 221-261. University of Minnesota Press, Minneapolis, London.

Winograd, I.J., Coplen, T.B., Landwehr, J.M., Riggs, A.C., Ludwig, K.R., Szabo, B.J., Kolesar, P.T., and Revesz, K.M. (1992) Continuous 500,000-year climate record from vein calcite in Devils Hole, Nevada. **Science, 258**, 255-260.

Wu, T.-W. (1984) Geochemistry and Petrogenesis of Some Granitoids in the Grenville Province of Ontario and Their Tectonic Implications. Ph.D. Thesis (University of Western Ontario), 662pp.

Xue, X.X. (1981) An early Pleistocene mammalian fauna and the stratohorizon in Weinan, Shaanxi Province. **Vertebrate Paleontology and Paleoanthropology 19**, 35-44. (in Chinese).

Yatsu, E. (1988) **The Nature of Weathering**. Chapter 5: Mineral transformation in the weathering zone, 401-504. Sozosha, Tokyo.

Young, C.C. (1934a) Introduction to the Hominid fossils and Cenozoic Geology of China. **Bulletin of Geolology Series B (5)**, 12-31 (in Chinese).

Young, C.C. (1934b) A historic review of the Sanmen Series. **Geological Reviews 1 (3)**, 323-330. (in Chinese).

Young, H.J. and Young, T.P. (1983) Local distribution of C-3 and C-4 grasses in sites of overlap on Mount Kenya. **Oecologia 58**, 373-377.

Zhang, L.Y. (1981) The influence of the Qinghai-Xizang Plateau on the Quaternary environmental evolution in China. **Journal of Lanzhou University (Natural Sciences) 1981**(3), 142-156.

Zhao, S.L. and Qin, Y.S. (1982) Transgressions and sea level changes in the eastern coastal region of China in the last 300,000 years. In: **Quaternary Geology and Environment of China** (Liu, T.S., ed.), China Ocean Press, Beijing. 147-154.

Zhao, X.T., Zhang, J., Jiao, W., and Li, G. (1980) Chenier ridges on the west coast of the Bohai Gulf. **Science Bulletin Sinica 25**, 243-247.

Zhao, X.T., Geng, X.S., and Zhang, J. (1982) Sea level changes in eastern China during the past 20 000 years. **Acta Oceanologica Sinica 1(2)**, 248-258.

Zhao, X.T. and Zhang, J. (1985) Basic characteristics of the Holocene sea level changes along the coastal areas in China. **Quaternaria Sinica 6(2)**, 104-109.

Zheng, H.B., An, Z.S., Shaw, J., and Liu, T.S. (1991a) A detailed terrestrial geomagnetic record for the interval 0-5.0 Ma. In: Liu, T.S. (ed.) **Loess, Environment and Global Change**, 147-156. Science Press, Beijing, China.

Zheng, H., Oldfield, F., Yu, L. Shaw, J., and An, Z.S. (1991b) The magnetic properties of particle-sized samples from the Luo Chuan loess section: Evidence for pedogenesis. **Physics of the Earth and Planetary Interiors 68**, 250-258.

Zhou, L.P., Oldfield, F., Wintle, A.G., Robinson, S.G., and Wang, J.T. (1990) Partly pedogenic origin of magnetic variations in Chinese loess. **Nature 346**, 737-739.

Zhu, H.Z. (1963) Some characterristics of the grain size and texture of Malan loess in the middle reaches of the Yellow River. **Scientia Geologica Sinica 2**, 88-102 (in

Chinese).

Zhu, X.M. (1958) Discussion on the problems of red layers intercalated in the loess section. **Quaternaria Sinica 1(1)**, 74-82 (in Chinese).

Zhu, X.M. (1965) Paleosols in loessic sediments of China. **Quaternaria Sinica 4(1)**, 9-19 (in Chinese).

Zoback, M.L. (1992) First- and second-order patterns of stress in the lithosphere: The world stress map project. **Journal of Geophysical Research, 97(B8)**, 11703-11728.

Zoback, M.D., Anel, R., Baumgartner, J., Brudy, M., Emmermann, R., Engeser, B., Fuches, K., Kessels, W., Rischmuller, H., Rummel, F., and Vernik, L. (1993) Upper-crustal strength inferred from stress measurements to 6 km depth in the KTB borehole. **Nature 365**, 633-635.